An-Najah National University
Faculty of Graduate Studies

Design and Techno-Economical Analysis of a Grid Connected with PV/ Wind Hybrid System in Palestine (Atouf Village-Case study)

By
Mohammad Husain Mohammad Dradi

Supervisor
Dr. Imad Ibrik

This Thesis is Submitted in Partial Fulfillment of the Requirements for the Degree of Master of Program in Clean Energy and Conservation Strategy Engineering, Faculty of Graduate Studies, An-Najah National University, Nablus-Palestine
2012

www.manaraa.com

Design and Techno-Economical Analysis of a Grid Connected with PV/ Wind Hybrid System in Palestine (Atouf Village-Case study)

By
Mohammad Husain Mohammad Dradi

This Thesis was defended successfully on 26/4/2012 and approved by:

Defense Committee Members	**Signature**
1. Dr. Imad Ibrik / Supervisor	.....
2. Dr. Abedel Karim Daud / External Examiner	.....
3. Prof. Marwan Mahmoud / Internal Examiner	.....

DEDICATION

To my father ….

To my mother, brothers and sisters…….

To my wife, daughters, and son……

To my uncle……

To the soul of my aunt ……..

To all friends and colleagues……

To every one working in this field……

To all of them,

I dedicate this work

www.manaraa.com

ACKNOWLEDGMENTS

It is an honor for me to have the opportunity to say a word to thank all people who helped me to complete this study, although it is impossible to include all of them here.

All appreciations go to my supervisor, Dr. Imad Ibrik for his exceptional guidance and insightful comments and observations throughout the duration of this project.

My thanks and appreciations go to the staff of Clean Energy and Conservation Strategy Engineering Master Program in An-Najah National University, especially Prof. Marwan Mahmoud for his valuable suggestions and assistance.

This project would not have been possible without the endless support and contributions from my family, especially my mother for her kindness, my wife for here encouragement and patience, my brothers and sisters for their support, also for my friends and colleagues for their useful help, and to everyone who contributed to complete this effort.

www.manaraa.com

الإقرار

إنا الموقع أدناه مقدم الرسالة التي تحمل عنوان

Design and Techno-Economical Analysis of a Grid Connected with PV/ Wind Hybrid System in Palestine (Atouf Village-Case study)

التقييم والتحليل التقني والاقتصادي لربط شبكات الكهرباء مع الأنظمة الهجينة خلايا شمسية رياح في فلسطين/ قرية عطوف : دراسة حالة

اقر بان ما اشتملت عليه هذه الرسالة إنما هو نتاج جهدي الخاص ، باستثناء مـــا تمـــت الإشارة إليه حيثما ورد، وان هذه الرسالة ككل من أو جزء منها لم يقدم من قبل لنيل أية درجة أو بحث علمي أو بحثي لدى أية مؤسسة تعليمية أو بحثية أخرى .

Declaration

The work provided in this thesis, unless otherwise referenced, is the researcher's own work, and has not been submitted elsewhere for any other degree or qualification.

Student's name: **اسم الطالب:**

Signature: **التوقيع:**

Date: **التاريخ:**

المنارة للاستشارات
www.manaraa.com

List of Abbreviations

AC	Alternative current
GTI	Grid tie inverter
GS	Gaza Strip
GW	Giga watt
GWh	Giga watt hour
IEC	Israel electric corporation
kVA	Kilo volt ampere
kWh	Kilo watt hour
NIS	New Israeli shekel
PSH	Peak sun hour
PT	Palestinian Territories
FIT	Feed in Tariff
STC	Standard Test Condition
LCC	Life Cycle Cost
PCC	Point of common coupling
ERC	Energy Research Center
CV	Constant voltage method
IC	Incremental Conductance method
CCM	Continues Conduction Mode
rpm	Revolution per minute

www.manaraa.com

Table of Contents

المنارة للاستشارات
www.manaraa.com

www.manaraa.com

www.manaraa.com

List of Tables

www.manaraa.com

List of Figures

www.manaraa.com

المنارة للاستشارات
www.manaraa.com

www.manaraa.com

www.manaraa.com

www.manaraa.com

List of Equations

www.manaraa.com

www.manaraa.com

www.manaraa.com

List of Maps

www.manaraa.com

List of Appendices

www.manaraa.com

Design and Techno-Economical Analysis of a Grid Connected with PV/ Wind Hybrid System in Palestine (Atouf Village-Case study)

By
Mohammad Husain Mohammad Dradi
Supervisor
Dr. Imad Ibrik

Abstract

As renewable energy becomes more prevalent, more information on how different technologies will behave needs to be available. This research based on modeling the Grid tie PV/Wind hybrid system using Matlab Simulink software program in order to study the techno-economic performance analysis of building these systems according to our environmental conditions and collecting data such as temperature, solar radiation and wind speed.

By creating a Simulink program which predicts the power output as a function of solar radiation, temperature and wind speed, a side-by-side comparison of different sizes and configurations can be made. Current predictive models are very useful for a grid tie system, which is limited to operate at the maximum power point, thus adaptations to previous models have been made. This model accurately predicts the power output of different PV hybrid system based on side data specification.

The program is dynamic, and fit with the changes of parameters, which are related to the reduced power output caused by increased temperature, as well as the effect of non-linear absorption of solar radiation on power output. Data was collected and analyzed as a case study for Atouf village.

www.manaraa.com

This research is important because it exposes weaknesses of different environmental conditions of the locations, and allows for a direct comparison of modeling different configurations of hybrid systems. This research shows that tacking random value for determining the size of PV system is not the best performance indicators of grid tie system. Specifically, this research shows that the penetration factor of PV hybrid system has a different effect on the power output of each PV array. The size of this affect can be evaluated technically and economically by using this software program.

www.manaraa.com

INTRODUCTION

www.manaraa.com

Introduction

Clean, economic and secure energy production gains importance with the increasing of the world's power demand. So, a new type of energy sources has gained popularity. The sun and the wind energy are more common alternative energy sources. Previously, they were used to supply local loads in remote areas outside the national grid. Later, they have become some of main sources [1], [2].

Alternative energy sources are operates in stand alone mode or grid tie mode. It is difficult to obtain an efficient operation in stand-alone mode and usually high capacity battery groups are required. Since the energy produced from the wind and the solar are transferred to grid line, the way of the transforming direct current (DC) energy to alternating current (AC) is very important. This process has generally been achieved by a grid tie inverter; inverter supplies the local loads and if the generated energy higher than the demand the excess energy is export to the grid, so battery groups are unneeded. On the other hand, control of the grid tied inverter is more complex than the stand alone one [2].

The electric power generation system, which consists of renewable energy sources connected to grid, has the ability to provide 24-hour electricity to the load. This system offers a better reliability, efficiency, flexibility of planning and environmental benefits compared to the stand-alone system.

www.manaraa.com

Each kilowatt-hour (kWh) generated from renewable resources saves the environment from the burning of fossil fuels. The coal fired and the natural gas fired power plants produce 1.05 Kg and 0.75 Kg carbon dioxide, respectively, to generate 1kWh electricity [3].

Objectives of Work

The main objective of the present work is to design a grid tie PV/Wind hybrid system by using Matlab Simulink program and apply this system on Atouf village as a case study. To achieve this objective I study the mathematical models which characterize each part of grid tie hybrid system such as PV module, wind turbine, MPPT controller and diesel generator, and then I convert the mathematical models to Simulink models. After that I Investigate the design connection topologies for all components of grid tie PV/wind hybrid system in order to study the operation of system for different environmental conditions.

Organization of Thesis

The work carried out in this thesis has been summarized in eight chapters

Chapter 1 studies the potential of solar energy, solar radiation and temperature in Palestine, also describes Photovoltaic (PV) Implemented Projects in Palestine.

www.manaraa.com

Chapter 2 describes the potential of wind energy, wind resource, wind distribution, wind data calculation for Ramallah and Nablus cities in Palestine.

Chapter 3 consists of the main building constructions of grid tie PV/wind system and basic information about PV systems, wind turbine system, maximum power point tracker (MPPT), three-phase DC-AC inverter, DC-DC converter, and also diesel generator.

Chapter 4 describes the mathematical modeling and Simulink for each part of the grid tie PV/Wind hybrid system such as PV system, wind turbine and diesel generator.

Chapter 5 describes the overall system and the simulation of it, with different environmental conditions, and then observes operation results.

Chapter 6 introduces some information about Atouf village, potential of solar energy, also, sizing the elements of the grid tie system for this village and simulation results in different conditions such as solar radiation, temperature and load.

Chapter 7 studies the economic and environmental impacts of grid tie PV system, describes the grid tie tariffs such as net metering or feed in tariff, evaluation the economic and environmental impacts of Atouf Grid tie PV system.

Chapter 8 describes the main conclusions about grid tie hybrid system and future scope of work**.**

المنارة للاستشارات
www.manaraa.com

CHAPTER ONE

POTINTIAL OF SOLAR ENERGY IN PALESTINE

www.manaraa.com

Chapter One
Potential of Solar Energy in Palestine

Introduction

Palestine is located between 34º:20′ - 35:30′ E and 31º: 10′ - 32º:30′ N, it consists of two separated areas from one another. The Gaza Strip is located on the western side of Palestine adjacent to the Mediterranean Sea and the West-Bank which extends from the Jordan River to the center of Palestine [4].

Palestine's elevation ranges from 350m below sea level in Jordan Valley, to sea level along the Gaza Strip sea shore and exceeding 1000m above sea level in some mountains areas in the West Bank [4].

Climate conditions in Palestine vary widely. The coastal climate in the Gaza Strip is humid and hot during summer and mild during winter. These areas have low heating loads, while cooling is required during summer. The daily average temperature and relative humidity range between: (13.3 – 35.4) C° and (67 – 75) % respectively [13].

In the hilly areas of the West-Bank, cold winter conditions and mild summer weather are prevalent. Daily average temperature and relative humidity vary in ranges: (8 – 23) Cº and (51 – 83) % respectively [13]. In some areas, the temperature decline below 0 ºC. Hence, high heating loads are required, while little cooling is needed during summer.

Solar radiation and temperature affect on electric solar energy production, so we should have to study these elements for Palestine.

www.manaraa.com

1.1 Solar Radiation in Palestine

Since the area of Palestine is relatively small and the solar radiation (W/m²) doesn't change significantly within such short distance (31° 10′ - 32° 30′ N), the measuring data for all regions (West-Bank & Gaza Strip) may considered to be the same. Table (1.1) shows the measurement of the global radiation on a horizontal surface in the Tubas District [13].

Table (1.1): Hourly average solar radiation of typical summer day (11/6/2011) [13]

Hours	Solar Radiation (w/m²)	Hours	Solar Radiation (w/m²)
1:00	0	13:00	990
2:00	0	14:00	917
3:00	0	15:00	780
4:00	0	16:00	585
5:00	30	17:00	375
6:00	140	18:00	154
7:00	343	19:00	20
8:00	532	20:00	0
9:00	747	21:00	0
10:00	910	22:00	0
11:00	1019	23:00	0
12:00	1062	24:00	0

These measurements are obtained from the Energy Research Center (ERC).

They have been done by horizontally oriented measuring devices, and done on a 5-minute interval basis.

Figure (1.1) shows the daily irradiation-curve plotted from data of table (1.1).

www.manaraa.com

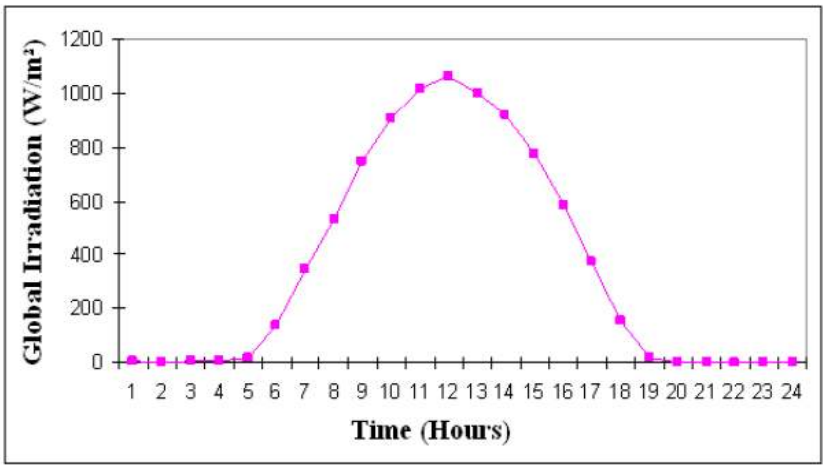

Figure (1.1): The global irradiation (W/m²) versus time (hours)-2011.

From table(1.1) & figure(1.1), it is obvious that the solar radiation is more than 900 W/m² during the hours : 10, 11, 12, 13, and 14 pm and it is also more than 135 W/m² in the morning hours 6, 7, 8, and 9 am, and in the evening hours 15, 16, 17, and 18 pm. This means that we have enough potential for solar radiation and we can obtain electric energy even in the morning or evening.

1.2 Ambient Temperature in Palestine

As we mentioned before, temperature affects the PV generators efficiency. The relation between temperature and efficiency is inversed. The ambient temperature is the main factor that affects the PV generator's temperature. Table (1.2) shows, for an example, the ambient temperature of the target area.

The shown data is the average of two days measurement in June 2011. The original measurements are done on a 5-minute interval basis [13].

www.manaraa.com

Table (1.2): Ambient temperature in Tubas [13].

Hours	Ambient temperature (C°)	Hours	Ambient temperature (C°)
1:00	22	13:00	32
2:00	22	14:00	32
3:00	22	15:00	31
4:00	21	16:00	31
5:00	21	17:00	29
6:00	22	18:00	28
7:00	23	19:00	26
8:00	24	20:00	24
9:00	25	21:00	24
10:00	27	22:00	23
11:00	28	23:00	22
12:00	31	24:00	22

Figure (1.2) shows the daily curve of the ambient temperature drawn from the data table (1.2). It shows that the maximum temperature occurs around noon time (32°C), and the minimum temperature occurs in the early morning (21°C).

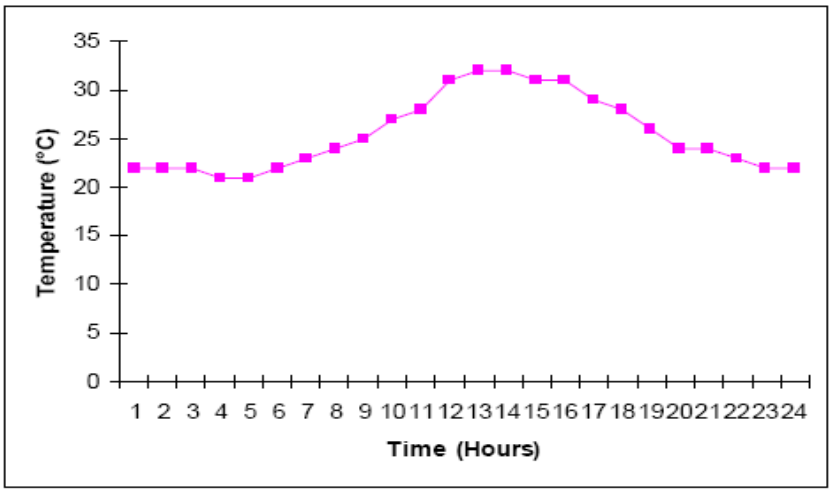

Figure (1.2): The daily ambient temperature curve-2011.

1.3 Solar Energy in Palestine

Palestine has high potential of solar energy. It has around 3000 sunshine hours / year and high annual average solar energy radiation which is about 5.45 kWh / m² - day.

www.manaraa.com

As shown in table (1.3), the lowest average solar energy is in December which is about 2.84 kWh /m² - day and the highest one is in June which is about 8.245 kWh/m² - day.

Table (1.3): Monthly solar energy on horizontal surface for Tubas District –2011 [13]

Month	kWh/m²-day	Month	kWh/m²-day
January	2.885	July	8.167
February	3.247	August	8.099
March	5.226	September	6.304
April	6.247	October	4.700
May	7.565	November	3.562
June	8.245	December	2.840

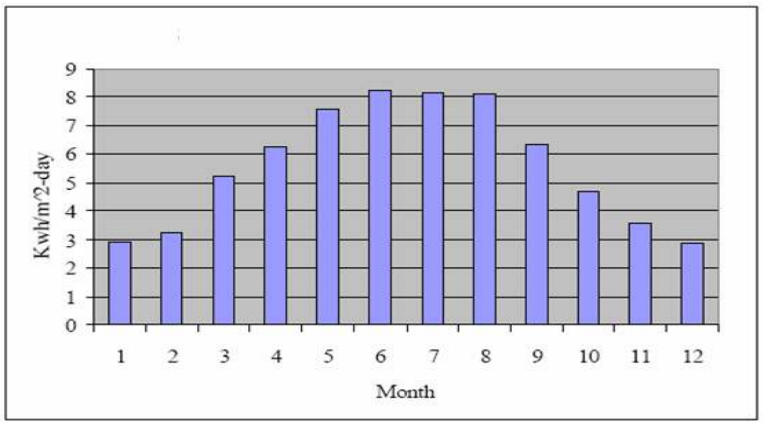

Figure (1.3): Monthly solar energy for Tubas district-2011 on horizontal surface.

1.4 Photovoltaic (PV) Implemented Projects in Palestine

Palestine has a large number of remote small villages that lack electricity and the probability of connecting them with high voltage grid in the near future is very poor due to financial and political situations .So new solar PV projects are implemented in order to provide these rural villages with electricity.

www.manaraa.com

A) Imnazel Photovoltaic (PV) Project:

Imnazel village is located south of Yatta in the Hebron District near the Separation Wall, where a population is about 400 people, and there are about 40 houses, a school and a mosque. The village was connected to electricity, for the first time, through 13kW central system of solar cells as shown in figure (1.4), and has been linked with a generator to help recharge the batteries in case there is lack of energy [13].

Figure (1.4): Imnazel photovoltaic (PV) project [13].

B) Atouf Photovoltaic (PV) Project

Atouf village is located in north of West Bank, where the population is about 200 people, and there are about 21 houses, a school and a mosque. The village was connected to electricity, for the first time, through 12kW central system of solar cells, and has been linked with a generator to help recharge the batteries in case there is lack of energy. I will speak in details about this village in chapter six.

المنارة للاستشارات
www.manaraa.com

Also there are new under construction projects using photovoltaic PV system to feed other small villages and communities far from the electricity grid such as Mkehel village and khirbit Alsaaed near Yabbad in Jenin District [13].

In this chapter, I studied the potential of solar energy in Palestine and the two main elements, solar radiation and temperature, which affecting this energy.

www.manaraa.com

CHAPTER TWO

POTINTIAL OF WIND ENERGY IN PALESTINE

www.manaraa.com

Chapter Two
Potential of Wind Energy in Palestine

Introduction

Wind energy has been used for thousands of years for milling grains, pumping water and other mechanical power applications. But the use of wind energy as an electrical supply with free pollution what makes it attractive and takes more interest and used on a significant scale.

Attempts to generate electricity from wind energy have been made since the end of nineteenth century. Small wind machines for charging batteries have been manufactured since the 1930s. Wind now is one of the most cost effective methods of electricity generation available in spite of the relatively low current cost of fossil fuels.

The wind technology is continuously being improved both cheaper and more reliable, so it can be expected that wind energy will become even more economically competitive over the coming decades [12].

2.1 The Wind Resource

The main consideration for implementing a wind project in a certain site is the wind resource. Other considerations include site accessibility, terrain, land use and proximity to transmission grid for grid-connected wind farms.

The main sources of the global wind movements are the earth rotation, regional and seasonal variations of sun irradiance and heating.

www.manaraa.com

Local effects on wind include differential heating of the land and the sea (land heats up faster), topographical nature such as mountains and valleys, existence of trees and artificial obstacle such as buildings.

At any location, wind is described by its speed and direction. The speed of the wind is measured by anemometer in which the angular speed of rotation is translated into a corresponding linear wind speed (in meters per second or miles per hour). A Standard anemometer averages wind speed every 10 minutes. Wind direction is determined by weather vane [6].

Average (mean) wind speed is the key in determining the wind energy potential in a particular site. Although long-term (over 10 years) speed averages are the most reliable data for wind recourse assessment, this type of data is not available for all locations. Therefore, another technique based on measurement, correlation and perdition is used. Wind speed measurements are recorded for a 1-year period and then compared to a nearby site with available long-term data to forecast wind speed for the location under study [6].

2.2 Wind Speed Distribution

Average value for wind speed for a given location does not alone indicate the amount of energy which wind turbine could produce there. To assess the climatology of wind speeds at a particular location, a probability distribution function is often fit to the observed data. Different locations will have different wind speed distributions. The distribution model which

www.manaraa.com

most frequently used to model wind speed climatology is a two-parameter Weibull distribution because it is able to confirm a wide variety of distribution shapes, from Gaussian to exponential.

Weibull Distribution

The measured wind speed variation for a typical site throughout a year indicates that the strong gale force winds are rare, while moderate and fresh winds are quite common, and this is applicable for most areas. Figure (2.1) shows the Weibull distribution describing the wind variation for a typical site.

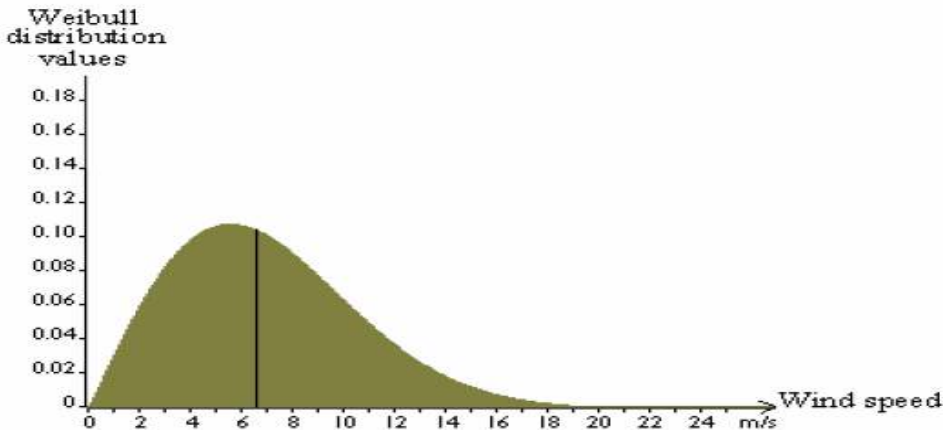

Figure (2.1): Weibull probability density distribution [12].

The area under the curve is always exactly 1, since the probability that the wind will be blowing at some wind speeds including zero must be 100 percent. The distribution of wind speeds is skewed; it is not symmetrical.

Sometimes there are very high wind speeds, but they are very rare. The statistical distribution of wind speeds varies from place to another around the globe depending upon local climate conditions, the landscape,

www.manaraa.com

and its surface. The Weibull distribution may thus vary, both in its shape, and in its mean value. The Weibull probability density distribution function is given by:

$$F(v) = K * \frac{v^{(K-1)}}{C^{K}} * e^{-(\frac{V}{C})^{K}} \quad (2.1)$$

Where

K: is the Weibull shape factor; it gives an indication about the variation of hourly average wind speed about the annual average,

C: is the Weibull scale factor [12].

Each site has its own K and C. Both can be found if the average wind speed V and the available power in wind (flux) are calculated using the measured wind speed values. Graph shown in figure C.1 in appendix C gives a relation between the Weibull scale parameter C and average wind speed V as a function of shape parameter K, and Graph shown in figure C.2 in appendix C gives a relation between Weibull scale parameter C and the available power in wind (flux) as a function of shape parameter K.

Using these two graphs, beginning from K=2, and manipulating the number of iterations until certain tolerance is achieved, the values of both K and C can be found [12].

The second wind speed distribution is the Rayleigh distribution, which is a specific form of the Weibull function in which the shape

www.manaraa.com

parameter equals 2 and very closely mirrors the actual distribution of hourly wind speeds at many locations.

2.3 Evaluation of Wind Data in Different Cities in the West Bank (Ramallah and Nablus Cities).

Different wind measurements were carried out for each month through the year 2006. The wind data obtained includes hourly average wind speeds for each hour in the month. Calculations were performed on these data for each month to obtain the duration in hours for each 1 m/s speed range selected. The total wind speed range was divided into 1 m/s speed ranges taking the ranges: 0-1, 1-2, 2-3, 3-4, and so on [12].

Table (2.1) shows in detail average wind speed, values for percentage of occurrence for each wind speed range , power available in the wind for each range per unit area using equation (4.14) , power density by multiplying percentage of occurrence with power available in wind for each range, Weibull values using equation (2.1), energy available in wind by multiplying power density for each range with Weibull value, and finally energy available in wind by multiplying power density for each range with occurrence percentage for this range [12].

www.manaraa.com

Table (2.1): Yearly wind calculations/Ramallah-2006 [12]

Speed range (m/s)	Mid range (m/s)	Duration (hours)	Occurrence percentage (%)	Power (W/m²)	Power density (W/m²)	Weibull values	Energy (kWh/m using Weibull	Energy (kWh/ m²) using data
0-1	0.5	82	0.936	0.08	0.001	0.03601	0.02	0.01
1-2	1.5	589	6.724	2.04	0.137	0.08230	1.47	1.20
2-3	2.5	1058	12.078	9.45	1.142	0.11133	9.22	10.00
3-4	3.5	1209	13.801	25.94	3.580	0.12520	28.45	31.36
4-5	4.5	1242	14.178	55.13	7.816	0.12616	60.93	68.47
5-6	5.5	1240	14.155	100.66	14.248	0.11736	103.48	124.81
6-7	6.5	961	10.970	166.15	18.227	0.10235	148.96	159.67
7-8	7.5	728	8.311	255.23	21.211	0.08443	188.76	185.81
8-9	8.5	563	6.427	371.55	23.879	0.06626	215.66	209.18
9-10	9.5	390	4.452	518.71	23.093	0.04968	225.75	202.30
10-11	10.5	218	2.489	700.36	17.429	0.03569	218.98	152.68
11-12	11.5	159	1.815	920.13	16.701	0.02463	198.50	146.30
12-13	12.5	103	1.176	1181.64	13.894	0.01635	169.22	121.71
13-14	13.5	60	0.685	1488.53	10.195	0.01046	136.34	89.31
14-15	14.5	56	0.639	1844.42	11.791	0.00645	104.24	103.29
15-16	15.5	28	0.320	2252.94	7.201	0.00384	75.86	63.08
16-17	16.5	15	0.171	2717.74	4.654	0.00221	52.70	40.77
17-18	17.5	14	0.160	3242.42	5.182	0.00123	35.02	45.39
18-19	18.5	10	0.114	3830.63	4.373	0.00066	22.30	38.31
19-20	19.5	9	0.103	4486.00	4.609	0.00035	13.64	40.37
20-21	20.5	4	0.046	5212.15	2.380	0.00018	8.02	20.85
21-22	21.5	7	0.080	6012.72	4.805	0.00009	4.54	42.09
22-23	22.5	7	0.080	6891.33	5.507	0.00004	2.47	48.24
23-24	23.5	8	0.091	7851.61	7.170	0.00002	1.30	62.81
Sum		8760	100%		229.225	1.00328	2025.85	2008.01

Yearly average wind speed V= 5.521 m/s

Weibull shape factor K = 1.81 (calculated using special graphs in appendix C)

Weibull scale factor C = 6.35 m/s (calculated using special graphs in appendix C)

Density of air ρ = 1.21 kg/m³

Figure (2.2) shows a graphical representation of the distribution of hourly duration for different ranges of wind speed.

www.manaraa.com

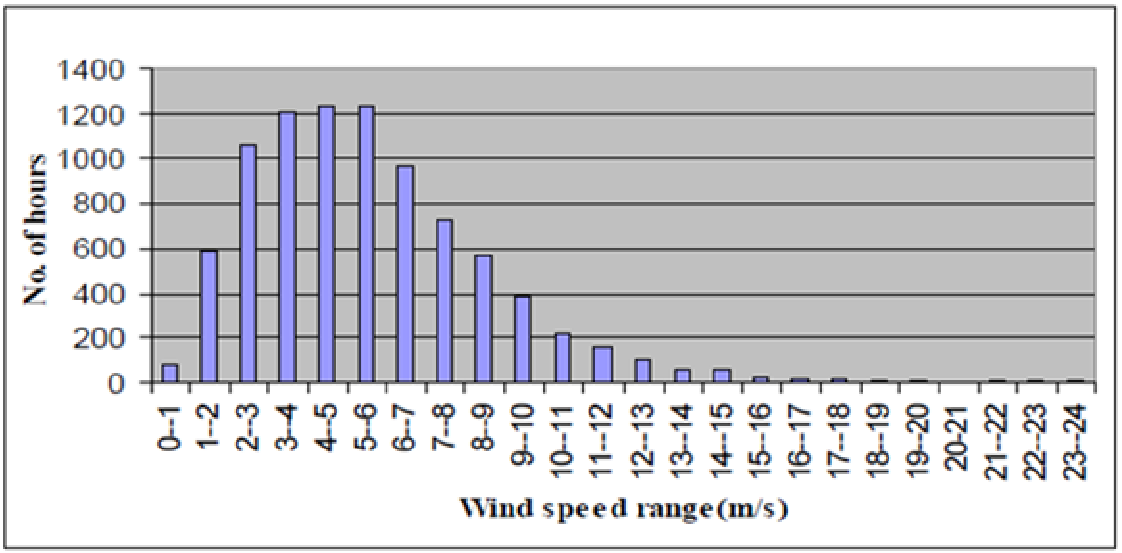

Figure (2.2): Number of hours per year for each wind speed range/Ramallah-2006

Figure (2.3) shows the distribution of energy and Weibull distribution for the wind measurements.

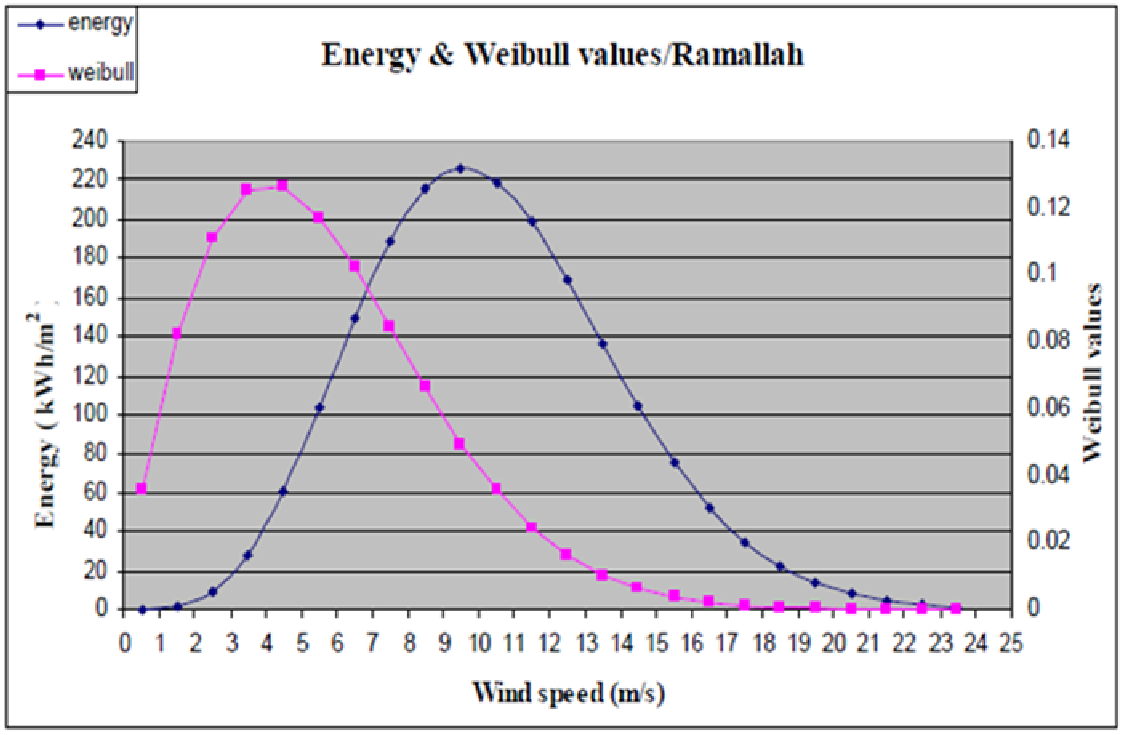

Figure (2.3): Yearly energy and Weibull distributions/Ramallah site-2006

Figure (2.4) shows the wind duration curve for Al-Mazra'a Al-Sharqiyyah site. It is a cumulative frequency diagram. Its horizontal

www.manaraa.com

axis represents the cumulative time duration in hours as wind speed group decreases starting at the highest wind speed group. It can be used to calculate graphically the energy produced by a certain wind turbine if its power curve is known [12].

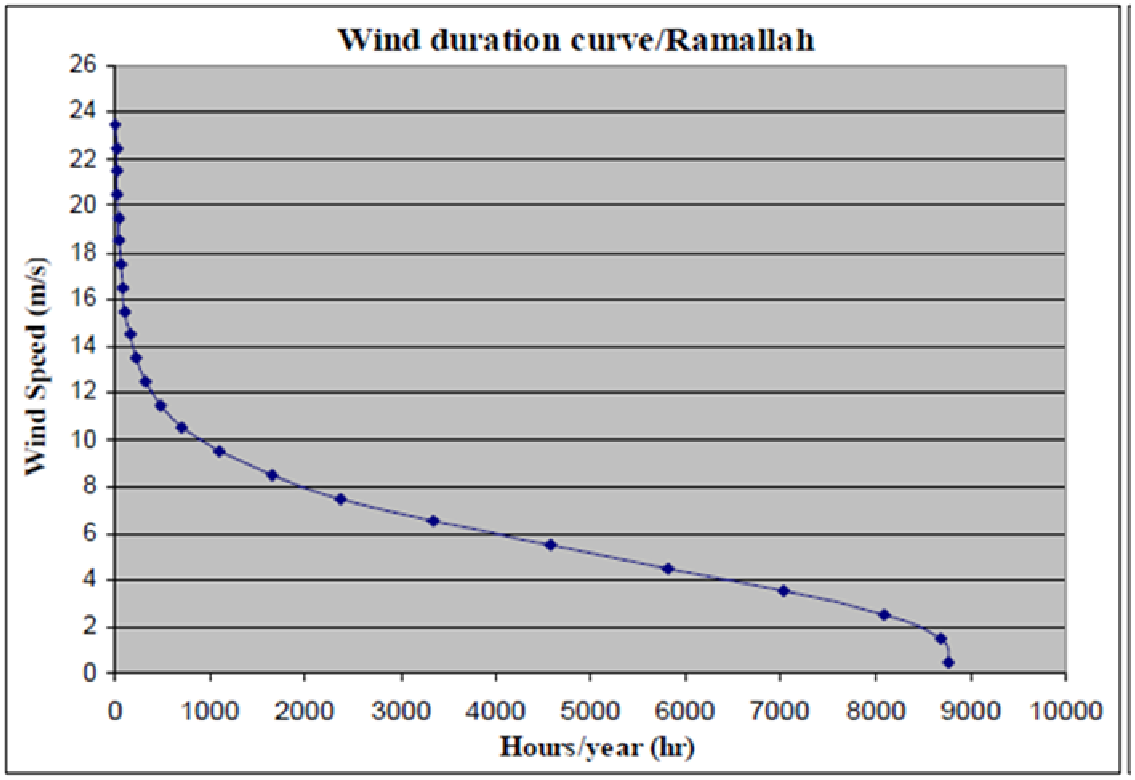

Figure (2.4): Wind duration curve for Ramallah site-2006

Table (2.2) shows percentage of occurrence for each wind speed range, power available in wind for each range per unit area, power density, Weibull values, energy available in wind using Weibull values, and finally energy available in wind using wind data available.

www.manaraa.com

Table (2.2): Yearly wind calculations/Nablus-2006 [12].

Speed range (m/s)	Mid range (m/s)	Duration (hours)	Occurrence percentage (%)	Power (W/m²)	Power density (W/m²)	Weibull values	Energy (kWh/ m²) (using Weibul)	Energy (kWh/ m²) (using data)
0-1	0.5	733.68	8.375	0.08	0.006	0.05334	0.03	0.06
1-2	1.5	376.64	4.300	2.04	0.088	0.12065	2.08	0.77
2-3	2.5	1105.78	12.623	9.45	1.193	0.15541	12.90	10.45
3-4	3.5	1786.15	20.390	25.94	5.289	0.16174	37.70	46.33
4-5	4.5	1802.06	20.572	55.13	11.341	0.14702	73.62	99.35
5-6	5.5	1285.92	14.679	100.66	14.776	0.12044	110.12	129.44
6-7	6.5	788.24	8.998	166.15	14.950	0.09039	135.01	130.97
7-8	7.5	440.14	5.024	255.23	12.824	0.06274	141.05	112.34
8-9	8.5	205.65	2.348	371.55	8.723	0.04054	128.66	76.41
9-10	9.5	101.65	1.160	518.71	6.019	0.02450	104.17	52.73
10-11	10.5	55.81	0.637	700.36	4.462	0.01389	75.74	39.09
11-12	11.5	25.93	0.296	920.13	2.724	0.00741	49.87	23.86
12-13	12.5	9.67	0.110	1181.64	1.304	0.00372	29.94	11.42
13-14	13.5	5.17	0.059	1488.53	0.878	0.00177	16.47	7.69
14-15	14.5	2.83	0.032	1844.42	0.597	0.00079	8.33	5.23
15-16	15.5	8.17	0.093	2252.94	2.100	0.00034	3.89	18.40
16-17	16.5	3.83	0.044	2717.74	1.189	0.00014	1.68	10.42
17-18	17.5	0.83	0.010	3242.42	0.308	0.00005	0.67	2.70
18-19	18.5	0.67	0.008	3830.63	0.292	0.00002	0.25	2.55
19-20	19.5	0.50	0.006	4486.00	0.256	0.00001	0.09	2.24
20-21	20.5	1.00	0.011	5212.15	0.595	0.00000	0.03	5.21
21-22	21.5	7.83	0.089	6012.72	5.377	0.00000	0.01	47.10
22-23	22.5	0.67	0.008	6891.33	0.524	0.00000	0.00	4.59
23-24	23.5	11.17	0.127	7851.61	10.009	0.00000	0.00	87.68
Sum		**8760**	**100.00**		**105.824**	**1.00490**	**932.33**	**927.02**

Yearly average wind speed V= 4.346 m/s
Weibull shape factor K = 1.9(calculated using special graphs in appendix C)
Weibull scale factor C = 6 m/s(calculated using special graphs in appendix C)
Density of airρ= 1.21 kg/m³

Figures (2.5), (2.6) show yearly energy, Weibull values and yearly wind duration curve for Nablus site respectively.

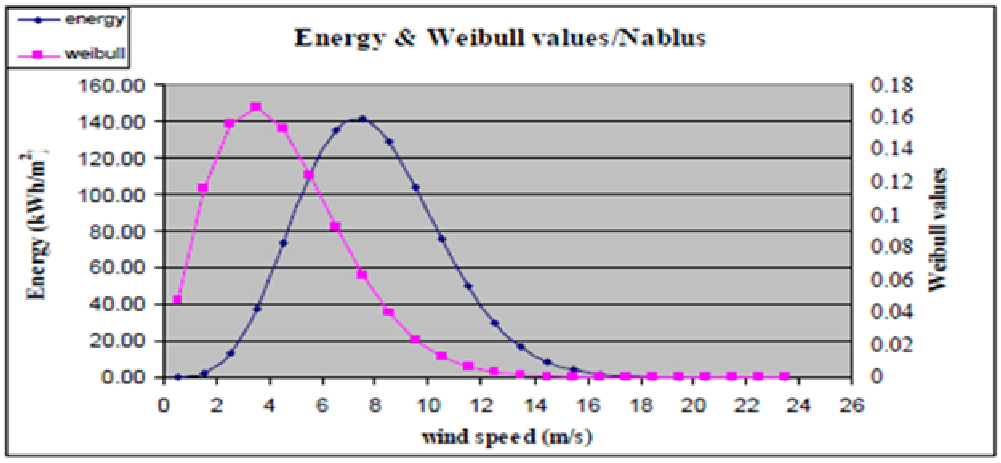

Figure (2.5): Yearly energy and Weibull distributions for Nablus site.

www.manaraa.com

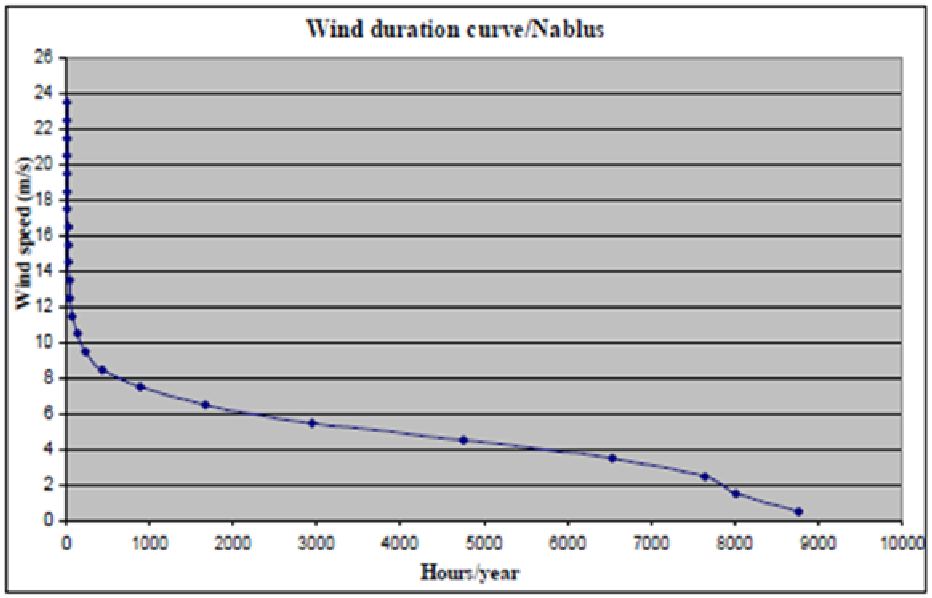

Figure (2.6): Wind duration curve for Nablus site.

In this chapter, I studied the potential of wind energy in Palestine. In the next chapter I will study and analyze the components of grid tie PV/Wind hybrid system.

www.manaraa.com

CHAPTER THREE

COMPONENTS OF GRID TIE PV/WIND HYBRID SYSTEM

www.manaraa.com

Chapter Three
Components of Grid Tie PV/ Wind Hybrid System

3.1 Grid Tie System configurations

The aim of this chapter is to present an overview of the main building blocks in a grid tied PV/wind system. These systems can be classified in terms of their connection to the power system grid into the following:

A. Centralized AC-bus architecture

In this architecture, the generators and the battery are all installed in one place and are connected to a main AC bus bar before being connected to the grid .This system is centralized in the sense that the power delivered by all the energy conversion systems and the battery is fed to the grid through a single point. In this case, the power produced by the PV system and the battery is inverted into AC before being connected to the main AC bus [14].

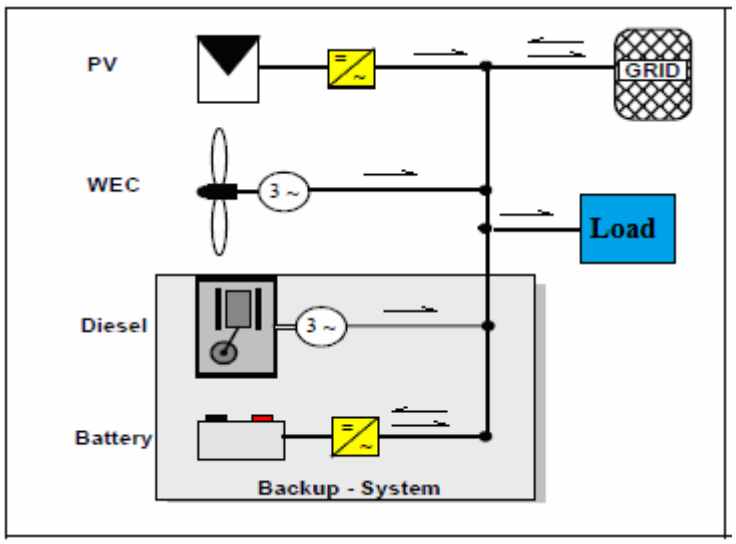

Figure (3.1): Centralized AC-bus architecture

www.manaraa.com

B. Centralized DC-bus architecture

The second architecture utilizes a main centralized DC bus bar as in figure (3.2). The wind turbine and the diesel generator, firstly deliver their power to rectifiers to be converted into DC before it is being delivered to the main DC bus bar. A main inverter takes the responsibility of feeding the AC grid from this main DC bus [14].

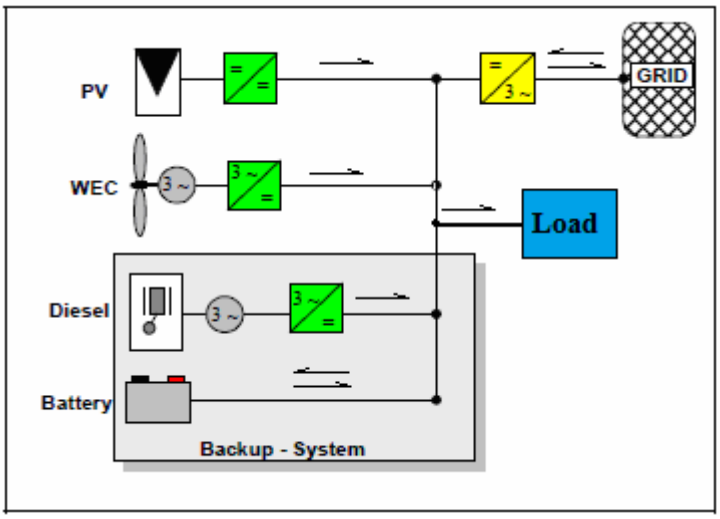

Figure (3.2): Centralized DC-bus architecture

C. Distributed AC-bus architecture

The power sources in this architecture do not need to be installed close to each other as in figure (3.3), and they do not need to be connected to one main bus bar. Otherwise, the sources are distributed in different geographical locations as appropriate and each source is connected to the grid separately. The power produced by each source is conditioned separately to be identical with the form required by the grid. The main disadvantage of this architecture is the difficulty of controlling the system [14].

www.manaraa.com

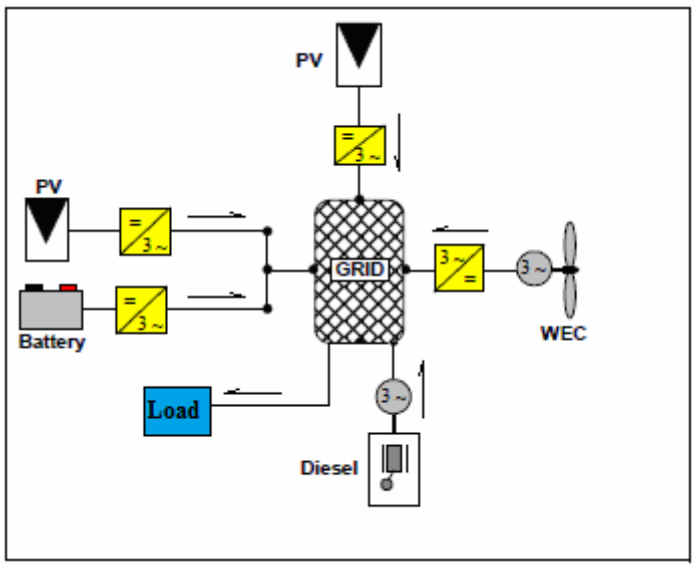

Figure (3.3): Distributed AC-bus architecture

D. Modified Distributed Ac Bus Architecture

The following architecture is the one upon which the submitted thesis is based. It is an improved version of the distributed AC-bus architecture shown in figure (3.3).The improvement exists mainly in the addition of a DC/DC converter for each energy conversion system and the remove of storage battery. By this addition of the DC/DC converters, the state values of the energy conversion sources become completely decoupled from each other and from the state values of the grid the power production of the different sources becomes now freely controllable without affecting the state values of the grid.

Decoupling the state values means that the variations of the renewable resources like the velocity of the wind and the intensity of the solar radiation will not influence the state values of the electrical grid.

www.manaraa.com

The main disadvantage of this architecture is the difficulty of controlling the system, but this problem is not effective since the improvement of wireless communications.

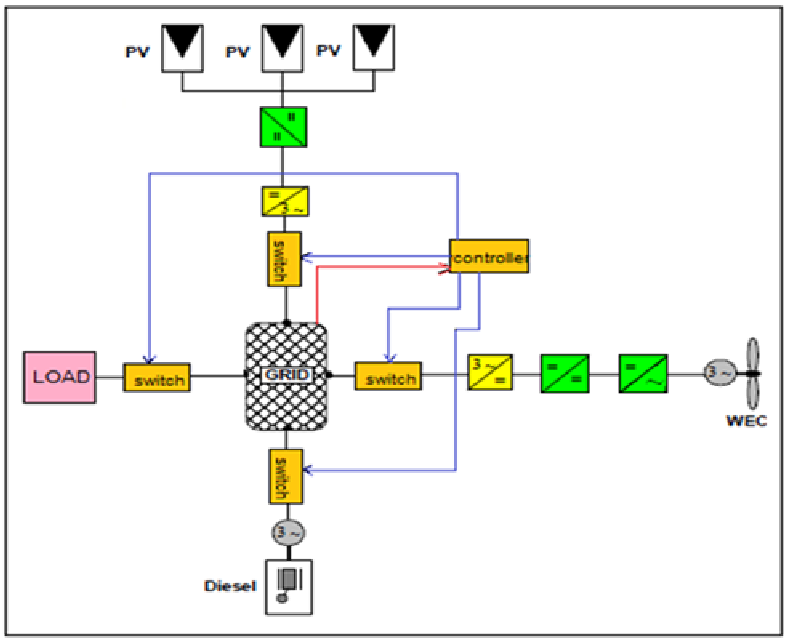

Figure (3.4): The modified distributed Ac bus architecture.

3.2 Photovoltaic PV Technology

The physics of the PV cell is very similar to that of the classical diode with a pn junction. When the junction absorbs light, the energy of absorbed photons is transferred to the electron–proton system of the material, creating charge carriers that are separated at the junction. The charge carriers in the junction region create a potential gradient, get accelerated under the electric field, and circulate as current through an external circuit [15].

www.manaraa.com

The PV cell is the elementary unit, the interconnection of the number of PV cell forms the module and similarly PV array is formed from number of module as shown in Figure (3.5).

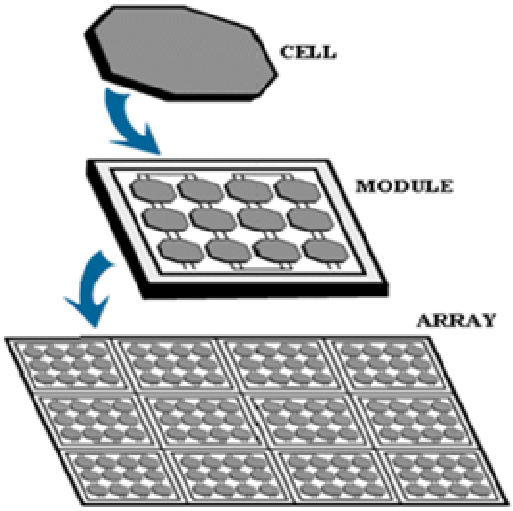

Figure (3.5): Transition of cell, module and arrays.

The main industrialized PV technologies are shown in figure (3.6).

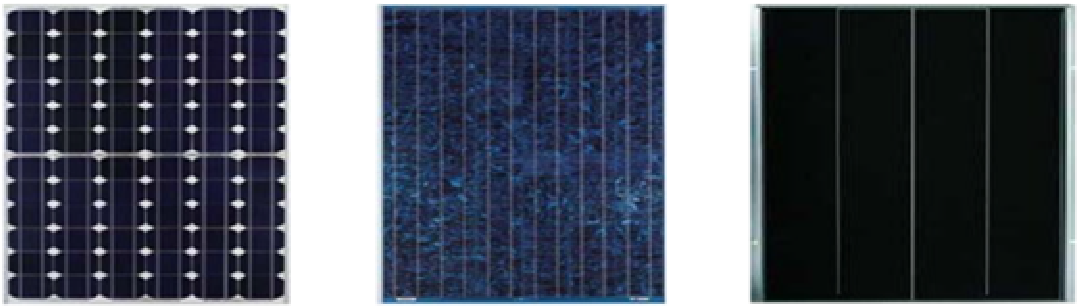

Figure (3.6): The main industrialized PV technologies
a) Mono-crystalline PV b) Poly-crystalline PV c) Amorphous PV

3.2.1 Mono Crystalline Silicon PV cells

Comprising 20% of the earth's crust composition, Silicon is considered the second most abundant element on earth. it exists in nature in the form of silicon dioxide minerals like quartz and silicate based minerals.

www.manaraa.com

It has first to reach a high degree of purity before it can be used for manufacturing single crystal PV cells.

High grade quartz or silicates are first treated chemically to form an intermediate silicon compound (Liquid trichlorosilane $SiHCl_3$), which is then reduced in a reaction with hydrogen to produce chunks of highly pure Silicon, about 99.9999% in purity. After that, these chunks of silicon are melted and formed into a single large crystal of Silicon through a process called the Czochralski process. The large Silicon crystal is then cut into thin wafers using special cutting equipment. These wafers are then polished and doped with impurities to form the required p-n junction of the PV cell.

Antireflective coating materials are added on top of the cell to reduce light reflections and allow the cell to better absorb sunlight. A grid of contacts made of silver or aluminum is added to the cell to extract the electric current generated when it is exposed to light. PV modules' efficiency is in the range of 12%-15% .The process of producing PV cells using this technology is quite expensive, so this led to development of new technologies that do not suffer from this drawback [16].

3.2.2 Multi-crystalline Silicon PV cells

In order to avoid the high cost of producing single crystal solar cells, cheaper multi-crystalline cells were developed. As the name implies, multi-crystalline Silicon solar cells do not have a single crystal structure. They are rather derived from several smaller crystals that together form the

www.manaraa.com

cell. The grain boundaries between each crystal reduce the net electric current that can be generated because of electron recombination with defective atomic bonds. However, the cost of manufacturing cells using this technology is less than what would be in the case of a single crystalline cell. The efficiency of modules produced using this technology ranges from 11%-14% [16].

3.2.3 Thin Film PV technologies

Thin film PV cells are manufactured through the deposition of several thin layers of atoms or molecules of certain materials on a holding surface. They have the advantage over their crystalline Silicon counter parts in their thickness and weight. They can be 1 to 10 micrometers thin as compared to 300 micrometers for Silicon cells. Another advantage is that they can be manufactured using an automated large area process that further reduces their cost. Thin film PV cells do not employ the metal grid required for carrying current outside the cell. However, they make use of a thin layer of conducting oxides to carry the output current to the external circuit.

The electric field in the p-n junction of the cell is created between the surface contacts of two different materials, creating what is called a hetero junction PV cell. Thin film PV can be integrated on windows and facades of buildings because they generate electricity while allowing some light to pass through. Two common thin film materials are Copper indium diselenide (CIS for short) and Cadmium Telluride (CdTe). CIS thin films

www.manaraa.com

are characterized by their very high absorption. PV cells that are built from this material are of the hetero junction type. The top layer can be cadmium sulfide, while the bottom layer can be gallium to improve the efficiency of the device. Efficiency for these technologies is about 10-13% [16].

3.3 Maximum Power Point Tracking

When a PV module is directly coupled to a load, the PV module's operating point will be at the intersection of its I–V curve and the load line which is the I-V relationship of load. For example in figure (3.7), a resistive load has a straight line with a slope of $1/R_L$ as shown in figure (4.8). In other words, the impedance of load dictates the operating condition of the PV module. In general, this operating point is seldom at the PV module's MPP. Thus it is not producing the maximum power.

A study shows that a direct-coupled system utilizes a more 31% of the PV capacity. A PV array is usually oversized to compensate for a low power yield during winter months.

This mismatching between a PV module and a load requires further over-sizing of the PV array and thus increases the overall system cost. To mitigate this problem, a maximum power point tracker (MPPT) can be used to maintain the PV module's operating point at the MPP. MPPTs can extract more than 97% of the PV power when properly optimized [17].

www.manaraa.com

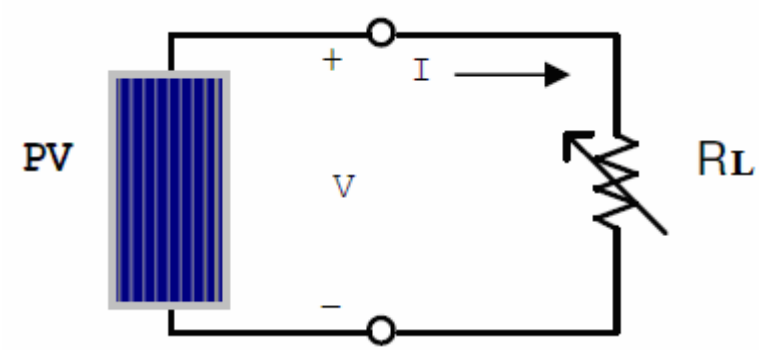

Figure (3.7): PV module is directly connected to a (variable) resistive load.

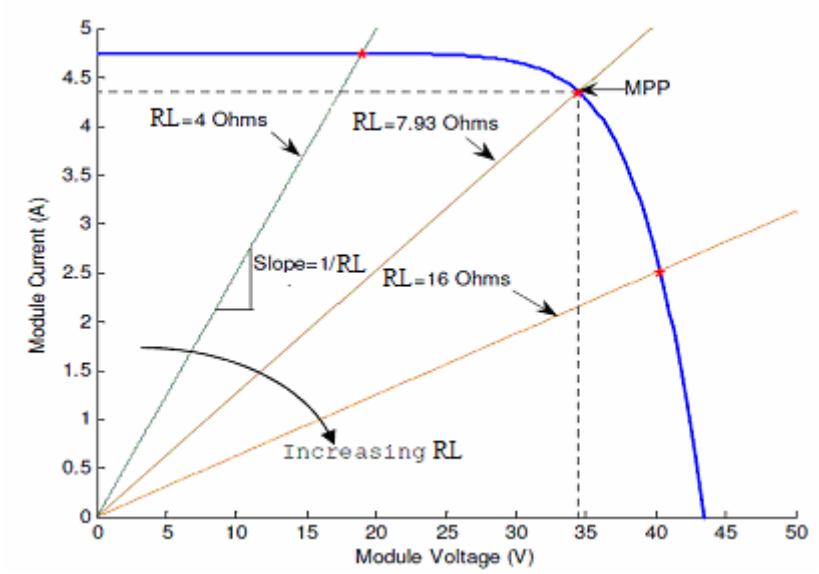

Figure (3.8): I-V curves of BP SX 150S PV module and various resistive loads Simulated with the MATLAB model (1kW/m2, 25°C)

3.3.1 Maximum Power Point Tracking (MPPT) Techniques

MPPT techniques are used to control DC converters in order to extract maximum output power from a PV array under a given weather condition. The DC converter is continuously controlled to operate the array at its maximum power point despite possible changes in the load impedance. Several techniques have been proposed to perform this task [18].

- Constant Voltage (CV) Method

www.manaraa.com

- Open Voltage (OV) Method

- Incremental Conductance (IC) Methods

- Perturb and Observe (P&Oa and P&Ob) Methods

- Three Point Weight Comparison

- Fuzzy Logic Method

- Sliding Mode Method

- Artificial neural network Method

Constant Voltage (CV) Method

The principle of the Constant Voltage (CV) Method is simple: the PV is supplied using a constant voltage, Temperature and Solar Irradiance impacts are neglected, The reference voltage is obtained from the MPP of the P(i) characteristic directly. Figure (3.9) shows the CV algorithm and the code of the Matlab embedded function [18].

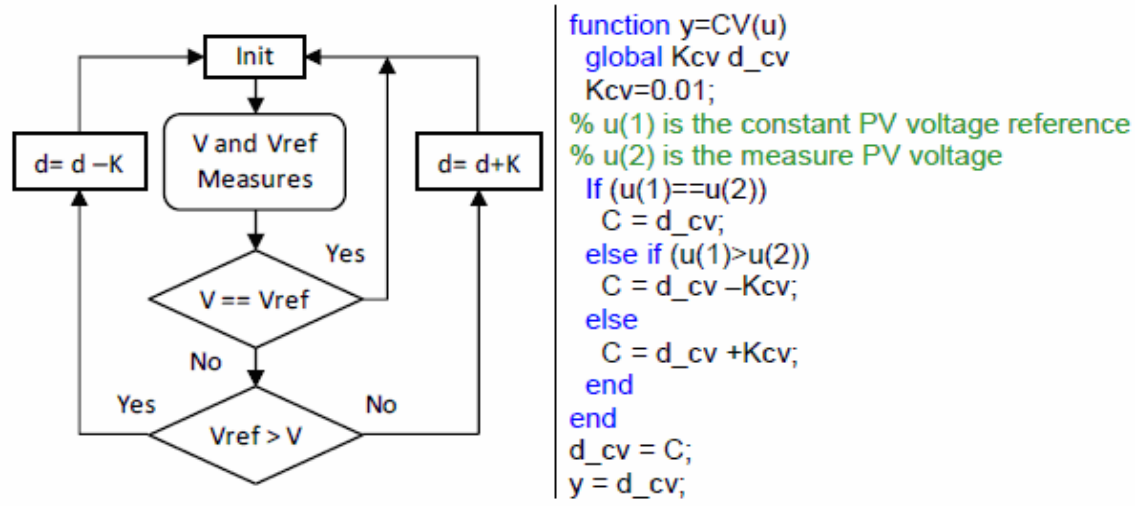

Figure (3.9): CV algorithm and the code of Matlab embedded function [18].

www.manaraa.com

This Constant Voltage Method cannot be very effective, regarding Solar Irradiance impact and certainly not regarding the temperature's influence.

The Open Voltage (OV) Method is based on the CV method, but it makes the assumption that the MPP voltage is always around 75% of the open-circuit voltage V_{OC}. So mainly, this technique takes into account the temperature. But it requests a special procedure to regularly disconnect the PV and to measure the open-circuit voltage [18].

B) Incremental Conductance (IC) Methods

The principle of the Incremental Conductance (IC) Method is based on the property of the MPP: the derivative of the power is null as in equation (3.1). So, the IC method uses an iterative algorithm based on the evolution of the derivative of conductance G, as in equation (3.2). Where the conductance is the I / V ratio.

$$\frac{dP}{dV} = 0, \quad with \quad P = V \cdot I \tag{3.1}$$

$$\frac{dP}{dV} = V \cdot \frac{dI}{dV} + I\frac{dV}{dV} = 0, \quad Thus: \quad \frac{dI}{dV} + \frac{I}{V} = 0 \quad \rightarrow dG + G = 0 \tag{3.2}$$

This method (ICa) has been improved, because when the voltage is constant, dG is not defined. So, a solution is to mix the CV method with the IC method. It is known as the Two- Method MPPT Control (or ICb). Figure (3.10) shows the Two-Method MPPT Control algorithm and the code of the Matlab embedded function [18]:

www.manaraa.com

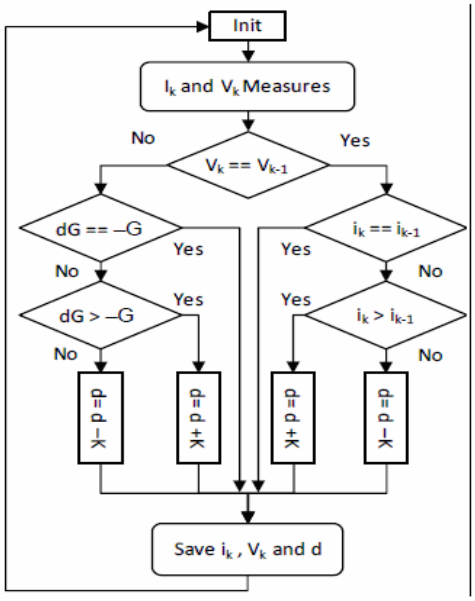


```
function y=IC(u)
  global i v Kic d_ic
  Kic=0.01;
% u(1) is the measure PV current
% u(2) is the measure PV voltage
G=u(1) / u(2); %G is the conductance
dv = u(2) – v;
di  = u(1) – i;
if (dv==0)  %equivalent to the CV method
  if (di==0)          C = d_ic;
    else if (di > 0)  C = d_ic + Kic;
    else              C = d_ic – Kic;
    end
  end
else
  dG = di / dv; % here start the IC method
  if (dG==–G)         C = d_ic;
    else if (dG > –G) C = d_ic – Kic;
    else              C = d_ic + Kic;
    end
  end
end
i= u(1); %save old current value
v=u(2); %save old voltage value
d_ic=C; %save old conductance value
y=d_ic;
```

Figure (3.10): Two-Method MPPT algorithm and the code of Matlab function [18].

C) Perturb and Observe (P&O) Methods

The principle is based on perturbing the voltage and the current of the PV regularly and then, in comparing the new power measure with the previous to decide the next variation. Two Perturb and Observe (P&O) Methods are well known [18]:

1- P&Oa with a fixed perturbing value.

2- P&Ob with a variable perturbing value.

The P&Ob method is similar to the P&Oa except for the constant coefficient K_{pnoa} which is replaced by a variable coefficient K_{pnob}:

$$Kpnob = 0.02 \cdot |\Delta P| \qquad (3.3)$$

Figure (3.11) shows the P&Oa algorithm and the code of the Matlab embedded function.

www.manaraa.com

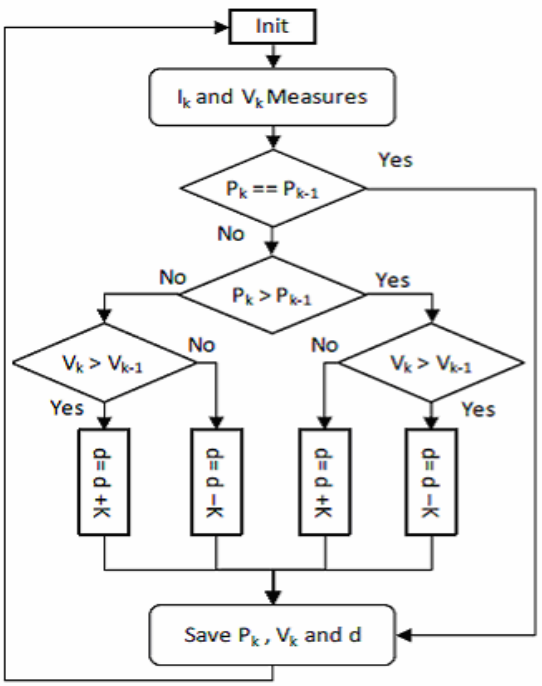


```
function y=PnOa(u)
  global p v Kpnoa d_pnoa
  Kpnoa=0.01;
% u(1) is the measure PV power
% u(2) is the measure PV voltage
  if ((u(1)==p)    C = d_pnoa;
  else
    if ((u(1)>p)
      if ((u(2)>v)  C= d_pnoa – Kpnoa;
      else          C= d_pnoa + Kpnoa;
      end
    else
      if ((u(2)>v)  C= d_pnoa + Kpnoa;
      else          C= d_pnoa – Kpnoa;
      end
    end
  end
p= u(1); %save old power value
v= u(2); %save old voltage value
d_pnoa =C;
y= d_pnoa;
```

Figure (3.11): P&Oa algorithm and the code of Matlab embedded function [18].

3.4 Switched Mode DC-DC Converters

DC/DC converters are used in a wide variety of applications including power supplies, where the output voltage should be regulated at a constant value from a fluctuating power source or achieve multiple voltage levels from the same input voltage. Several topologies exist to either increase or decrease the input voltage or perform both functions together using a single circuit [16].

3.4.1 Buck Converter

The schematic diagram of a buck DC converter is shown in figure (3.12). It is composed with DC chopper and an output LC filter to reduce the ripples in the resulting output. The output voltage of the converter is less than the input as determined by the duration the semiconductor switch

www.manaraa.com

Q is closed. Under continuous conduction mode (CCM), the current IL passing through the inductor does not reach zero. The time integral of the inductor voltage over one period in steady state equals zero. From that, the relation between the input and output voltages can be obtained [16].

$$(V_{in} - V_{out})\, t_{on} - V_{out} t_{off} = 0$$

$$\frac{V_{out}}{V_{in}} = \frac{t_{on}}{t_{on} + t_{off}} = d \qquad where \quad d = duty\ cycle \qquad (3.4)$$

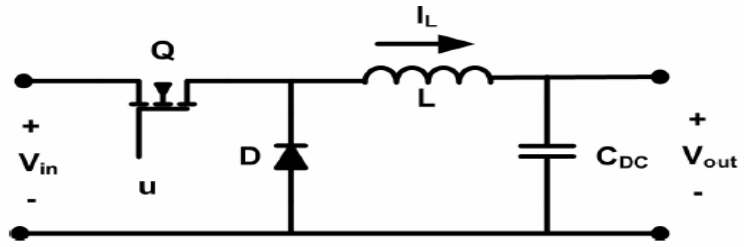

Figure (3.12): Buck converter

3.4.2 Boost Converter

The boost DC converter is used to step up the input voltage by storing energy in an inductor for a certain time period, and then uses this energy to boost the input voltage to a higher value.

The circuit diagram for a boost converter is shown in figure (3.13). When switch Q is closed, the input source charges up the inductor while diode D is reverse biased to provide isolation between the input and the output of the converter. When the switch is opened, energy stored in the inductor and the power supply is transferred to the load. The relationship between the input and output voltages is given by [16]:

www.manaraa.com

$$V_{in}t_{on} + (V_{in} - V_{out})t_{off} = 0$$

$$\frac{V_{out}}{V_{in}} = \frac{t_{on} + t_{off}}{t_{off}} = \frac{1}{1-d} \qquad (3.5)$$

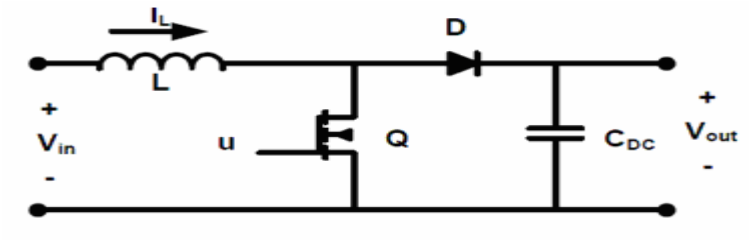

Figure (3.13): Boost converter

3.4.3 Buck-Boost Converter

This converter topology can be used to perform both functions of stepping the input voltage up or down, but the polarity of the output voltage is opposite to that of the input as in figure (3.14).

The input and output voltages of this configuration are related through [16].

$$V_{in}t_{on} + V_{out}t_{off} = 0$$

$$\frac{V_{out}}{V_{in}} = \frac{-t_{on}}{t_{off}} = \frac{-d}{1-d} \qquad (3.6)$$

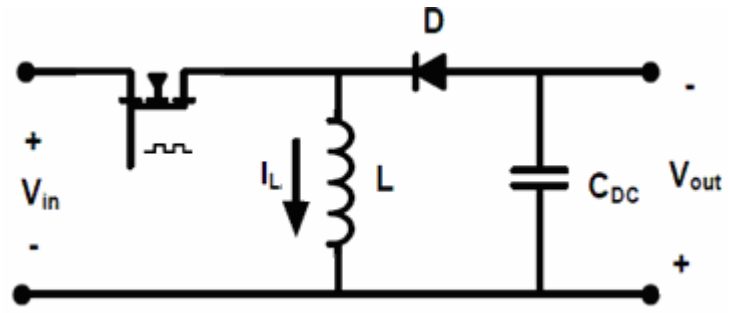

Figure (3.14): Buck Boost converter

www.manaraa.com

3.5 Wind Turbine Technology

Wind turbines operate in an unconstrained air fluid. The force is transferred from air fluid to the blades of the wind turbine. It can be considered to be equivalent to two component forces acting in two perpendicular directions, known as the drag force and the lift force. The magnitude of these drag and lift forces depends on the shape of the blade, its orientation to the direction of air, and the velocity of air [12].

The drag force is the component that is in line with the direction of air. The lift force is the component that is at right angles to the direction of the air. These forces are shown in figure (3.15).

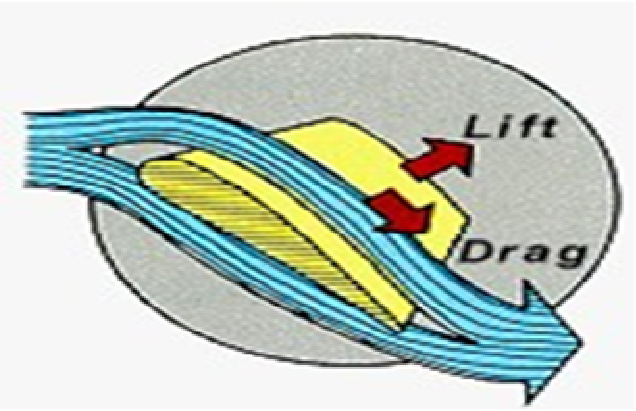

Figure (3.15): Lift and drag force components [12].

A low pressure region is created on the downstream side of the blade as a result of an increase in the air velocity on that side. In this situation, there is a direct relationship between air speed and pressure: the faster the airflow, the lower the pressure. The lift force acts as a pulling force on the blade, in a direction at right angles to the airflow.

www.manaraa.com

Wind turbines can be categorized according to the axis of rotation: vertical and horizontal axis. The vertical wind turbines are suitable for low power applications. The power efficiency is limited to 25%. The advantage of the vertical wind turbines is that the generator and transformer can be placed on the ground near the rotor blades. This results in low installation and maintenance cost [9].

A more popular type of wind turbines shown in figure (3.16) is the horizontal wind turbines. It can be built with two or three blades [9].

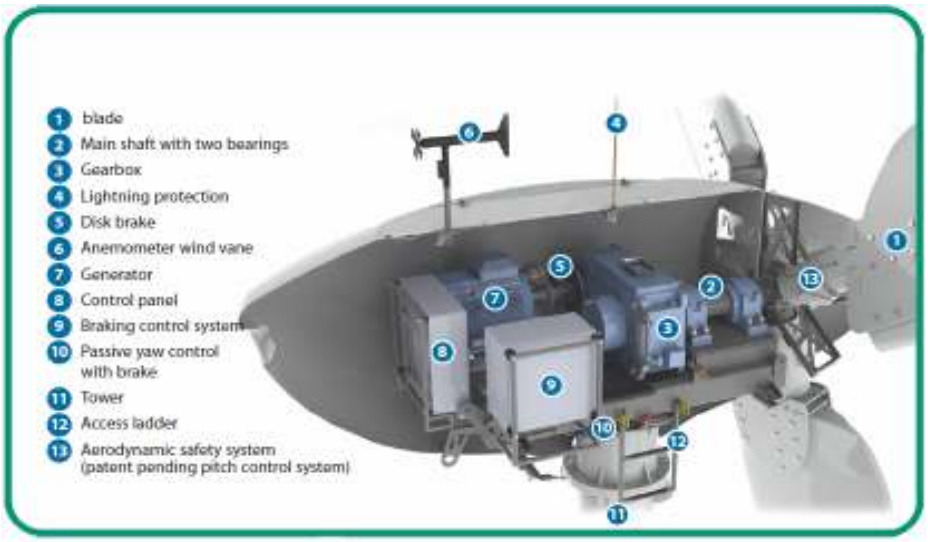

Figure (3.16): Horizontal wind turbine.

Each wind turbine has its own characteristic known as wind speed power curve. The shape of this curve is influenced by the blades area, the choice of airfoil, the number of blades, the blade shape, the optimum tip speed ratio, the speed of rotation, the cut-in wind speed, the shutdown speed, the rated speed, and gearing and generator efficiencies.

The power output of a wind turbine varies with wind speed and wind

www.manaraa.com

turbine power curve. An example of such curve is shown in figure (3.17) [12].

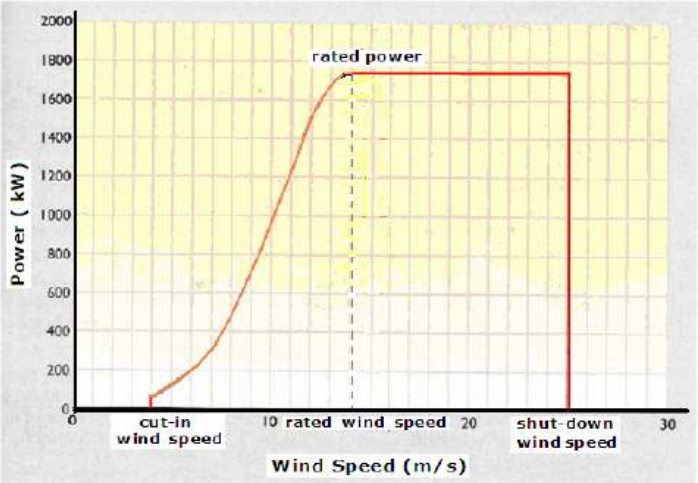

Figure (3.17): Typical wind turbine power curve [12].

3.5.1 Types of Wind Turbine Grid Tie Connections

In the context of the grid interconnection, it is inevitable to learn about the wind generators. Each type of the generators requires different power electronic grid interconnection.

Induction generator is widely used in the wind industry. There are two types of the induction generators. The squirrel-cage induction generator can be directly connected to the utility grid or connected with a full-rated power electronic interface at a variable speed [9].

The system with a fixed speed is inexpensive due to its simplicity and low maintenance requirements. Nonetheless, the direct connection of the wind turbines and the utility grid causes mechanical stress problems and high inrush current during start up. This problem can be solved by a soft-starter mechanism.

www.manaraa.com

A soft starter is comprised of thyristors, a power electronic semiconductor device, limiting the maximum inrush current. After start up, the thyristors are bypassed to avoid thermal breakdown, as shown in figure (3.18) [9].

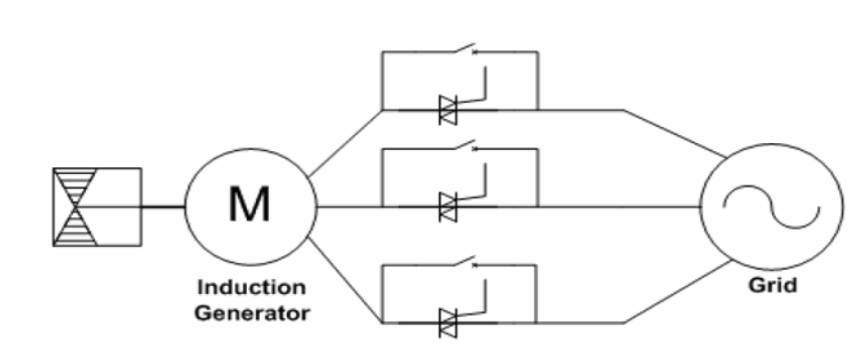

Figure (3.18): Soft starter

Additionally, the induction generator requires reactive power from the utility grid that causes unacceptable conditions such as the voltage drop or low power factor. The compensated reactive power can be supplied from a switched capacitor bank or a power converter. For the fixed speed or direct connection induction generators, the switched capacitor banks can supply the reactive power as shown in figure 3.19.a).

For the variable speed squirrel-cage induction generator, the power converter, therefore, must be able to provide reactive power to the generators.

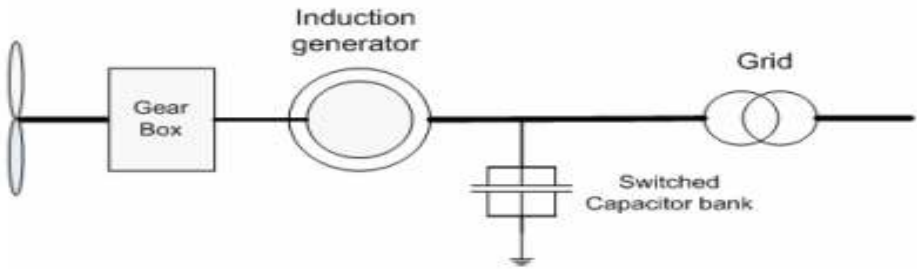

Figure (3.19 a): Squirrel-cage induction generator with direct connection to the grid

www.manaraa.com

For the direct connection, the induction generator has to operate at the synchronous frequency of the grid. Thus, there must be a gearbox to increase the low speed shaft of the rotor blades to the speed of the grid.

The simplest topology for the variable speed is the back-to-back converter as shown in figure 3.19 b) [9].

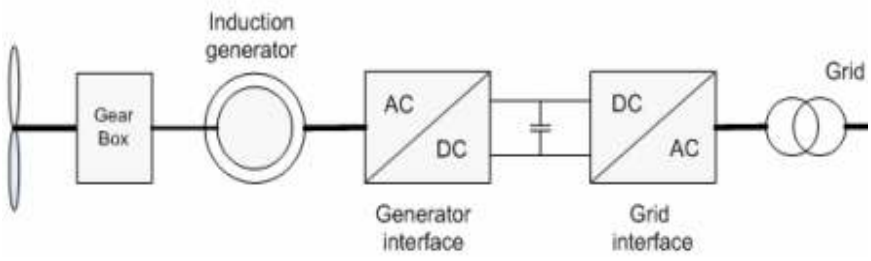

Figure (3.19 b): Squirrel-cage induction generator with power converters

The doubly-fed induction generator is partly connected to the grid. That allows only a part of the power feed through the power converter. Therefore, the nominal power of the converter is less than the nominal power of the generator. The stator of the generator is directly connected to the grid whereas the rotor is connected to the power converter decoupling the angular frequency of generator rotor from the grid, as shown in figure (3.20).

To supply the power to the grid, the doubly-fed induction generator must operate at super-synchronous frequency of the grid. Therefore, it is necessary to increase the speed of the rotor blade shaft with the gearbox [9].

www.manaraa.com

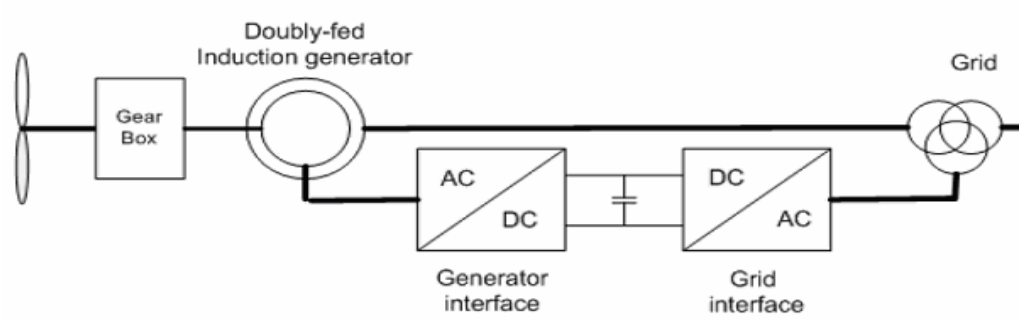

Figure (3.20): Doubly-fed induction generator

Another type of the generators utilized in a wind farm is a synchronous generator. The rotor winding of the synchronous generator can be excited by an external field exciter, which requires the field current supplied from the grid with an AC-DC converter as shown in figure (3.21). The stator winding is connected to the full-rated power converters supporting the variable speed concept. A multi-pole synchronous generator can eliminate the gear box as mentioned previously. This results in a simpler system and reduction in maintenance cost. The relationship of the multiple poles and frequency can be expressed as

$$f_{(elec)} = \frac{P}{2} f_{(rotor)} \qquad (3.7)$$

Where

P*:* is number of poles

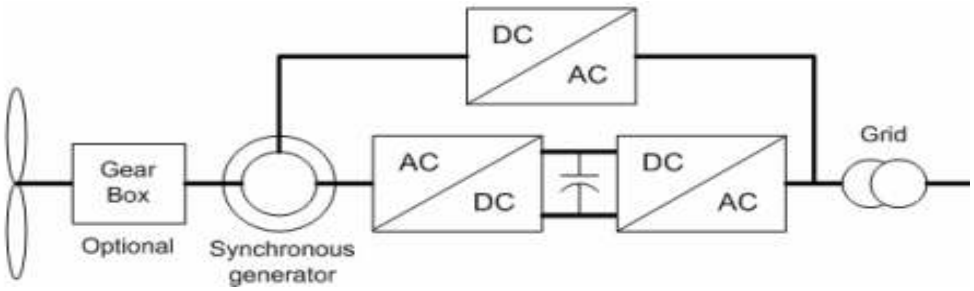

Figure (3.21): Synchronous generator with a field exciter

www.manaraa.com

The synchronous generator can be also excited by an internal permanent magnet, as shown in figure (3.22). The gearless multi-pole permanent magnet synchronous generator is attractive because it is light and requires low maintenance cost. It also reduces the cost of transportation and installation. Furthermore, it is considerably efficient compared to the other types of generators [9].

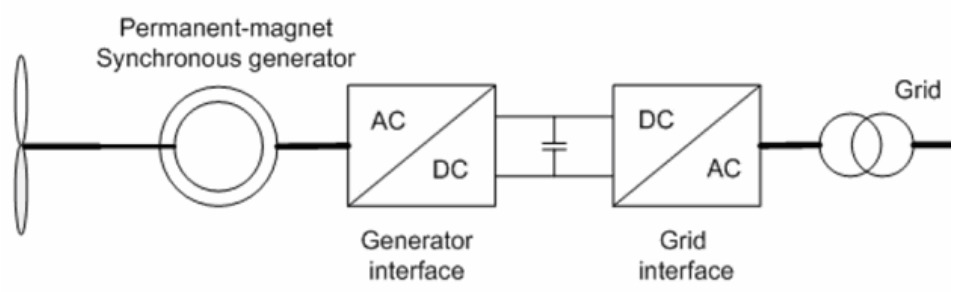

Figure (3.22): Permanent magnet synchronous generator.

3.5.2 Control Types of Wind Turbine

A wind turbine has control system that regulates the speed of rotor blades. The anemometer measures the wind speed and transmits the data to the controller. The pitch angle of the rotor blades is controlled by the controller to attain the maximum wind power and to limit the mechanical power in case of the strong wind. The rotor blades are pitched to decrease the angle of attack from the wind when the rated power is reached. The yaw drive can turn the wind turbine compartment or so called nacelle according to the direction of the wind measured by the wind vane [9].

In addition to the pitch control, the maximum power from the wind can be limited by passive stall control for small and medium-size wind

www.manaraa.com

turbines. The stall control avoids the rotation of the blades. Contrary to the pitch-angle control, passive stall control has fixed pitch-angle rotor blades.

The passive stall control relates to the design of the rotor blades that leads to turbulence or so called stall on the back of the blades to reduce the power extracted from the wind.

As the capacity of wind turbines is increasing, active stall control is used for large wind turbines, more than 1MW. The active stall control is similar to the pitch-angle control. The rotor blades are rotated to obtain the maximum power extract. When the extracted power reaches the rated power, opposite to the pitch-angle control, the active stall control turns the rotor blades to increase the angle of attack from the wind to provoke the turbulence [9].

3.6 Diesel generator

A diesel generator is the combination of a diesel engine with an electrical generator (often called an alternator) to generate electrical energy and used in places without connection to the power grid, as emergency power-supply if the grid fails [19].

www.manaraa.com

Figure (3.23): Diesel generator

3.6.1 Diesel generator set

The packaged combination of a diesel engine, a generator and various ancillary devices (such as base, canopy, sound attenuation, control systems, circuit breakers, jacket water heaters and starting system) is referred to as a "generating set" or a "genset" for short [19].

3.6.2 Operating Characteristics of Diesel generator

A) Rotation speed

The Corresponding speeds of 50 Hz generators are 3000 rpm and 1500 rpm synchronous generators obtained from the equation (3.8).

$$120 \times f = n \times P \qquad (3.8)$$

Where

n: speed (rpm)

www.manaraa.com

f: frequency

P: number of poles

The 3000 rpm units are 2-pole machines and are of simpler construction, resulting in lower acquisition cost. The 1500-rpm machines are 4-pole machines and are somewhat more expensive, but more common in the larger sizes or heavy duty units [19].

In general, higher rpm will apply more wear and tear on the bearings. This means more frequent maintenance requirements. Two-pole generators are most convenient for use in relatively light duty applications that require less than 400 hours per year of operation. Four-pole generators are recommended when there is more than 400 hours of operation.

B) Fuel types

Diesel engines differ from gasoline engines in that they do not have spark plugs to ignite the fuel mixture, and work at much higher pressures. Diesel engines need less maintenance than gasoline engines, and they are more efficient [19].

C) Efficiency and fuel consumption

Electrical and mechanical losses are present in all generators. However, the greatest losses in a generator system are attributable to the prime mover engine. The efficiency of a diesel generator is proportional to the size of the operated load by the diesel generator .Manufactures

www.manaraa.com

endeavor to produce maximum efficiency at somewhere between 80-90% of rated full load. Figure (3.24) shows approximate plots of efficiency vs. percentage of rated electrical load [19].

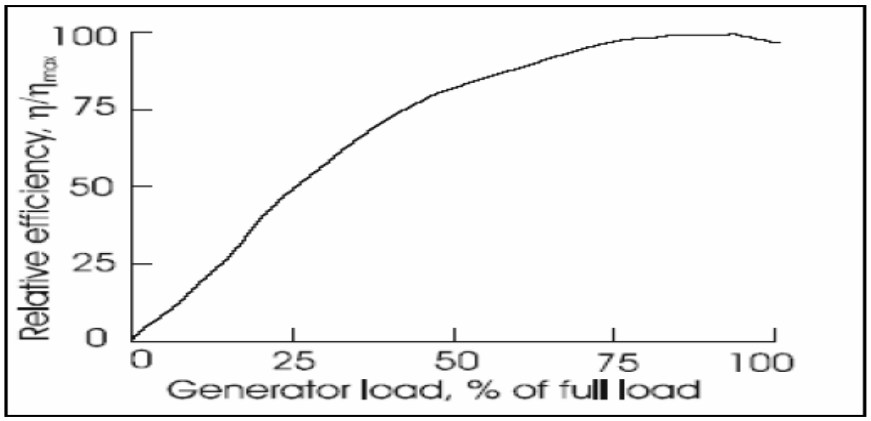

Figure (3.24): Diesel generator overall efficiency vs. rated load [19].

D) Life cycle of diesel and regular maintenance requirements

A diesel generator can operate for between 5000–50000 hours (average 20000 hours), depending on the quality of the engine, whether it has been installed correctly, and whether O&M has been properly carried out. Regular maintenance and low load operation are the main factors that affect the diesel generators life [19].

E) Low load operation.

Another factor that affects the diesel generators life is the low load operation which defined as when the engine operates for a prolonged period of time below 40 – 50 % of rated output power [19]. During periods of low loads, the diesel generator will be poorly loaded with the consequences of poor fuel efficiency and low combustion temperatures. The low temperatures cause incomplete combustion and carbon deposits

www.manaraa.com

(glazing) on the cylinder walls, causing premature engine wear. Therefore, to avoid glazing, we operate the diesel generator near its full rated power.

F) Pollutant emissions

The number of kg of CO_2 produced per liter of fuel consumed by the diesel generator depends upon the characteristics of the diesel generator and of the characteristics of the fuel and it usually fall in the 2.4–2.8 kg/L range [19].

3.8 Grid Tie Inverter

A grid-tie inverter (GTI) is a special type of inverter that converts direct current (DC) electricity into alternating current (AC) electricity and feeds it into an existing electrical grid. GTIs are often used to convert direct current produced by many renewable energy sources, such as solar panels or wind turbines, into the alternating current used to power homes and businesses. The technical name for a grid-tie inverter is "grid-interactive inverter". They may also be called synchronous inverters. Grid-interactive inverters typically cannot be used in standalone applications where utility power is not available [31].

Figure (3.25): Grid tie inverter [31].

www.manaraa.com

Inverters take DC power and invert it to AC power so it can be fed into the electric utility company grid. The grid tie inverter must synchronize its frequency with that of the grid (e.g. 50 or 60 Hz) using a local oscillator and limit the voltage to no higher than the grid voltage.

A high-quality modern GTI has a fixed unity power factor, which means its output voltage and current are perfectly lined up, and its phase angle is within 1 degree of the AC power grid. The inverter has an on-board computer which will sense the current AC grid waveform, and output a voltage to correspond with the grid [31].

Grid-tie inverters are also designed to quickly disconnect from the grid if the utility grid goes down to prevent the energy produced from harming any line workers who are sent to fix the power grid [31].

Properly configured, a grid tie inverter enables a home owner to use an alternative power generation system like solar or wind power without extensive rewiring and without batteries. If the alternative power being produced is insufficient, the deficit will be sourced from the electricity grid [31].

www.manaraa.com

CHAPTER FOUR

MATHMATICAL MODELING AND SIMULINK OF GRID TIE PV/WIND HYBRID SYSTEM

www.manaraa.com

Chapter Four

Mathematical Modeling and Simulink of Grid Tie PV/Wind Hybrid System

4.1 Configuration of Grid Tie PV / Wind Hybrid System

The configuration of grid tie PV/wind hybrid system under study is shown in figure (4.1). It consists of grid tie PV system, grid tie wind turbine system, standby diesel generator and the load.

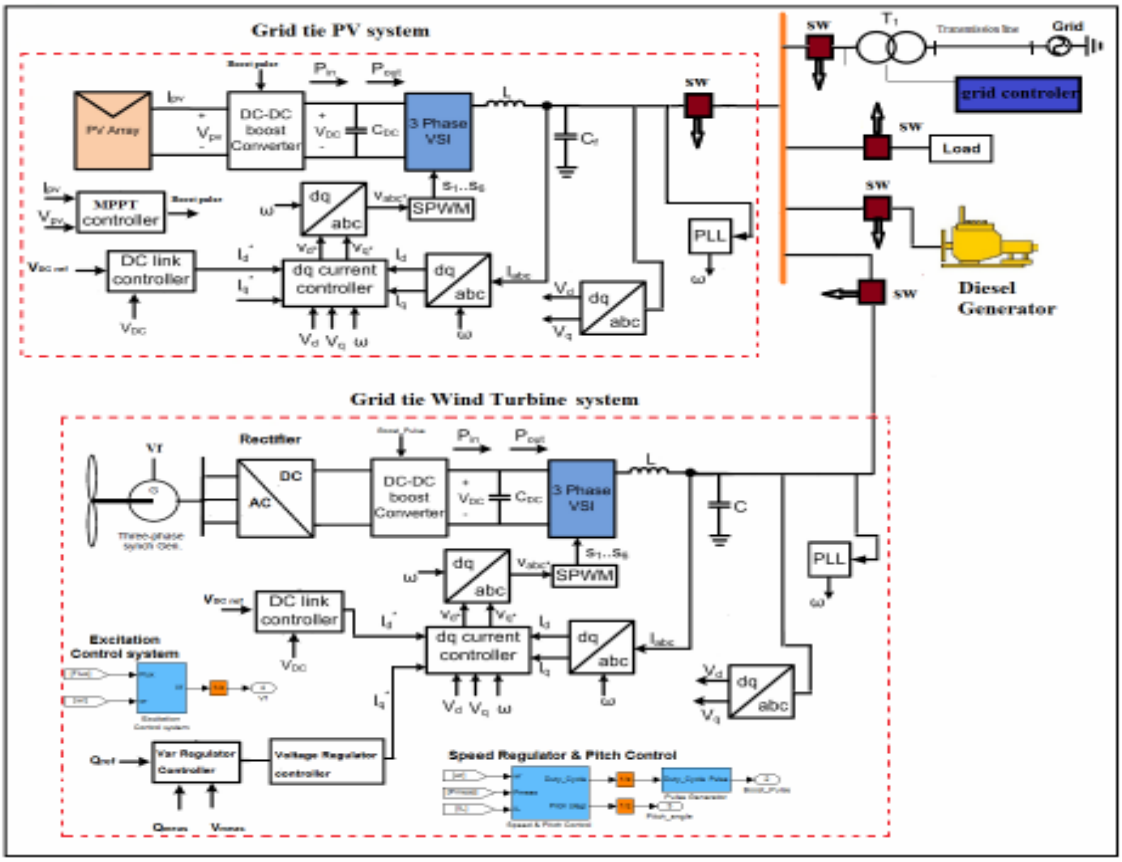

Figure (4.1): Grid tie PV/wind hybrid system structure

For grid tie PV system the output of the PV array is connected to DC-DC boost converter that is used to perform MPPT functions and increase the array terminal voltage to a higher value so it can be interfaced to the distribution system grid.

www.manaraa.com

A DC link capacitor is used after the DC converter and acts as a temporary power storage device to provide the voltage source inverter with a steady flow of power. The capacitor's voltage is regulated using a DC link controller that balances input and output powers of the capacitor.

The voltage source inverter is controlled in the rotating *dq* frame to inject a controllable three phase AC current into the grid. To achieve unity power factor operation, current is injected in phase with the grid voltage. A phase locked loop (PLL) is used to lock on the grid frequency and provide a stable reference synchronization signal for the inverter control system, which works to minimize the error between the actual injected current and the reference current obtained from the DC link controller[18].

RL load are connected to the grid to simulate some of the loads that are connected to a distribution system network.

An LC low pass filter is connected at the output of the inverter to attenuate high frequency harmonics and prevent them from propagating into the power system grid.

For grid tie wind turbine the AC voltage out from three phase salient pole synchronous generator is rectified to DC voltage then connected to DC-DC boost converter that is used to regulate the speed and control the output power.

The main difference between control system for wind turbine and PV Array is the reactive power controller, which is used to regulate the reactive power of wind turbine under grid voltage variations.

www.manaraa.com

A standby diesel generator is connected to the load and works when the grid fails in order to cover the load demand. A grid controller is connected to the system in order to sense the grid voltage and sends control signal to the switches in case of grid failure.

4.2 Modeling of Grid Tie PV System

Figure (4.2) shows the Simulink model of grid tie PV system which consists of photovoltaic Array, DC-DC Boost converter, maximum power point tracking controller, three phase voltage source inverter, system controller and LC filter.

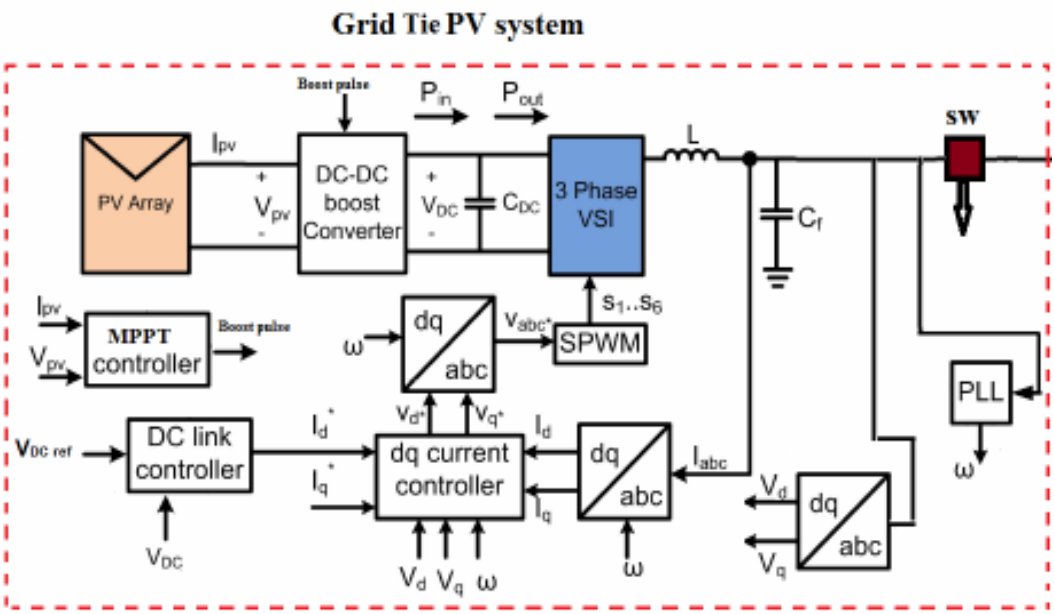

Figure (4.2): Simulink model of PV system [18].

4.2.1 Modeling of Photovoltaic Array

A) Mathematical Modeling of Photovoltaic Array

The equivalent circuit model of a PV cell is needed in order to simulate its real behavior as in figure (4.3). Using the physics of p-n

www.manaraa.com

junctions, a cell can be modeled as a DC current source in parallel with two diodes that represent currents escaping due to diffusion and charge recombination mechanisms. Two resistances, Rs and Rp, are included to model the contact resistances and the internal PV cell resistance respectively. The values of these two resistances can be obtained from measurements or by using curve fitting methods based on the I-V characteristic of the cell [16].

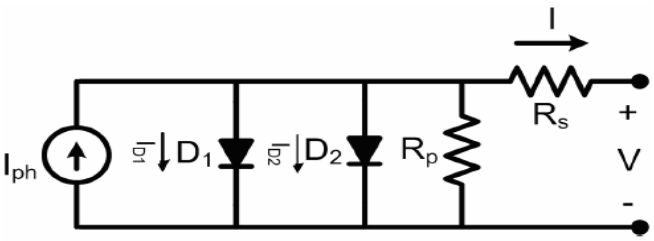

Figure (4.3): Double exponential PV cell model.

The relationship between the PV cell output current and terminal voltage is governed by:

$$I = I_{ph} - I_{D1} - I_{D2} - \frac{V + IR_s}{R_p} \qquad (4.1)$$

$$I_{D1} = I_{01}\left[\exp\left(\frac{q(V + IR_s)}{akT}\right) - 1\right] \qquad (4.2)$$

$$I_{D2} = I_{02}\left[\exp\left(\frac{q(V + IR_s)}{akT}\right) - 1\right] \qquad (4.3)$$

Where

I_{ph} : is the PV cell internal generated photocurrent.

I_{D1} and **I_{D2} :** are the currents passing through diodes D_1 and D_2.

www.manaraa.com

a : is the diode ideality factor.

k : is the Boltzmann constant ($1.3806503 \times 10^{-23}$ J/K).

T: is the cell temperature in degrees Kelvin.

***q* :** is the electron charge (1.6021×10^{-19} C).

$\mathbf{I_{01}}$ and $\mathbf{I_{02}}$ **:** are the reverse saturation currents of each diode respectively.

Assuming that the current passing in diode D_2 due to charge recombination is small enough to be neglected, a simplified PV cell model can be reached as shown in figure (4.4).

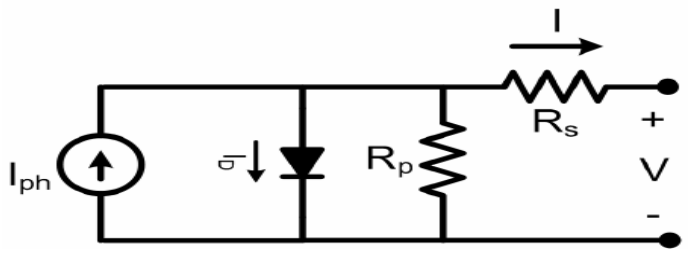

Figure (4.4): Simplified PV cell model.

This model provides a good compromise between accuracy and model complexity and has been used in several previous works. In this case, current I_{D2} can be omitted from equation (4.1) and the relation simplifies to [16]:

$$I = I_{ph} - I_0\left[\exp\left(\frac{q(V+IR_s)}{akT}\right)-1\right]-\frac{V+IR_s}{R_p} \qquad \textbf{(4.4)}$$

It is clear that the relationship between the PV cell terminal voltage and output current is nonlinear because of the presence of the exponential term in equation (4.1) and (4.4).

www.manaraa.com

The presence of the p-n semiconductor junction is the reason behind this nonlinearity. The result is a unique I-V characteristic for the cell where the current output is constant over a wide range of voltages until it reaches a certain point where it starts dropping exponentially.

Another important relationship in PV cells is the power-voltage characteristic. The product of current and voltage is evaluated at each point in the curve to find out how much power can be obtained as voltage changes. Power starts increasing as voltage increases. A certain point in the curve is reached where maximum power output can be obtained; this point is therefore referred to as the Maximum Power Point (MPP). After this point, power starts dropping as the terminal voltage increases until it eventually reaches zero at open circuit voltage.

The PV cell characteristics also depend on external factors including temperature and solar irradiation level. To incorporate these effects into the model, two additional relations are used.

Output current varies with solar irradiation and temperature through [16]:

$$I = (I_n + K_I \Delta T)\frac{G}{G_n} \qquad (4.5)$$

Where

I_n : is the nominal PV cell output current (at 25 °C and 1000 W/m^2).

K_I : is the current/temperature variation coefficient (A/°C).

www.manaraa.com

ΔT : is the variation from the nominal temperature (25°C).

G_n : is the nominal solar irradiation (1000 W/m^2).

The value of K_I is relatively small and this makes the cell output current linearly dependent on solar radiation level more than temperature. Temperature, however, has a strong effect on the reverse saturation current, I_0 in equation (4.6) [16].

$$I_0 = \frac{I_{sc,n} + K_I \Delta T}{\exp(q(V_{oc,n} + K_V \Delta T) / akT) - 1} \qquad (4.6)$$

Where

$I_{sc,n}$: is the nominal short circuit current of the PV cell.

$V_{oc,n}$: is the nominal open circuit voltage.

K_I and **K_V :** are the current and voltage temperature variation coefficients, in A/ °C and V/ °C, respectively.

A PV module is the result of connecting several PV cells in series to order to increase the output voltage. The characteristic has the same shape except for changes in the magnitude of the open circuit voltage [16].

The PV array is composed of several interconnected photovoltaic modules. The modeling process is the same as the PV module from the PV cells. The same parameters from the datasheet are used. To obtain the required power, voltage and current, the PV modules are associated in series and parallel the number of modules connected in series and

www.manaraa.com

connected in parallel must be calculated. Figure (4.5) shows a photovoltaic array, which consists of multiple modules, linked in parallel and series. N_{ss} is the total quantity of modules within the series and N_{pp} is the amount of modules in parallel. The number of modules modifies the value of resistance in parallel and resistance in series. The value of equivalent resistance series and resistance parallel of the PV array are [20]:

$$R_{s,array} = \frac{R_{s,module} \cdot N_{ss}}{N_{pp}} \quad (4.7)$$

$$R_{p,array} = \frac{R_{p,module} \cdot N_{ss}}{N_{pp}} \quad (4.8)$$

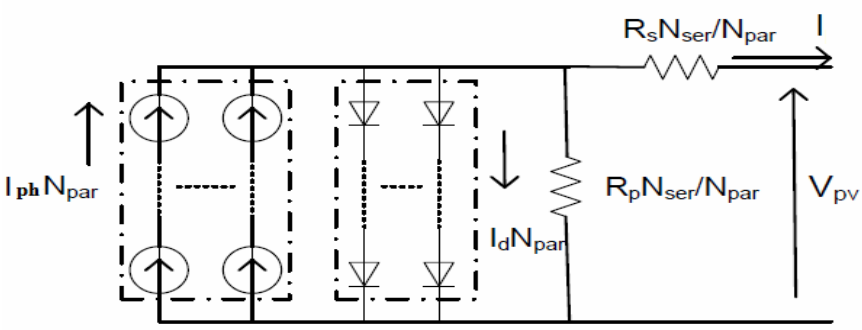

Figure (4.5): PV array composed of Nss x Npp modules [16]

After extending the relation current voltage of the PV modules to a PV array, the new relation of current voltage of the PV array is calculated in by [20].

$$I = I_{ph} N_{pp} - I_0 N_{pp} \left[exp\left(\frac{V + R_s \left(\frac{N_{ss}}{N_{pp}}\right) I}{V_t a N_{ss}} \right) - 1 \right] - \frac{V + R_s \left(\frac{N_{ss}}{N_{pp}}\right) I}{R_p \left(\frac{N_{ss}}{N_{pp}}\right)} \quad (4.9)$$

Where I_0, I_{ph}, V_t are the same parameters used for a PV modules.

This equation is valid for any given array formed with identical modules.

www.manaraa.com

The photovoltaic array will be simulated with this equation. The simulation circuit must include the number modules series and parallel. Figure (4.6) shows the circuit model of the PV array.

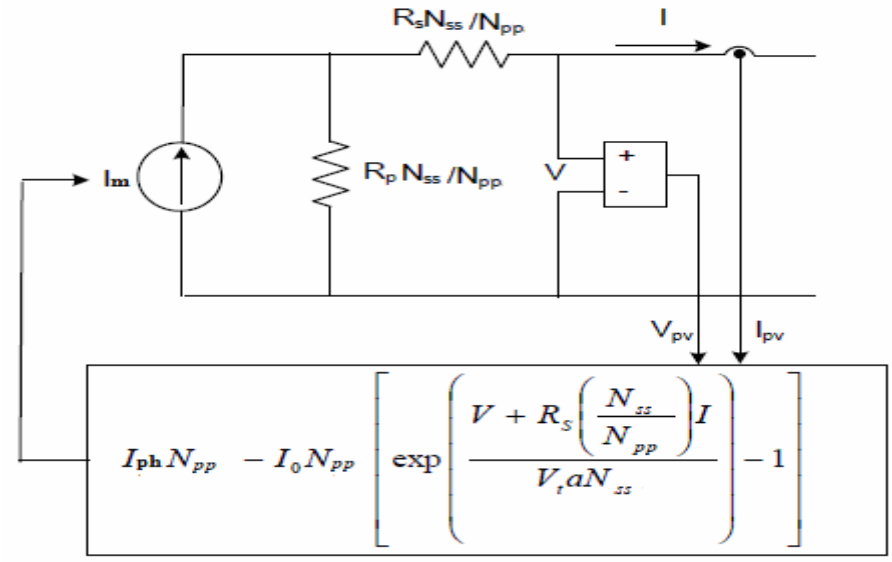

Figure (4.6): Model structure of the photovoltaic array [20].

B) Simulink Modeling of the Photovoltaic Array

The simulation of the photovoltaic array is realized with Simulink block. Certain variables are modified for the application with maximum power point tracking. The input parameters required for the model are:

Ns: number of cells in series

N_{pp}: number modules in parallel

N_{ss}: number of modules in series

A: 1.3977, diode constant

k: $1.38e^{-23}$, boltzmann constant

www.manaraa.com

$I_{sc,n}$: nominal short-circuit voltage

K_p: voltage temperature constant

Ki: current temperature coefficient

V_{mp}: voltage maximum power at STC

I_{mp}: current at maximum power at STC

The PV characteristics from data sheet are used to generate the file necessary for Rs, Rp and other parameters for the maximum power point. The initial setup is used to obtain the I-V curve characteristics of the PV array and show the maximum power point of the PV. The model of the PV is used with the boost converter to determine the performance of the maximum power point tracker [21].

The model of the photovoltaic array has been implemented in Simulink as shown in figure (4.7). The temperature and the irradiance are specified. The simulation allows having the curve I-V and P-V characteristics.

The Simulink model uses a current source and the value of the resistance in series and parallel of the PV [21].

www.manaraa.com

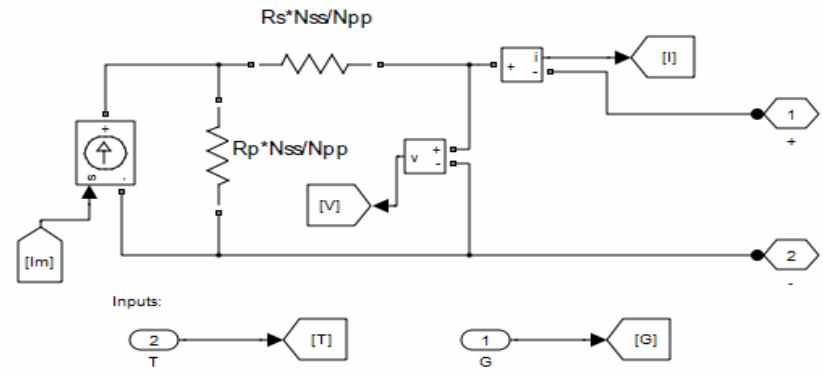

Figure (4.7): Simulation of the PV module

The number of modules in series and parallel are set with N_{ss} and N_{pp}. The I_m result is used for the Simulink block as a current source to obtain the voltage and current delivered from the PV.

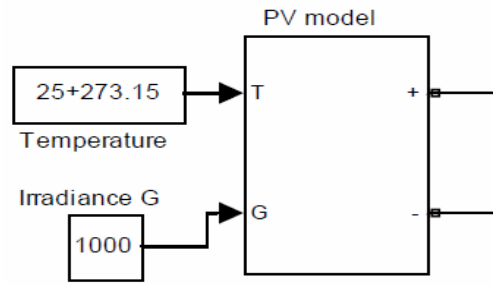

Figure (4.8): Simulink block of the photovoltaic array

Figure (4.9) shows the Simulink model for the reverse current saturation (Io) at the reference temperature which is given by the equation (4.10) [21]:

$$I_0 = \frac{I_{sc,n} + K_I \Delta_T}{\exp\left(\frac{V_{oc,n} + K_V \Delta_T}{a V_t}\right) - 1} \qquad \textbf{(4.10)}$$

www.manaraa.com

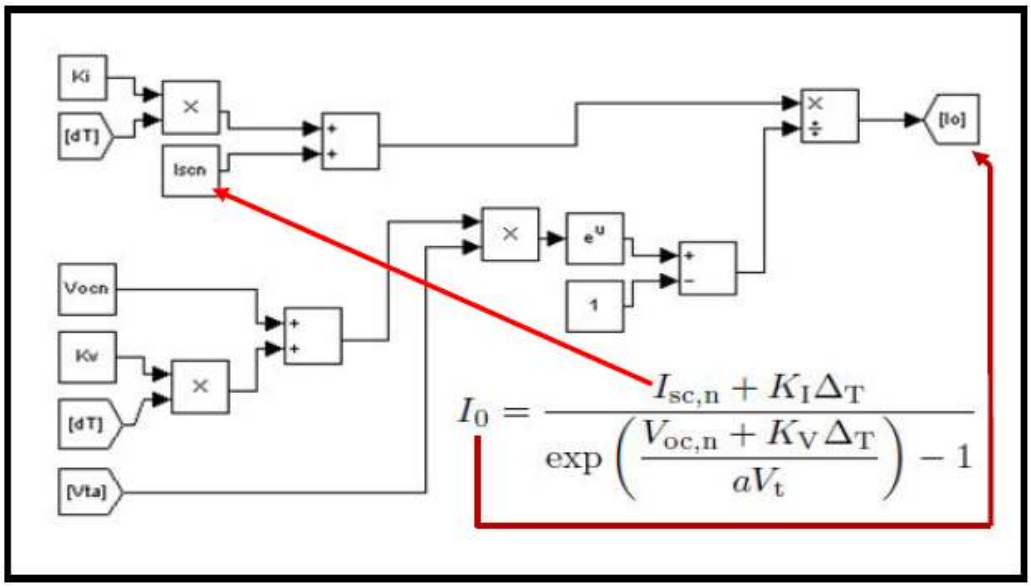

Figure (4.9): Simulink modeling implementation for Io [21].

Figure (4.10) shows the Simulink model for the light generated current of the photovoltaic cell which depends linearly on the influence of temperature and solar radiation as given by the equation (4.11) [21]:

$$\mathbf{Iph = (I_{ph,n} + K_I \Delta T) \frac{G}{Gn}} \qquad \mathbf{(4.11)}$$

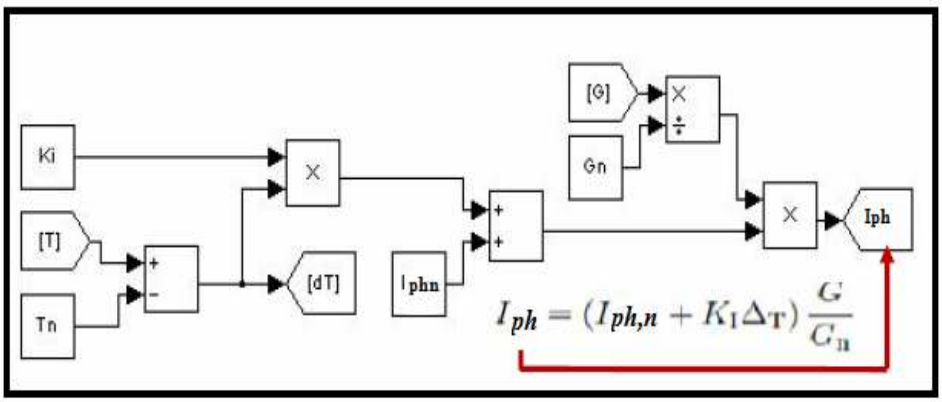

Figure (4.10): Simulink modeling implementation for Iph [21].

Figure (4.11) shows the Simulink model for the model current I_m which given by the equation (4.12) [21]:

www.manaraa.com

$$I_m = I_{ph} - I_0 \left[\exp\left(\frac{V + Rs\, I}{Vt\, a} \right) - 1 \right] \quad (4.12)$$

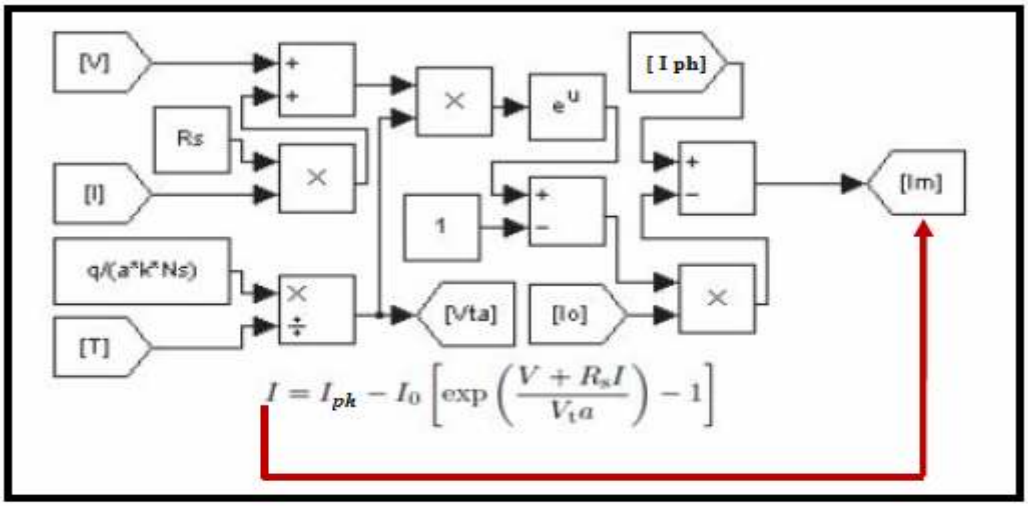

Figure (4.11): Simulink modeling implementation for Im [21]

Figure (4.12) depicts the PV array modeling, Figure (4.13) and table (4.1) depicts PV array mask menu and parameter.

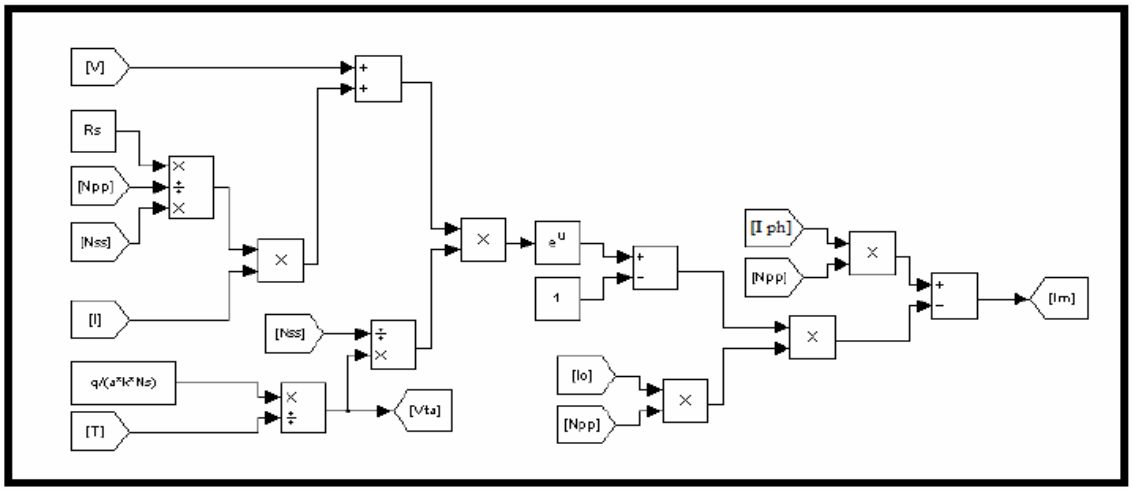

Figure (4.12): PV array modeling [21].

C) Validation of PV Simulink Model

In order to validate the PV model, I substituted the PV model parameters from a real PV module (KD 135SX), then I simulated the PV

www.manaraa.com

model under different temperatures and radiations. As a result, I achieved the same curves from the simulation model and from data sheet PV model as shown in figure (4.15) to (4.22).

Table (4.1): KD135SX PV characteristics parameters (Appendix B) [22].

Maximum Power (Pmax)	135W (+5%/–5%)
Maximum Power Voltage (Vmpp)	17.7V
Maximum Power Current (Impp)	7.63A
Open Circuit Voltage (Voc)	22.1V
Short Circuit Current (Isc)	8.37A
Max System Voltage	600V
Temperature Coefficient of Voc	-8.0×10^{-2} V/°C
Temperature Coefficient of Isc	5.02×10^{-3} A/°C

*STC : Irradiance 1000W/m², AM1.5 spectrum, cell temperature 25°

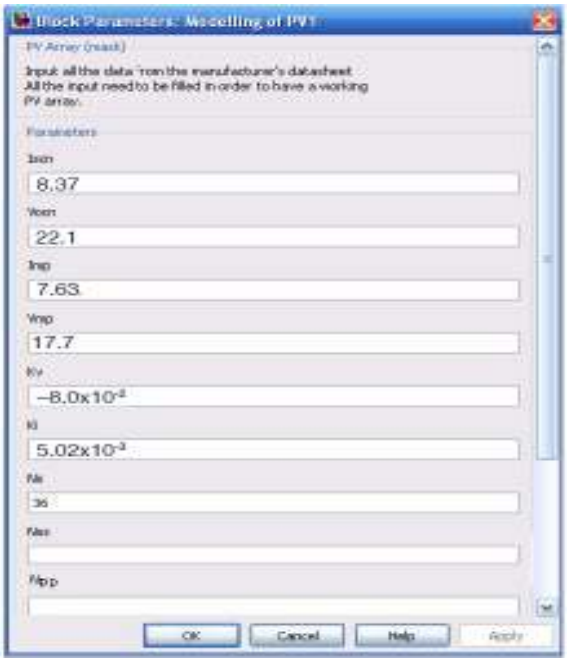

Figure (4.13): The PV Menu after mask process.

www.manaraa.com

Validation of PV Module Model for Different Temperatures

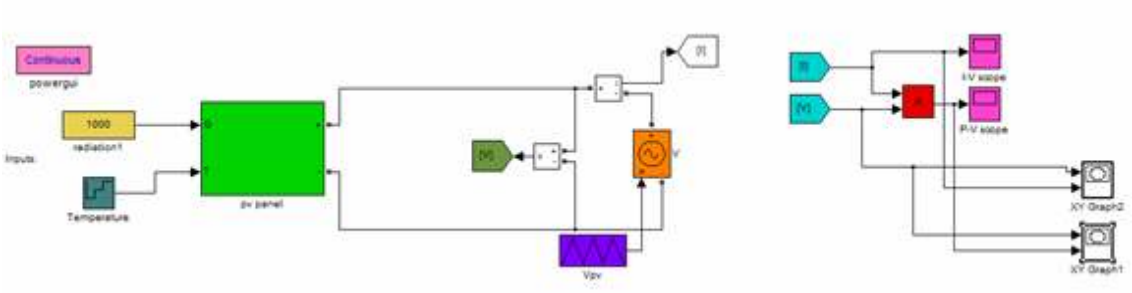

Figure (4.14): PV model simulation at different temperatures.

Figure (4.15) shows the main effect of temperature on the PV module voltage, which decreases when the temperature increases.

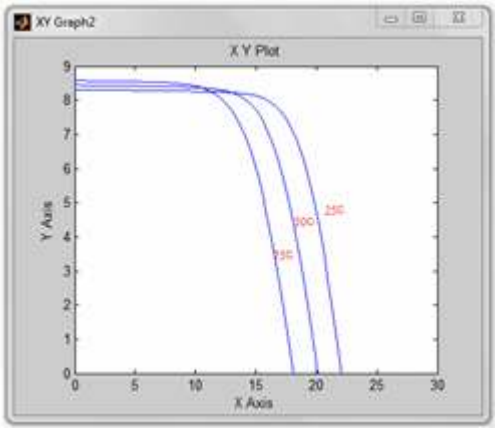

Figure (4.15): Simulink IV characteristic curves for different temperatures.

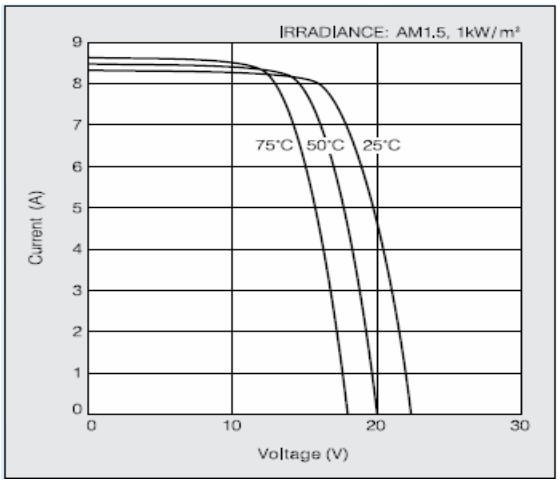

Figure (4.16): Datasheet IV characteristic curves for different temperatures [22].

www.manaraa.com

Validation of the PV Module Model for Different Radiations

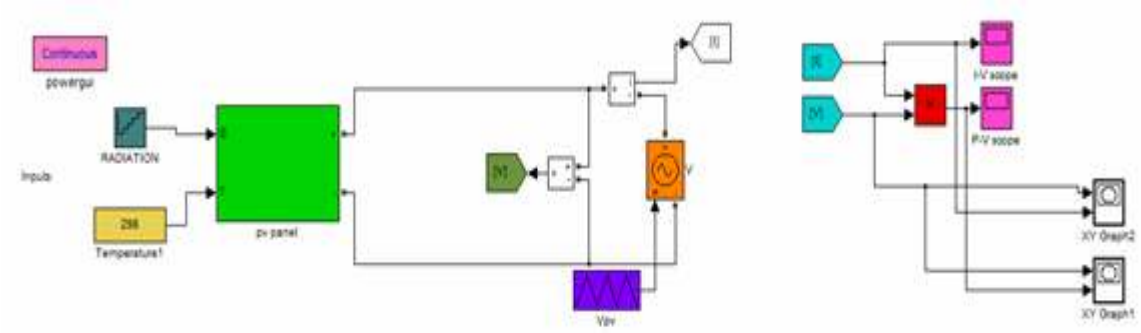

Figure (4.17): PV model simulation at different radiations.

Figure (4.18) shows the main effect of radiation on the PV module current, which decreases when the radiation decreases.

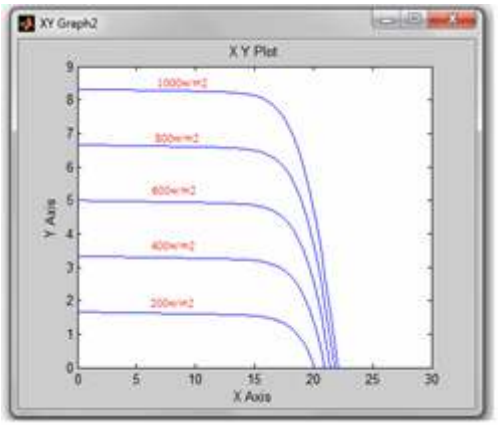

Figure (4.18): Simulink IV characteristic curves for different radiations.

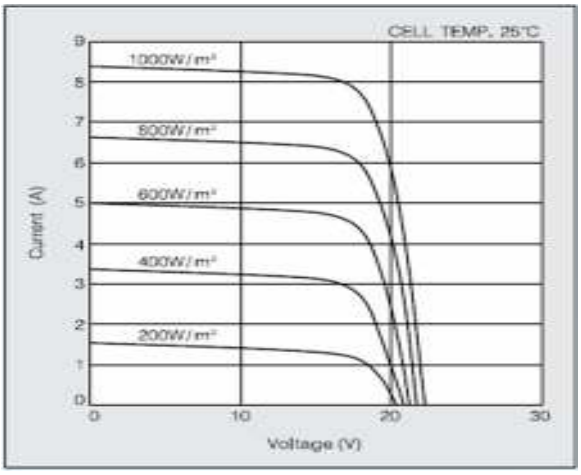

Figure (4.19): Data sheet IV characteristic curves for different radiations [22].

www.manaraa.com

Figure (4.20) shows the effect of temperature on the PV module power, which decreases when the temperature increases.

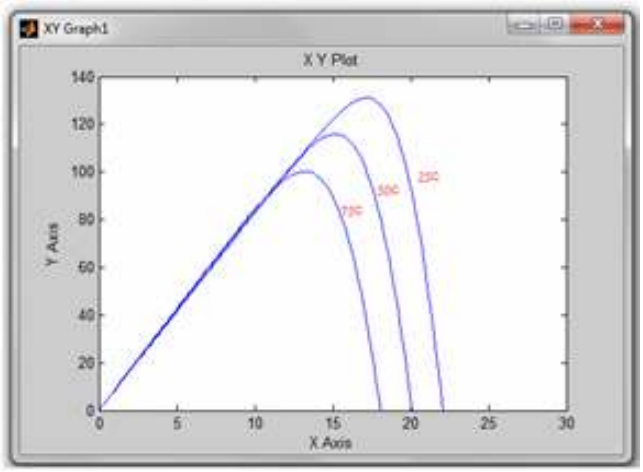

Figure (4.20): Simulink P-V characteristic curves for different temperatures.

Figure (4.21) shows the effect of radiation on the PV module power, which decreases when the radiation decreases.

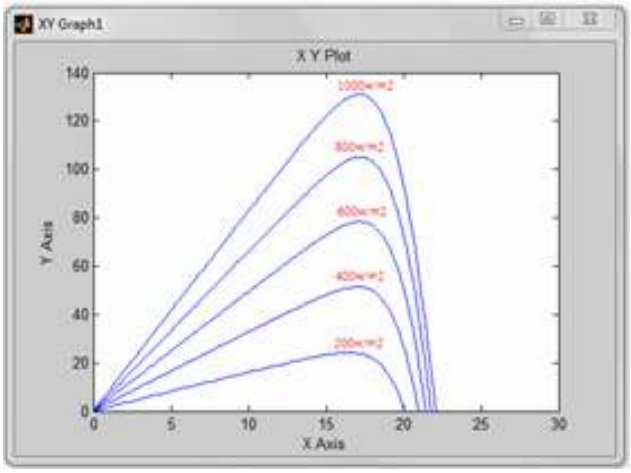

Figure (4.21): Simulink P-V characteristic curves for different radiations.

4.2.2 Modeling of Boost Converter

Figure (4.22) shows the Simulation of the boost converter. The input of the boost converter is the photovoltaic output voltage. The inductance

www.manaraa.com

and the capacitor need to be specified. The switching command of the IGBT is obtained from the MPPT controller.

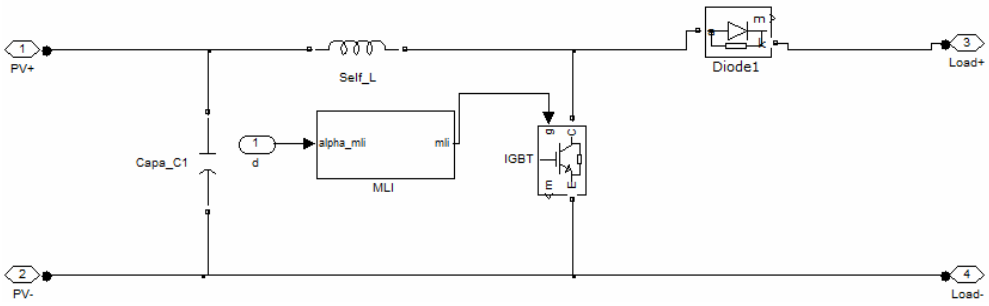

Figure (4.22): Boost converter in Simulink [14].

The design specifications of boost controller are shown in table (4.2). The specifications are for a variable value of input voltage of the boost controller where the input voltage comes from the renewable source of the hybrid system and the output voltage of the boost controller is fixed 800V DC.

Table (4.2): Specification of Boost Controller.

Parameter	Value
Input voltage	**0–240 V**
Output voltage	**380 V**
Output current	**140 A**
Switching frequency	**30 KHz**

Based on the specification for input voltage and output voltage as shown in table (4.2), the required duty cycle can be determined by using Equation (4.13).

In this boost controller circuit, the duty cycle of the boost controller changes with the value of its input voltage. Therefore, in order to determine

www.manaraa.com

the value of minimum inductor L_{min} and minimum capacitor C_{min} of the boost controller, the minimum of the duty cycle D of the boost controller is used in which this duty cycle can be achieved when the input voltage of the boost controller is at maximum value and the output voltage is fixed at 800V.

$$D = 1 - \frac{Vo,max}{Vs} \quad (4.13)$$

$$Vo = \frac{Vs}{1 - D}$$

$$\mathbf{D = 1 - \frac{240}{800} = 0.7}$$

D = 70%

The minimum inductance can be determined by using Equation (4.12).

$$Lmin = \frac{D(1 - D)^2 R}{2f} \quad (4.14)$$

$$\mathbf{Lmin = \frac{0.7\ (1 - 0.7)^2\ 10}{2\ (30\ k)} = 10.5\,\mu H}$$

The capacitance is calculated using Equation (4.15). Let the peak-to-peak ripple voltage equal to 0.05.

$$\Delta Vo = 0.05$$

$$Cmin = \frac{VoD}{\Delta VoRf} \quad (4.15)$$

$$\mathbf{Cmin = \frac{800(\ 0.7)}{0.05\ (10)\ (30k)} = 37\,mF}$$

www.manaraa.com

4.2.3 Modeling of MPPT Controller

The maximum power point controller block is shown in figure (4.23). The voltage and the current of the photovoltaic array are the input, and the duty cycle is the output. The duty cycle is compared to a triangle wave signal to generate the PWM. The frequency of the triangle wave is the pulsation frequency of the boost converter [18].

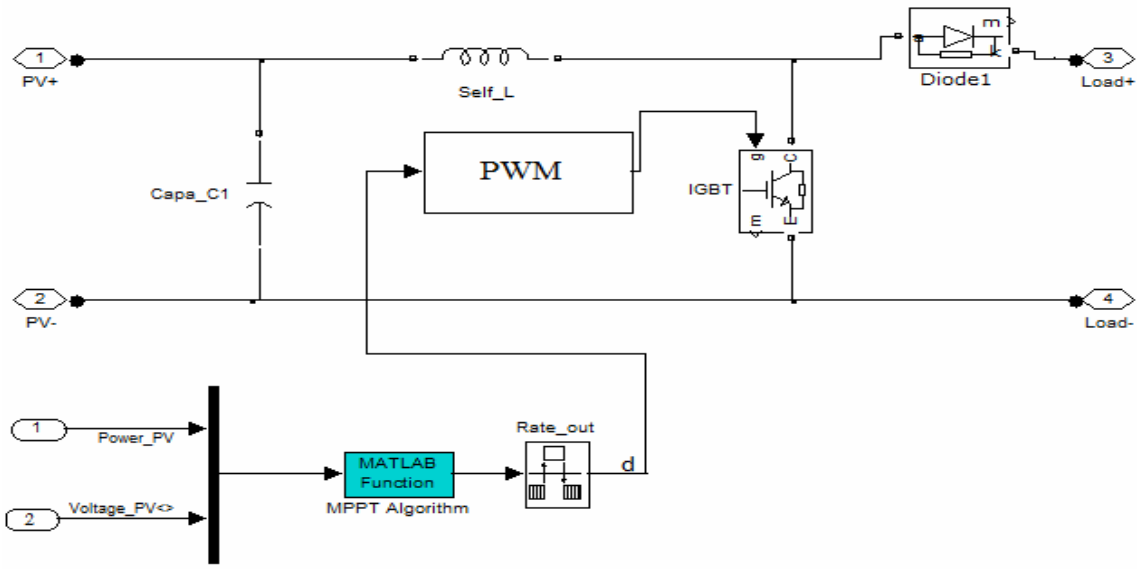

Figure (4.23): MPPT Simulink modeling [18].

The perturb and observe algorithm is implemented and shown in (Appendix E). The duty cycle is increased or decreased until the maximum power point of the photovoltaic is reached. The step of the duty cycle is variable, and it determines the efficiency and accuracy of the MPPT controller [18].

www.manaraa.com

4.2.4 Modeling of Three Phase Voltage Source Inverter

A) Three Phase Inverter Construction

Voltage source inverters (VSI) are mainly used to convert a constant DC voltage into 3-phase AC voltages with variable magnitude and frequency. Figure (4.24) shows a schematic diagram of a 3 phase VSI. The inverter is composed of six switches S1 through S6 with each phase output connected to the middle of each "inverter leg". Two switches in each phase are used to construct one leg. The AC output voltage from the inverter is obtained by controlling the semiconductor switches ON and OFF to generate the desired output.

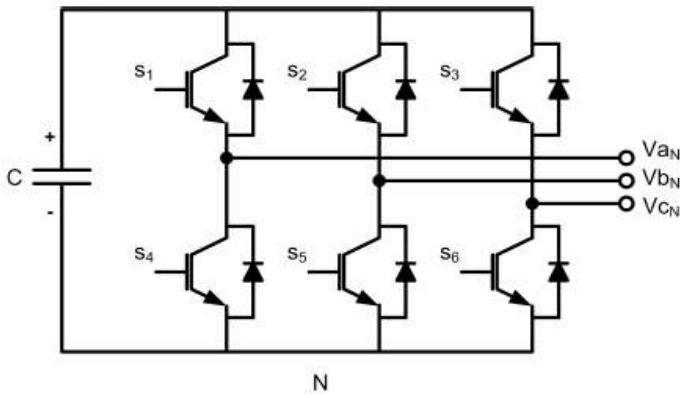

Figure (4.24): Three phase voltage source inverter (VSI)

Insulated Gate Bipolar Transistors (IGBTs) and power MOSFET devices can be used to implement the switches. Each device varies in its power ratings and switching speed. IGBTs are well suited for applications that require medium power and switching frequency [11].

In order to discuss the modeling of inverter control, an overview about abc/dq conversion will introduce in the following section.

www.manaraa.com

B) The *abc/dq* Transformation

The *dq* transformation is used to transform three phase system quantities like voltages and currents from the synchronous reference frame (abc) to a synchronously rotating reference frame with three constant components when the system is balanced [16].The relationship that govern the transformation from the abc to *dq frame* is

$$\begin{bmatrix} x_d \\ x_q \\ x_0 \end{bmatrix} = T \times \begin{bmatrix} x_a \\ x_b \\ x_c \end{bmatrix} \qquad (4.16)$$

$$T = \sqrt{\frac{2}{3}} \times \begin{bmatrix} \cos(\omega t) & \cos(\omega t - 2\pi/3) & \cos(\omega t + 2\pi/3) \\ -\sin(\omega t) & -\sin(\omega t - 2\pi/3) & -\sin(\omega t + 2\pi/3) \\ 1/\sqrt{2} & 1/\sqrt{2} & 1/\sqrt{2} \end{bmatrix}$$

Where x can be either a set of three phase voltages or currents to be transformed, T is the transformation matrix or ω is the angular rotation frequency of the frame. The angle between the direct axis (d-axis) and phase a-axis is defined as θ as shown in figure (4.25).

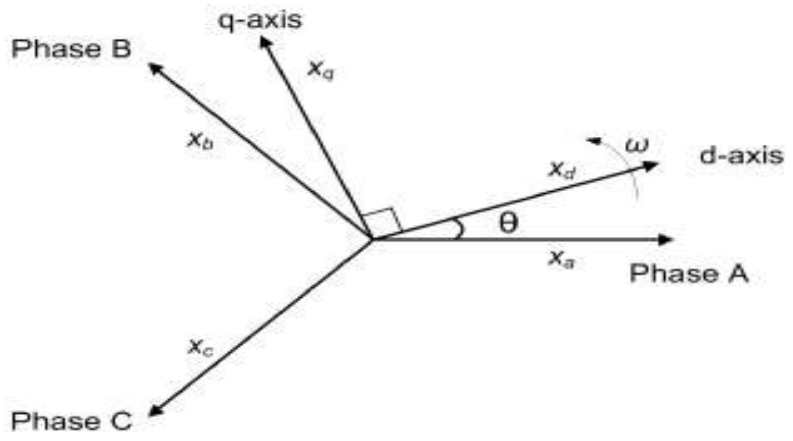

Figure (4.25): Relationship between the abc and dq reference frames.

www.manaraa.com

The result of this transformation is three constant rotating components: the direct (d), quadrature (q) and zero (0) components. In balanced three phase systems, the zero component can be ignored since

$$x_a + x_b + x_c = 0 \tag{4.17}$$

The inverse transformation from the dq frame to the abc frame can be obtained by applying

$$\begin{bmatrix} x_a \\ x_b \\ x_c \end{bmatrix} = T^{-1} \times \begin{bmatrix} x_d \\ x_q \\ x_0 \end{bmatrix}$$

$$T^{-1} = \sqrt{\frac{2}{3}} \times \begin{bmatrix} \cos(\omega t) & -\sin(\omega t) & 1/\sqrt{2} \\ \cos(\omega t - 2\pi/3) & -\sin(\omega t - 2\pi/3) & 1/\sqrt{2} \\ \cos(\omega t + 2\pi/3) & -\sin(\omega t + 2\pi/3) & 1/\sqrt{2} \end{bmatrix} \tag{4.18}$$

This transformation is useful in developing the control system for the voltage source inverter under current control to regulate the output of the PV system.

C) Simulink Modeling of Three Phase VSI Control

The structure of control system blocks is introduced at figure (4.26).The function of each block is examined in detail [16].

www.manaraa.com

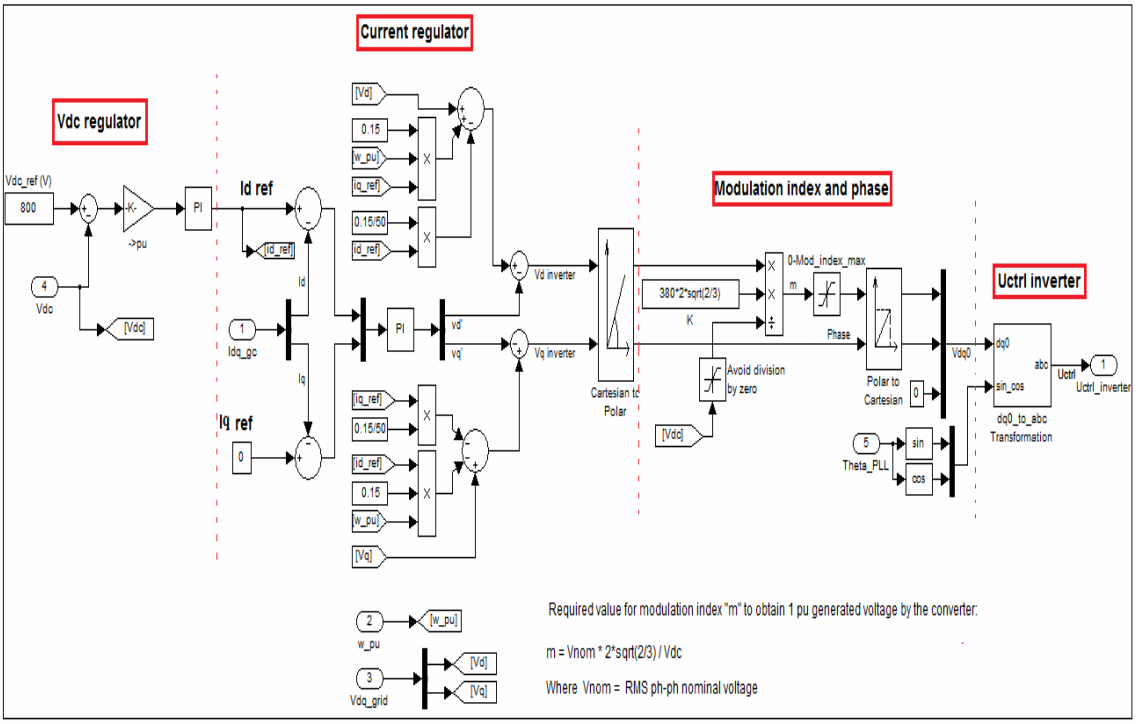

Figure (4.26): Grid tie PV inverter control model.

The state equations describing the dynamics of the output currents and voltages of the voltage source inverter are derived in this section. The time derivatives of the inverter output current and voltage are:

$$L_f \frac{d}{dt} I_{inv} = V_{inv} - V_C \qquad (4.19)$$

$$C_f \frac{d}{dt} V_C = I_{inv} - I_G \qquad (4.20)$$

Where L_f and C_f are the filter's inductance and capacitance respectively, Vc is the capacitor voltage and I_G is the current injected into the grid as shown in figure (4.27).

Equations (4.21) and (4.22) are in matrix format [16] where

$$I_{inv} = \begin{bmatrix} I_{inv,a} & I_{inv,b} & I_{inv,c} \end{bmatrix}^T, \quad V_C = \begin{bmatrix} V_{Ca} & V_{Cb} & V_{Cc} \end{bmatrix}^T \qquad (4.21)$$

www.manaraa.com

$$L_f = \begin{bmatrix} L_f & 0 & 0 \\ 0 & L_f & 0 \\ 0 & 0 & L_f \end{bmatrix}, \quad C_f = \begin{bmatrix} C_f & 0 & 0 \\ 0 & C_f & 0 \\ 0 & 0 & C_f \end{bmatrix}$$

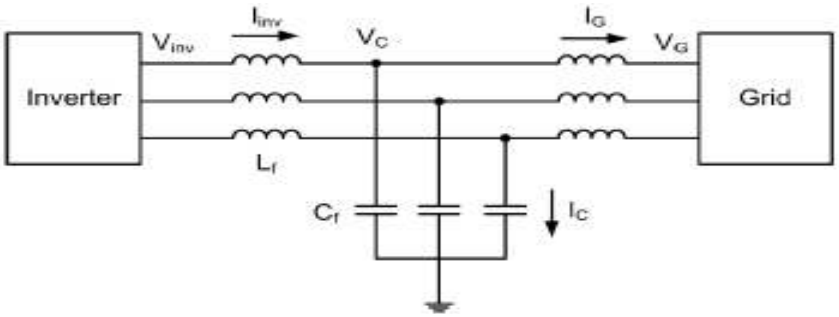

Figure (4.27): Circuit diagram of a three phase grid connected inverter.

Multiplying both sides of equation (4.21) by the transformation matrix T in (4.18), the VSI model in the dq frame can be obtained [27]. The following procedure is adopted to find the result of the transformation

$$TL_f \frac{d}{dt} I_{abc} = T(V_{inv} - V_C)$$

$$TL_f \frac{d}{dt} T^{-1} \hat{I}_{inv} = T(V_{inv} - V_C)$$

$$TL_f \hat{I}_{inv} \frac{d}{dt} T^{-1} + TL_f T^{-1} \frac{d}{dt} \hat{I}_{inv} = \hat{V}_{inv} - \hat{V}_C \qquad (4.22)$$

Where (^) is used to denote dq quantities.

The previous steps use the relationship governing the inverse transformation, which is:

$$I_{abc} = T^{-1} I_{dqo} \qquad (4.23)$$

As a result, equation (4.21) becomes:

$$\begin{bmatrix} 0 & \omega L_f & 0 \\ -\omega L_f & 0 & 0 \\ 0 & 0 & 0 \end{bmatrix} \hat{I}_{inv} + L_f \frac{d}{dt} \hat{I}_{inv} = \begin{bmatrix} 1 & 0 & 0 \\ 0 & 1 & 0 \\ 0 & 0 & 0 \end{bmatrix} (\hat{V}_{inv} - \hat{V}_C) \qquad (4.24)$$

www.manaraa.com

Since the 0-component is not contributing to both sides of the equation, it can be omitted and equation (4.24) can be written as:

$$\begin{bmatrix} \dot{I}_{inv,d} \\ \dot{I}_{inv,q} \end{bmatrix} = \begin{bmatrix} 0 & -\omega \\ \omega & 0 \end{bmatrix} \begin{bmatrix} I_{inv,d} \\ I_{inv,q} \end{bmatrix} + \begin{bmatrix} 1/L_f & 0 \\ 0 & 1/L_f \end{bmatrix} \begin{bmatrix} V_{inv,d} \\ V_{inv,q} \end{bmatrix} - \begin{bmatrix} 1/L_f & 0 \\ 0 & 1/L_f \end{bmatrix} \begin{bmatrix} V_{Cd} \\ V_{Cq} \end{bmatrix} \quad (4.25)$$

This represents the state equation of the inverter output current in the dq frame. Applying the same procedure on equation (4.22), the state equation for the capacitor voltage is:

$$\begin{bmatrix} \dot{V}_{Cd} \\ \dot{V}_{Cq} \end{bmatrix} = \begin{bmatrix} 0 & \omega \\ -\omega & 0 \end{bmatrix} \begin{bmatrix} V_{Cd} \\ V_{Cq} \end{bmatrix} + \begin{bmatrix} 1/C_f & 0 \\ 0 & 1/C_f \end{bmatrix} \begin{bmatrix} I_{Ld} \\ I_{Lq} \end{bmatrix} - \begin{bmatrix} 1/C_f & 0 \\ 0 & 1/C_f \end{bmatrix} \begin{bmatrix} I_{Gd} \\ I_{Gq} \end{bmatrix} \quad (4.26)$$

The output current from the VSI is regulated using proportional-integral controllers to force the error signal in each dq-component to zero. The error signal is defined as the difference between the measured output current and the reference current.

Control laws shown in equation (4.27) generate the required command voltages at the inverter output such that the error in the output current is minimized [28]

$$v_d^* = K_P\left(I_d^* - I_d\right) + K_I \int \left(I_d^* - I_d\right) dt - \omega L_f I_q + V_{Gd}$$
$$v_q^* = K_P\left(I_q^* - I_q\right) + K_I \int \left(I_q^* - I_q\right) dt + \omega L_f I_d + V_{Gq} \quad (4.27)$$

Where Id^* and Iq^* are the dq reference currents, V_{Gd} and V_{Gq} are the dq voltages at the point of common coupling. The command voltages, vd * nd vq*, are transformed back to the natural frame to be sent to the sinusoidal PWM block to generate the switching signals for the inverter.

www.manaraa.com

Under unity power factor operation, the PV system injects real power only into the grid. In that case, reactive power injection is forced to zero by setting the reference current Iq* to zero. The real power injection is controlled by Id* which is extracted from the power mismatch of the DC link capacitor. The capacitor voltage changes according to equation (4.28):

$$\frac{d}{dt}V_{DC}^2 = \frac{2}{C}(P_{in} - P_{out}) \qquad (4.28)$$

Where P_{in} is the input power to the capacitor coming from the DC converter, P_{out} is the output power going to the inverter and then to the grid ignoring power losses, and C is the capacitance of the DC link. To keep the voltage constant, it is necessary to balance Pin and Pout.

Since the input power is controlled by the DC converter to be the maximum output power from the PV array, the control system of the inverter performs the task of controlling the real output power by controlling Id*. This is achieved by using a separate DC link voltage PI controller using

$$I_d^* = \frac{1}{V_{Gd}}\left(K_P(P_{in} - P_{out}) + K_I\int(P_{in} - P_{out})\,dt\right) \qquad (4.29)$$

A schematic diagram of the controller is shown in figure (4.28) . It accepts the power mismatch of the DC link capacitor as an input, and uses a proportional integral controller to generate a power control signal necessary to drive the mismatch to zero. The power control signal is then divided by the direct component of the grid voltage to obtain the reference

www.manaraa.com

current Id*. This reference is sent to the current controllers to regulate the output current of the inverter [16].

The PI controller had a low bandwidth due to slow variations in the DC link power and to ensure that the reference current signal does not suffer any abrupt changes.

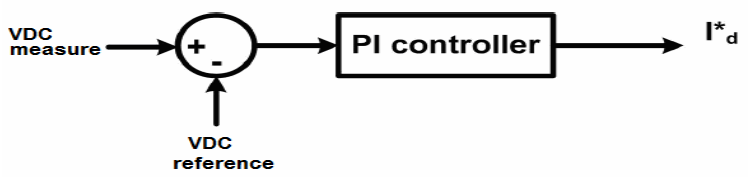

Figure (4.28): Schematic diagram of the DC link controller.

Active and reactive powers injected from the PV system can be calculated using equation (4.30) [16]:

$$P = V_d I_{d,injected} + V_q I_{q,injected}$$
$$Q = -V_d I_{q,injected} + V_q I_{d,injected} \quad \textbf{(4.30)}$$

Where V_d , V_q are the *dq* voltages at PCC at the grid side of the transformer, $I_{d,injected}$ and $I_{q,injected}$ are the *dq* components of the injected current at the grid side. It is evident that in the computation of reactive power Q, there is cross coupling between the direct and quadrature current and voltage components. This can be eliminated through the use of a phase locked loop (PLL) that locks on the grid frequency in such a way that the quadrature component of the voltage at the point of PV system connection is forced to zero. In this case, equation (4.30) simplifies to:

$$P = V_d I_{d,injected}$$
$$Q = -V_d I_{q,injected} \quad \textbf{(4.31)}$$

www.manaraa.com

This means that the direct and quadrature components of the inverter output current can be used to control the active and reactive output powers from the PV array system, as they are related to the injected currents by the transformer turns ratio. This is based on the assumption that the voltage at the point of common coupling (PCC) is relatively constant. In current practice, distribution systems have regulation mechanisms to keep voltage within specified limits.

D) Phase Locked Loop (PLL)

The role of the phase locked loop is to provide the rotation frequency, direct and quadrature voltage components at the point of common coupling (PCC) by resolving the grid voltage *abc* components.

Multiple control blocks of the PV system rely on this information to regulate their output command signals. As stated earlier, the PLL computes the rotation frequency of the grid voltage vector by first transforming it to the *dq* frame, and then force the quadrature component of the voltage to zero to eliminate cross coupling in the active and reactive power terms [26]. A proportional-integral controller is used to perform this task as shown in figure (4.29).

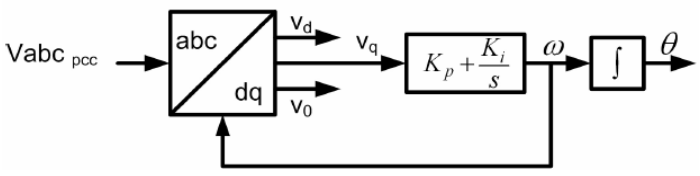

Figure (4.29): Schematic diagram of the phase locked loop (PLL).

www.manaraa.com

The output from the PI controller is the rotation frequency ω in rad/s. Integrating this term results in the rotation angle θ in radians. The operation of the PLL is governed by:

$$\omega = K_P V_q + K_I \int V_q \, dt$$
$$\theta = \int \omega \, dt \qquad (4.32)$$

E) Sinusoidal Pulse Width Modulation (SPWM)

The sinusoidal pulse width modulation technique is used to control the voltage source inverter by producing the gating signals for the semiconductor switches. This technique is used to obtain three phase output voltages that can be controlled in magnitude and frequency. A reference or modulating signal is compared to a high frequency carrier signal; the result of this comparison in each phase is used to activate the switches accordingly. A separate modulating signal is used for each phase with a phase shift of 120° between them as shown in figure (4.30). Two important quantities in SPWM are the amplitude and frequency modulation indices, ma and mf respectively. The amplitude modulation index, ma, is defined as the ratio between the amplitude of the modulating signal to the carrier signal, while the frequency modulation index, mf, is the ratio between the frequency of the carrier signal to that of the modulating signal as in equation (4.33) and (4.34) [16].

$$m_a = \frac{V_m}{V_{carrier}} \qquad (4.33)$$

$$m_f = \frac{f_{carrier}}{f_m} \qquad (4.34)$$

www.manaraa.com

When the amplitude of the modulating signal is greater than that of the carrier signal, the upper switch in the corresponding phase leg in figure (4.24) is activated.

This leads to the output voltage to have the same magnitude of the DC link voltage. The switches in each phase leg operate in a complementary fashion in order to avoid shorting the DC kink capacitor. Figure (4.30) shows the modulating signals for a three-phase inverter and phases A and B output voltages. The line voltage between these two phases is obtained by subtracting V_b from V_a. It is clear that the output voltages need to be filtered to obtain clean sinusoidal voltages. The harmonic content in the output voltages of the inverter depends on the choice of the frequency of the carrier signal. Any even harmonics in the output line voltages in addition to harmonic orders below mf – 2 will be eliminated if the following conditions hold [16].

$$m_f > 9$$
$$m_f = odd\ multiple\ of\ 3$$

In addition to that, harmonics will be centered at mf and its multiples 2 mf, 3 mf …etc., which helps ease the filtering requirements determined by the cutoff frequency. A possible choice is to have mf = 99 which means that

$$f_{carrier} = 99 \times f_m = 99 \times 50 = 4950\ Hz$$

www.manaraa.com

The magnitude of the output phase voltage (rms) can be determined using

$$V_{rms} = m_a \frac{V_{DC}}{2\sqrt{2}} \qquad (4.35)$$

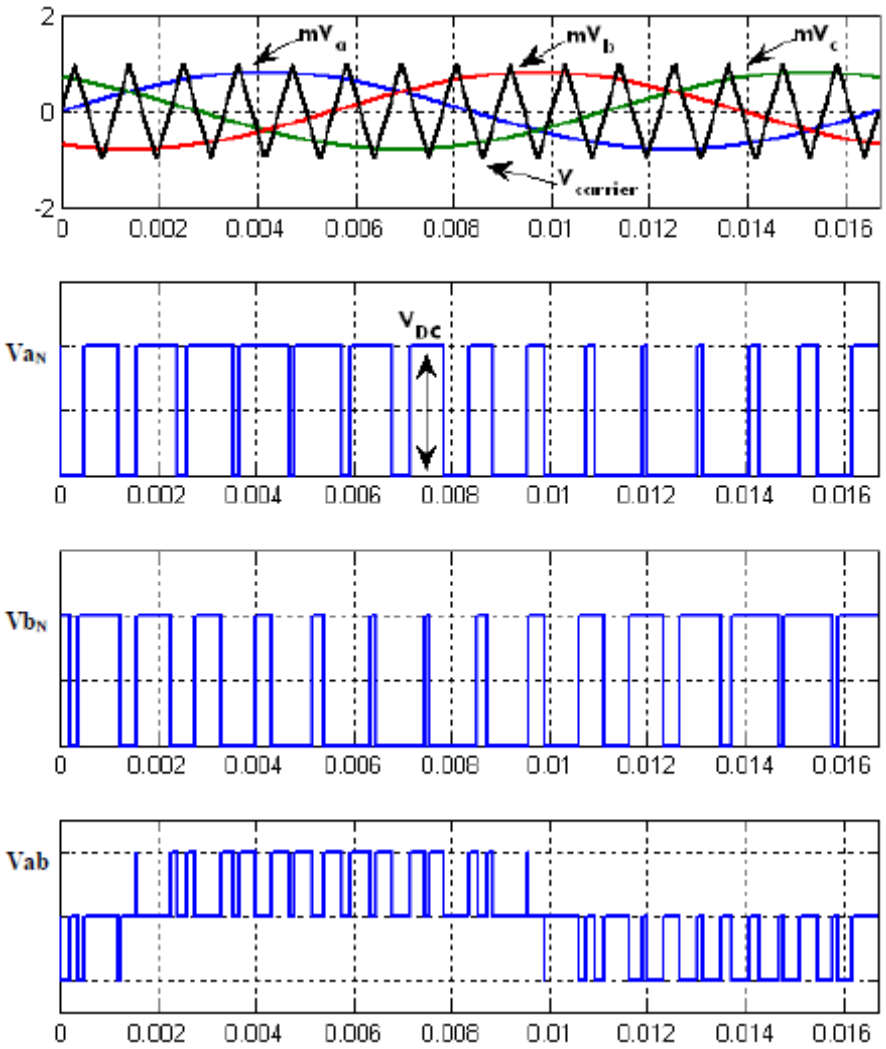

Figure (4.30): SPWM modulation signals for the VSI shown in fig (4.32)

4.3 Modeling of Wind Turbine

In this section, the electrical and mechanical components of the wind generator system are modeled depend on the wind turbine model from Matlab Simulink library as shown in figure (4.31).

www.manaraa.com

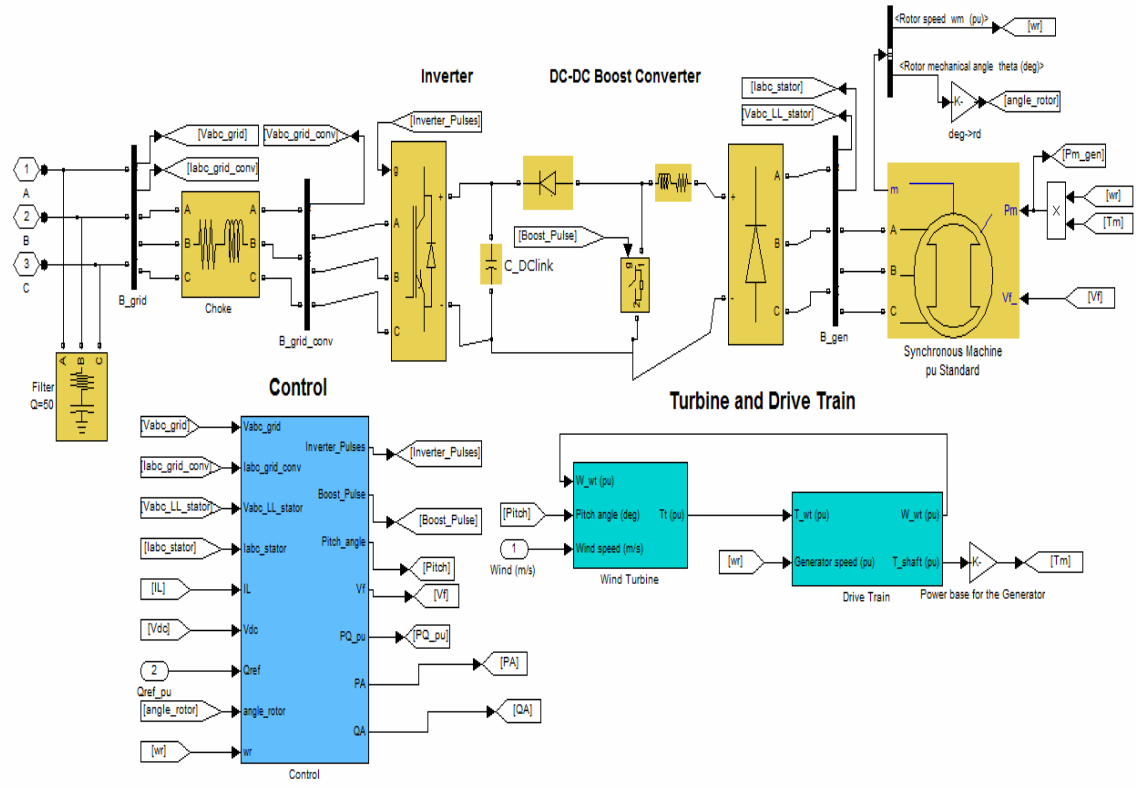

Figure (4.31): Simulink model for grid tie wind turbine [23].

The grid tie wind turbine system consists of aerodynamic model, drive train, synchronous generator, three phase diode rectifier, DC-DC boost converter three phase voltage source inverter, LC filter and different control systems.

4.3.1 Modeling of Wind Turbine Aerodynamic

The wind turbine continuously extracts kinetic energy from the wind by decelerating the air mass, and feeds it to the generator as mechanical power. The aerodynamic model of the wind turbine is necessary because it gives a coupling between the wind speed and the mechanical torque produced by the wind turbine. The mechanical power, PM, produced by the wind turbine rotor can be defined as [25]:

www.manaraa.com

$$P_m = C_p(\lambda, \beta)\, P_v = \frac{1}{2}\rho_{air} v^3 A C_p(\lambda, \beta) \qquad (4.36)$$

Where

A: swept wind turbine rotor area

Cp: performance coefficient of the wind turbine

Pv: wind power available in the rotor swept area

v: wind speed

ρ_{air} : air density

λ: tip speed ratio of the rotor blade tip speed to wind speed

β: blade pitch angle.

Figure (4.32) shows the aerodynamic Simulink model of wind turbine and the relation between wind speed and the mechanical torque.

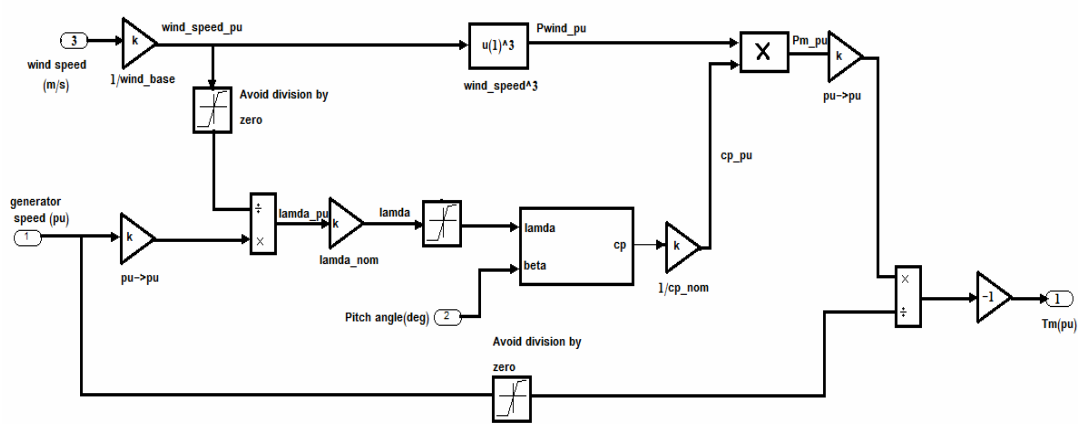

Figure (4.32): Simulink block of wind turbine torque.

The relation between C_P and λ is normally established by the C_P/ λ curve. This curve can be approximated using the power/wind curve,

www.manaraa.com

provided by wind turbine manufacturers. To perform this calculation, it is supposed that the rotor speed does not depend on wind speed in steady-state operation. Here, a generic equation is used to model the performance coefficient, $C_P(\lambda,\beta)$. This equation based on the turbine model characteristics [25]:

$$C_p(\lambda, \beta) = C_1 \left(\frac{C_2}{\lambda} - C_3\,\beta - C_4\right) e^{\left(\frac{-C_5}{\lambda}\right)} + C_6 \qquad (4.37)$$

Where **C1** = 0.5176, **C2** = 116, **C3**= 0.4, **C4** = 5, **C5**= 21, **C6** = 0.0068. The C_p- λ characteristics, for different values of the pitch angle β, are illustrated in figure (2.9). The maximum value of C_p (C_p max= 0.48) is achieved for β = 0 degree and for λ = 8.1. This particular value of λ is defined as the nominal value (λ_nom) [23].

Figure (4.33) shows the Simulink model for equation (4.37).

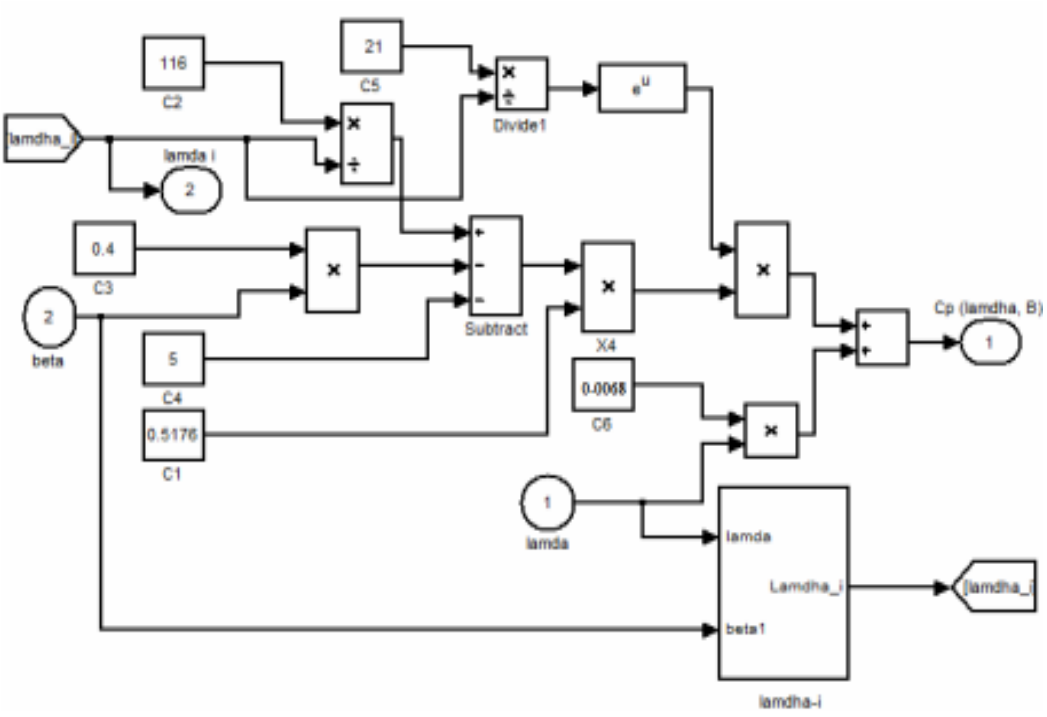

Figure (4.33): Simulink block of performance coefficient C_p (λ,β) [20],[21].

www.manaraa.com

The C_p- λ characteristic of Figure (4.34) shows that the values of performance coefficient Cp were increased when reducing the value of blade pitch angle (degree) β. The maximum value of performance coefficient C_p was obtained when the value of blade pitch angle (degree) β was set to $\beta = 0^o$ [22].

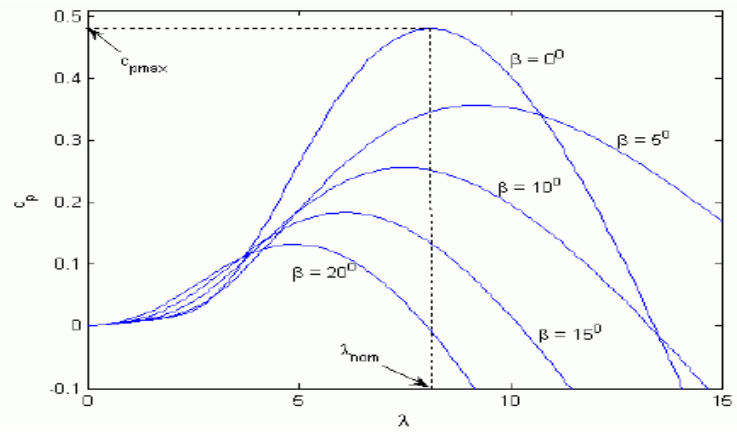

Figure (4.34): Cp- λ Characteristics of wind turbine [22].

Also,

$$1/\lambda_i = 1/(\lambda + 0.08\,\beta) - 0.035/(\beta^3 + 1) \qquad \textbf{(4.38)}$$

Figure (4.35) shows the Simulink model for equation (4.38).

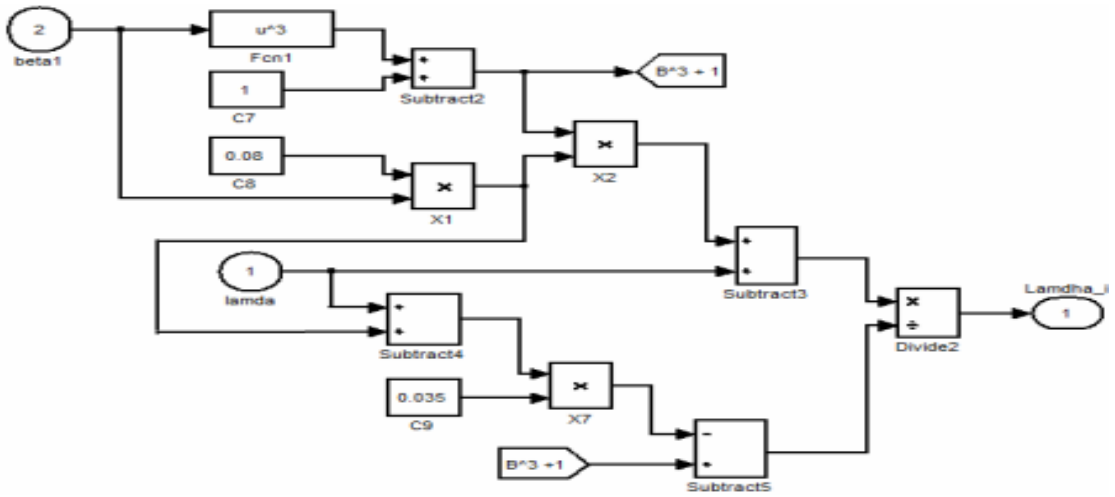

Figure (4.35): Simulink block of tip speed ratio λi model [20],[21].

www.manaraa.com

4.3.2 Modeling of Drive Train

The drive train model simulates the elastic connection between the low-speed wind turbine shaft and the high-speed generator shaft. It consists of the inertia of both the turbine and generator (2-mass system). The elastic coupling between the two masses is modeled by spring, k, and damper, B. The equivalent model for the drive train of the wind turbine referred to the generator side is shown in figure (4.36).

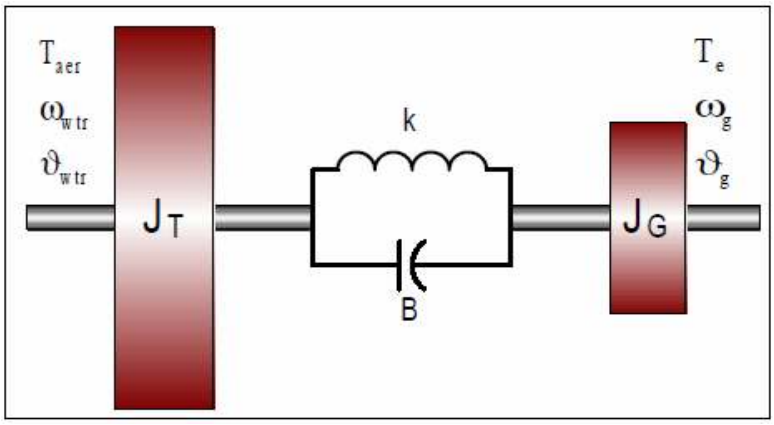

Figure (4.36): Model of drive train (2-mass system).

The dynamics of the drive train on the generator side can be written in equation (4.39) and (4.40) [9]:

$$T_{aer} = J_T \frac{d\omega_{wtr}}{dt} + k \cdot \Delta\vartheta + B \cdot \Delta\omega \qquad (4.39)$$

$$k \cdot \Delta\vartheta + B \cdot \Delta\omega = J_G \frac{d\omega_g}{dt} + T_e \qquad (4.40)$$

Where

$$\Delta\omega = \omega_{wtr} - \omega_g$$

$$\Delta\vartheta = \vartheta_{wtr} - \vartheta_g$$

www.manaraa.com

$$\omega_{wtr} = \frac{d\vartheta_{wtr}}{dt}$$

$$\omega_g = \frac{d\vartheta_g}{dt}$$

J_T (kg .m^2) is the turbine moment of inertia,
J_G (kg .m^2) is the generator moment of inertia,
k (N.m/rad) is the stiffness of the shaft,
B (N.m.sec/rad) is the absorption of the shaft,
T_{aer} (N.m) is the wind turbine torque,
T_e (N.m) is the electromagnetic generator torque,
ω_{wtr}, ω_g (rad s^{-1}) are the angular speed of the turbine and of the generator, respectively, and $\vartheta_{wtr}\vartheta_g$ (rad) are the positions of the turbine and generator shafts, respectively.

Figure (4.37) shows wind turbine drive train based on 2-mass model

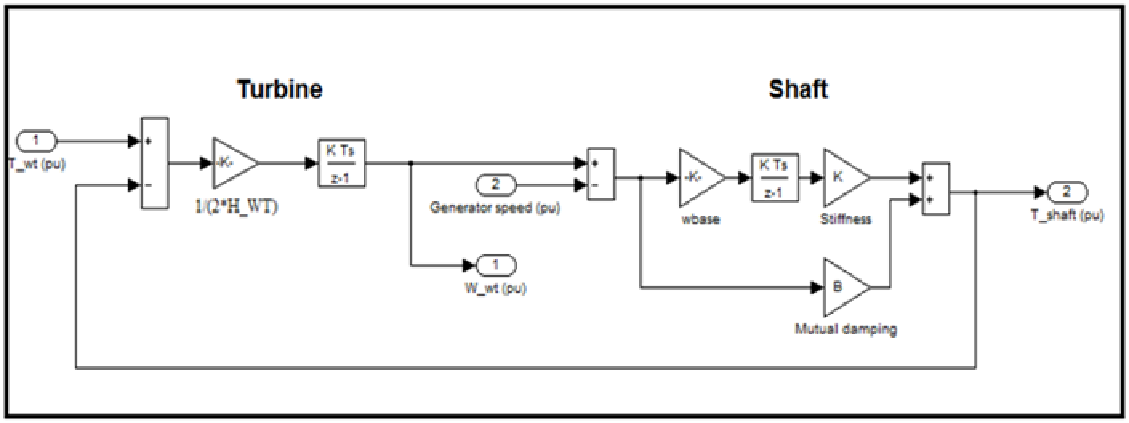

Figure (4.37): Equivalent diagram of the drive train model.

4.3.3 Modeling of Grid Tie Wind Turbine Control

The control system for wind turbine consisting of four main parts, inverter control, excitation control, speed regulator and pitch control.

Simulink Modeling of Grid Tie Wind Turbine Inverter Control

Figure (4.38) shows the control strategy for grid tie wind turbine inverter which is the same control strategy used in grid tie PV inverter, but

www.manaraa.com

with the addition of reactive power controller. During the voltage sag the control systems try to regulate reactive power at their set points (0 kvar).

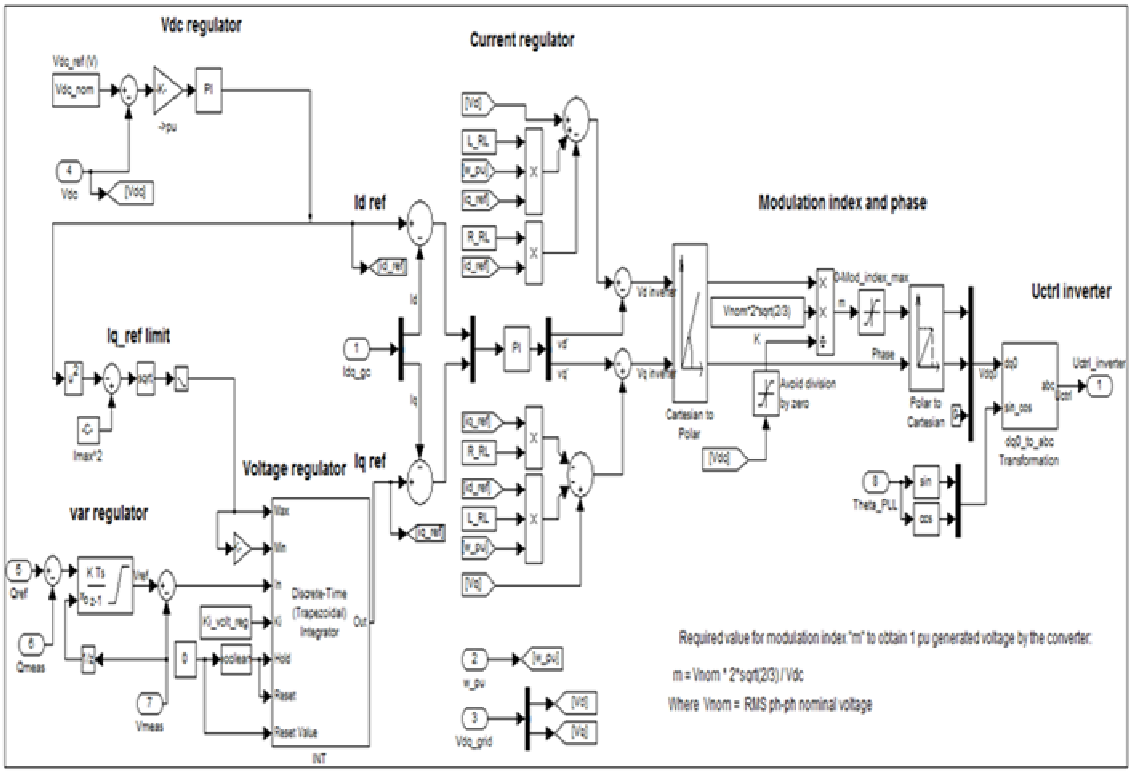

Figure (4.38): Equivalent diagram for grid tie wind turbine control model[23].

The second part of grid tie wind turbine control is the excitation control:

A) Simulink Modeling of Excitation Control

The objective of this controller is to regulate the field winding voltage of the synchronous generator. Higher excitation voltages increase the maximum torque capability of the generator but result also in increased iron losses. Hence, for operation at low wind speeds, and therefore at low rotor speeds, the field voltage may be decreased since the generator torque

www.manaraa.com

requirements are reduced. At high winds, on the other hand, a higher excitation is needed for the generator to develop its full torque.

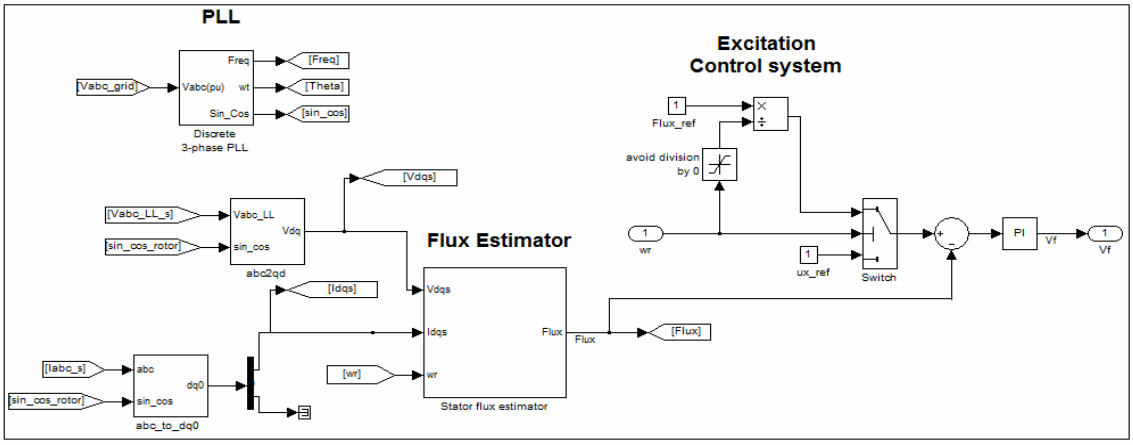

Figure (4.39): Equivalent diagram of generator excitation control model [23].

The third part of grid tie wind turbine control is the speed controller:

B) Simulink Modeling of Speed Controller

The goal of speed control is to maximize energy capture for wind speeds below rated as shown in figure (4.40).

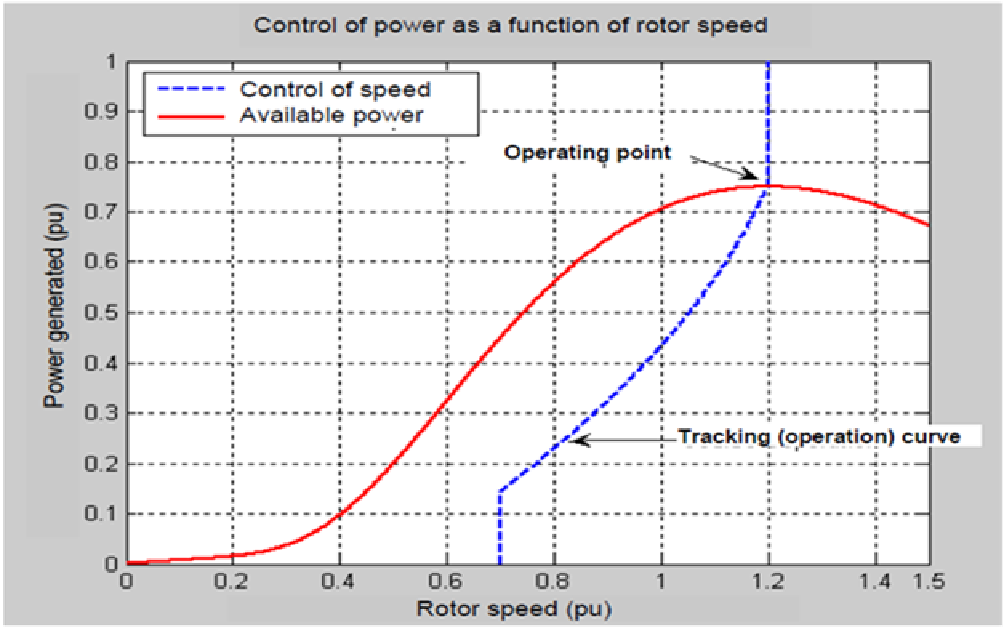

Figure (4.40): Stabilization of power and speed through a single operating point.

www.manaraa.com

The available power (solid red line) characterizes the turbine's response to a given wind speed (12 m/s), as a function of rotation speed. The tracking curve (dotted blue line) characterizes the operation strategy, which consists in establishing speed set-points as a function of the power generated. The intersection of the two curves defines the operating point. This unique point is the key to maintaining the rotational speed [33].

If this unique point did not exist, it would not be possible to maintain rotor speeds near those required for maximum available power. To maintain the system at this point, the velocity error signal, provided by comparing the required set-point speed and the actual speed, is converted to an electromagnetic torque command signal using a P.I. controller. The regulator obtains the required torque (T) by taking advantage of the equation (4.41) [33]:

$$T_{em} = \frac{P}{\omega_r} \qquad (4.41)$$

The speed controller shown in figure (4.41) regulates the speed of the rotor by controlling the generator electrical power (and therefore torque) according to the optimal speed vs. power control characteristic discussed in the following. The measured turbine power determines the reference rotor speed, and then the error of the rotor speed determines the DC current set-point via a PI-controller. The DC current is then regulated at the reference value by the PI controller of the boost converter.

www.manaraa.com

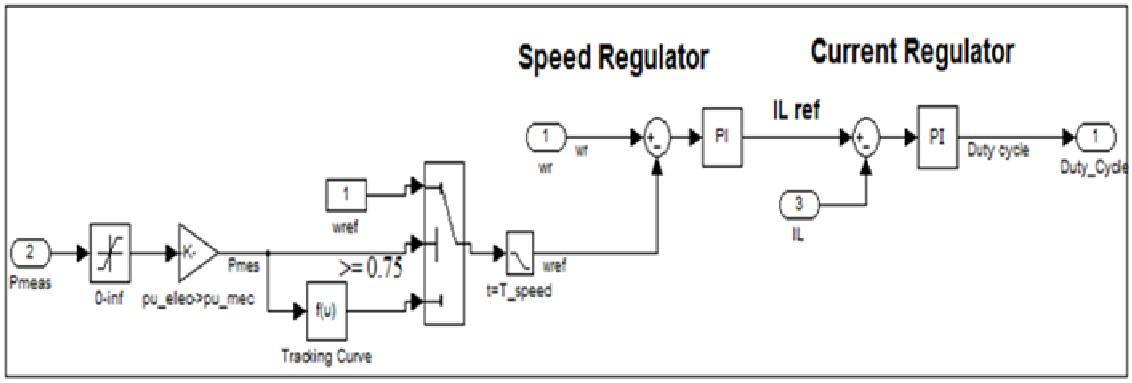

Figure (4.41): Equivalent flow diagram for speed regulator.

C) Simulink Modeling of Pitch Control

Blade pitch angle can be modified to reduce the power transmitted to the rotor. The pitch angle is adjusted by a mechanical controller attached to the blades at the rotor hub[33].

Figures (4.42), (4.43) and (4.44) show various curves characterizing available power as a function of wind speed and blade pitch angle.

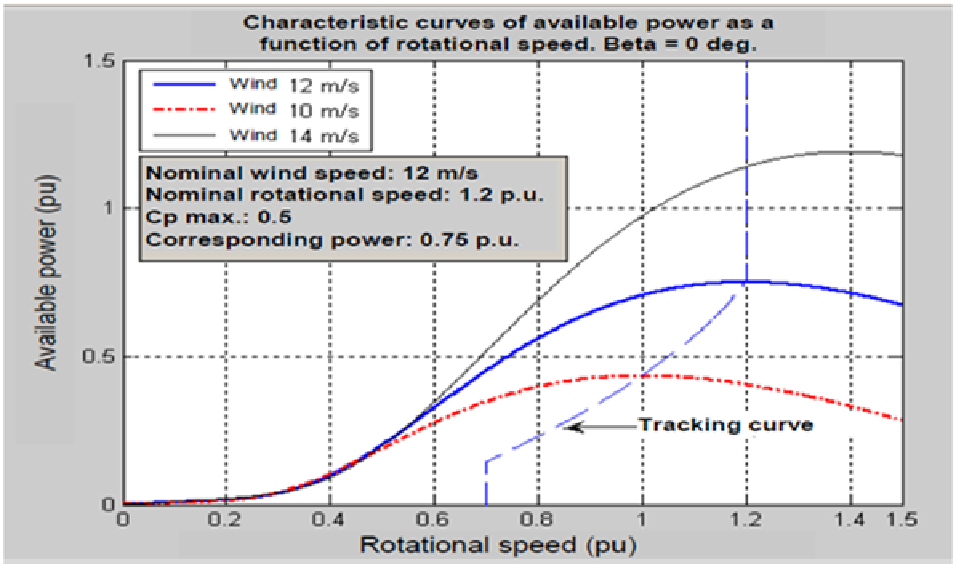

Figure (4.42): Available power for different wind speeds; blade pitch angle of zero.

www.manaraa.com

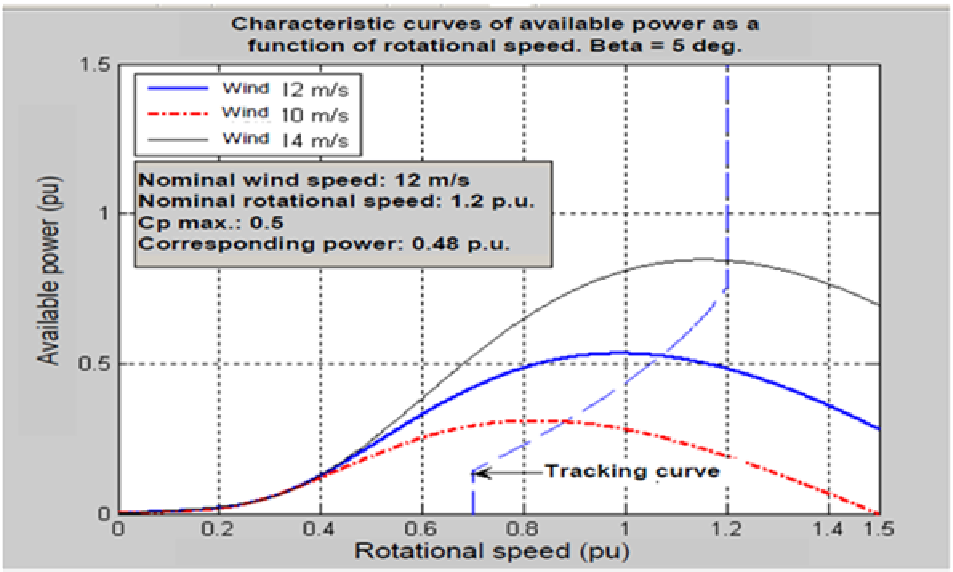

Figure (4.43): Available power for different wind speeds; pitch angle of 5 degrees.

Figure (4.44) shows that, when wind speed is 15 m/s, but design speed is 12 m/s, the blade pitch angle (Beta) must be greater than 5 degrees to satisfy the maximum power constraint of 1 p.u [33].

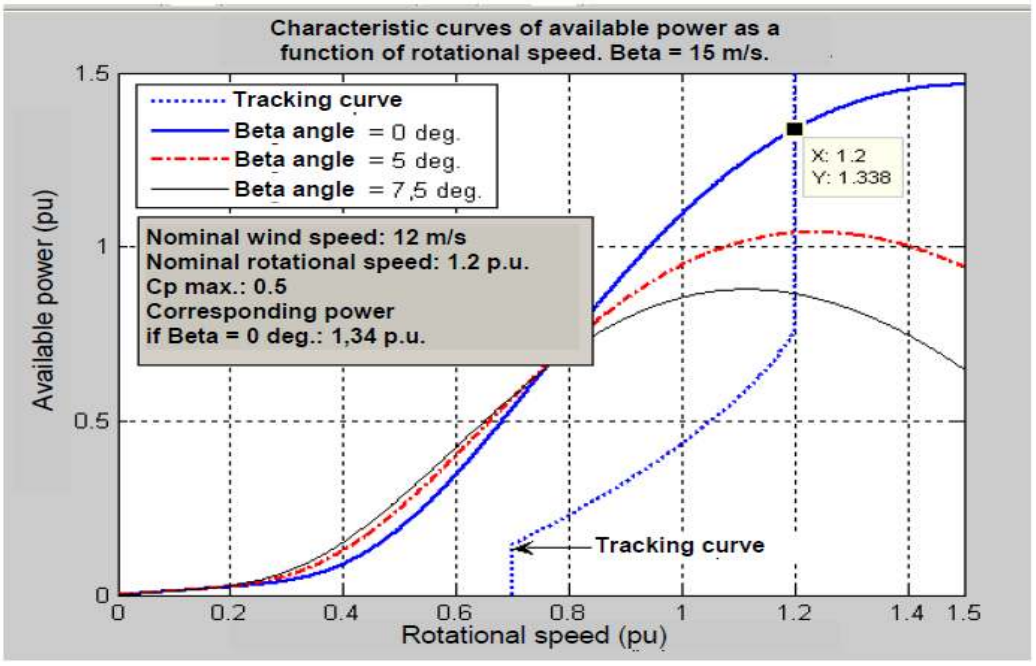

Figure (4.44): Available power for different blade pitch angles; wind speed 15 m/s.

The Simulink model of pitch angle controller shown in figure (4.45), the generator power is regulated at its rated value to avoid overloading the

www.manaraa.com

generator and converters, while the blade pitch angle is increased in order to reduce Cp and the resulting mechanical torque. The objective is to prevent the rotor speed from increasing beyond its maximum value. For operation below rated wind speed, the pitch angle is approximately zero, for maximum aerodynamic efficiency.

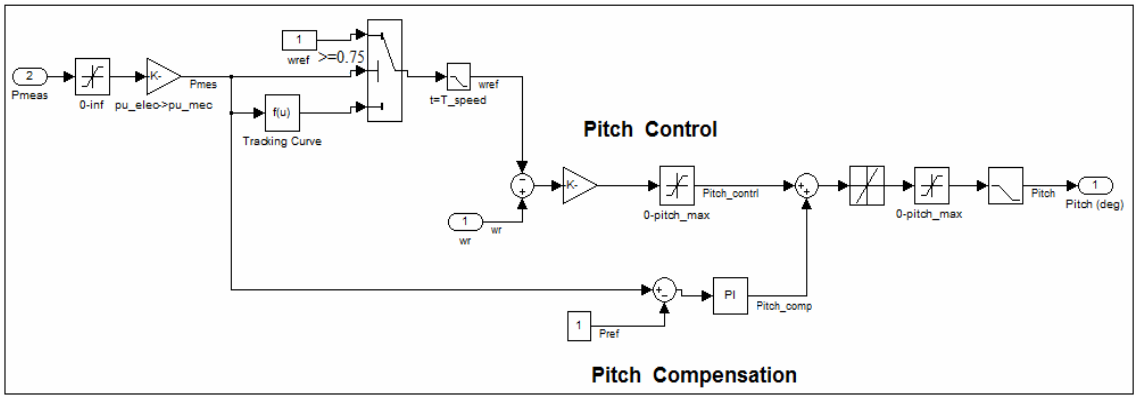

Figure (4.45): Equivalent flow diagram for pitch control.

4.4 Modeling of Diesel Generator

A diesel electricity generator is simulated by using an alternator having its mechanical energy from diesel engine. Also, alternator gets its field voltage from an excitation system, this system depend on the diesel generator model from Matlab Simulink library as shown in figure (4.46).

4.4.1 Modeling of Diesel Engine

To simulate the complete dynamics of a diesel engine system, a very large order model will be required. However for most studies on speed dynamics of internal combustion engines, it is sufficient to use a lower order model. Similar approaches have been adopted in diesel engine simulation studies.

www.manaraa.com

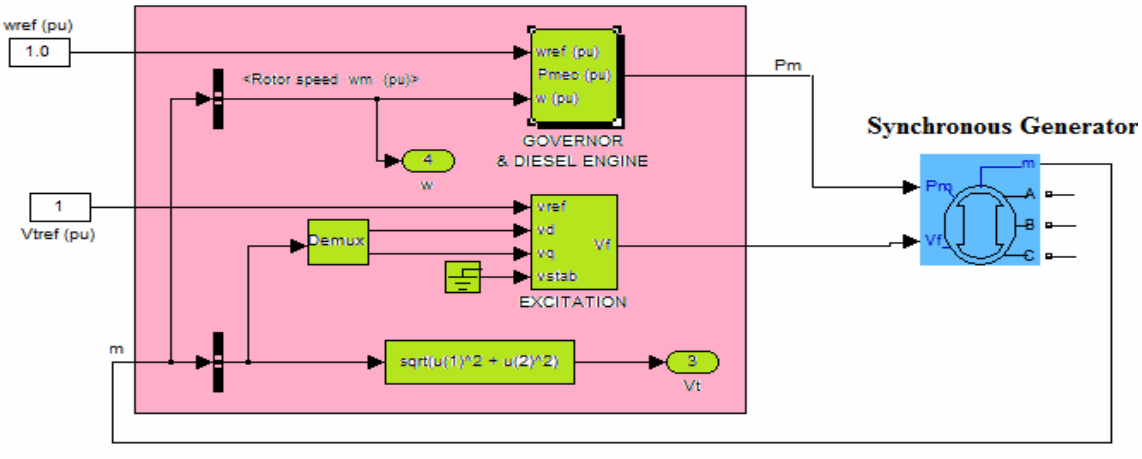

Figure (4.46): Simulink model of diesel generator.

The engine consists of three parts: the actuator, the engine and the flywheel. The speed control system designed to control the speed of diesel engine is shown in Figure (4.47).

Diesel engines in the range of 100 to 1000 horsepower are generally referred to as small to medium sized diesel engines. When being used to drive electrical generator sets, a Proportional, Integral, Derivative (PID) controller typically controls this type of engine. Suitable values for the three gains in a PID compensator are usually found by trial and error [25].

PID controller is the Laplace transform of the classic:

$$u(s) = Pe(s) + \frac{Ie(s)}{s} + \frac{Dse(s)}{\mu s + 1} \qquad \textbf{(4.42)}$$

Where

e(s): is difference of reference value given and feedback value obtained (error).

u(s): is the output of the controller.

www.manaraa.com

A lag has been added to the denominator of the derivative term, because high frequency noise tends to dominate a pure derivative function. The time constant of this lag, μ, is typically made much smaller than the time constants of any modeled system dynamics.

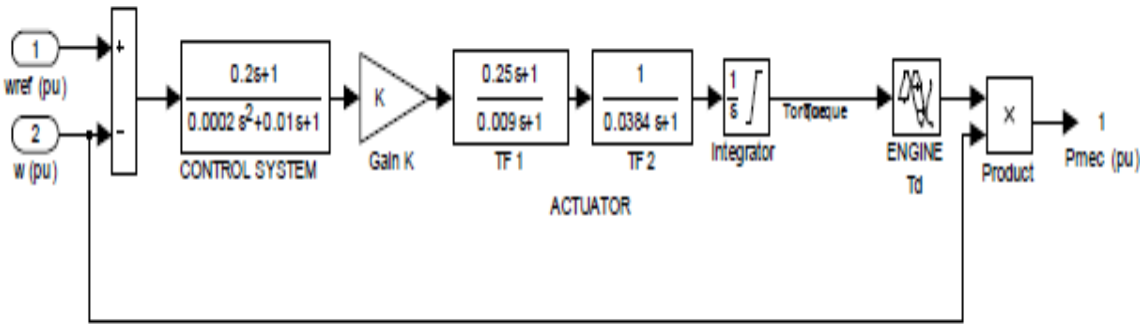

Figure (4.47): Speed Control of Diesel Engine [25].

A dead time TD in figure (5.47) represents un-modeled high frequency dynamics, as well as the almost pure dead time associated with an engine.

This dead time is the result of having several cylinders. Not all cylinders will be in a position to accept more fuel at a given instant. The dead time TD is largely made up of the time required for all cylinders to come into position to be filled with more or less fuel [25].

In the simulated system, speed control for diesel engine and supplying the torque obtained from it to a synchronous generator. The diesel engine is assumed to be simulated and the speed obtained from it is basically controlled by designing a speed control system for it.

www.manaraa.com

The blocks basically take speed of engine as input and gives mechanical power as its output. The speed of the diesel engine is the same as that of the synchronous generator. To the summing block of the control system, the reference angular speed ω provided is 1 pu. The actual speed of the diesel engine is provided from the measurement port of the synchronous machine which happens to be the same for both the engine and generator.

The speed error is provided to the PID controller with Transfer function:

$$H(s) = \frac{40(1+0.2s)}{1+0.01s+0.0002s^2} \quad \textbf{(4.43)}$$

The control system passes the output signal to the actuator, which converts it to a torque signal.

The transfer function of the actuator is given by the two transfer function blocks in cascade and the resultant transfer function is given by:

$$G(s) = \frac{1+0.25s}{s(1+0.009s)(1+0.0384s)} \quad \textbf{(4.44)}$$

The control signal after passing through the integrator is made to have a delay of 0.024 units. The integrator takes care that torque remains between the limits from 0 to 1.2.

$$T_D = e^{-0.024s} \quad \textbf{(4.45)}$$

The time delay block, which is referred to as the input dead time of

www.manaraa.com

the system, comprises of three parts:

(i) Time from a load disturbance to time when the cylinders respond.

(ii) Time between the fuel rack change and when a certain amount of fuel has been injected into the chamber.

(iii) Time for fuel to burn and the generation of torque required.

Usually, the first one is called a "power-stroke delay" and the latter two are regarded as an "ignition delay". The engine dead time is a function of the engine speed and can be considered as a nonlinear part of the system.

The torque signal obtained is then fed to a product box along with the velocity; the result of which gives the mechanical power, which is then fed to the synchronous machine [25].

$$P_{mec} = \text{Torque X angular velocity} \quad (4.46)$$

4.4.2 Excitation System of Alternator Model

This model, described by the block diagram of figure (4.48), is used to represent field-control dc commutator exciters with continuously acting voltage regulators. Because this model has been widely implemented by the industry, it is sometimes used to represent other types of systems when detailed data for them are not available or when a simplified model is required [25].

www.manaraa.com

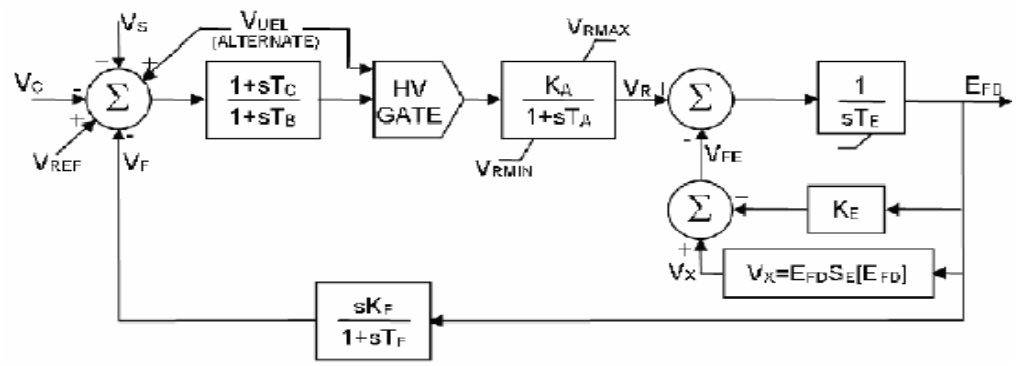

Figure (4.48): Field-Controlled DC Commutator Exciters.

The principal input to this model is the output from the terminal voltage transducer, V_C. At the summing junction, terminal voltage transducer output, V_C, is subtracted from the set point reference, V_{REF}. The stabilizing feedback, V_F, is subtracted and the power system stabilizing signal, VS, is added to produce an error voltage. In the steady state, these last two signals are zero, leaving only the terminal voltage error signal. The resulting signal is amplified in the regulator. The major time constant, T_A, and gain, K_A, associated with the voltage regulator are showing limits typical of saturation or amplifier power supply limitations.

These voltage regulators utilize power sources that are essentially unaffected by brief transients on the synchronous machine or auxiliary buses [25].From the block diagram shown in Figure (4.48), the equation (4.47) is obtained:

$$V_{comp} = V_s + V_{uel} - V_c + V_{ref} - Vf \qquad \textbf{(4.47)}$$

Where **Vc:** Voltage of Transducer output, **Vref:** reference Voltage, **Vf:** stabilizing feedback, **Vs:** stabilizing signal, **Vuel:** terminal field voltage

www.manaraa.com

The voltage regulator output, V_R, is used to control the exciter, which may be either separately excited or self-excited. When a self-excited shunt field is used, the value of K_E reflects the setting of the shunt field rheostat. In some instances, the resulting value of K_E can be negative and allowance should be made for this. Most of these exciters utilize self-excited shunt fields with the voltage regulator operating in a mode commonly termed buck-boost [25].

The majority of station operators manually track the voltage regulator by periodically trimming the rheostat set point so as to zero the voltage regulator output. This may be simulated by selecting the value of K_E so that initial conditions are satisfied with $V_R = 0$. In some programs, if K_E is entered as zero, it is automatically calculated by the program for self-excitation.

If a nonzero value for K_E is provided, the program should not recalculate K_E, as a fixed rheostat setting is implied. For such systems, the rheostat is frequently fixed at a value that would produce self- excitation near rated conditions. Systems with fixed field rheostat settings are in widespread use on units that are remotely controlled. A value for $K_E = 1$ is used to represent a separately excited exciter.

The term $S_E[E_{FD}]$ is a nonlinear function with values defined at two or more chosen values of E_{FD}. The output of this saturation block, V_X, is the product of the input, EFD, and the value of the nonlinear function $S_E[E_{FD}]$ at this exciter voltage.

www.manaraa.com

A signal derived from field voltage is normally used to provide excitation system stabilization, V_F, via the rate feedback with gain, K_F, and time constant, T_F. Figure (4.49) shows the model simulated in Matlab Simulink environment [25].

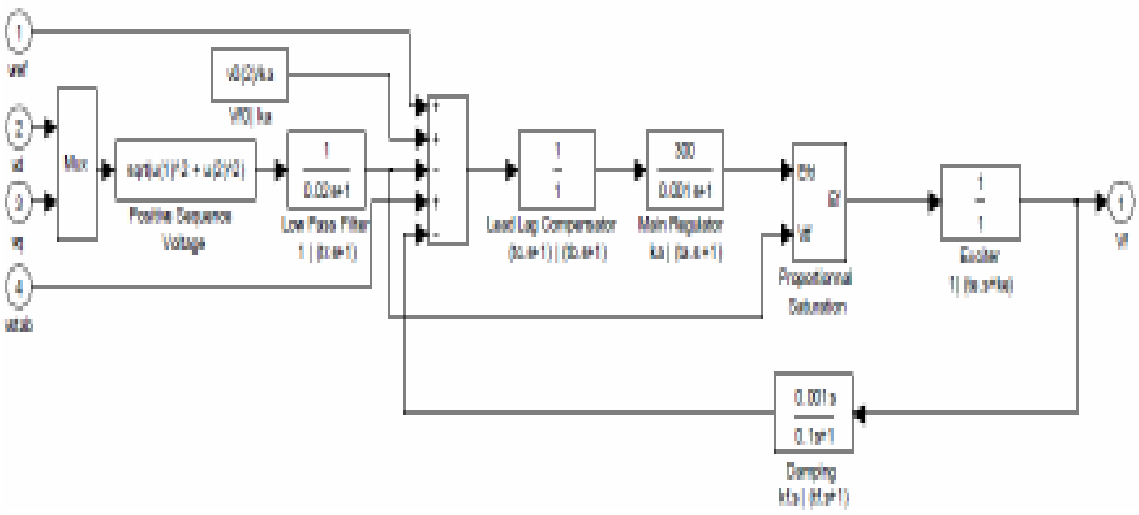

Figure (4.49): Simulink model of Excitation System [25].

Here also, the input given to the Lead Lag Compensator can be written as:

$$V_{comp} = V_{ref} + V_{fo}/k_a - \sqrt{(V_d^2 + V_q^2)}/(1 + T_r s) + V_{stab} - V_f(k_f s/(1+t_f s)) \quad \textbf{(4.48)}$$

Where

V_{comp}: is the input voltage given to compensator.

V_{ref}: is the reference voltage if exciter.

V_{fo}: is initial value of field voltage.

K_a: is regulator gain.

www.manaraa.com

$\mathbf{V_f}$ **:** is field voltage.

$\mathbf{k_f}$ **:** is damping function gain.

$\mathbf{t_f}$**:** is filter time constant.

Comparing equations (4.48) and (4.47), it is inferred that:

$V_s = V_{stab}$ = stabilizing voltage signal and

$$V_F = \frac{V_f ks}{1 + T_r s} \tag{4.49}$$

The terminal field voltage is calculated as:

$$V_{tF} = \frac{\sqrt{V^2_d + V^2_q}}{1 + T_r s} \tag{4.50}$$

Where

$\mathbf{V_d}$ and $\mathbf{V_q}$ **:** are direct and quadrature axis voltages,

$\mathbf{T_{rs}}$ **:** is Low Pass filter time constant.

Also, V_C Voltage of Transducer output is given by:

$$V_c = \frac{V_{fo}}{k_a} \tag{4.51}$$

Figure (4.50) shows complete grid tie PV/Wind hybrid Simulink model.

www.manaraa.com

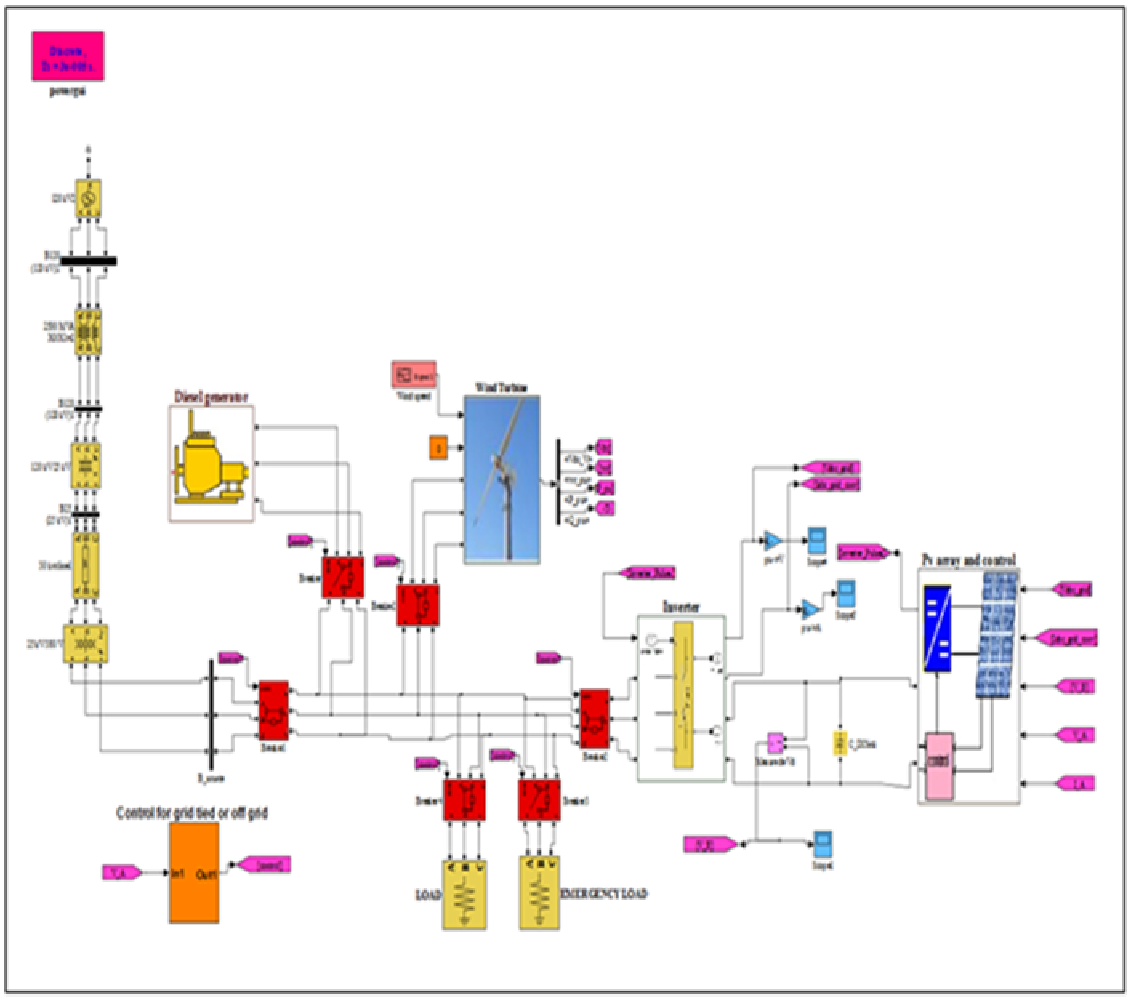

Figure (4.50): Simulink model for Grid tie PV/Wind hybrid system.

In this chapter I discussed the mathematical modeling and simulink of grid tie PV/Wind hybrid system; in the next chapter I will study the simulation of grid tie PV/Wind system.

www.manaraa.com

CHAPTER FIVE

SIMULATION OF GRID TIE PV/WIND HYBRID SYSTEM

www.manaraa.com

Chapter Five
Simulation of Grid Tie PV/Wind Hybrid System

5.1 Grid Tie PV/Wind Hybrid System Constructions

There are two designs for grid tie system:

A-Grid Tie System without Battery:

When the grid is disconnected or in off mode the system will stop working and the inverter disconnect the renewable generators, so in order to cover the load demand we need a diesel generator.

B-Grid Tie System with Battery:

In this system, when the grid is disconnected or on off mode, the system will work isolated from the grid and takes its stability from the battery via converter.

In my thesis, I will study and analyze the first system as shown in figure (5.1) for safety issues in electrical network. This system contain PV array with its controller and inverter, wind turbine system with its controller and inverter, diesel generator, two loads one of them is the main load and the other is the emergency load, and the controller with breakers to check if the grid in off mode or not.

www.manaraa.com

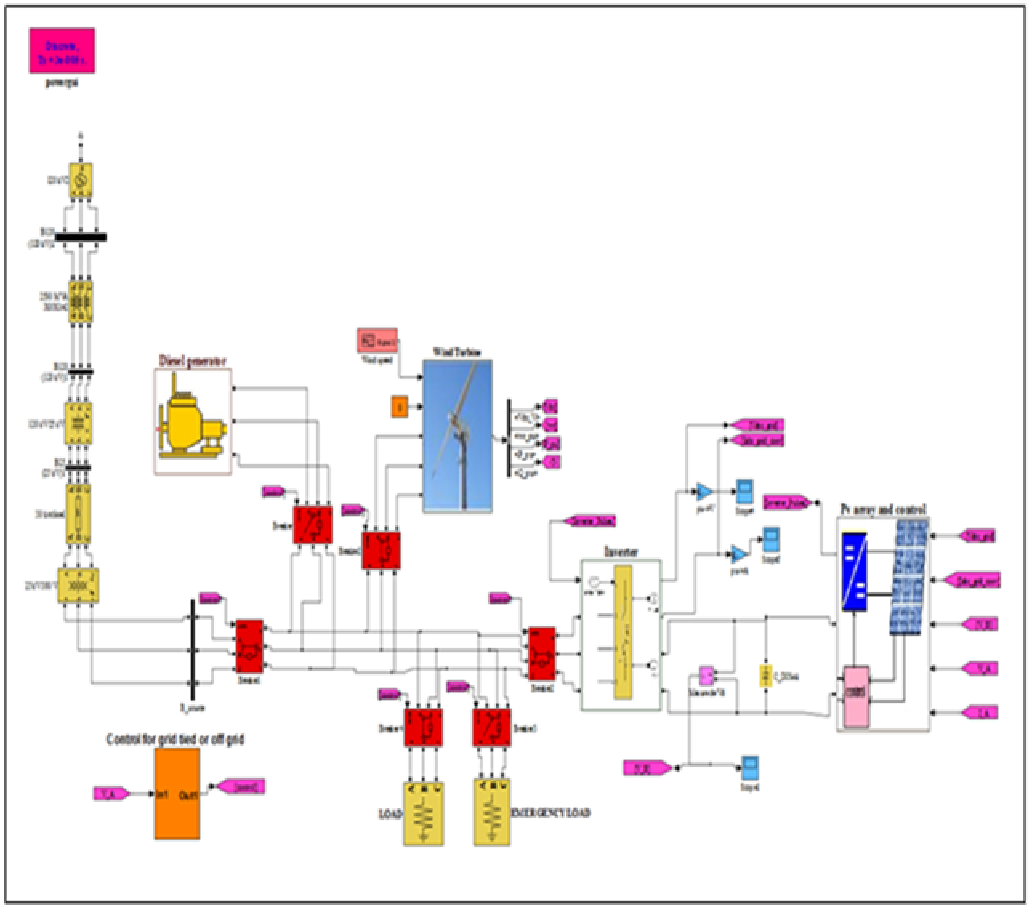

Figure (5.1): Complete grid tie PV/Wind Simulink system

I simulate the grid tie PV/Wind hybrid system for two different conditions:

1- Grid tie hybrid system for different radiations, temperatures, wind speeds and loads (Normal condition).

2- Grid tie hybrid system during on and off grid process.

5.2 Simulation of Grid Tie PV/ Wind Hybrid System

5.2.1 Simulation of the System for Different Radiations.

The system consists of 45kW PV array, 110kW wind turbine and 150kw load. These conditions are applied on the Simulink system to find the performance of it.

www.manaraa.com

1-The input temperature for the PV array is equal 25Cº.

2-The input radiation for PV array is equal 1000 W/m^2 until 8s then change to 500 W/m^2.

3-The input wind speed for wind turbine is equal 15 m/s,

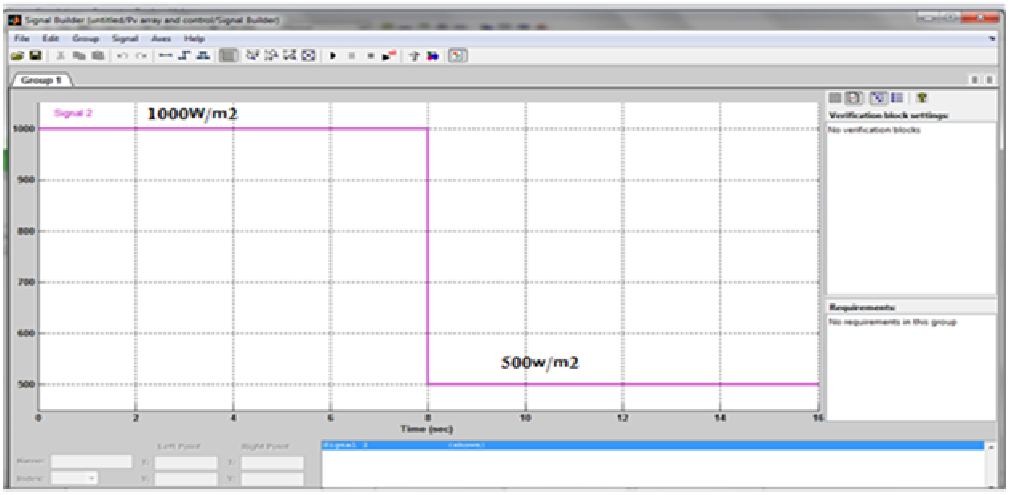

Figure (5.2): Two different input radiations for PV array.

Figure (5.3) shows that the output power from PV array decreases when the input radiation decreases from 1000W/m^2 to 500W/m^2 .

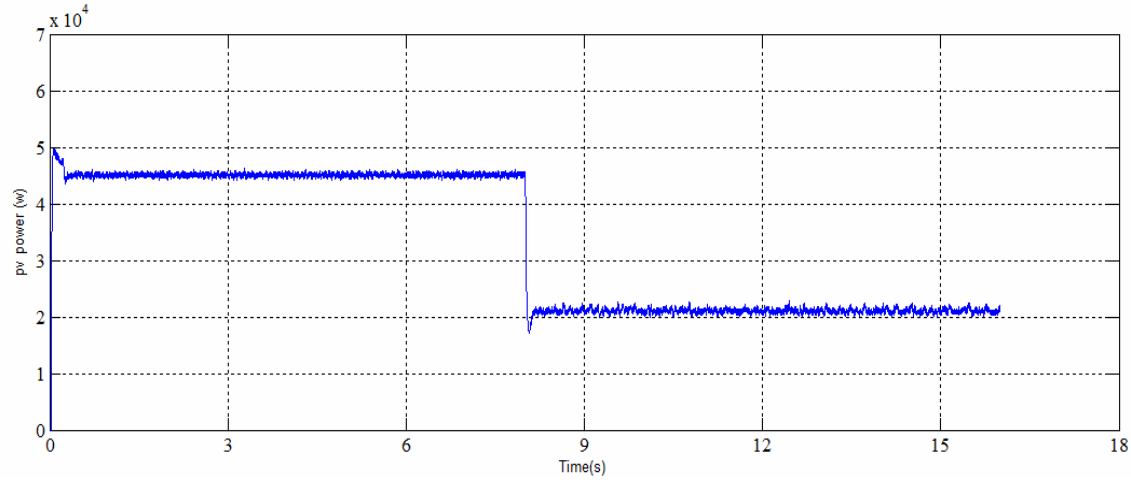

Figure (5.3): PV Inverter power output for two different radiations.

www.manaraa.com

Figure (5.4) shows that the output current from PV array inverter decreases to half when the input radiation decreases from 1000W/m^2 to 500W/m^2 .

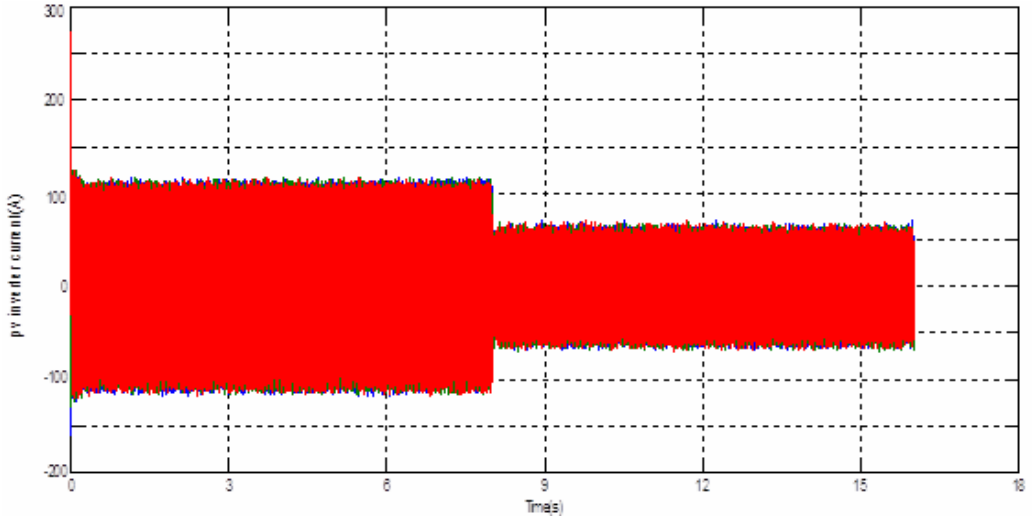

Figure (5.4): Three phase PV inverter current for two different radiations.

Figure (5.5) shows that the voltage is still constant on the input capacitor of the PV inverter when the input radiation decreases from 1000W/m^2 to 500W/m^2 . This happens because of the active power controller of the inverter.

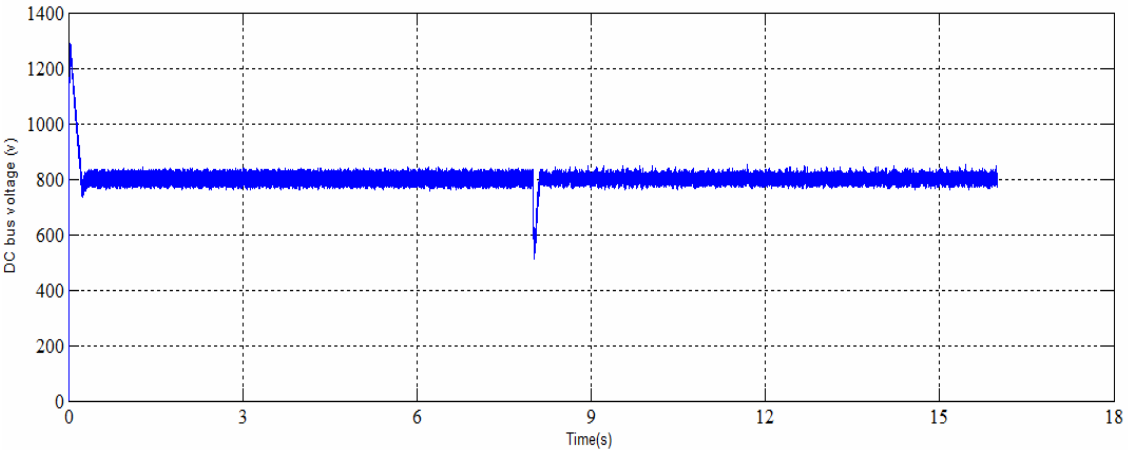

Figure (5.5): PV inverter dc bus voltage for two different radiations.

www.manaraa.com

Figure (5.6) shows that the output power from wind turbine is still constant at 110 kW because the wind speed is constant and equals 15m/s.

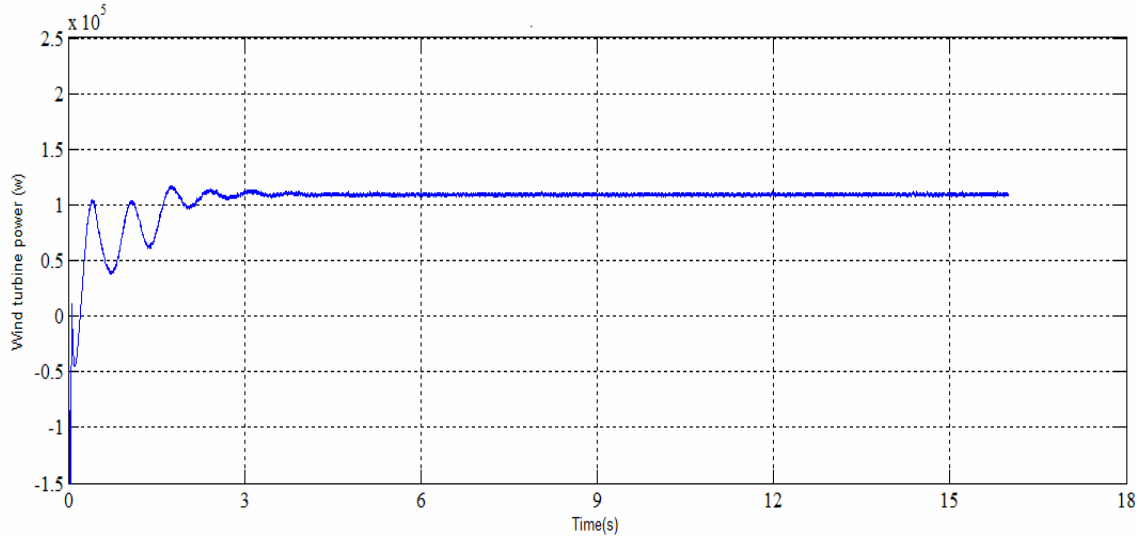

Figure (5.6): Wind turbine output power for the variation of input radiation of pv.

Figure (5.7) shows that the output power from grid is in minus which means that the power from PV and wind turbine is more than the load. This condition lasts 8s, and then the grid power is positive and this means that the grid source the load with power, this happens because of the reduction in solar radiation.

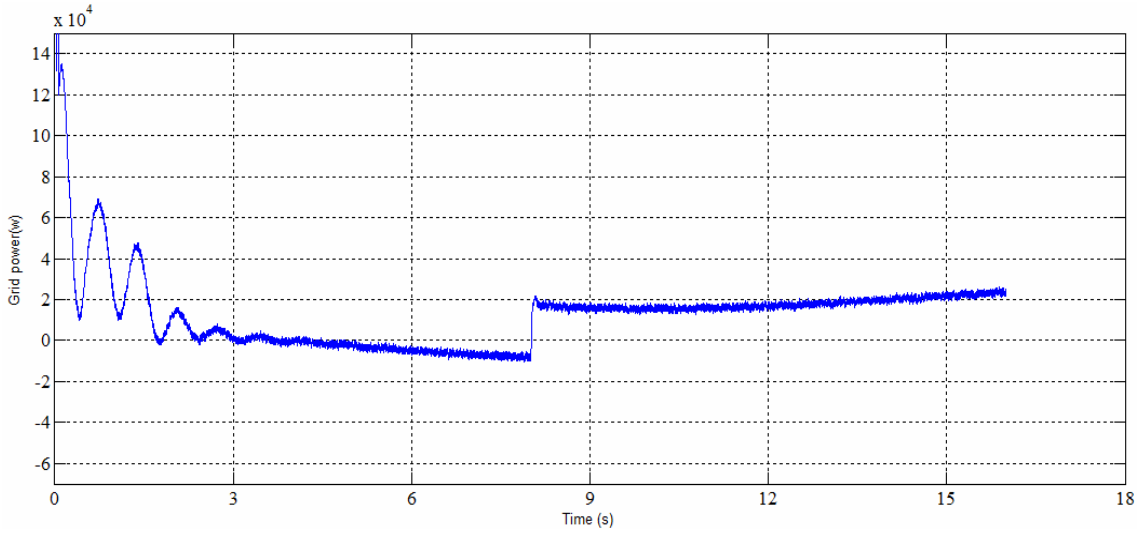

Figure (5.7): Grid power output for two different radiations.

www.manaraa.com

5.2.2 Simulation of the System for Different Temperatures.

The system consists of 45kW PV array, 110kW wind turbine and 150kw load. These conditions are applied to the system to find the system performance.

1-The input temperature of the PV array equals 25ºC until 8s then changes to 50 ºC.

2-The input radiation of PV array equals 1000 W/m^2.

3-The input wind speed for wind turbine equals 15 m/s.

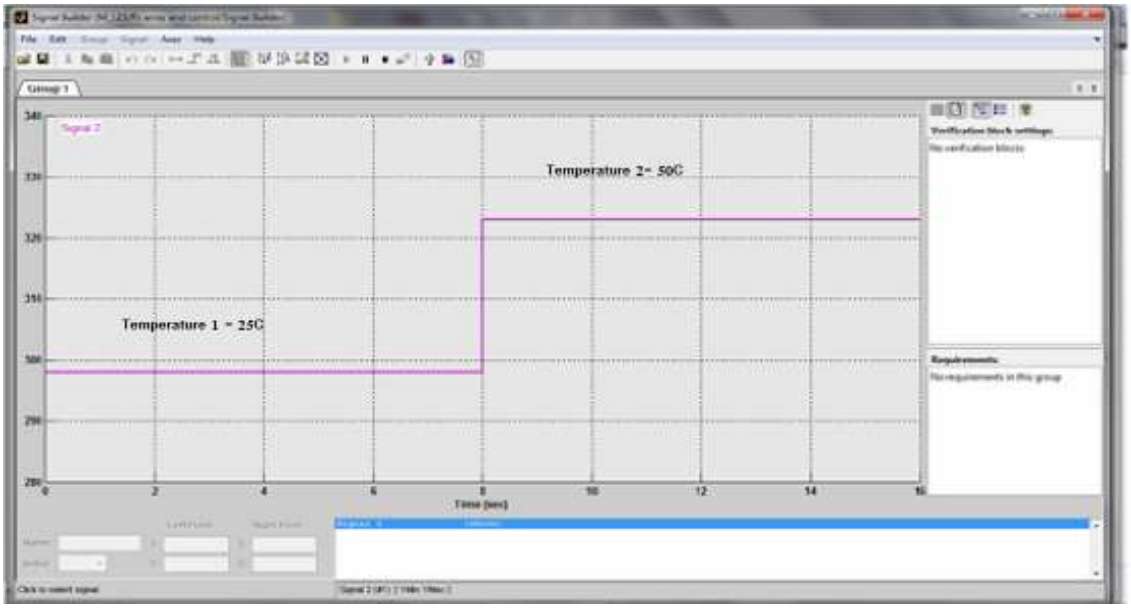

Figure (5.8): Two different input temperatures for PV array.

Figure (5.9) shows that the output power from PV array slightly decreases because the temperature increases from 25 ºC to 50 ºC.

www.manaraa.com

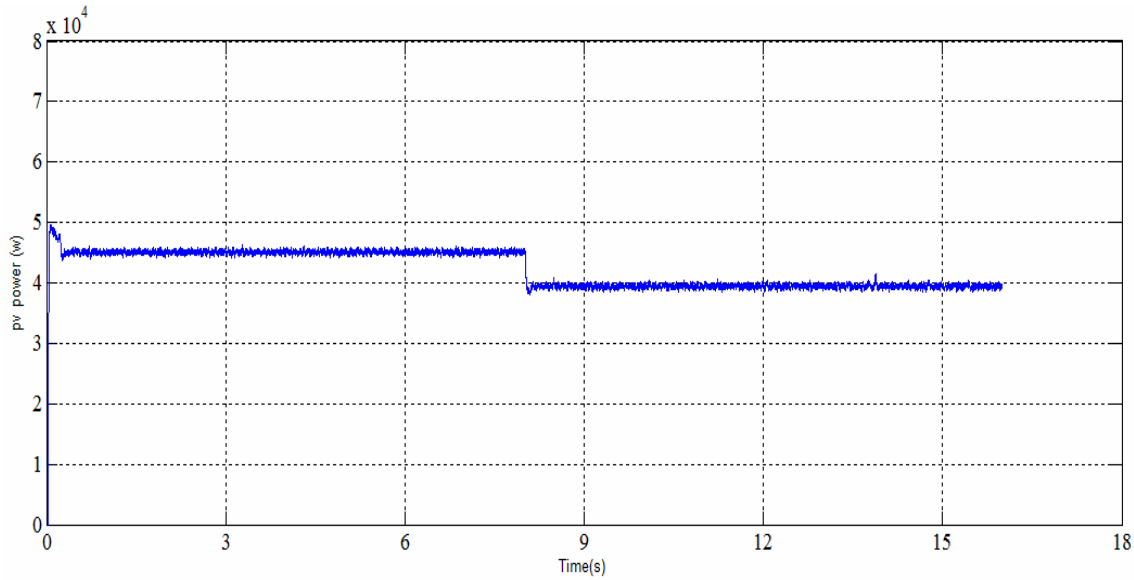

Figure (5.9): PV Inverter power output for two different temperatures.

Figure (5.10) shows that the output current from PV array inverter slightly decreases because the temperature increases from 25 ºC to 50 ºC .

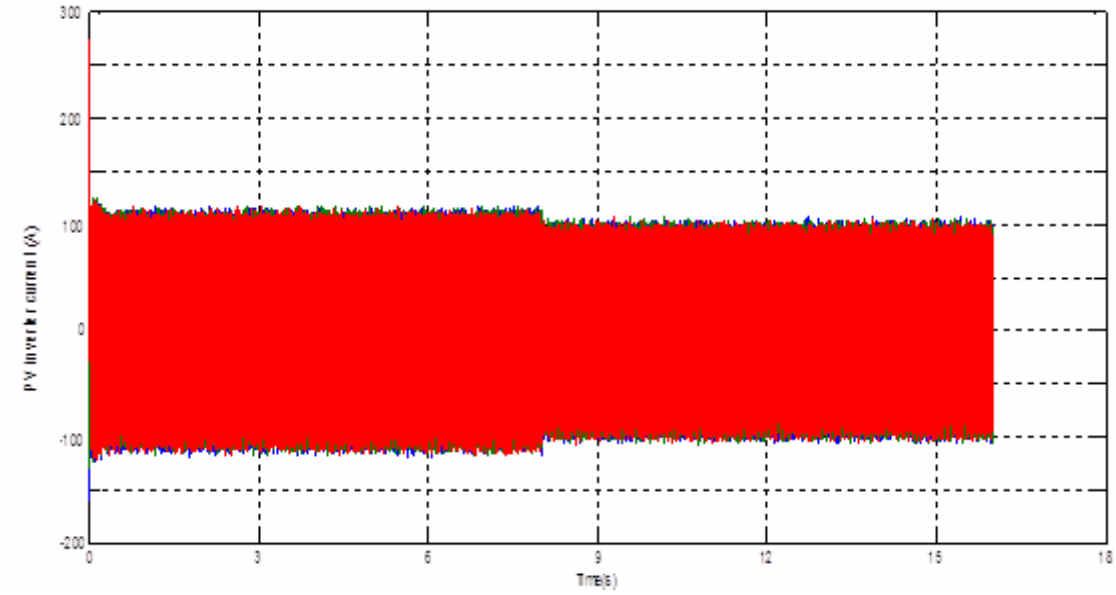

Figure (5.10): Three phase PV inverter current for two different temperatures.

The output power from wind turbine is still constant at 110 kW because the wind speed is constant on15m/s as shown in figure (5.11).

www.manaraa.com

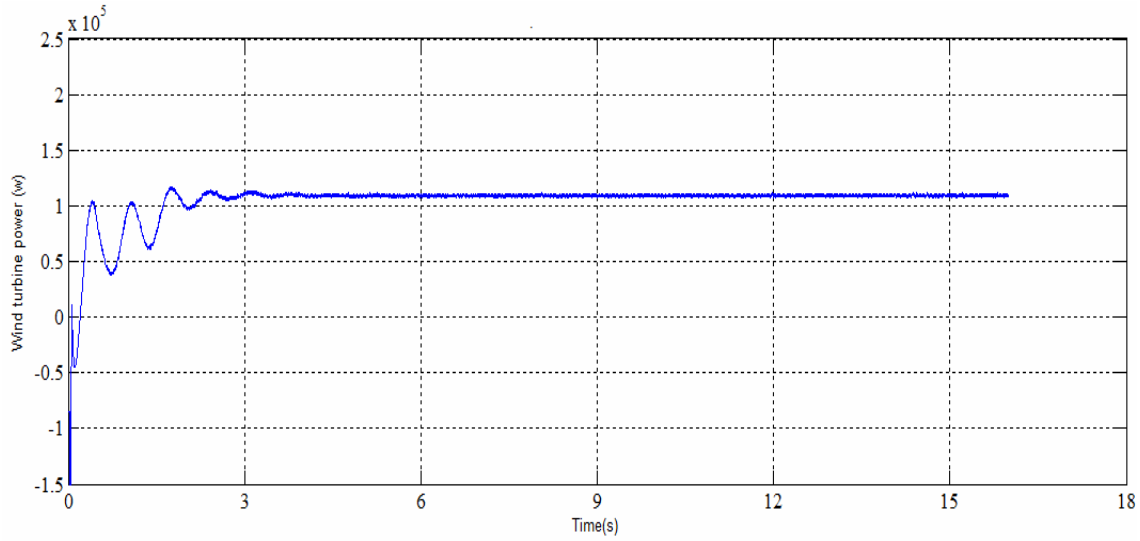

Figure (5.11): Wind turbine power for the variation of input temperature on PV.

Figure (5.12) shows that the grid power sinks about 5kW because the power from PV and wind is more than load, but after 8s the grid power equal zero due to the reduction in PV array power.

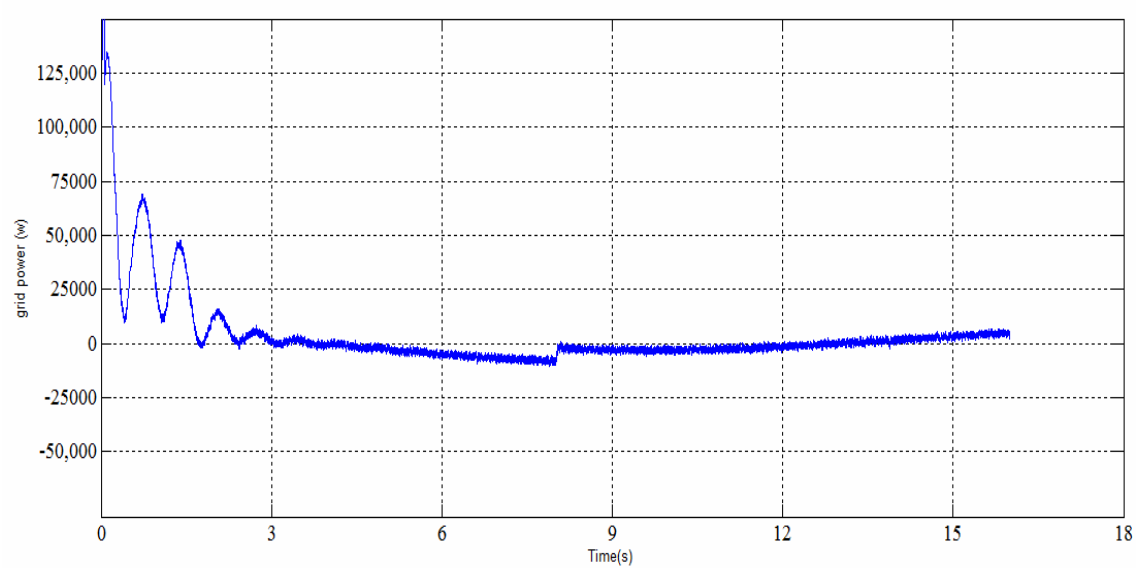

Figure (5.12): Performance of Grid power for two different temperatures.

www.manaraa.com

5.2.3 Simulation of the System for Different Wind Speed

The system consists of 45kW PV array, 110kW wind turbine and 190kw load. These conditions are applied to the system to find the system performance.

1-The input temperature of the PV array equals 25 ºC.

2-The input radiation of the PV array equals 1000 W/m^2.

3-The **input wind speed for wind turbine equals 12 m/s until 7s then changes to 7m/s.**

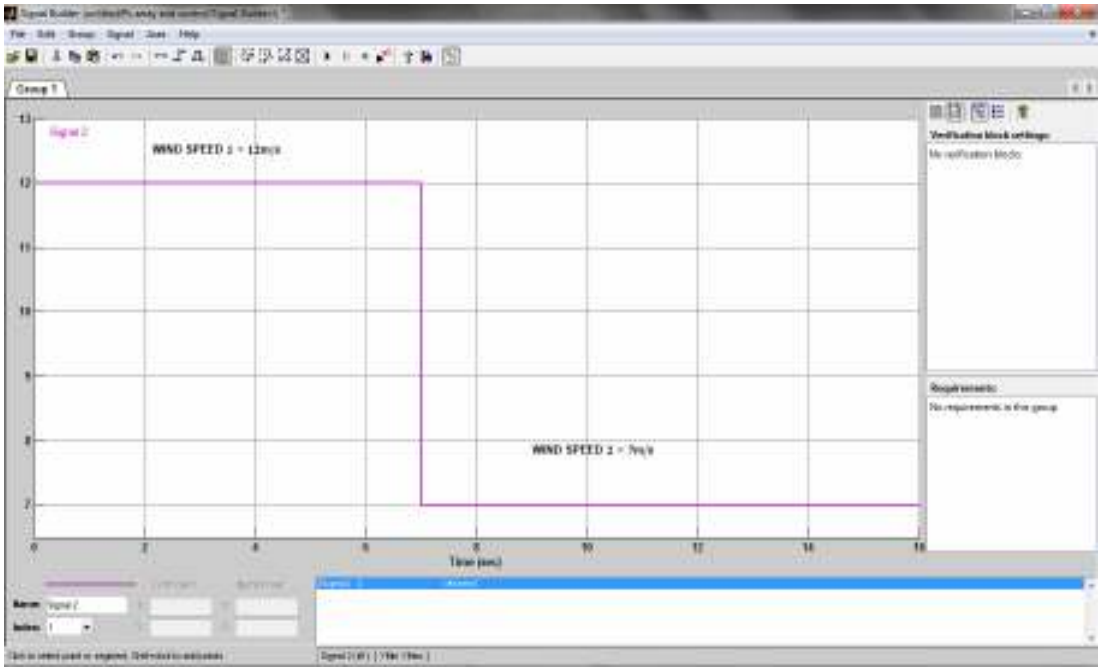

Figure (5.13): Two different input wind speeds for wind turbine.

Figure (5.14) shows that the output power from PV array is still constant at 45 kW because the solar radiation is constant at 1000W/m^2 .

www.manaraa.com

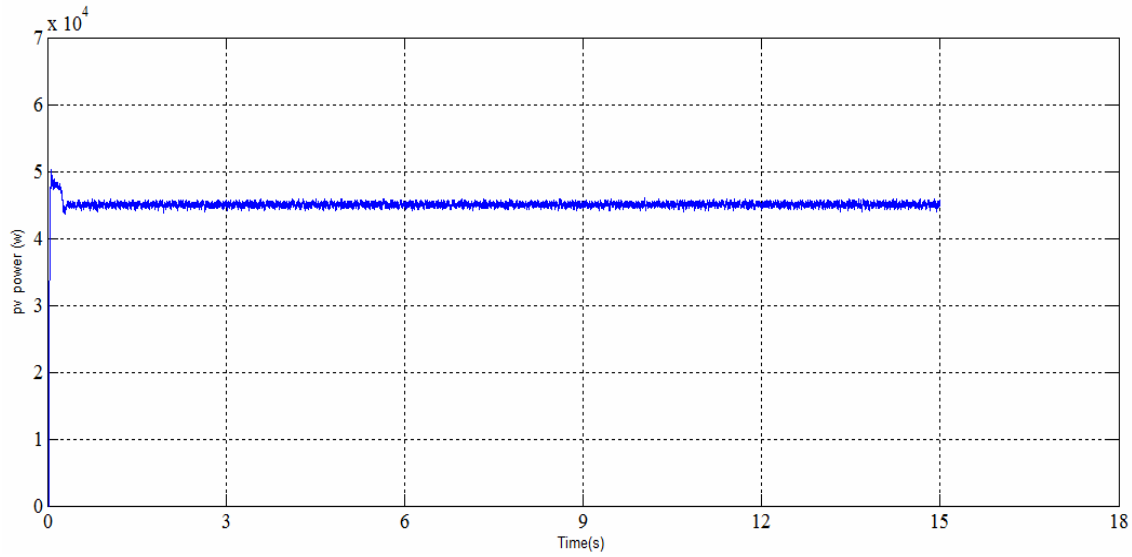

Figure (5.14): PV Inverter power under the variation of wind speed on wind turbine.

Figure (5.15) shows that the output power from wind turbine decreases when the input wind speed decreases from 12m/s to 7m/s .

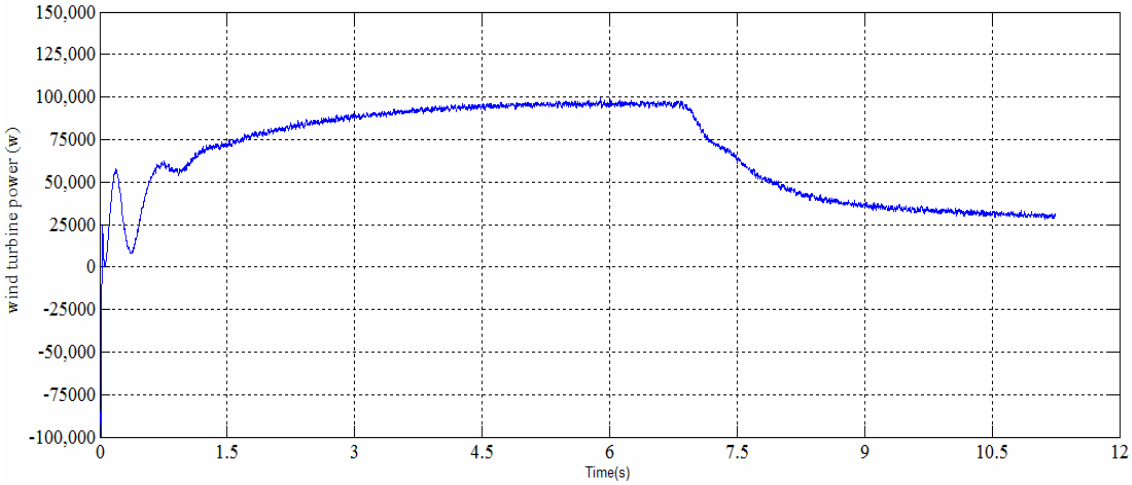

Figure (5.15): Wind turbine power for two different wind speeds.

Figure (5.16) shows that the grid provides about 42kW to the load because the wind resources are less than the load until 7s, and then the grid provides the load with about 120kW, this is due to the reduction of wind speed.

www.manaraa.com

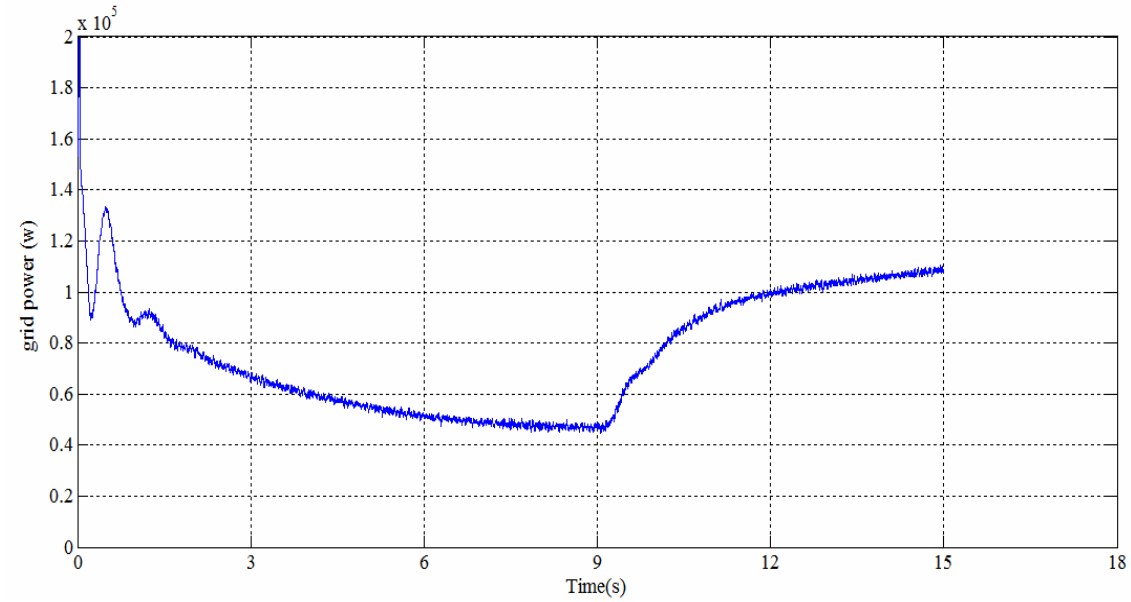

Figure (5.16): Performance of Grid power for two different wind speeds.

5.2.4 Simulation of the System for Different loads

The system consists of 45 kW PV array, 110 kW wind turbine. These conditions are applied to the system to find the system performance.

1-The input temperature of the PV array equals 25 ºC.

2-The input radiation of the PV array equals 1000 W/m^2.

3-The input wind speed for wind turbine equals 15 m/s.

4-The load equals 100 kW for 7s, and then changes to 200 kW.

Figure (5.17) shows that the output power from PV array is still constant because it is not affected by the variation of load.

www.manaraa.com

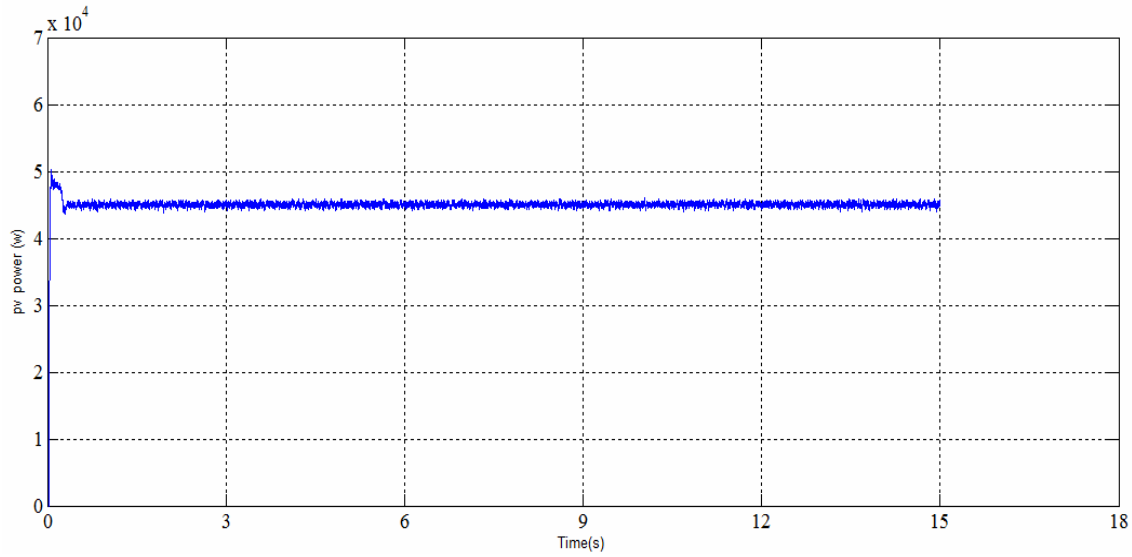

Figure (5.17): PV Inverter power output for two different loads.

Figure (5.18) shows that the output power from wind turbine is still constant because the wind speed is constant at 15m/s .

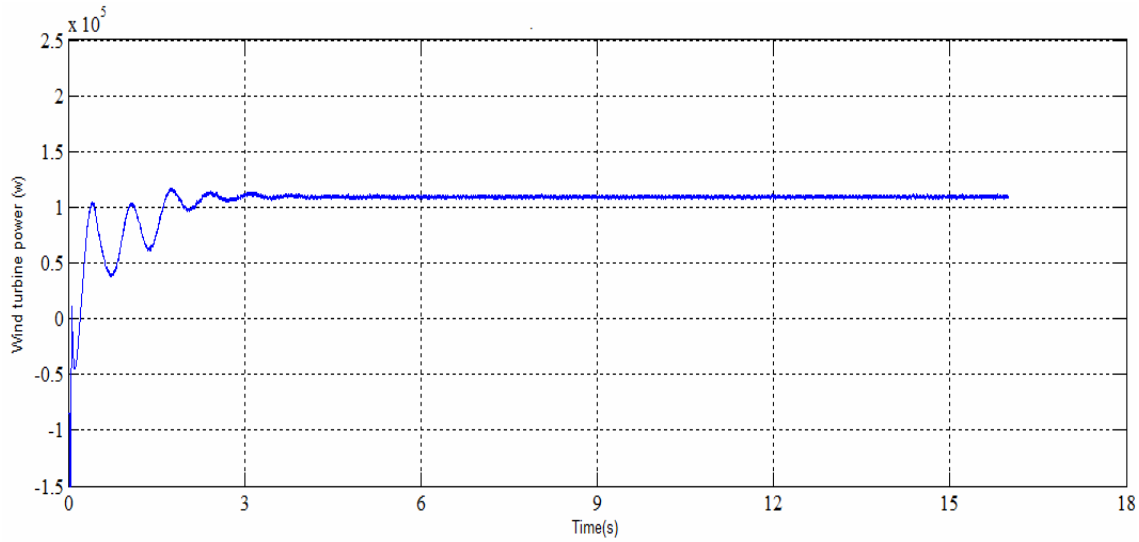

Figure (5.18): Wind turbine power for two different loads.

Figure (5.19) shows that the electrical grid sinks about 55 kW because the renewable resource power is more than the load until 7s, and then the grid power provides the load with 45 kW, this happens due to increase of the load.

www.manaraa.com

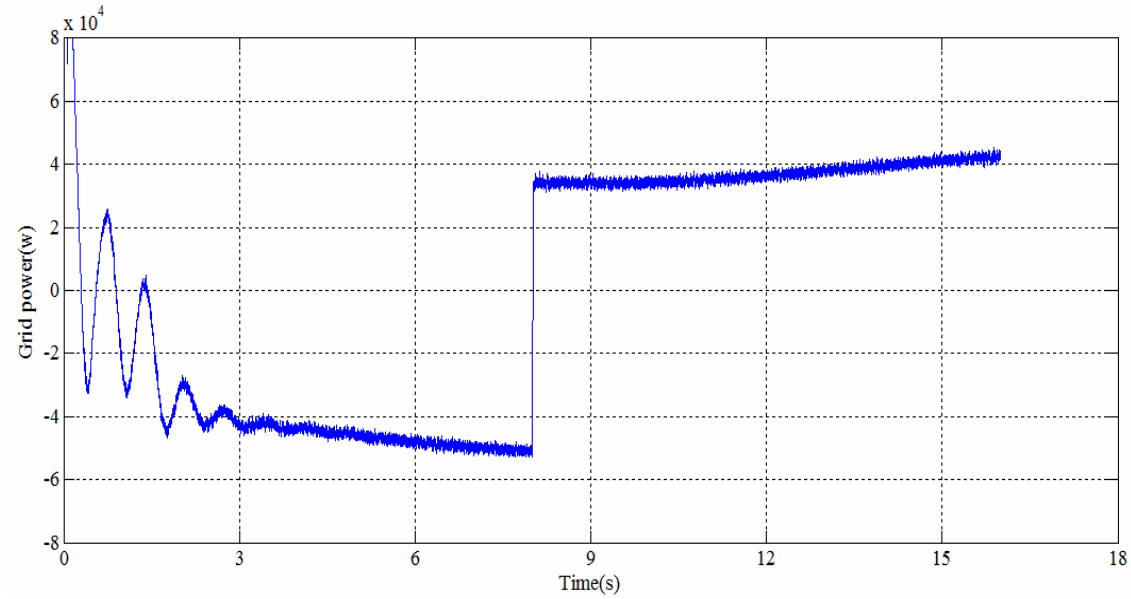

Figure (5.19): Performance of Grid power for two different loads.

5.3 Simulation of the System for On and Off Grid Connection

The system consists of 45kW PV array, 110kW wind turbine, 200kW load, 40kW emergency load and 100kW diesel generator. These conditions are applied to the system to find the system performance.

1-The input temperature of the PV array equals 25 ºC.

2-The input radiation of the PV array equals 1000 W/m^2.

3-The input wind speed for wind turbine equals 12 m/s.

Figure (5.20) shows that the output power from PV array is still 45 kW for 7s, and then from 7s to 13s the PV power equals zero because the grid is at off mode, so the controller disconnects the PV array. After 13s the grid is at on mode so the controller reconnects the PV array.

www.manaraa.com

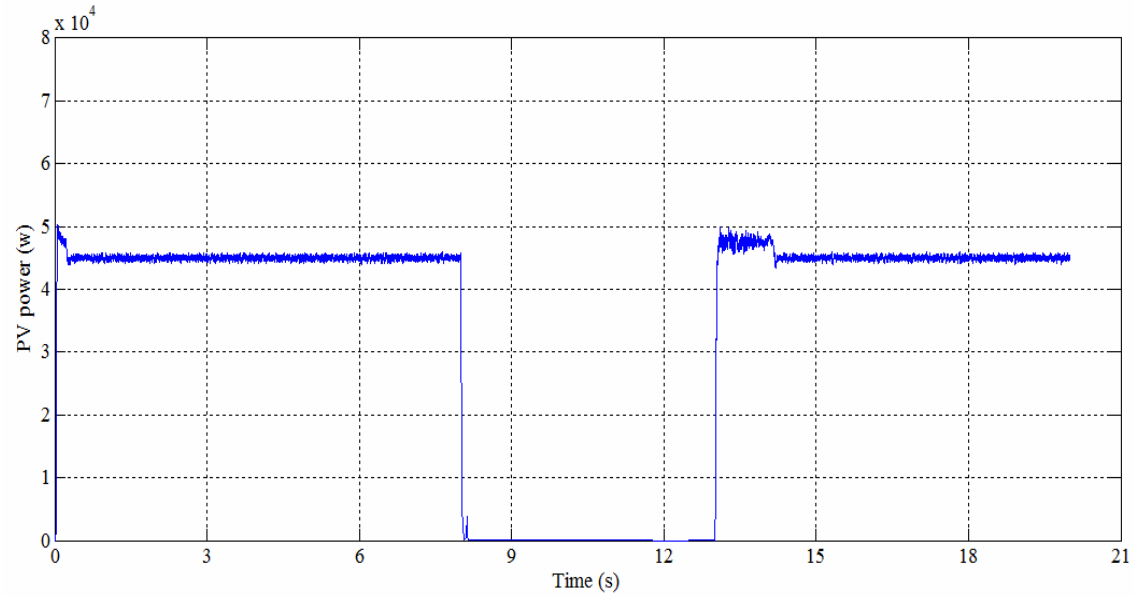

Figure (5.20): PV Inverter power output for on and off grid.

Figure (5.21) shows that the capacitor voltage of the PV inverter is still constant at 800v for 7s, and then from 7s to13s the voltage equals zero because the grid is at off mode, so the controller disconnects the PV array. After 13s, the grid is at on mode so; the controller reconnects the PV array. The increase in voltage is due to the reconnection of PV array to the grid, but this increase lasts about one second, and then the controller stabilized the voltage again to 800v.

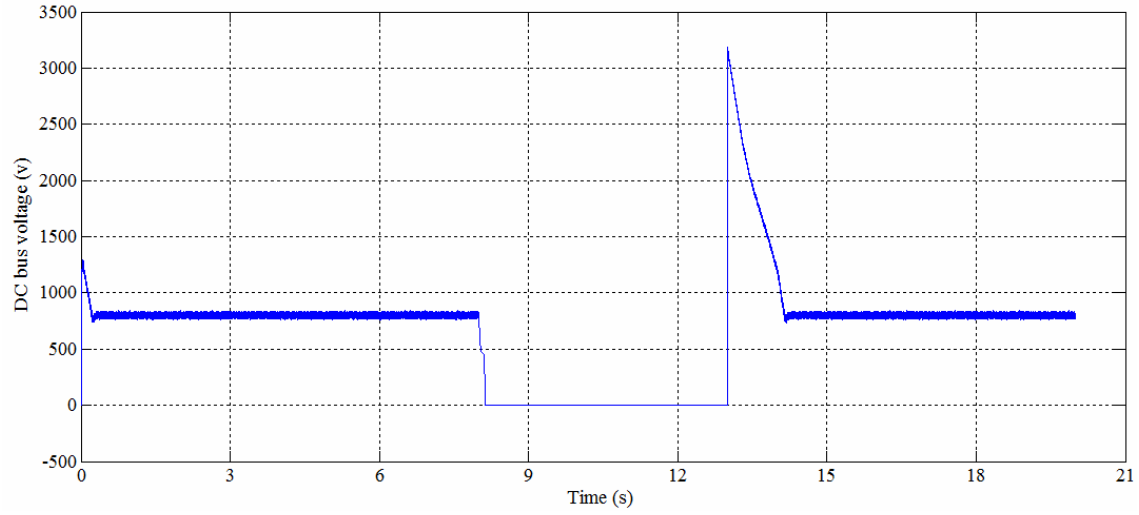

Figure (5.21): PV inverter dc bus voltage for on and off grid.

www.manaraa.com

Figure (5.22) shows the value of PV inverter current at on and off grid

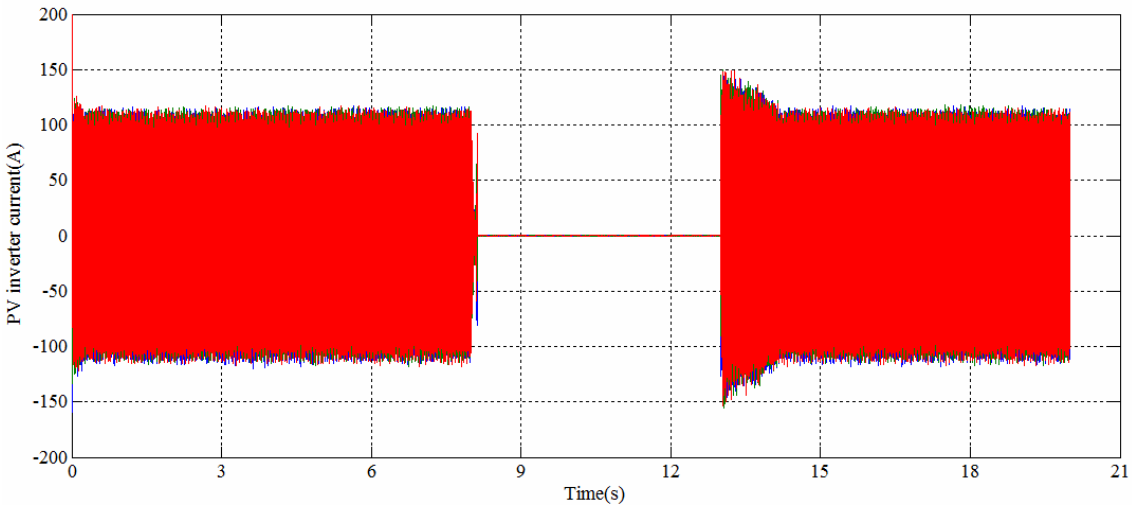

Figure (5.22): Three phase PV inverter current for on and off grid.

Figure (5.23) shows the value of grid voltage for on and off grid

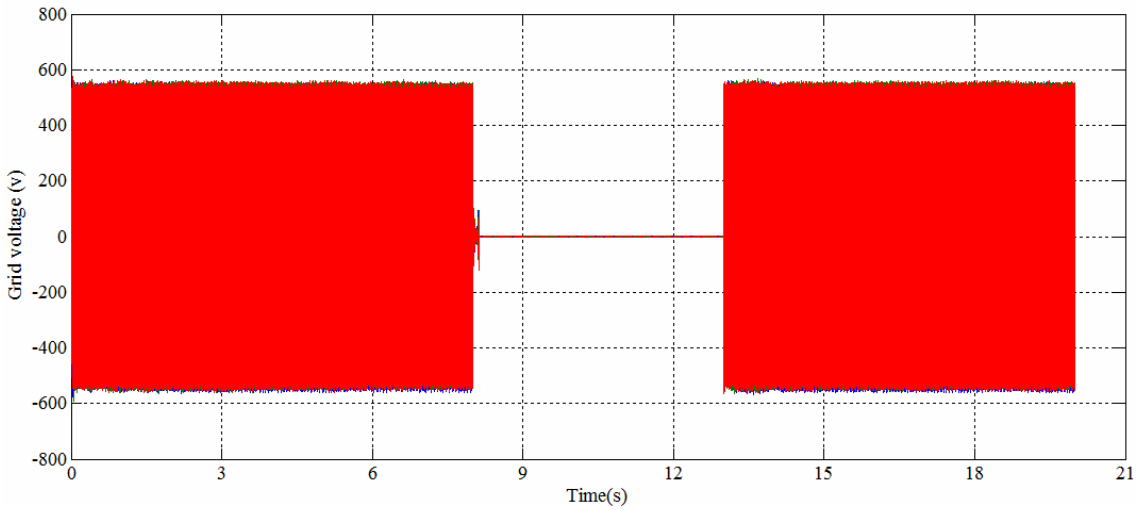

Figure (5.23): Three phase grid voltage for on and off grid.

Figure (5.24) shows the value of power at on and off grid.

www.manaraa.com

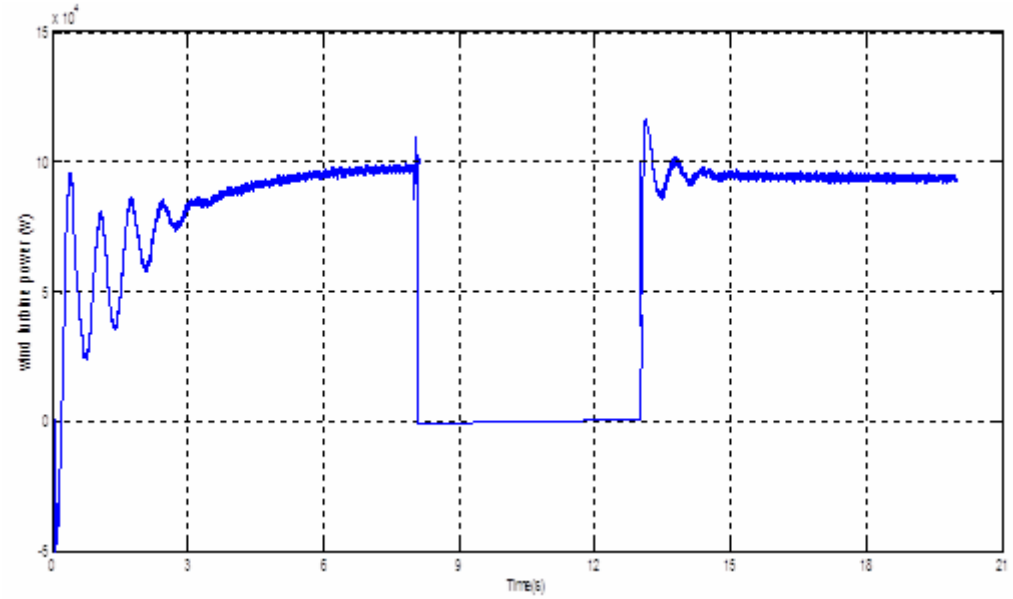

Figure (5.24): Wind turbine output power for on and off grid

Figure (5.25) shows the performance of grid power source for on and of grid, the grid sources the load with about 50kW at on grid and zero at off grid.

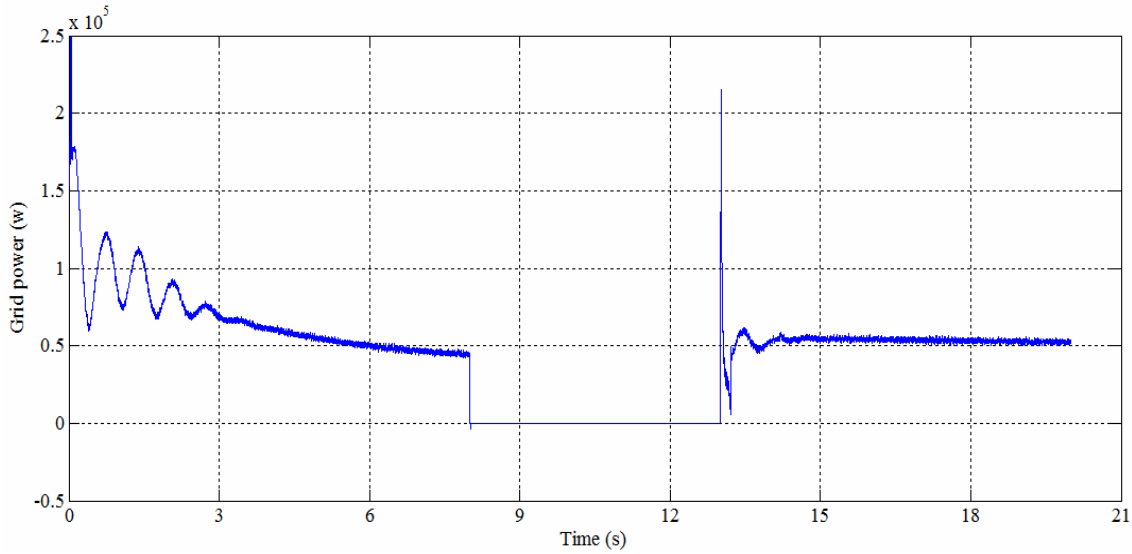

Figure (5.25): Performance of Grid power for on and off grid.

Figure (5.26) shows the pu diesel generator mechanical power at on and off grid. When the grid is at on mode, the mechanical power of diesel generator equals zero, but if the grid is at off mode, the pu of diesel

www.manaraa.com

generator mechanical power will equal 0.4 because the controller connects 40kW emergency load to 100kW diesel generator.

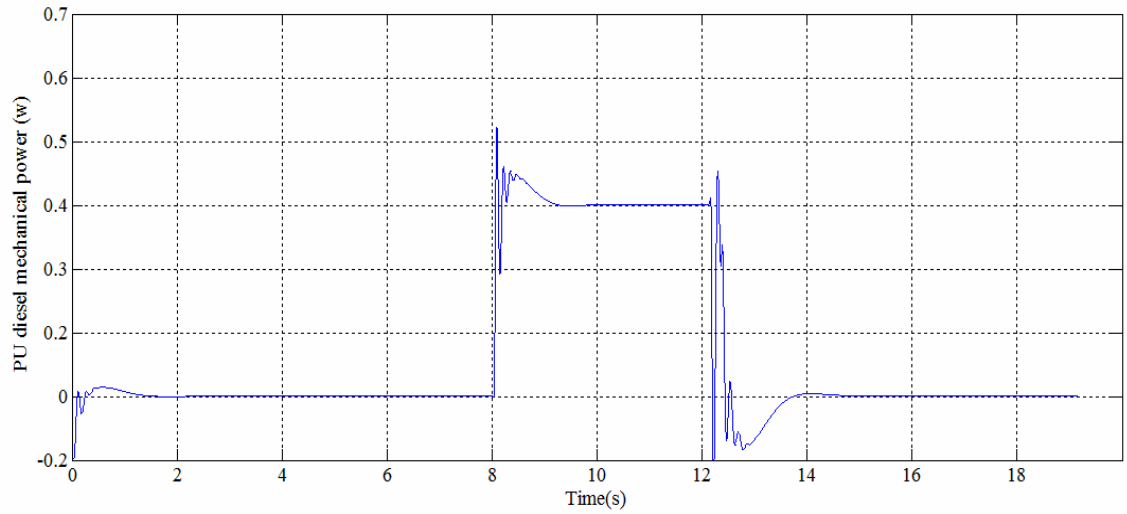

Figure (5.26): pu diesel generator mechanical power for on and off grid.

www.manaraa.com

CHAPTER SIX

DESIGN AND SIMULATION OF ATOUF GRID TIE PV SYSTEM

www.manaraa.com

Chapter Six

Design and Simulation of Atouf Grid Tie PV System

6.1 Introduction about Atouf Village

Depending on a comprehensive assessment for electrified Villages which have PV array, Atouf was found to be one of the most appropriate villages to be subjected to a techno-economic analyses study on a grid tie PV system [5].

Figure (6.1): Picture for Atouf village

Atouf is located in the Jordan valley (West of Jordan valley) at the coordinates 32°15/N and 35°30/E and near Tamun town Map (6.1). Its inhabitants work mainly in farming and cattle breeding. The population amounts to about 200 living in 21 houses. A mosque, clinic and school are available in Atouf. Drinking water is obtained from artesian wells in the village area [5].

www.manaraa.com

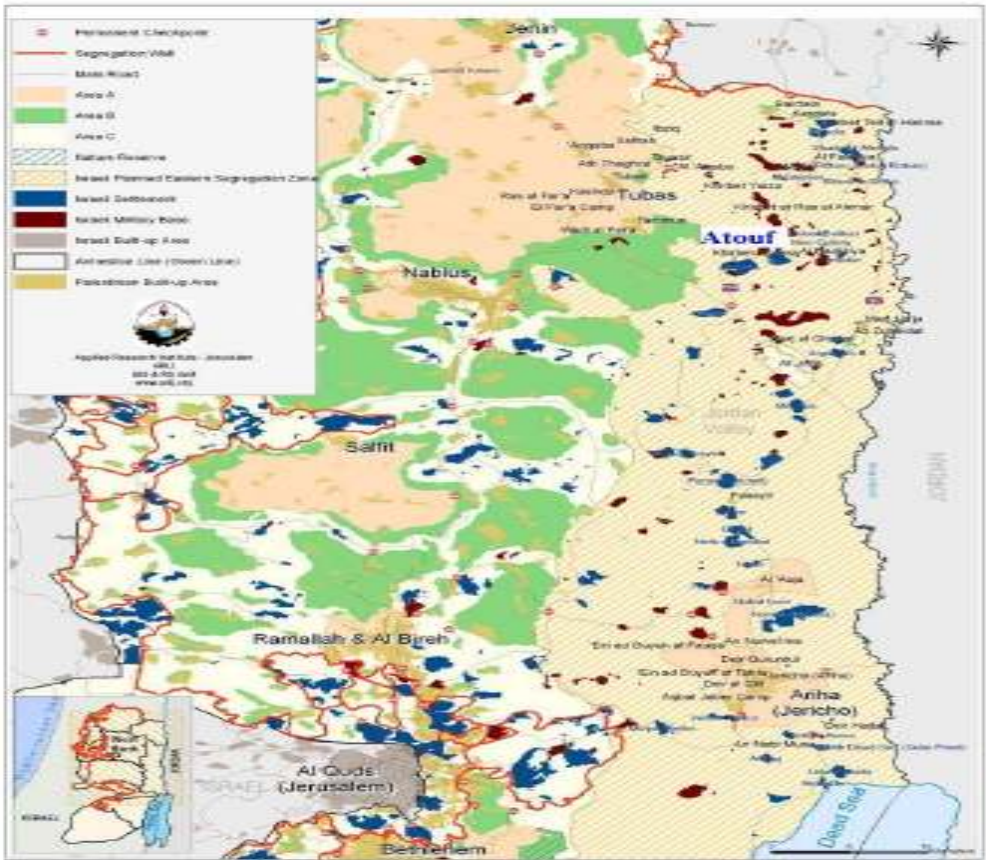

Map (6.1): Location of Atouf village.

The daily energy needs in such villages are very low. The households use mainly wood and biomass for cooking and baking bread.

The village is connected to the nearest high voltage grid (33kV) in Tamun town which is 10 km far from the village. Most houses of the village have solar water heaters, which is enough to cover the total daily hot water needs [30].

6.2 Potential of Solar Energy of Atouf Village

The solar radiation data has a great effect on the performance of photovoltaic (PV) systems. Figure (6.2) shows the monthly values of solar energy.

www.manaraa.com

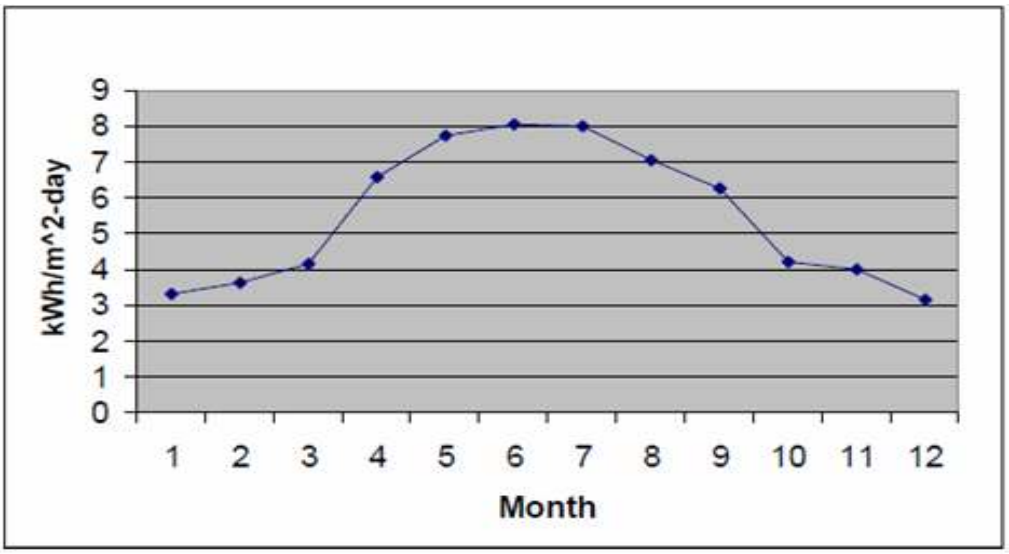

Figure (6.2): The monthly average value of solar energy in Atouf village [13].

It is clear from the figure that solar energy in this region is very high during summer months, when it exceeds 8kWh/m^2/day, while the lowest average intensity is during January with a value of 3.2kWh/m^2/day.

The village has around 3000 sun shine hours per year. The annual average temperature amounts to 22 ^{o}C while it exceeds 37 ^{o}C during summer months [9].

6.3 Energy Demand and Electrical Grid of Atouf Village

The electrical load in the village is mainly concentrated at night since the people work during the day in the fields and cattle pasture. The main electrical loads in the village are: house hold appliances (lighting, TV, refrigerator, radio, washing machine and fan), street lighting (sodium lamps), school appliances (lighting, educational TV and lab equipment).

www.manaraa.com

6.4 Current Situation of Consumers Connections

Atouf village is connected with municipality grid with 100KVA transformer 33KV/0.4KV as shown in figure (6.3).

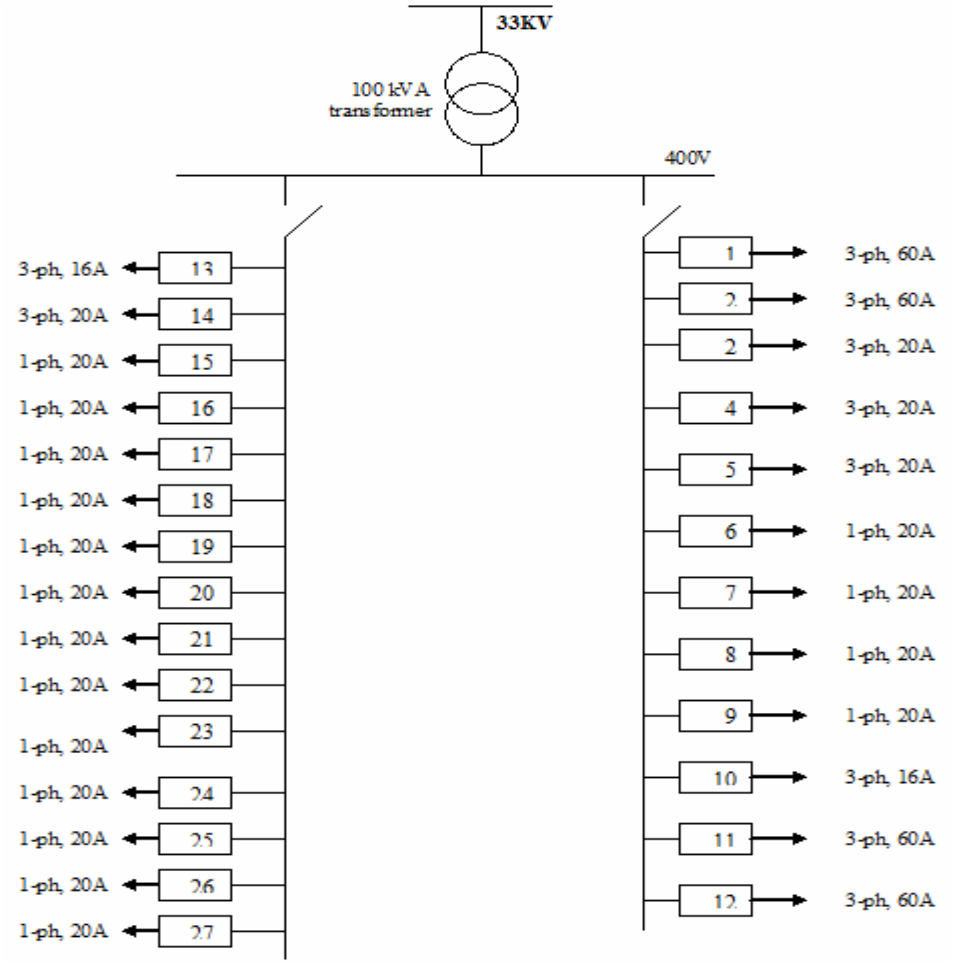

Figure (6.3): Atouf main distribution board [13].

The village has unconnected 90 PV modules (135Wp for each) and 20KVA diesel generator as shown in figure (6.4) and (6.5).

www.manaraa.com

Figure (6.4): Diesel generator used in Atouf village.

Figure (6.5): Atouf PV array (90 modules 135Wp).

Map (6.2) shows the electrical network of Atouf village.

www.manaraa.com

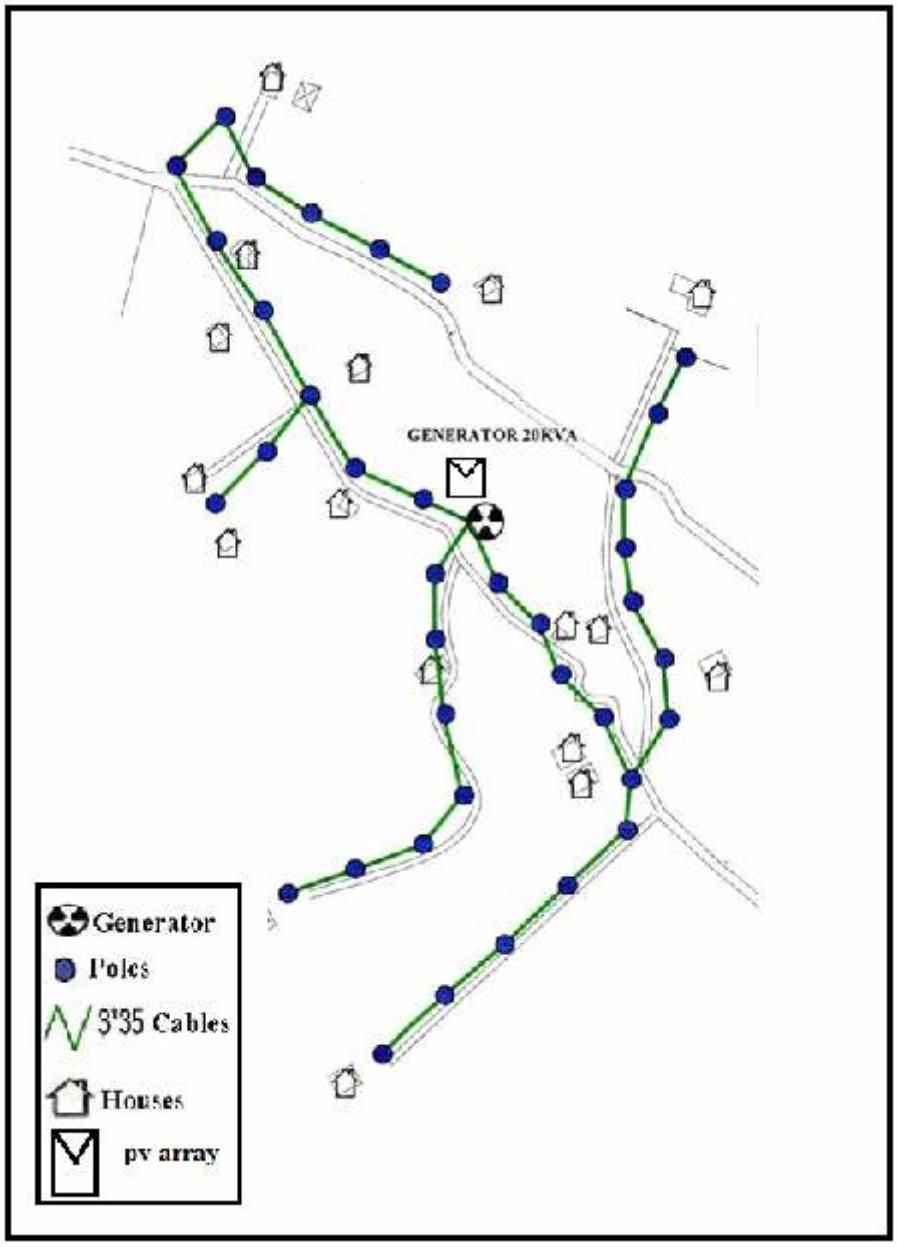

Map (6.2): Electrical network in Atouf village [5].

6.5 Design of Grid Tie PV System for Atouf Village

6.5.1 Electricity Consumption for Atouf Village

The electrical load in the village is mainly concentrated at night, so electricity consumption in Atouf village is not high compare to other villages as shown in table (6.1) and figure (6.6).

www.manaraa.com

Table (6.1): Monthly Energy consumption of Atouf village [13].

Month	Energy consumption (kWh)
January	2316
February	2124
March	2576
April	2891
May	3020
June	3637
July	4624
August	6346
September	4982
October	3210
November	2894
December	2267
Total	40887

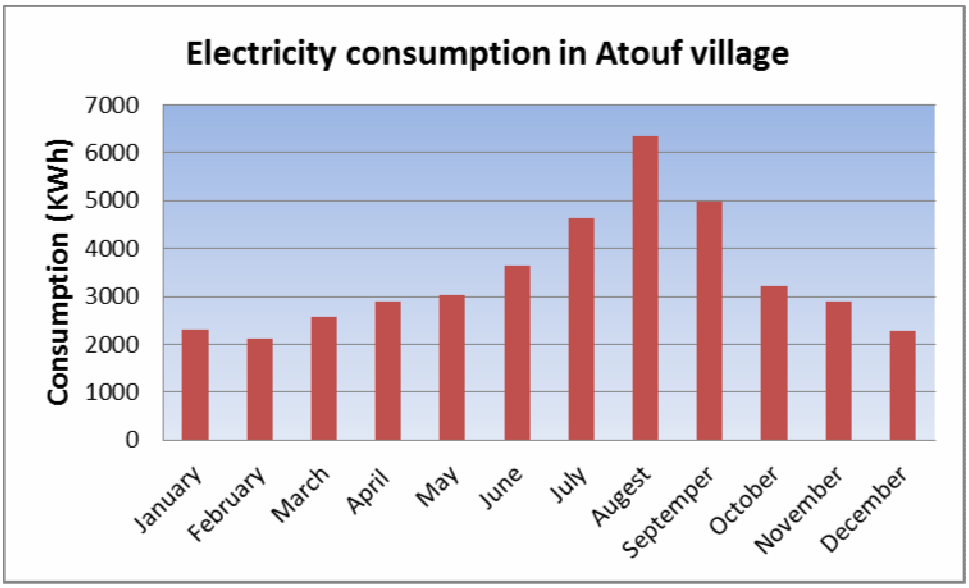

Figure (6.6): Monthly electricity consumption in Atouf village.

6.5.2 Design Grid Tie PV System at 100% penetration

A) PV Array Sizing

The peak power (Wp) of the PV generator is obtained from the equation (6.1):

www.manaraa.com

$$P_{PV} = \frac{E_L}{\eta_V \eta_R PSH} S_f \qquad (6.1)$$

Where

E_L : Energy consumption per day =40887/365 = 112 kWh

η_v : Inverter efficiency (grid tie inverter efficiency = 0.95)

η_R : Charge controller efficiency (because of grid tied inverter so this efficiency omit from the equation).

PSH : (the peak sun hours) = 5.587

S_F :(the safety factor =1 because of grid tied and it not necessary to put safety factor).

$$P_{PV} = \frac{112}{0.95 * 5.578} * 1 = 21 \text{ KW}_P$$

To obtain this peak value, we select a multicrystalline-36 cells module (KD135SX) of a 1m² area, rated at 12 VDC, and P_{mpp}=135 W_P as shown in (appendix B). The number of necessary PV modules is obtained as:

$$No._{PV} = \frac{P_{PV}}{P_{mpp}} \qquad (6.2)$$

$$No._{PV} = \frac{21000}{135} = 156 \text{ PV modules}$$

We select the voltage of the PV generator to be =280V, so number of modules in series is obtained as:

www.manaraa.com

$$No._{PVS} = \frac{V_{PV}}{V_{mpp}} = \frac{280v}{17.7} = 16 \text{ modules}$$

$$\text{And number of strings} = \frac{No._{PV}}{No._{PVs}} = \frac{156}{16} = 9.75 \approx 10$$

The configuration will be as shown in Figure (6.1). The area of the array is (0.668*1.5) (16*10) = 160.3 m²

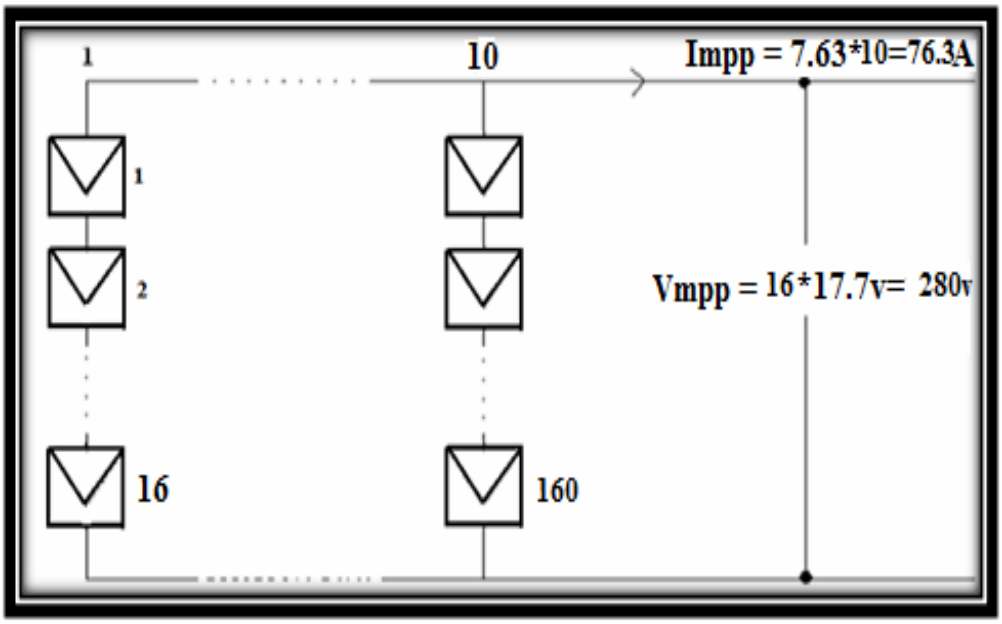

Figure (6.7): The configuration of PV generator for Atouf village at 100% penetration

B) Inverter Sizing

In order to size the grid tied inverter suitable to PV system the main parameters should be determined from (appendix B):

- V_{input} should be located in the inverter MPPT voltage range (DC100~500V) and V rated = 280v.

www.manaraa.com

- V_{output} should fulfill the specification of the electric grid of the village specified as: V_{rated}=380V ± 5% AC, three phase 50 Hz, sinusoidal wave voltage.
- Power of inverter's size depends on PV array because of grid tied $P_{nominal}$ > 25kW.
- The efficiency = 95% - 97%

6.5.3 Design Grid Tie PV System at 56% penetration

A) PV Array Sizing

As I said previously, Atouf village has 90 module (135Wp), so the power =12.15kW, so I will size the system about this value which is 56% penetration

$$No._{PVS} = \frac{V_{PV}}{V_{mpp}} = \frac{\mathbf{280v}}{\mathbf{17.7}} = \mathbf{16\ modules}$$

$$\textbf{And number of strings} = \frac{No._{PV}}{No._{PVs}} = \frac{\mathbf{90}}{\mathbf{16}} = \mathbf{5.6} \approx \mathbf{6}$$

The configuration will be as shown in Figure (6.1). The area of the array is (0.668*1.5) (16*6) = 96.12 m²

www.manaraa.com

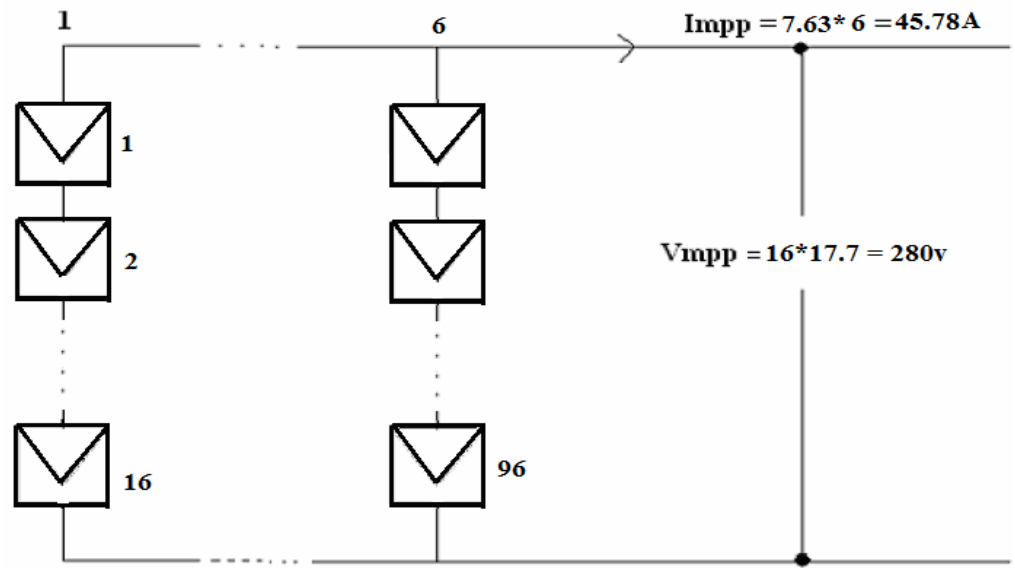

Figure (6.8): The configuration of PV generator for Atouf village at 56% penetration.

B) Inverter Sizing

In order to size the grid tied inverter suitable to PV system the main parameters should be determined from (appendix B):

- V_{input} should be located in the inverter MPPT voltage range (DC250~600V) and V rated = 280v.
- V_{output} should fulfill the specification of the electric grid of the village specified as: V_{rated}=380V ± 5% AC, three phase 50 HZ, sinusoidal wave voltage.
- Power inverter's size depends on PV array because of grid tied $P_{nominal}$ = 12.5kW.
- The efficiency > 92%

www.manaraa.com

6.5.4 Energy Analysis of Grid Tie PV System at 100% penetration for Atouf Village

Analysis of grid tied PV system for different months at 100% penetration shown in Table (6.2), this table contains the output energy produced from 21kWp PV array, energy consumption of the village and the difference between the two energies.

Table (6.2): Monthly energy production versus consumption [13].

Month	PV(kWh)	Consumption(kWh)	differences(kWh)
January	1729.35	2316	-586.6496434
February	2320.382	2124	196.3816112
March	3435.918	2576	859.9183797
April	4019.134	2891	1128.133703
May	5145.677	3020	2125.677294
June	5371.093	3637	1734.093174
July	5008.18	4624	384.1795795
August	4451.597	6346	-1894.40259
September	3796.264	4982	-1185.736469
October	2476.625	3210	-733.3753433
November	1974.014	2894	-919.985804
December	1575.08	2267	-691.9196578
Total	41303.31	40887	416.3142337

Figure (6.9) represent the graphical view of table (6.2).

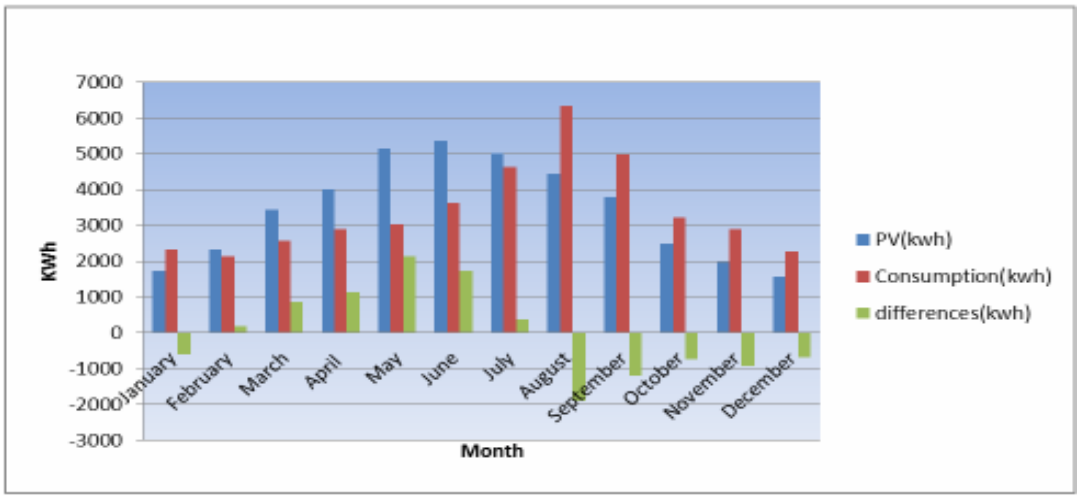

Figure (6.9): Monthly energy production versus consumption.

www.manaraa.com

6.5.5 Energy Analysis of Grid Tie PV System at 56% penetration for Atouf Village

Analysis of grid tied PV system for different months at 56% penetration shown in Table (3.2), this table contains the output energy produced from 21kWp PV array, energy consumption of the village and the difference between the two energies.

Table (6.3): Monthly energy production versus energy consumption [13].

Month	PV(kWh)	Consumption(kWh)	differences(kWh)
January	988.2002	2316	-1327.799796
February	1325.932	2124	-798.0676507
March	1963.382	2576	-612.6180687
April	2296.648	2891	-594.3521696
May	2940.387	3020	-79.61297504
June	3069.196	3637	-567.8039008
July	2861.817	4624	-1762.183097
August	2543.77	6346	-3802.230051
September	2169.293	4982	-2812.706554
October	1415.214	3210	-1794.78591
November	1128.008	2894	-1765.991888
December	900.0459	2267	-1366.95409
Total	23601.89	40887	-17285.10615

Figure (6.10) represent the graphical view of table (6.3).

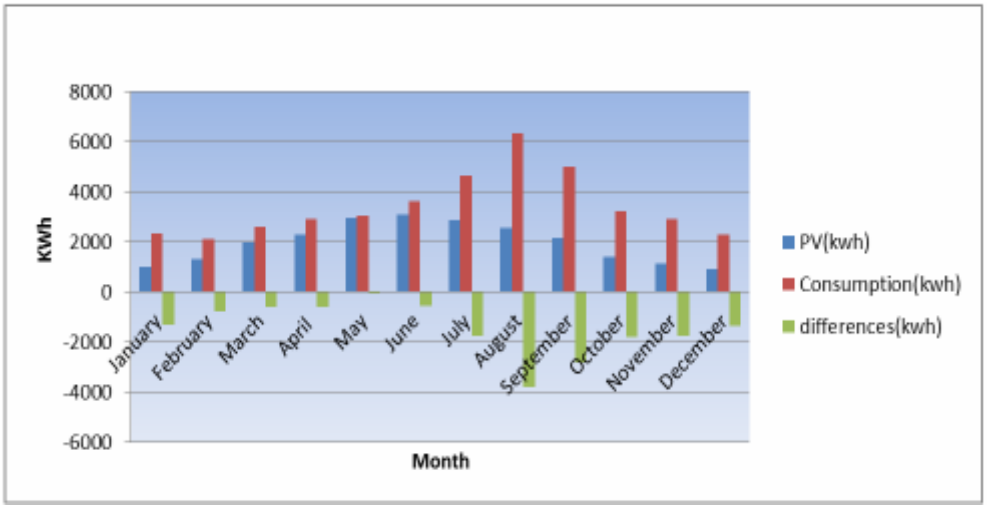

Figure (6.10): Monthly energy production versus energy consumption.

www.manaraa.com

6.6 Simulink Configuration of Atouf village

After designing and sizing all parts of Atouf village, figure (7.11) shows the whole Simulink model, the simulation results for this system for different conditions are in (Appendix F).

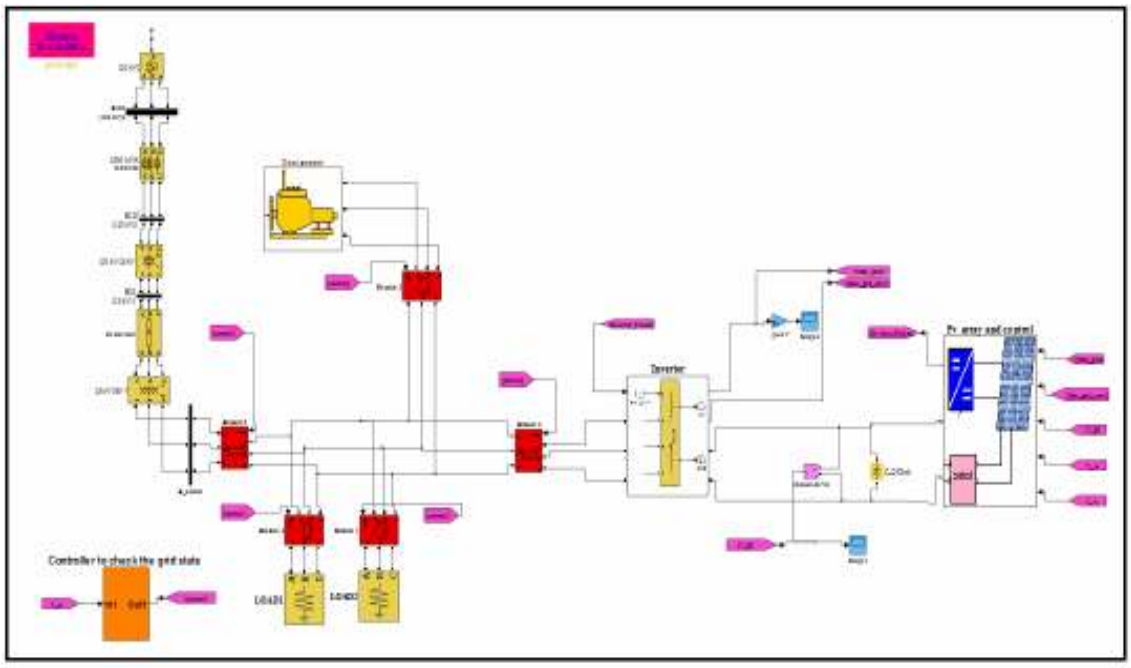

Figure (6.11): Simulink model of Atouf village.

In this chapter, I studied the simulation model of Atouf village, solar energy potential for the village and system sizing; in the next chapter, I will study the economic and environmental impact of grid tie system.

www.manaraa.com

CHAPTER SEVEN

ECONOMIC AND ENVIRONMENTAL IMPACT OF GRID TIE PV/WIND HYBRID SYSTEM

www.manaraa.com

Chapter Seven

Economic and Environmental Impact of the Grid Tie PV/Wind Hybrid System

7.1 Determining the Cost of Producing One kWh from Grid Tie PV/Wind Hybrid System

The economic analysis used in this work is based on the use of life cycle cost, cost annuity (NIS/kWh) and economic impact of grid tie PV/Wind hybrid system.

7.1.1 Life cycle cost (LCC)

The life cycle cost (LCC) is defined as the sum of the PWs of all the components. The life cycle cost may contain elements pertaining to original purchase price, maintenance costs, operation costs, and salvage costs or salvage revenues.

A) Initial Cost of Grid Tie PV/Wind Hybrid System

Initial cost includes purchasing equipment (PV-panels, grid tie inverter, wires and other components used in installation). Also includes labors and technicians costs for installation. These costs depend on the size and type of a component. All these costs are summed to give the overall initial cost.

$$\text{Initial cost} = \sum \text{components cost} + \text{installation cost} \qquad (7.1)$$

www.manaraa.com

Initial Cost of Photovoltaic Modules

PV-modules are available in different sizes and types, the size of PV is characterized by their peak watt at STC (rated power).The price of peak watt is the same for mono or poly crystalline, but the installation or Structure cost will differ depending on the installed PV area. The (NIS/Wp) will decrease as the size of module increases [32].

Initial Cost of Grid Tie PV Inverter

The grid tie inverter available in different sizes and types .The price of the grid tied inverter depend on its capacity, efficiency, contain MPPT controller or not, protection and other parameters[32].

Other Initial Costs

Shipping costs and accessories needed for installation and system protection, wiring, rooms, should be also considered. These costs depend on the system size and vary with the kind of the project; if it for public use (may be land available free), or for private use.

B) Operation and Maintenance Cost of Grid Tie PV/Wind Hybrid system

The operation costs considered are incurred after installation in order to run the system for a certain number of years (system life time).

www.manaraa.com

C) Salvage value

The salvage value is considered as the value of the project elements after the system life time finishes.

Figure (7.1) shows the cash flow which represents the initial, maintenance cost and salvages revenue.

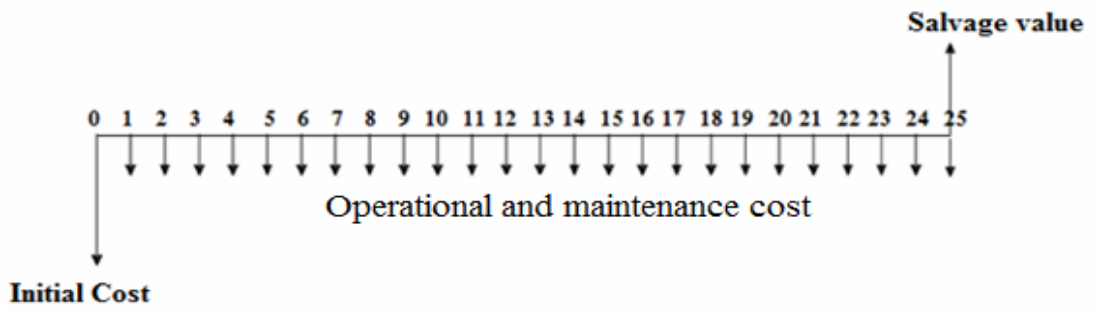

Figure (7.1): The cash flow which represent initial, operational cost and salvage revenue.

7.1.2 Economic Factors

In order to calculate the equivalent uniform annual series (Aw) of cash flow in figure (7.1), the most important fact to remember is to first convert everything to a present worth.

The life cycle cost of grid tie system= initial cost of PV system + present worth of maintenance and operation – present worth of salvage value.

The life cycle cost of grid tie system= initial cost of the system + Operation and maintenance X (P / A, i,n) – salvage value X (P / F, i ,n).

The term A (P/A, i ,n) is called the uniform-series present worth factor.

www.manaraa.com

This expression determines the present worth P of an equivalent uniform annual series A which begins at the end of year 1 and extends for n years at an interest rate i, and (P/A) can be found by equation (7.2):

$$P = A\left[\frac{(1+i)^n - 1}{i(1+i)^n}\right] \qquad i \neq 0 \qquad (7.2)$$

The term F (P/ $F_{i, n}$) is known as the single-payment present-worth factor, or the P/F factor. This expression determines the present worth P of a given future amount F after n years at interest rate i, and (P/F) can be found by equation (7.3):

$$P = F\left[\frac{1}{(1+i)^n}\right] \qquad (7.3)$$

In order to simplify the routine engineering economy calculations involving the factors, tables of factors values have been prepared for interest rates from 0.25 to 50% and time period from 1 to large n values, depending on the interest value 10% and interest table in appendix (D).

The equivalent annual worth AW is obtained with appropriate A/P, as follow: AW = PW (A / $P_{i , n}$)

Then the energy unit price calculated from equation (7.4)

$$(\text{NIS/kWh}) = \frac{\text{Aw}}{\text{Total yearly kWh produced}} \qquad (7.4)$$

www.manaraa.com

7.1.3 Cost of producing one kWh from Grid Tie PV/wind hybrid System for Atouf village

The price of the PV system and its installation are important factors in the economics of grid tied PV systems. These include the prices of PV modules, inverter, and all other auxiliaries as shown in table (7.1). The cost of installation must be taken into consideration.

Table (7.1): Cost of elements and installation of grid tie PV system [13].

Component material or work	Quantity	Price(NIS)	Life time(Year)
PV-module Kyocera	12 KWp	176000	25
Inverter	1	20000	25
Mechanical parts, installation material and various accessories		50000	
Total		246000	

For the present PV system, the life cycle cost will be estimated as follows:

1- The lifecycle of the system components will be considered as 25 years.

2- The interest rate is about 10%.

The initial cost of the PV system = PV array cost + inverter cost + installation cost.

The initial cost of the PV system = 176000+20000+50000 = 246000 NIS.

The annual maintenance and operation costs are about 2% of initial cost which is equal to 196.8 NIS/year, salvage value after 25 years is taken 15% from initial cost and it is equal to 36900 NIS.

www.manaraa.com

The life cycle cost of PV system is obtained by drawing cash flow as in figure (7.2):

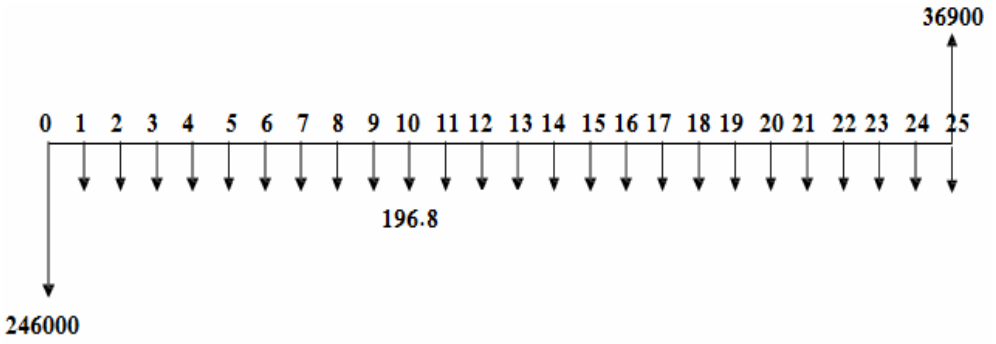

Figure (7.2): Cash flow of grid tie PV system for Atouf village.

The life cycle cost of PV system = 246000 + 196.8(P / A, i,n) – 36900 (P / F, i ,n).

PW = 246000 + 196.8 (P / A 10%, 25) – 36900 (P / F 10%, 25).

The factors in the above equation are taken from appendix (D):

PW = 246000 + 196.8 x 9.0770 – 36900 x 0.0923

= 244380.44 NIS.

AW = PW (A / P i , n) = 244380.44 (A / P 10% , 25).

From appendix (D), the term (A / P 10%, 25) is equal to 0.11017, then:

AW = 244380.44 (A / P 10%, 25)

AW =244380.44 x 0.11017 =26923.4NIS.

www.manaraa.com

The cost of 1 kWh from the PV generator = 26923.4NIS / 23601.3 kWh

= 1.14 NIS/kWh.

7.2 Grid Tie System Tariffs

Electricity delivered to the grid can be compensated in several ways such as net metering or feed-in tariff.

7.2.1 Net Metering Tariff

A solar PV system generates electricity by converting sunlight into electricity that can be used in your home or business. This reduces the amount of electricity you need to purchase from your utility. If your system produces more electricity than you need at any given time, it will actually spin your meter backwards to supply the grid. Your utility keeps track of how much electricity you supply to the grid as well as how much you purchase, and bills you only for your net electricity consumption (via net metering). At the end of any billing period, if overall electricity production exceeds consumption (indicated by a negative meter read), a billing credit is applied to your next bill [31].

www.manaraa.com

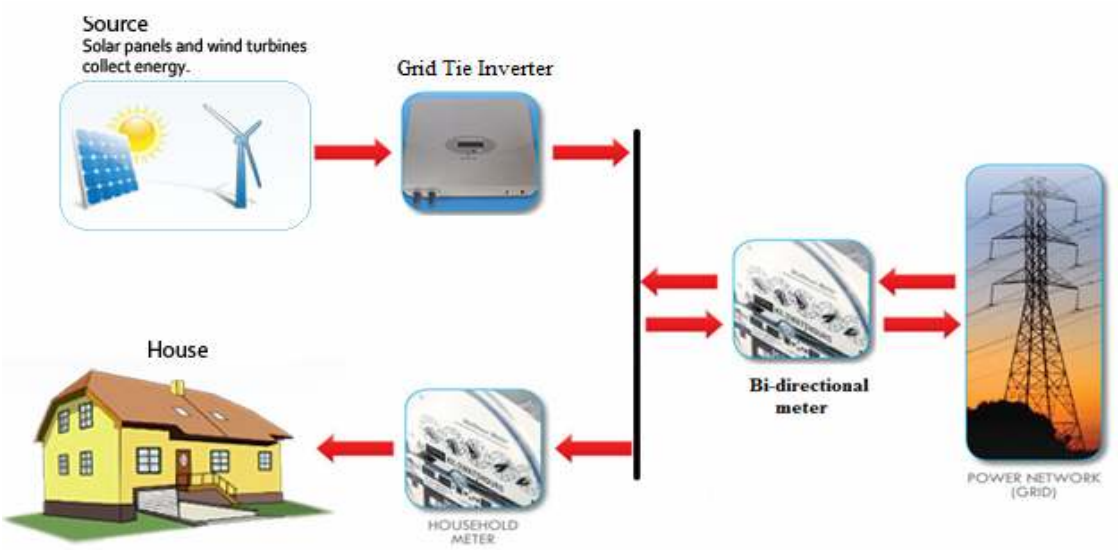

Figure (7.3): Grid tie net metering tariff.

7.2.2 Feed in Tariff

A feed-in tariff (FIT) encourages a new renewable energy development by creating a long-term financial incentive to customers who generate renewable electricity, offering a standardized and streamlined process to do so, and easing the entry for new systems. Under a feed-in tariff, a utility is contractually obligated to connect the renewable energy generator to the grid and pay that generator for electricity at a fixed rate for the life of the FIT contract, typically 10-20 years. The goal of a FIT is to create a robust market for renewable energy to lower technology costs and increase development of such resources for the duration of the program, and potentially pave the way for future growth. The design of FITs can vary considerably in how rates are calculated, eligibility of different technologies and resource sizes, and the contract terms [31].

www.manaraa.com

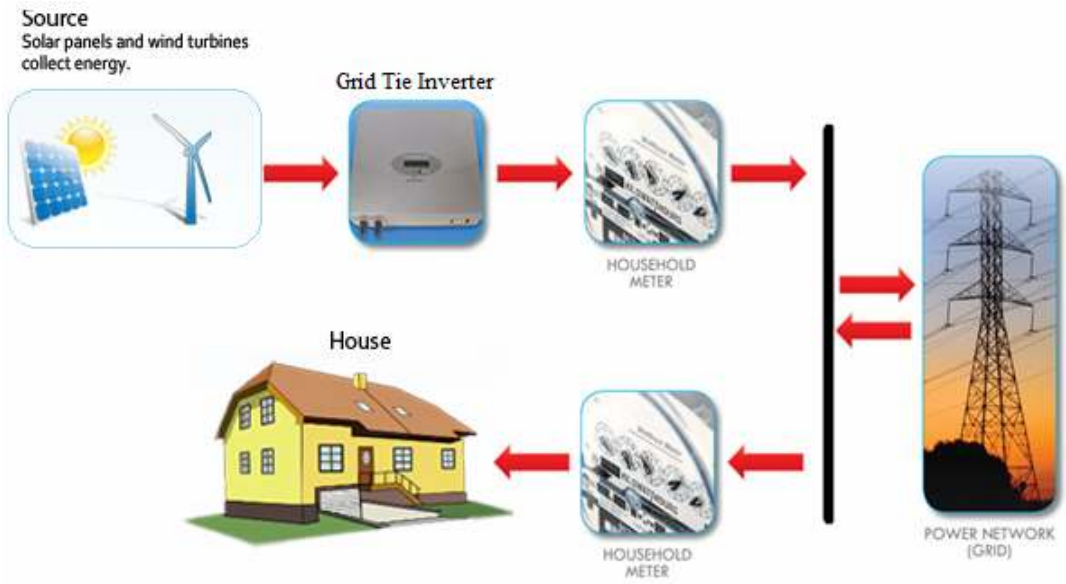

Figure (7.4): Grid tie feed in tariff

7.3 Evaluation the Economic Impact of Atouf Grid Tie PV system

As shown from figure (7.5) the bi-directional energy meter measures the net value between the energy consumption by the load and the energy transmitted to grid.

The following equation determines the cost of annual total energy measure by the bi-directional energy meter.

Annual cost for energy measured by the meter = (Energy consumption before PV installation – PV energy) X cost of 1kWh

= (40887 kWh - 23601.89 kWh) X 0.55 NIS = 9506.8105NIS

www.manaraa.com

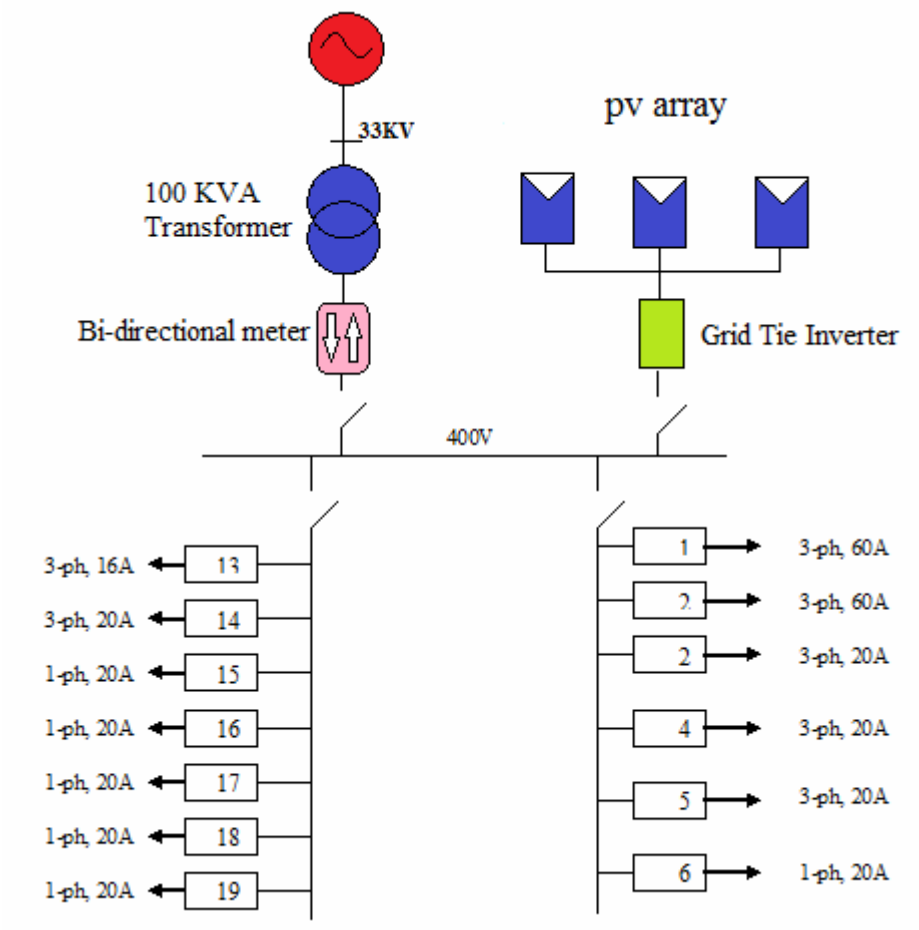

Figure (7.5): Atouf grid tie PV system electrical construction

In order to find the annual saving money for Atouf village:

Annual saving money for Atouf = cost of annual total bill before PV installation - cost of annual total bill after PV installation

= (40887 kWh X 0.55NIS) - 9506.8105NIS.

Saving = 22487.85 NIS - 9506.8105NIS = 12981.04 NIS.

7.4 Environment Impact of Grid Tie PV/ Wind system

In the long term, environmental benefits may be the most important reason for the implementation of grid-tied PV. The environmental impact

www.manaraa.com

of PV is small when compared with all nonrenewable energy sources. Coal plants produce huge quantities of CO_2 as well as particulates and oxides of sulfur and nitrogen. Of course, CO_2 is inherent in the combustion process and cannot be avoided. Scrubbers can reduce, but not eliminate sulfur and particulate emissions. Gas fired plants are cleaner than coal plants, but still produce greenhouse gases. Atmospheric emissions from nuclear plants are negligible, but radioactive waste is an incessant problem with no clear cut solution.

The amount of CO_2 produced from conventional source using fossil fuel is 1kg for 1kWh[13], so if I take Atouf village as a case study the reduction of CO_2 from energy saving 23601.89kWh is 23601.89kg annually.

www.manaraa.com

CHAPTER EIGHT

CONCLUSIONS AND FUTURE SCOPE OF WORK

www.manaraa.com

Chapter Eight
Conclusions and Future Scope of Work

8.1 Conclusions

From this research it was shown that it is possible to accurately predict the power output from grid connected photovoltaic arrays by including the effect of temperature and solar radiation. Furthermore, it was shown that it is possible to adapt the size of models and the different PV hybrid system configurations which are applicable to a grid connected and modify it in such a way that important information about techno-economic performance of these systems can be obtained.

Upon achieving this, a side-by-side comparison of different grid connected PV sizes was performed. The form of this model was justified by looking at different measured values over the collection period; such as; power output vs. radiation, voltage vs. radiation and output power vs. temperature. These plots gave an appropriate justification for the sizes and percentage of penetration factor for all parameters connecting with grid.

General information was presented about the solar resource for Atouf data collection, a temperature coefficient and non-linear radiation coefficient was determined, the power output from each configuration can be accurately predicted for general operating conditions.

Using this software Simulink program, and the determined the effect of temperature coefficient and non-linear radiation term, the maximum power output from each PV hybrid system sizes and configurations can

www.manaraa.com

now be predicted with accuracy. This can be done, not only for a single unrealistic value of solar radiation, but under general operating conditions. Being able to accurately predict the power output is very important for increased growth in the deployment of photovoltaic hybrid systems.

8.2 SCOPE FOR FUTURE WORK

After the completion of the simulation work, the scope is been identified as:

- Study effects of switching & fault conditions for grid tied systems.
- Technical and economic analysis comparison between grid tied system without storage battery and grid tied system with storage battery.
- Build Simulink dynamic smart system with all parts and controller.

www.manaraa.com

References

[1] S.B. KJAER, J.K. PEDERSON, F. BLAABJERG "**A review of single-phase grid connected inverters for photovoltaic modules**" IEEE Transactions on Industry Applications, September/October, Vol. 41, No.5, 2005, pp. 1292-1306.

[2] İ. SEFA, N. ALTIN "**Simulation of current controlled grid interactive inverter**" TPE-2006 3rd Conference on Technical and Physical Problems in Power Engineering, Ankara(Turkey), May 2006, pp. 964-968.

[3] U.S. Emission Data, Environment Energy-Related Emission Data & Environmental Analysis, Energy Information Administration, http://www.eia.doe.gov/environment.html [access date 10 April 2011]

[4] Bassam A. Abdel-Ghani "**Techno-Economic Evaluation of Electrification of Small Villages in Palestine by Centralized and Decentralized PV System**" A thesis presented to the University of An-Najah National University, Nablus, Palestine, 2008.

[5] Asma M. Yasin "**Optimal Operation Strategy and Economic Analysis of Rural Electrification of Atouf Village by Electric Network, Diesel Generator and Photovoltaic System**" A thesis presented to the University of An-Najah National University, Nablus, Palestine,2008.

www.manaraa.com

[6] Muthanna S. Abu-hamdeh "**Modeling of Bi-directional Converter for Wind Power Generation**" Master thesis presented to the Ohio State University, 2009.

[7] V. Quaschning, "**Understanding Renewable Energy Systems**," Earthscan, London, 2005.

[8] M.K. Patel "**Wind and Solar Power Systems: Design, Analysis, and Operation**" CRC Press, FL, 2006.

[9] Siriya Skolthanarat "**The Modeling and Control of a Wind Farm and Grid Interconnection in a Multi-machine System"** Doctor of Philosophy thesis presented to Virginia Polytechnic Institute and State University, August 26th, 2009

[10] David A. Spera "**Wind turbine technology: fundamental concepts of wind turbine engineering**" page 66, New York, 1994.ASME Press.

[11] Rudion K. "**Aggregated modeling of wind farm**" Dissertation in electrical engineering at University of Magdeburg, Chapter 4.

[12] Mahmoud S. Abdel-Qader "**Simulation of a Hybrid Power System Consisting of Wind Turbine, PV, Storage Battery and Diesel Generator with Compensation Network: Design, Optimization and Economical Evaluation**" A thesis presented to the University of An-Najah National University, Nablus, Palestine, 2008.

www.manaraa.com

[13] Energy Research Center (ERC) Meteorological measurements in West Bank Nablus: An-Najah National University; 2011

[14] E. Ortjohann , O. Omari " **A Simulation Model For Expandable Hybrid Power Systems**" University of Applied Sciences Südwestfalen **www.otti.de/ipv/ipvabstracts/6.4ortjohann.pdf** [Access Date 3-2- 2012]

[15] "**Introduction of photovoltaic system**" SECO, FACT SHEET NO.11, pp. 1-4. www.infinitepower.org [Access Date 7-9- 2011]

[16] Ahmed S. Khalifa "**Control and Interfacing of Three Phase Grid Connected Photovoltaic Systems**" A thesis presented to the University of Waterloo, Ontario, Canada, 2010

[17] AKIHIRO OIE "**Design and Simulation of Photovoltaic Water Pumping System**" A Thesis Presented to the Faculty of California Polytechnic State University, San Luis Obispo, Requirements for the Degree of Master of Science in Electrical Engineering,2005

[18] Ghislain Remy, Olivier Bethoux,"**Review of MPPT Techniques for Photovoltaic Systems**" Laboratoire de Génie Electrique deParis (LGEP)/ SPEE-Labs,Université Paris-Sud 11,france.

[19] Mo'ien A. Omar "**COMPUTER – AIDED DESIGN AND PERFORMANCE EVALUATION OF PV-DIESEL HYBRID SYSTEM**" A thesis presented to the University of An-Najah National University, Nablus, Palestine, 2007.

www.manaraa.com

[20] Falinirina F. Rakotomananandro "**Study of Photovoltaic System**" Master thesis presented to the Ohio State University, 2011.

[21] SURESH A/L THANAKODI "**Modeling and Simulation of Grid Connected Photovoltaic System Using Matlab / Simulink**" Master thesis presented to University Technology Malaysia November 2009.

[22] PV module from kyocera data sheet http://www.kyocerasolar.eu/index/products/download/English.-cps-7724-files-20802-File.cpsdownload.tmp/KD135SX-1PU_Eng_March%202011 .pdf [Access Date 2-1- 2012]

[23] MATLAB/Simulink simulation software 2009a.

[24] Slootweg, J.G.; Polinder, H. "**Initialization of Wind Turbine Models in Power System Dynamics Simulations**", this paper appears in: Power Tech Proceedings, 2001 IEEE Porto Issue Date: 2001 On page(s): 6 pp. vol.4 September 2001.

[25] Ashima Taneja" **Sustainable Energy Systems with HVDC Transmition**" Thesis submitted in the partial fulfillment for the award of the degree of Master of Engineering in Power Systems & Electric Drives, Thapar university Patiala,2011.

[26] Kroutikova, N.; Hernandez-Aramburo, C.A.; Green, T.C "**State-space model of grid-connected inverters under current control mode**" Electric Power Applications, IET , vol.1, no.3, pp.329-338,May 2007.

www.manaraa.com

[27] Kawabata, T.; Miyashita, T.; Yamamoto, Y. "**Dead beat control of three phase PWM inverter**" IEEE Transactions on Power Electronics, vol.5, no.1, pp.21-28, Jan 1990

[28] Y. Mohamed and E. F. El-Saadany, "**Adaptive Decentralized Droop Controller to Preserve Power Sharing Stability of Paralleled Inverters in Distributed Generation Microgrids**" IEEE Transactions on Power Electronics, vol. 23, pp. 2806-2816, 2008.

[29] Leland Blank, P.E. & Anthony Tarquin, P.E. "**Engineering Economy**" Singapore, McGraw-Hill; 1998

[30] Marwan M.Mahmoud, Imad H.Ibrik "Techno-**economic feasibility of energy supply of remote villages in Palestine by PV systems, diesel generators and electric grid**" Renewable and sustainable Energy Reviews 10(2006) 128 – 138.

[31] http://en.wikipedia.org/wiki/Grid-tie_inverter [Access Date 3-2-2012].

[32] www.affordable-solar.com [Access Date 3-2- 2012].

[33] Marc Langevin, Consulting Engineer ,"**Maximum Generating Capacity of A Wind Farm Connected to 25 KV Distribution Feeder**" Report Presented to David Beauvais, Project Leader Canmet ENERGY – Varennes Research Centre

www.manaraa.com

APPENDICES

Appendix A: Simulink blocks for each part of grid tied PV/wind system

Appendix B: Specifications of the grid tie PV/Wind system elements

Appendix C: Graphs to calculate K and C

Appendix D: Table of interest at i = 10%

Appendix E: Perturb and Observe Algorithm

Appendix F: Simulation Results of Atouf Village

www.manaraa.com

APPENDIX (A)

Simulink blocks for each part of grid tie PV/wind system

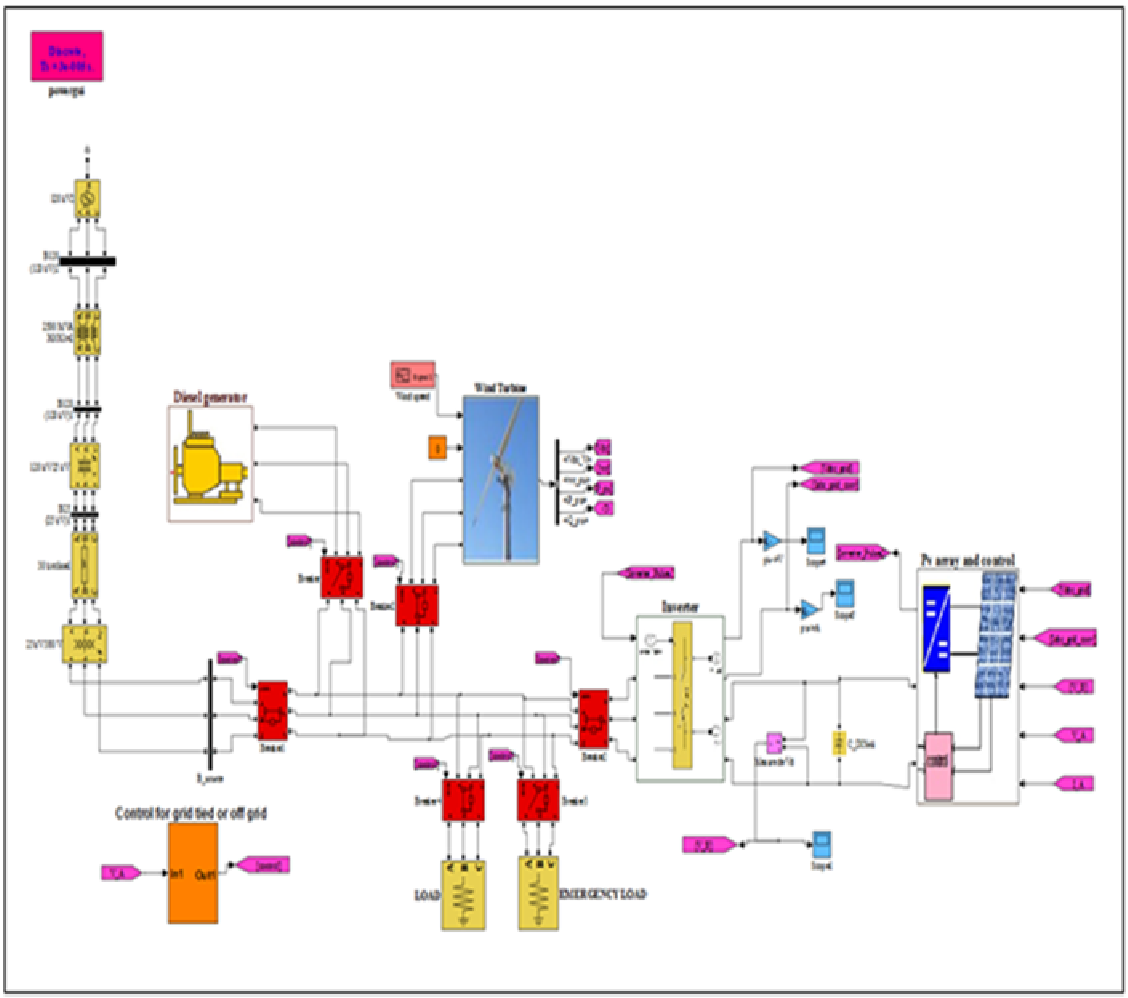

Figure (A.1): Simulink model of Grid tie PV/Wind hybrid system

www.manaraa.com

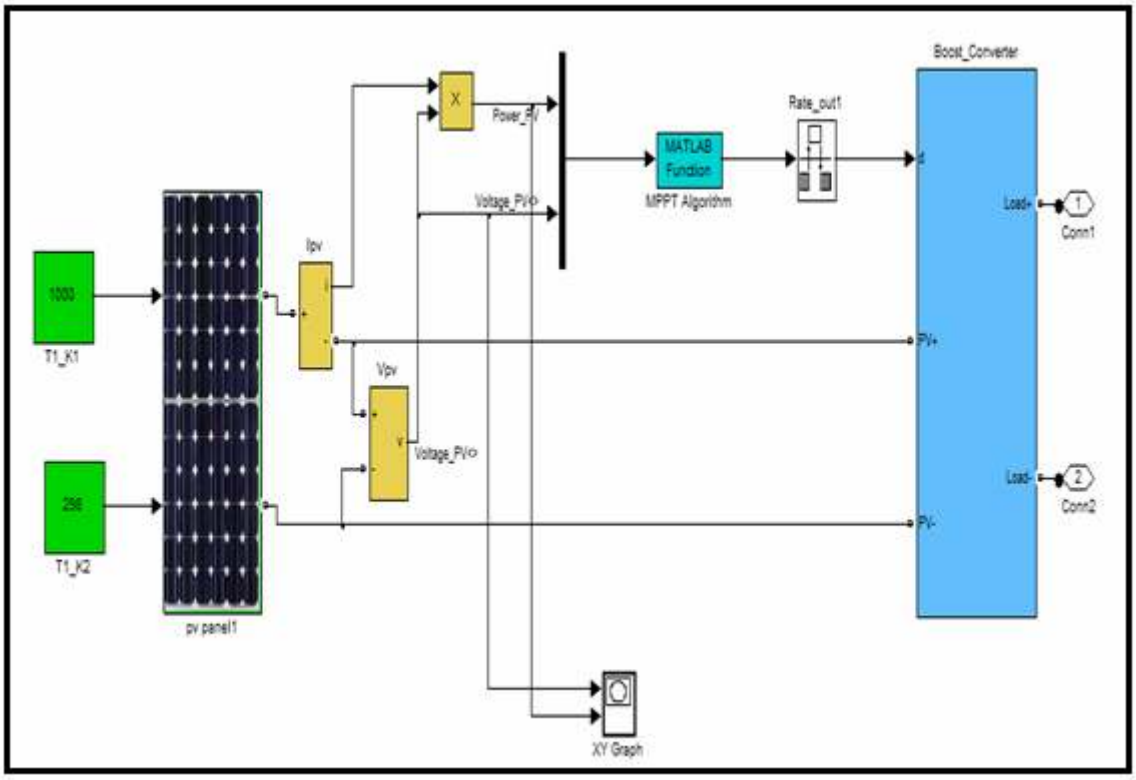

Figure (A.2): PV system with MPPT and boost converter.

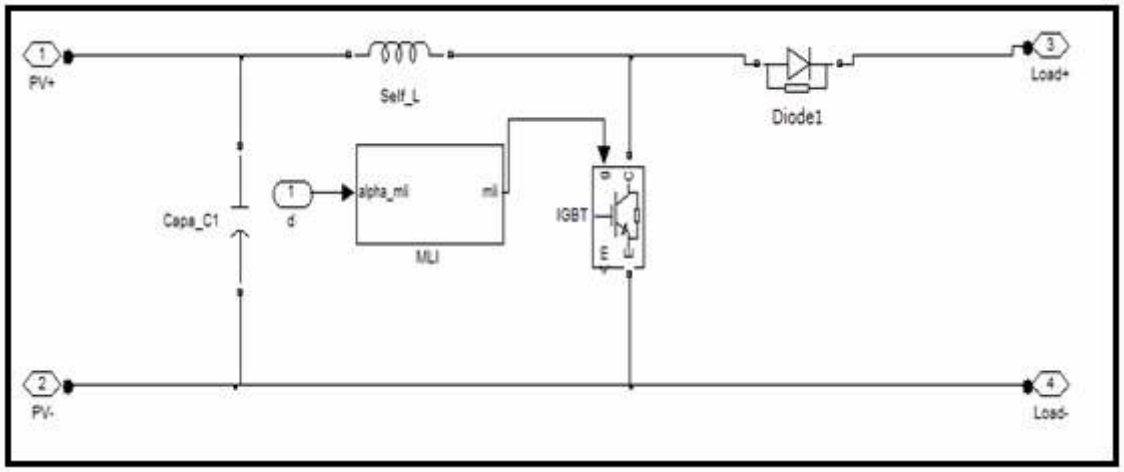

Figure (A.3): Boost dc-dc converter.

www.manaraa.com

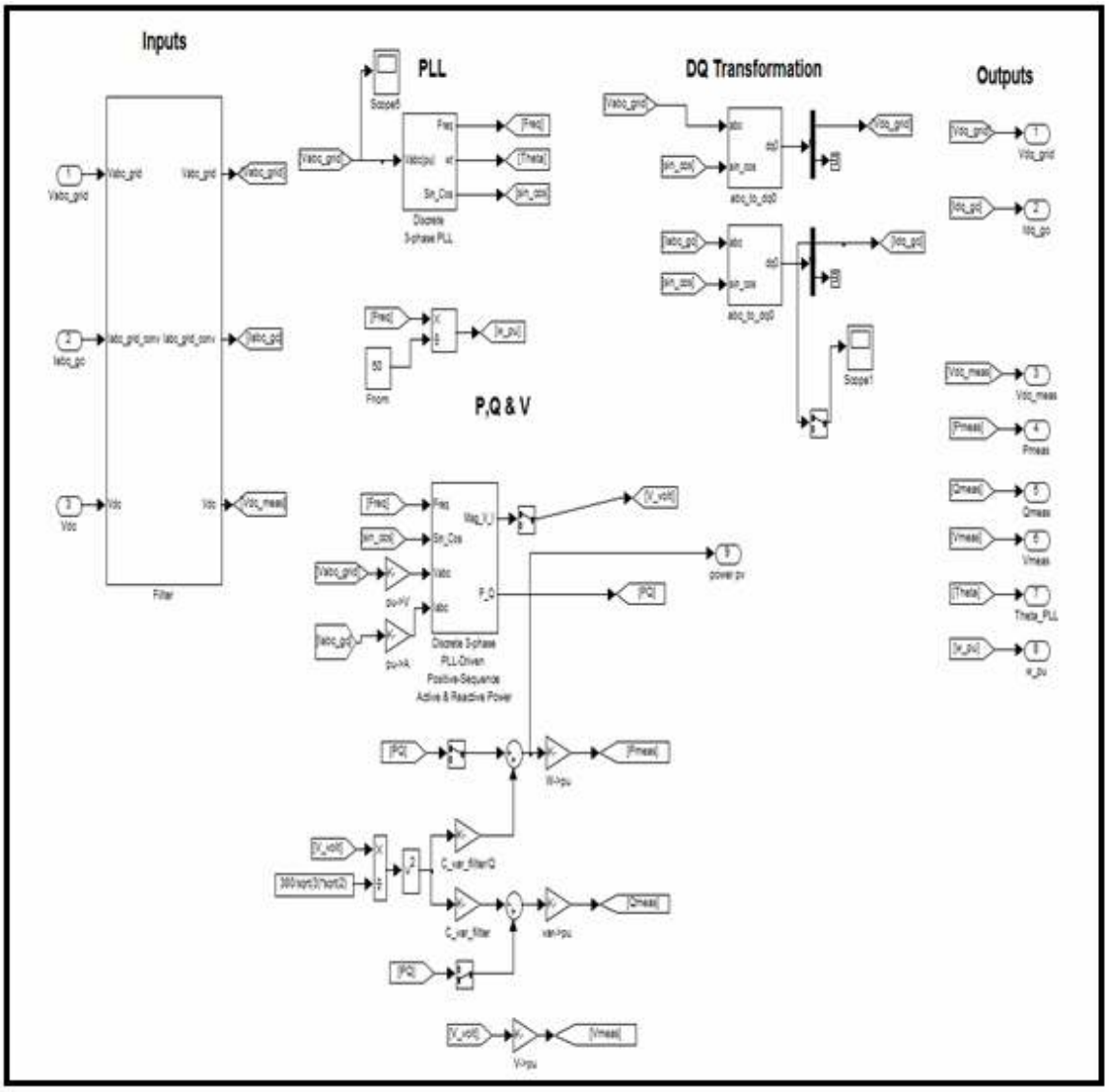

Figure (A.2): Unmask block of grid tie PV inverter measurement

www.manaraa.com

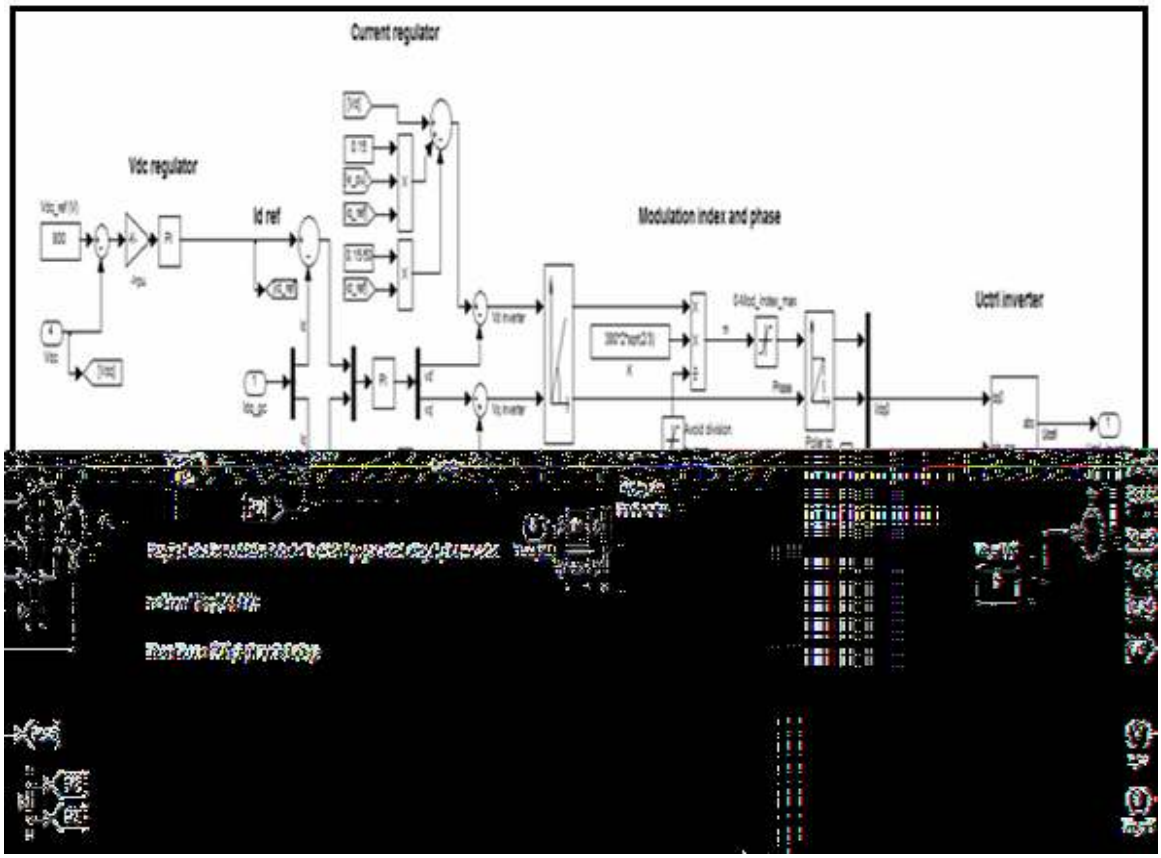

Figure (A.3): Unmask control block for grid tie PV inverter

www.manaraa.com

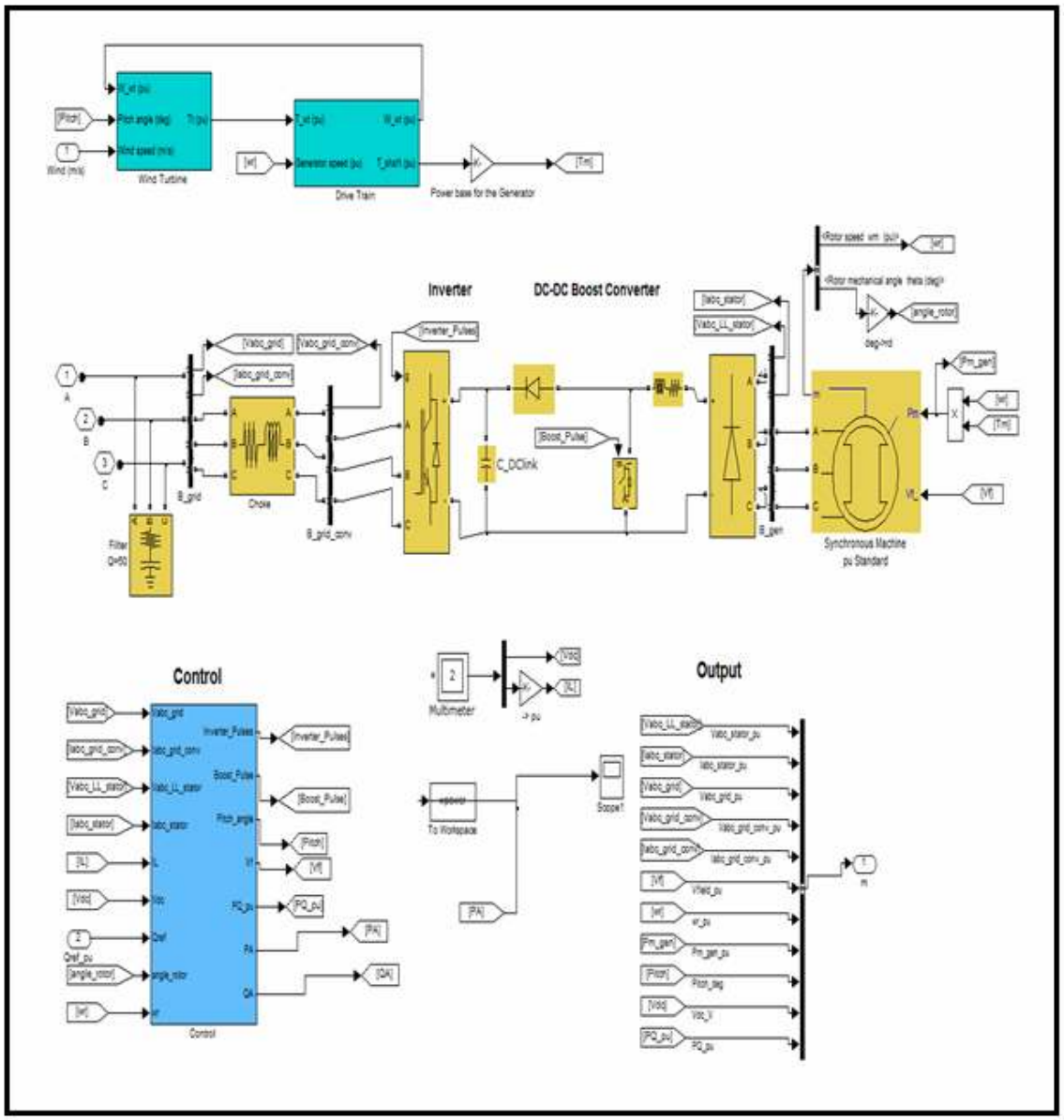

Figure (A.4): Unmasked Wind turbine model

www.manaraa.com

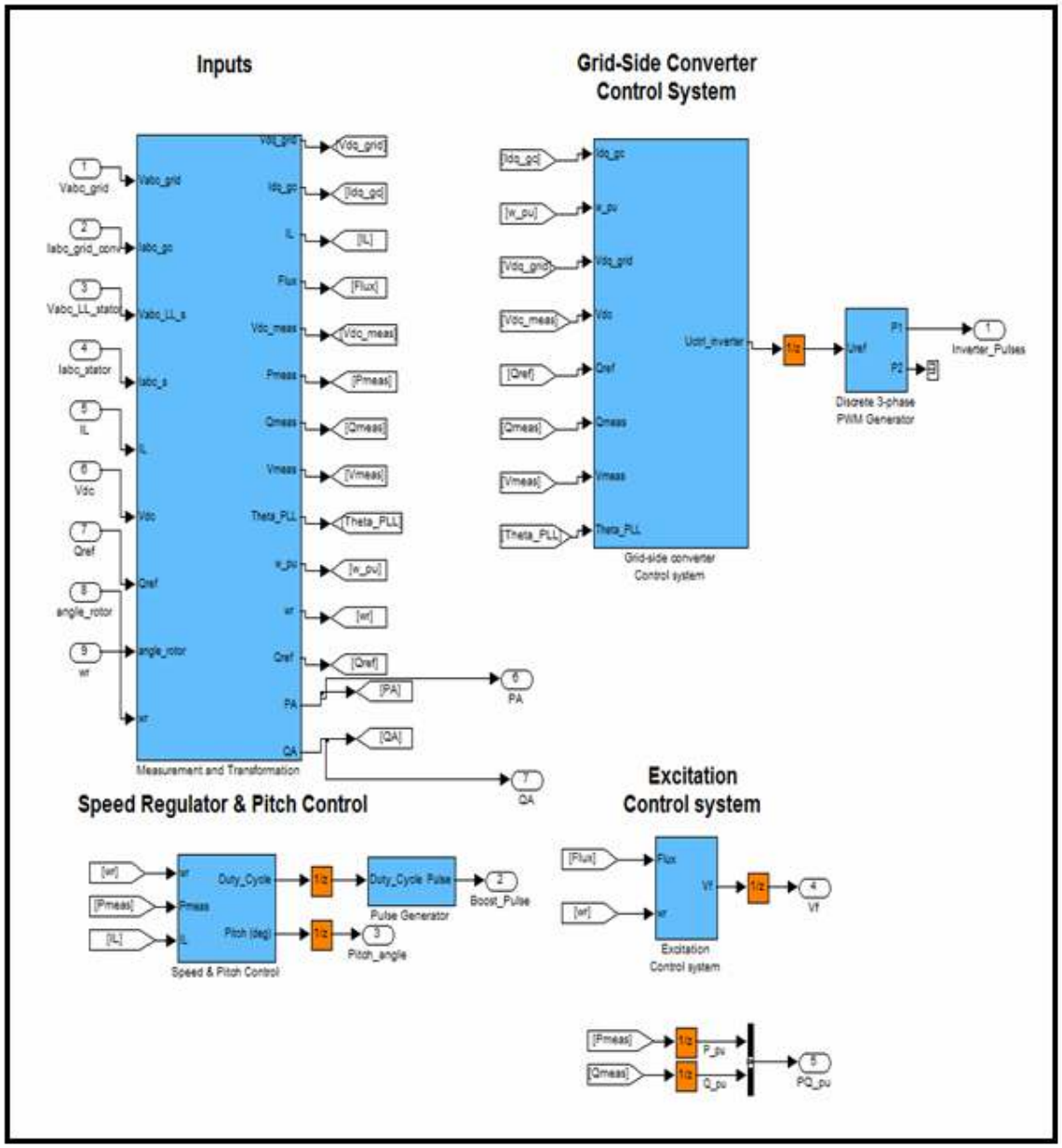

Figure (A.5): blocks of measurements, control, speed regulator & pitch control and excitation control

www.manaraa.com

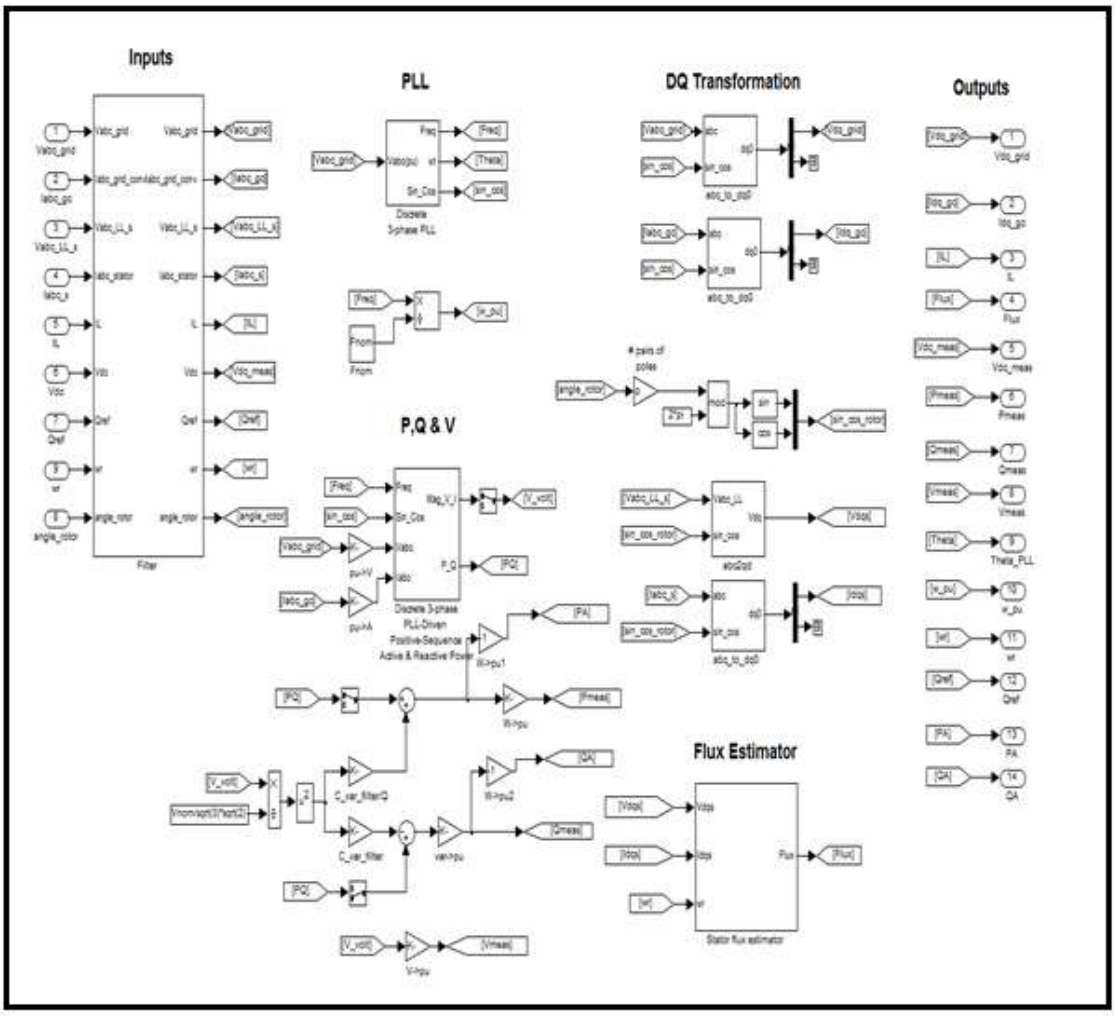

Figure (A.6): Unmask measurements block for wind turbine

www.manaraa.com

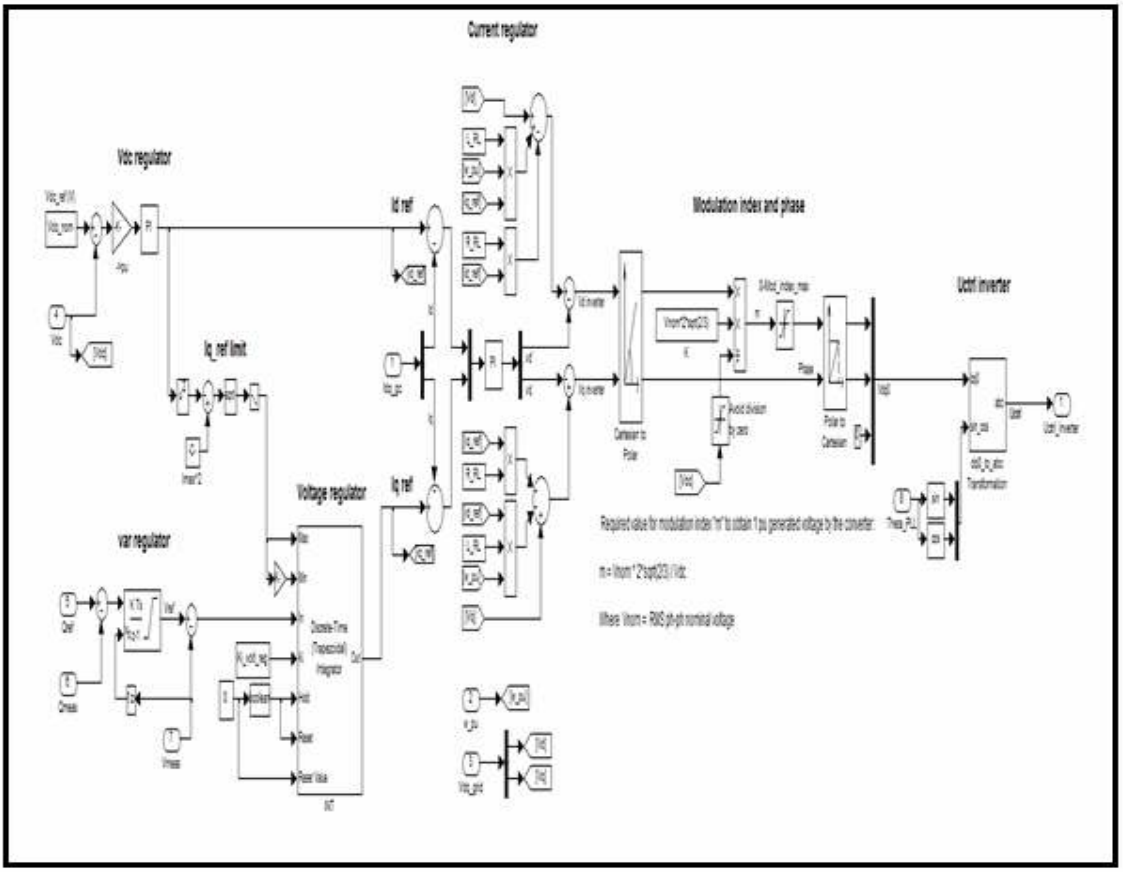

Figure (A.7): Unmask control block for wind turbine

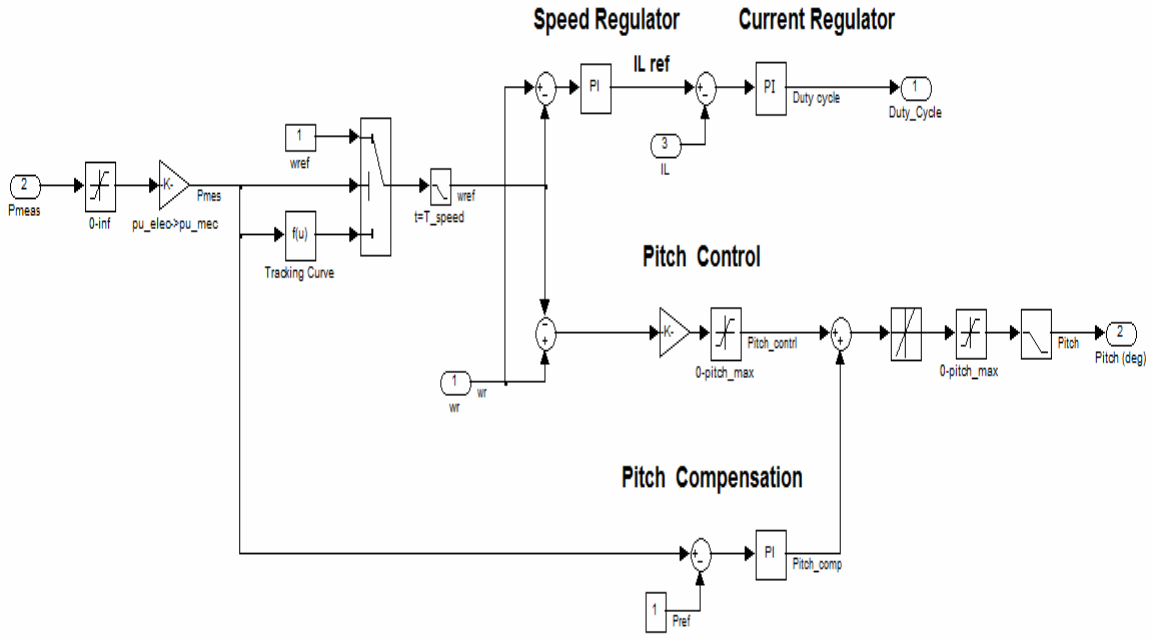

Figure (A.8): Unmask speed regulator and pitch control block

www.manaraa.com

APPENDIX (B)

Specifications of the grid tie PV/Wind hybrid system elements

(B.1): Solar PV module technical specifications

www.manaraa.com

SOLAR by KYOCERA

KD135SX-UPU

ELECTRICAL CHARACTERISTICS

Current-Voltage characteristics of Photovoltaic Module KD135SX-UPU at various cell temperatures

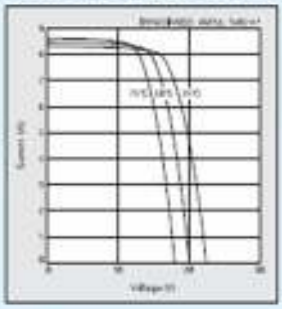

Current-Voltage characteristics of Photovoltaic Module KD135SX-UPU at various irradiance levels

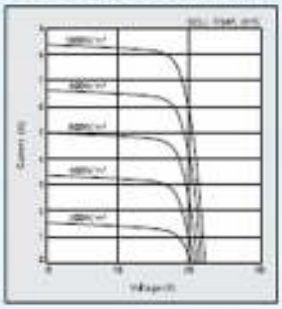

SPECIFICATIONS

■ Physical Specifications

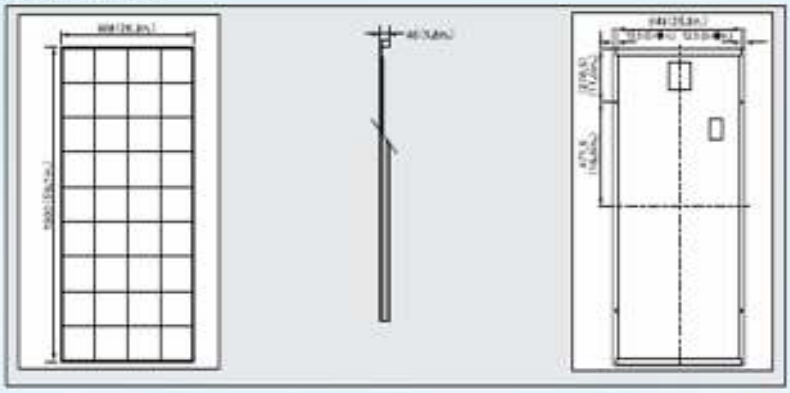

■ Specifications

■ Electrical Performance under Standard Test Conditions (*STC)

Maximum Power (Pmax)	135W (+5%/-5%)
Maximum Power Voltage (Vmpp)	17.7V
Maximum Power Current (Impp)	7.63A
Open Circuit Voltage (Voc)	22.1V
Short Circuit Current (Isc)	8.37A
Max System Voltage	600V
Temperature Coefficient of Voc	-8.0×10^{-1} V/°C
Temperature Coefficient of Isc	5.02×10^{-3} A/°C

*STC: Irradiance 1000W/m², AM1.5 spectrum, cell temperature 25°

■ Electrical Performance at 800W/m², *NOCT, AM1.5

Maximum Power (Pmax)	95W
Maximum Power Voltage (Vmpp)	15.7V
Maximum Power Current (Impp)	6.10A
Open Circuit Voltage (Voc)	20.0V
Short Circuit Current (Isc)	6.79A

*NOCT (Nominal Operating Cell Temperature): 47.5°C

■ Cells

Number per Module	36

■ Module Characteristics

Length x Width x Depth	1326mm(52.1inches) x 660mm(26.0inches) x 46mm(1.8in)
Weight	12.5kg(27.5lbs.)

■ Junction Box Characteristics

Length x Width x Depth	120mm(4.7inches) x 93mm(3.7inches) x 25mm(1.0in)
IP Code	IP65

■ Others

*Operating Temperature	-40°~90°C
Maximum Fuse	15A

*The temperature is based on cell temperature

ISO 9001 and ISO 14001 Certified and Registered

www.kyocerasolar.com
800-223-9580 toll free 800-523-2329 fax

KYOCERA

www.manaraa.com

(B.2) : Grid tied inverter technical specifications (12kW)

SUNNY TRIPOWER
10000TL / 12000TL / 15000TL / 17000TL

Efficient
- Maximum efficiency of 98.1%
- OptiTrac Global Peak for best tracking efficiency
- Bluetooth® communication

Safe
- Electronic string fuse and failure detection
- Optional DC overvoltage protector (Type II)
- String current monitoring

Flexible
- DC input voltage up to 1000 V
- Integrated grid management functions
- Custom plant design with Optiflex

Simple
- Three-phase feed-in
- Cable connection without tools
- SUNCLIX® DC plug system
- Easily accessible connection area

SUNNY TRIPOWER 10000TL / 12000TL / 15000TL / 17000TL

The three-phase inverter for easy system design

The Sunny Tripower is packed full of innovation. Thanks to the new SMA Optiflex technology, which features two MPP inputs and a very broad input voltage range, the three-phase Sunny Tripower is suited to almost any module configuration. This flexibility simplifies plant design and is perfect for systems up to the megawatt range. The Sunny Tripower also assists grid managers. It meets all the requirements for reactive power supply, utility interaction management and grid support. The Optiprotect safety concept, with its self-learning string failure detection, electronic string fuse and available DC overvoltage protector (Type II), ensures maximum uptime.

www.manaraa.com

Technical data	Sunny Tripower 10000TL	Sunny Tripower 12000TL	Sunny Tripower 15000TL	Sunny Tripower 17000TL
Input (DC)				
Max. DC power (@ cos φ = 1)	10200 W	12250 W	15340 W	17410 W
Max. DC voltage	1000 V	1000 V	1000 V	1000 V
MPP voltage range	320 V - 800 V	380 V - 800 V	360 V - 800 V	400 V - 800 V
DC nominal voltage	600 V	600 V	600 V	600 V
Min. DC voltage / start voltage	150 V / 188 V	150 V / 188 V	150 V / 188 V	150 V / 188 V
Max. input current / per string	A: 22 A, B: 11 A / 33 A	A: 22 A, B: 11 A / 33 A	A: 33 A, B: 11 A / 33 A	A: 33 A, B: 11 A / 33 A
Number of MPP trackers / strings per MPP tracker	2 / A: 4, B: 1	2 / A: 4, B: 1	2 / A: 5, B: 1	2 / A: 5, B: 1
Output (AC)				
AC nominal power (@ 230 V, 50 Hz)	10000 W	12000 W	15000 W	17000 W
Max. AC apparent power	10000 VA	12000 VA	15000 VA	17000 VA
Nominal AC voltage/ range	3 / N / PE; 220 V / 400 V; 160 V - 280 V			
AC grid frequency; range	50, 60 Hz; -6 Hz, +5 Hz	50, 60 Hz; -6 Hz, +5 Hz	50, 60 Hz; -6 Hz, +5 Hz	50, 60 Hz; -6 Hz, +5 Hz
Max. output current	16 A	19.2 A	24 A	24.6 A
Power factor (cos φ)	0.8 leading ... 0.8 lagging			
Phase conductors / connection phases / power balancing	3 / 3 / –	3 / 3 / –	3 / 3 / –	3 / 3 / –
Efficiency				
Max. efficiency / Euro-eta	98.1% / 97.7%	98.1% / 97.7%	98.1% / 97.7%	98.1% / 97.7%
Protection devices				
DC reverse-polarity protection / reverse current protection	●/electronic	●/electronic	●/electronic	●/electronic
ESS switch-disconnect	●	●	●	●
AC short circuit protection	●	●	●	●
Ground fault monitoring	●	●	●	●
Grid monitoring (SMA Grid Guard)	●	●	●	●
Galvanically isolated / all-pole sensitive leakage current monitoring unit	–/●	–/●	–/●	–/●
DC overvoltage protector (type II)	o	o	o	o
String failure detection	●	●	●	●
Protection class / overvoltage category	I / III	I / III	I / III	I / III
General data				
Dimensions (W / H / D) in mm (in)	665 / 690 / 265 (26 / 27 / 10)			
Weight	65 kg (143 lb)			
Operating temperature range	-25 °C ... +60 °C (-13 °F ... +140 °F)			
Noise emission (typical)	www.SMA-Solar.com	www.SMA-Solar.com	www.SMA-Solar.com	www.SMA-Solar.com
Internal consumption at night	1 W	1 W	1 W	1 W
Topology	transformerless	transformerless	transformerless	transformerless
Cooling concept	OptiCool®	OptiCool®	OptiCool®	OptiCool®
Electronics protection rating / connection area (as per IEC 60529)	IP65 / IP54	IP65 / IP54	IP65 / IP54	IP65 / IP54
Climatic category (per IEC 60721-3-4)	4K4H	4K4H	4K4H	4K4H
Features				
DC connection: SUNCLIX®	●	●	●	●
AC connection: screw terminal / spring-type terminal	–/●	–/●	–/●	–/●
Display: text line / graphic	–/●	–/●	–/●	–/●
Interfaces: RS485 / Bluetooth	o/●	o/●	o/●	o/●
Warranty: 5 / 10 / 15 / 20 / 25 years	●/o/o/o/o	●/o/o/o/o	●/o/o/o/o	●/o/o/o/o
Certificates and permits (more available on request)	CE, VDE 0126-1-1, DK 5940, G83/1-1, PPC, AS 4777, EN 50438*, C10/C11, IEC 61727			

● Standard features o Optional features – Not available

Provisional data, as of March 2010. Data at nominal conditions

* Does not apply to all national deviations of EN 50438

Type designation	STP 10000TL-10	STP 12000TL-10	STP 15000TL-10	STP 17000TL-10

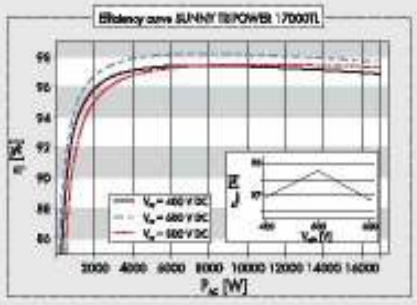

Accessories

Toll Free +1 888 4 SMA USA
www.SMA-America.com

SMA America, LLC

www.manaraa.com

(B.3): Grid tied inverter technical specifications (22kW)

Product Description: Solar inverter has CE, VDE0126-1, G83/1, AS4777, and AS3100 Certificate.

- Conversion efficiency is 98%.
- islanding protection & MPPT.
- High efficiency and Wide range of MPPT.
- Wide input voltage range.
- High reliability due to complete protection function.
- Powerful communication interfaces.
- Easy operation and installation.
- Easy-to-set multilingual LCD display.
- Adjustable protection / operation parameters.

Model		SDS 22KW
DC Input	MPPT Voltage Range	DC100~600 V
	Recommend PV Array Open Circuit Voltage	200~400V
	Control System	MPPT
AC Output	Output Power	22KW
	Rate voltage	AC380V
	voltage range	AC 342 ~ 418 V
	Normal Grid Frequency	50/60Hz (Grid frequency)
	Phases	3 phase 4 wire
	Power Factor	> 0.95
	Current THD	At rated power and in the sine wave < 5%
	Control System	PWM
	Anti-islanding	≤ 0.5 sec
	Output Overload	100%
	Max. Efficiency	97%
	Euro Efficiency	96.4%

www.manaraa.com

(B.4): Data sheet for grid tie 100 kW Wind Turbine

Pacific Tool & MACHINERY

www.PacificToolCompany.com
1.310.497.7374

100KW Wind Turbine

Start-up wind speed: 3.5m/s or 5.59 mph
Rated wind speed: 12.5m/s or 28 mph
Cut-out wind speed: 25m/s or 44.7 MPH
Survival wind speed: 50m/s or 101 mph
System Type: Grid Tie - 50HZ or 60HZ
YAW System: Normal: Free, 360 degrees
Rated Power: 100KW
Rotor Diameter: 21 meters or 45' 3"
Noise: 60 db @ 4m/s, 75db @10m/s

Rotor and Blade Information

Type of Hub: Variable Pitch Rotor
Number of Blades: 3
Rated rotation speed: 65 rpm
Blade Material: Fiber Glass
Blade length: 10 m
Max. rotation speed: 80 rpm

Rotor Speed Control

Normal Start up: Aerodynamic
Shut-down: Electromagnetic brakes / air brakes

Generator

Type: 3 phase Permanent-magnet
Maximal Power: 120kW
Rated AC Voltage: 380 V
Rated AC Current: 150 A
Max AC Voltage: 540 V
Amb. Parameters: -20°C ~ +45 °C; Humidity < 90 %

Tower Information

Type: Free stand, Hot-dip Galvanized
Height: 30m (Standard)

Controller Information

3.1. General Parameter

Rated Working Voltage: : 540Vdc
Maximum Voltage : 600Vdc
Rated Output Power : 100kW
Maximum Output Power : 120kW
Rated Rotor Speed: 65 rpm a) Voltage protection
Starting Loading Voltage : DC550V
Fully Loading Voltage : DC570V b) Rotor Speed Protection
Starting Loading rotor speed : 65rpm
Fully Loading rotor speed : 70rpm
Protection rotor speed : 72rpm
Maximum rotor speed : 80 rpm c) Operating data of Wind Turbine
Yaw speed : 0.55°/s
Yaw precision : <3.2°

www.manaraa.com

Pacific Tool & MACHINERY

3.2. Ambient Parameters

Ambient Temperature : -10℃~+50℃
Storage Temperature : -20℃~+70℃
Relative Humidity : ≤90%RH
Height above sea level : ≤1000m
(Remark: Capacity of controller will reduce 5% for using if height increases per km)

3.3. Basic Function

1) Autocontrol Voltage : Voltage will be adjusted by controller automatically when input voltage is too high.
2) Display : Check parameter and operating states by meter and LCD
3) Over Loading Protection : In order to protect whole system, controller will cut off output and alarm at exceeding 100 kW
4) Short Circuit Protection : Controller will start cutting off output and alarm if short circuit is found
5) Yaw Control : In order to improve generator efficiency, wind turbine automatically traces wind direction under rated wind speed. At the same time, the direction of wind turbine is adjusted at exceeded rated wind speed in order to protect it from damage.
6) Automatic Lubricatiom: Providing seasonal lubrication protection for bearing and yaw equipment.
7) Shut-down : Automatic air brake, blades pitch control and electromagnetic braking, Manual Parking brake for servicing
8) Automatic Untwist : It can avoid gnarling cable and has untwisted function in to protect cable.
9) Failure Alarm : Controller will alarm when the system failure is found.

Inner Structure

www.manaraa.com

POWER CURVE

Pacific Tool & MACHINERY

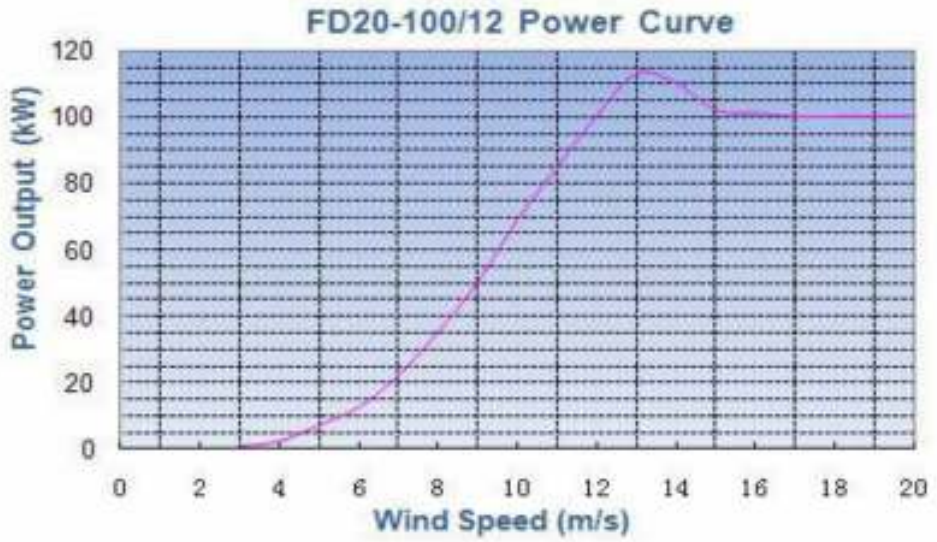

Pacific Tool & MACHINERY

www.PacificToolCo.com

//310.497.7374

DISTRIBUTED BY:

www.manaraa.com

APPENDIX (C)

Graphs to calculate K and C

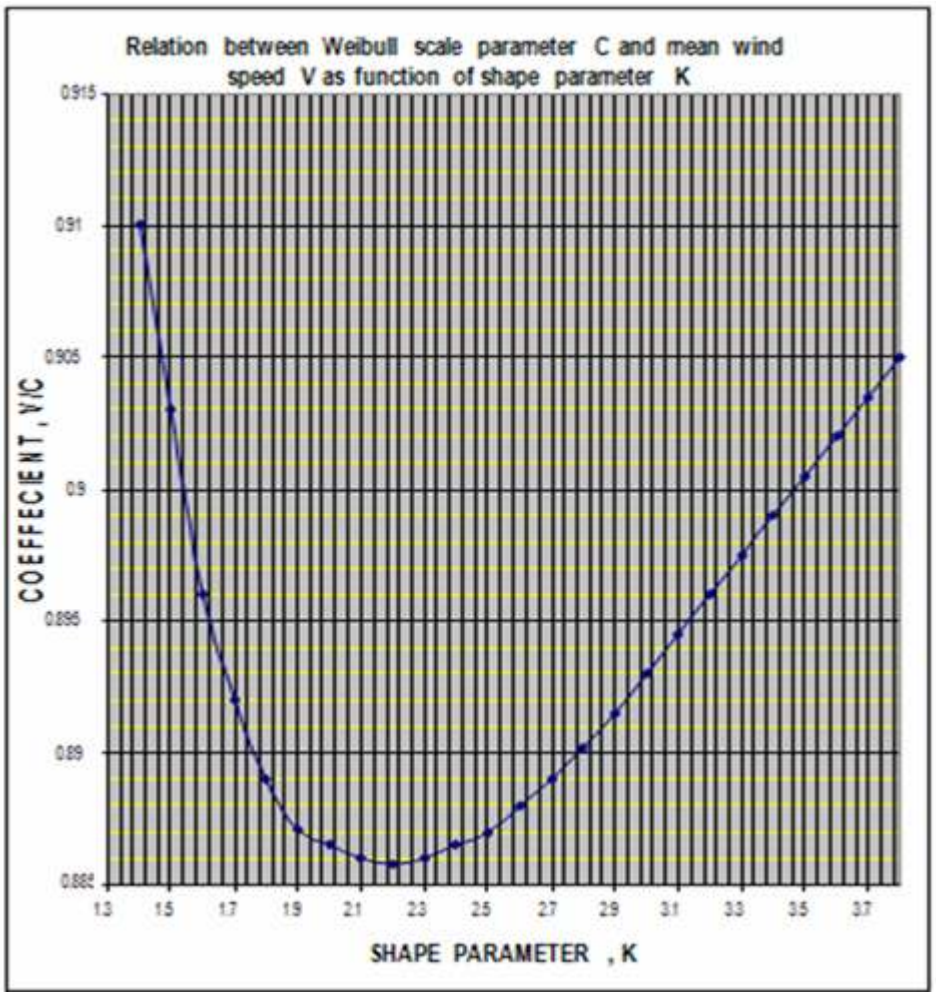

Figure (C.1): Relationship between coefficient V/C and shape parameter K

www.manaraa.com

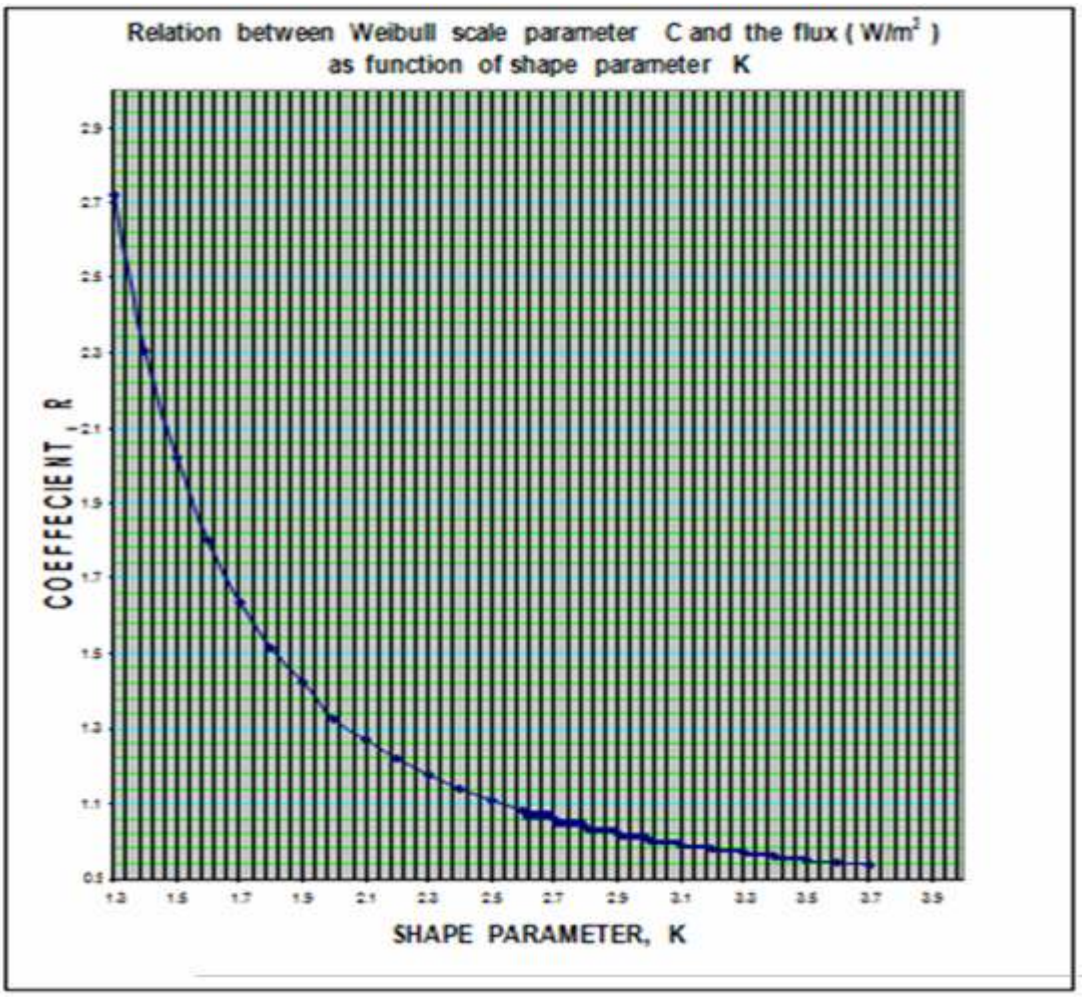

Figure (C.2): Relationship between coefficient R and shape parameter K

www.manaraa.com

Appendix (D)

Table of interest at i = 10%

10%								10%
	Single Payments		Uniform-Series Payments				Uniform Gradient	
n	Compound Amount F/P	Present Worth P/F	Sinking Fund A/F	Compound Amount F/A	Capital Recovery A/P	Present Worth P/A	Gradient Present Worth P/G	Gradient Annual Series A/G
1	1.1000	0.9091	1.00000	1.0000	1.10000	0.9091		
2	1.2100	0.8264	0.47619	2.1000	0.57619	1.7355	0.8264	0.4762
3	1.3310	0.7513	0.30211	3.3100	0.40211	2.4869	2.3291	0.9366
4	1.4641	0.6830	0.21547	4.6410	0.31547	3.1699	4.3781	1.3812
5	1.6105	0.6209	0.16380	6.1051	0.26380	3.7908	6.8618	1.8101
6	1.7716	0.5645	0.12961	7.7156	0.22961	4.3553	9.6842	2.2236
7	1.9487	0.5132	0.10541	9.4872	0.20541	4.8684	12.7631	2.6216
8	2.1436	0.4665	0.08744	11.4359	0.18744	5.3349	16.0287	3.0045
9	2.3579	0.4241	0.07364	13.5795	0.17364	5.7590	19.4215	3.3724
10	2.5937	0.3855	0.06275	15.9374	0.16275	6.1446	22.8913	3.7255
11	2.8531	0.3505	0.05396	18.5312	0.15396	6.4951	26.2963	4.0641
12	3.1384	0.3186	0.04676	21.3843	0.14676	6.8137	29.9012	4.3884
13	3.4523	0.2897	0.04078	24.5227	0.14078	7.1034	33.3772	4.6988
14	3.7975	0.2633	0.03575	27.9750	0.13575	7.3667	36.8005	4.9955
15	4.1772	0.2394	0.03147	31.7725	0.13147	7.6061	40.1520	5.2789
16	4.5950	0.2176	0.02782	35.9497	0.12782	7.8237	43.4164	5.5493
17	5.0545	0.1978	0.02466	40.5447	0.12466	8.0216	46.5819	5.8071
18	5.5599	0.1799	0.02193	45.5992	0.12193	8.2014	49.6395	6.0526
19	6.1159	0.1635	0.01955	51.1591	0.11955	8.3649	52.5827	6.2861
20	6.7275	0.1486	0.01746	57.2750	0.11746	8.5136	55.4069	6.5081
21	7.4002	0.1351	0.01562	64.0025	0.11562	8.6487	58.1095	6.7189
22	8.1403	0.1228	0.01401	71.4027	0.11401	8.7715	60.6893	6.9189
23	8.9543	0.1117	0.01257	79.5430	0.11257	8.8832	63.1462	7.1085
24	9.8497	0.1015	0.01130	88.4973	0.11130	8.9847	65.4813	7.2881
25	10.8347	0.0923	0.01017	98.3471	0.11017	9.0770	67.6964	7.4580
26	11.9182	0.0839	0.00916	109.1818	0.10916	9.1609	69.7940	7.6186
27	13.1100	0.0763	0.00826	121.0999	0.10826	9.2372	71.7773	7.7704
28	14.4210	0.0693	0.00745	134.2099	0.10745	9.3066	73.6495	7.9137
29	15.8631	0.0630	0.00673	148.6309	0.10673	9.3696	75.4146	8.0489
30	17.4494	0.0573	0.00608	164.4940	0.10608	9.4269	77.0766	8.1762
31	19.1943	0.0521	0.00550	181.9434	0.10550	9.4790	78.6395	8.2962
32	21.1138	0.0474	0.00497	201.1378	0.10497	9.5264	80.1078	8.4091
33	23.2252	0.0431	0.00450	222.2515	0.10450	9.5694	81.4856	8.5152
34	25.5477	0.0391	0.00407	245.4767	0.10407	9.6086	82.7773	8.6149
35	28.1024	0.0356	0.00369	271.0244	0.10369	9.6442	83.9872	8.7086
40	45.2593	0.0221	0.00226	442.5926	0.10226	9.7791	88.9525	9.0962
45	72.8905	0.0137	0.00139	718.9048	0.10139	9.8628	92.4544	9.3740
50	117.3909	0.0085	0.00086	1163.91	0.10086	9.9148	94.8889	9.5704
55	189.0591	0.0053	0.00053	1880.59	0.10053	9.9471	96.5619	9.7075
60	304.4816	0.0033	0.00033	3034.82	0.10033	9.9672	97.7010	9.8023
65	490.3707	0.0020	0.00020	4893.71	0.10020	9.9796	98.4705	9.8672
70	789.7470	0.0015	0.00013	7887.47	0.10013	9.9873	98.9870	9.9113
75	1271.90	0.0008	0.00008	12709	0.10008	9.9921	99.3317	9.9410
80	2048.40	0.0005	0.00005	20474	0.10005	9.9951	99.5606	9.9609
85	3298.97	0.0003	0.00003	32980	0.10003	9.9970	99.7120	9.9742
90	5313.02	0.0002	0.00002	53120	0.10002	9.9981	99.8118	9.9831
95	8556.68	0.0001	0.00001	85557	0.10001	9.9988	99.8773	9.9889
96	9412.34	0.0001	0.00001	94113	0.10001	9.9989	99.8874	9.9898
98	11389	0.0001	0.00001		0.10001	9.9991	99.9052	9.9914
100	13781	0.0001	0.00001		0.10001	9.9993	99.9202	9.9927

المنارة للاستشارات
www.manaraa.com

Appendix (E)

Perturb and Observe Algorithm

```
function y=pnob(u)
global A B Ka alpha_mli
Ka=.02*abs(u(1)-A); Ka=0.02*|DeltaP|
if (u(1)-A)==0
  C=alpha_mli;
else
if(u(1)-A)>0
    if(u(2)-B)>0
    else
      C=alpha_mli+Ka;
    end
  else
    if(u(2)-B)>0
      C=alpha_mli+Ka;
   else
      C=alpha_mli-Ka;
    end
  end
end
if(C<0) %saturation due negative
  C=0;
end
if(C>1) %saturation due over one
  C=1;
end
A=u(1); measure power
B=u(2); measure voltage
alpha_mli=C;
y=alpha_mli;
```

www.manaraa.com

Appendix (F)

Simulation Results of Atouf Village

Simulation of the System for Different Radiations

These conditions applied on the system, 1000 W/m^2 until 5s then change to 500 W/m^2, 25 ºC, 7kW load.

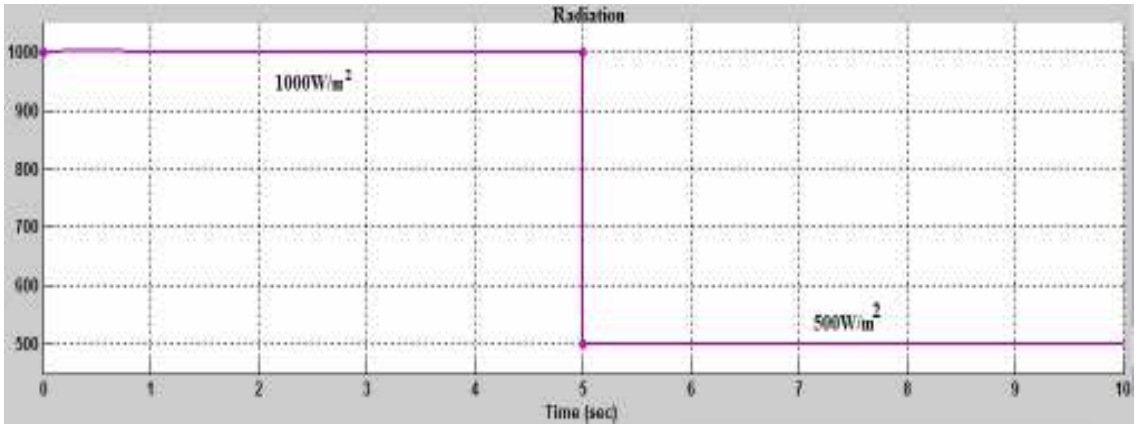

Figure (F.1): Different input radiations for PV array.

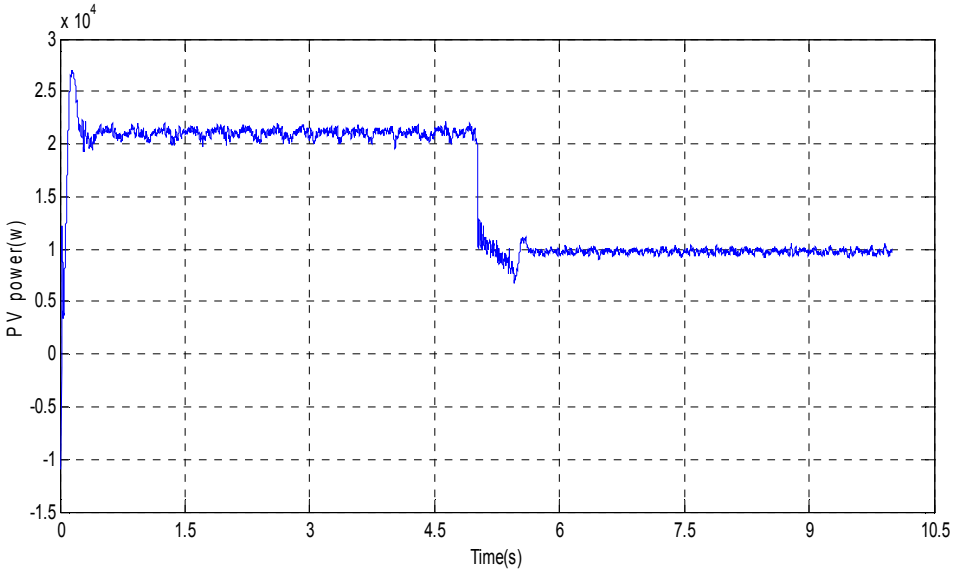

Figure (F.2): PV power for two different radiations.

www.manaraa.com

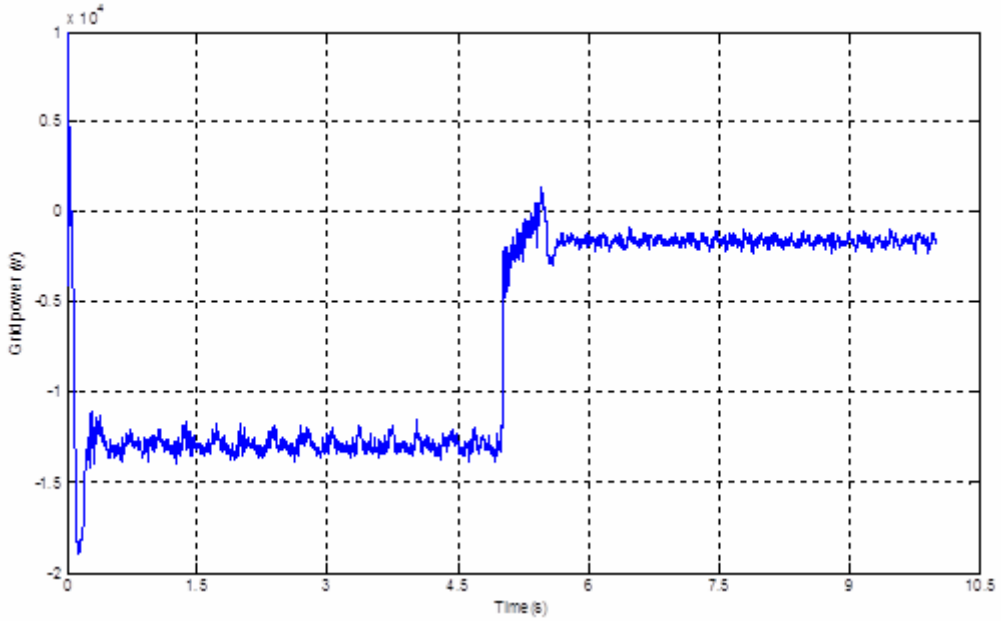

Figure (F.3): Grid power for two different radiations.

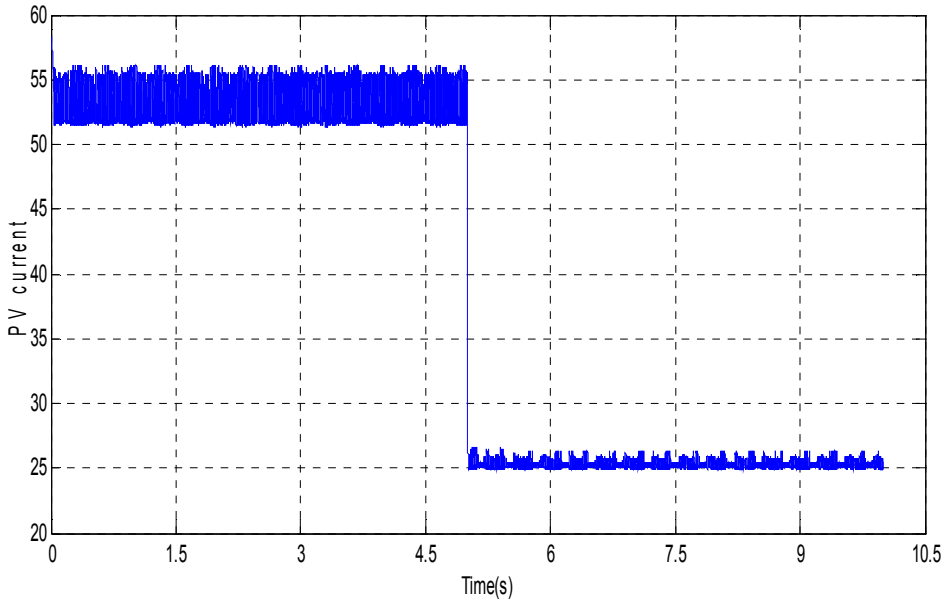

Figure (F.4): MPP current regulation for two different radiations.

www.manaraa.com

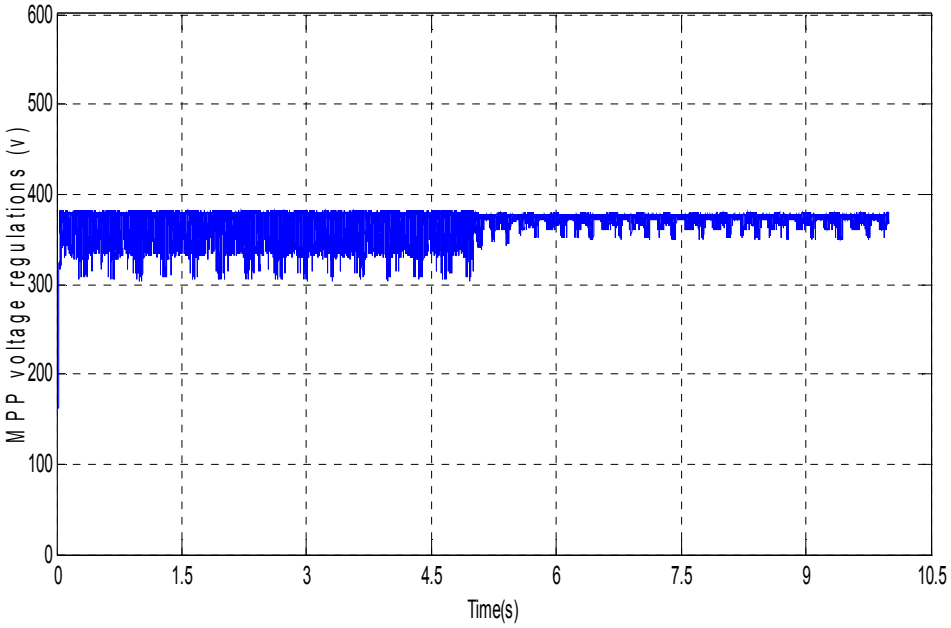

Figure (F.5): MPP voltage regulations for two different radiations.

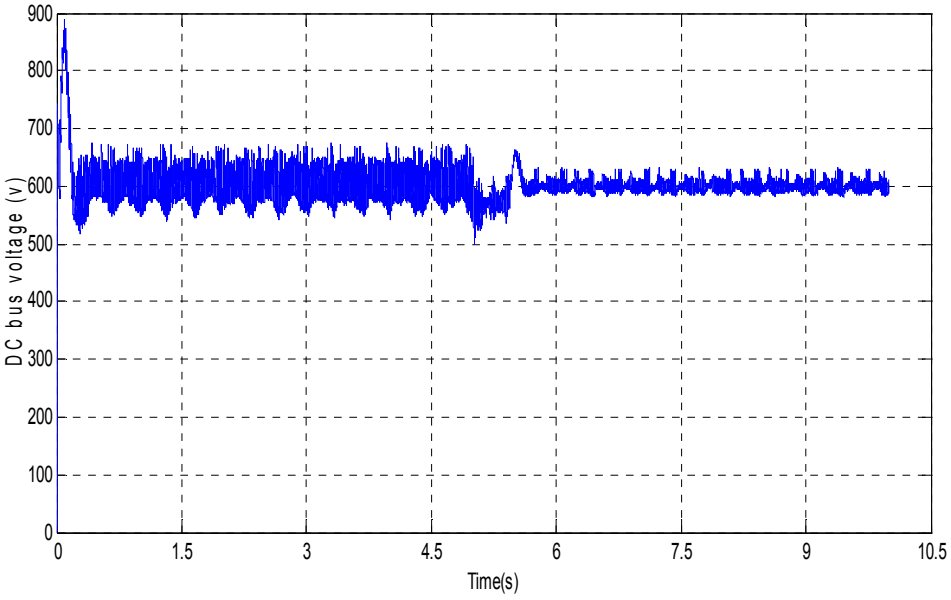

Figure (F.6): Bus dc voltage for two different radiations.

www.manaraa.com

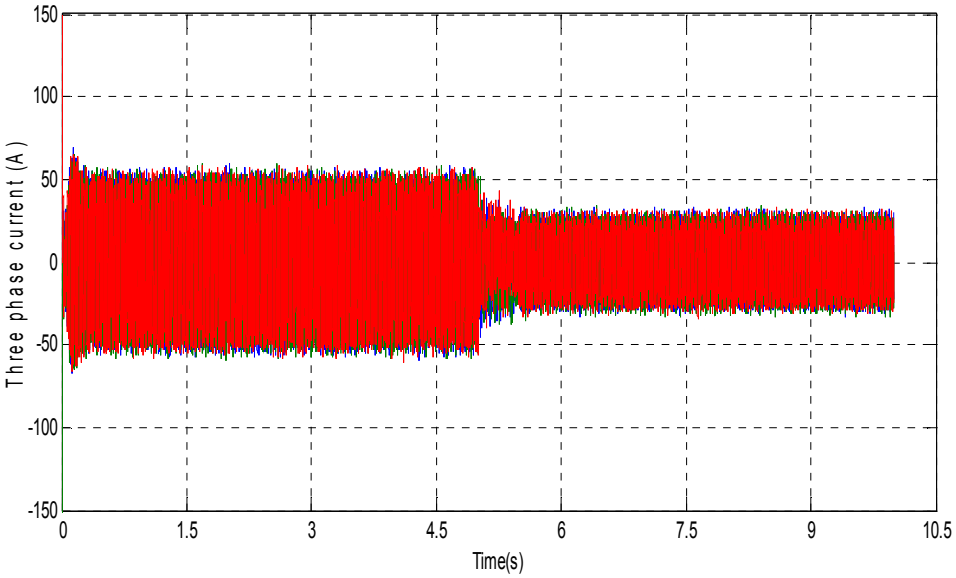

Figure (F.7): Three phase inverter current for two different radiations.

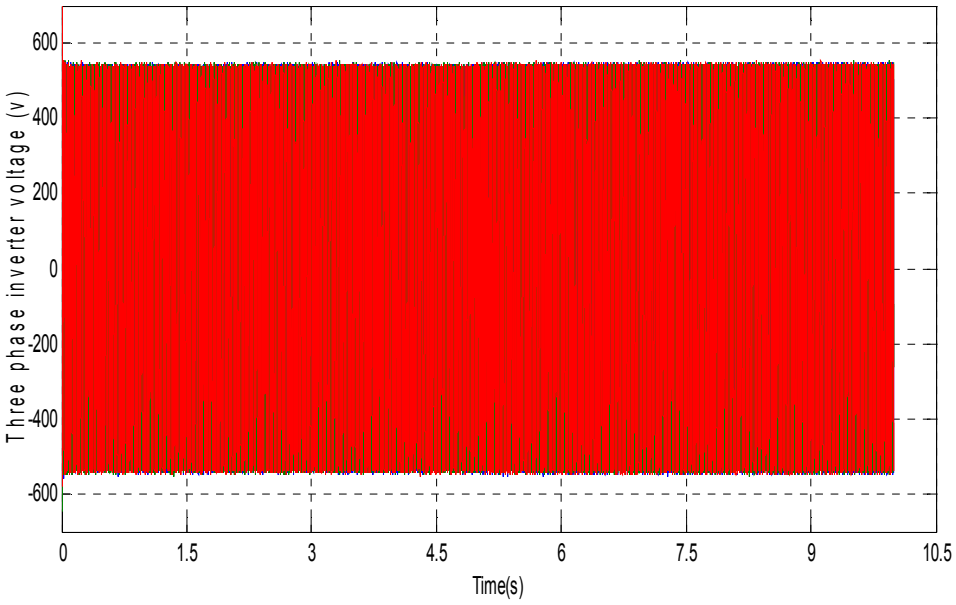

Figure (F.8): Grid voltage for two different radiations.

www.manaraa.com

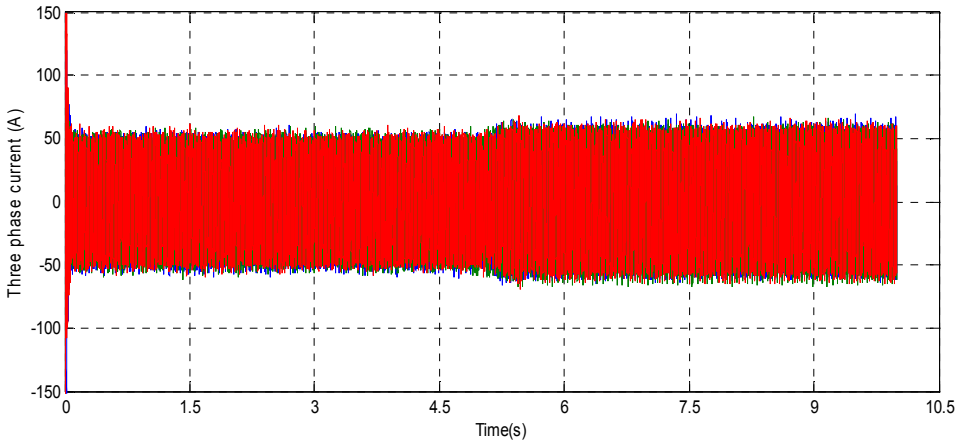

Figure (F.9): Three phase grid current for two different radiations.

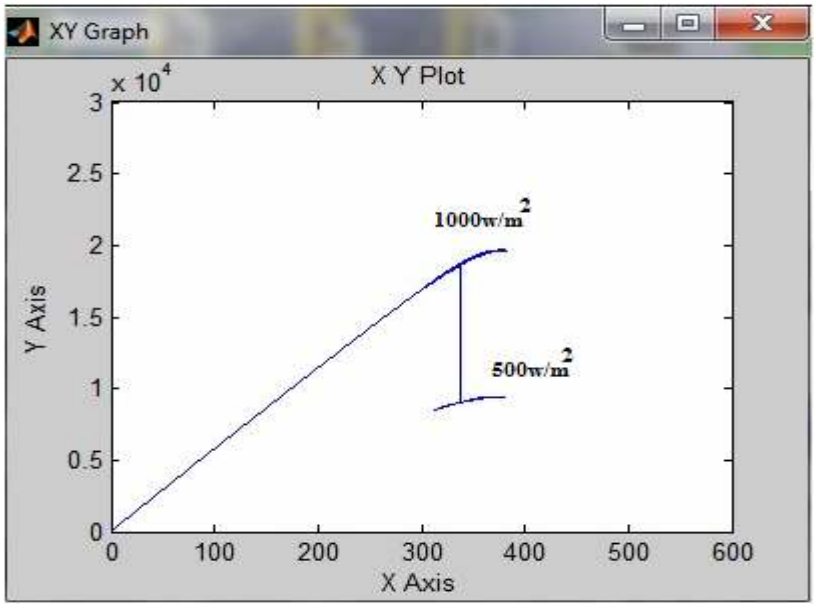

Figure (F.10): P-V Curve for two different radiations for MPP control.

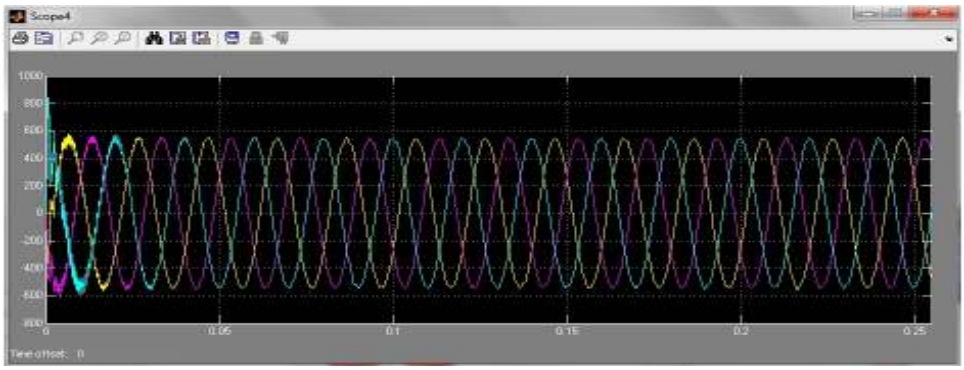

Figure (F.11): Three phase grid voltage.

www.manaraa.com

Simulation of the System for Different Temperatures

These conditions applied on the system, 25 ºC until 5s then change to 50 ºC, 1000 W/m^2, 7kW load

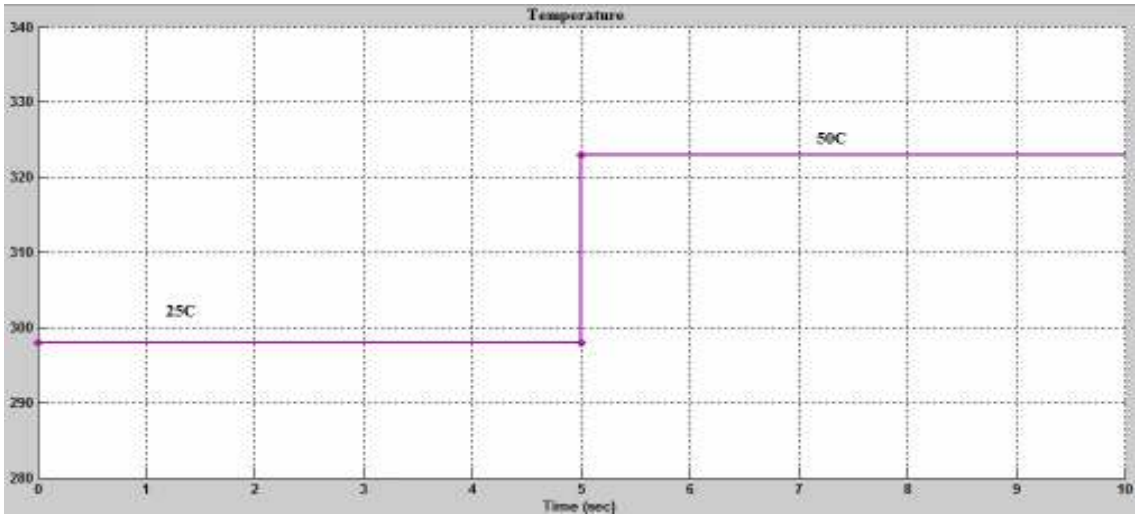

Figure (F.12): different input temperature for PV array.

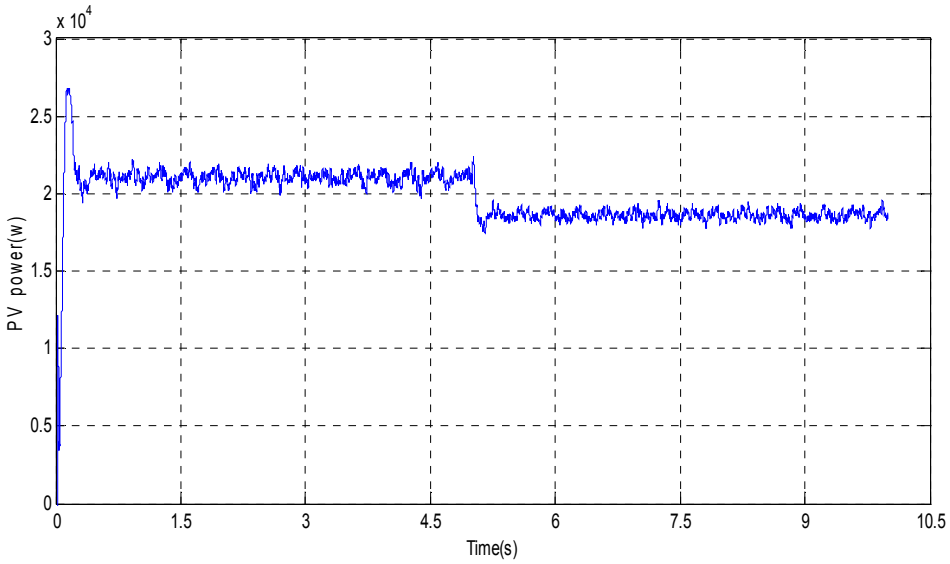

Figure (F.13): PV power for two different temperatures.

www.manaraa.com

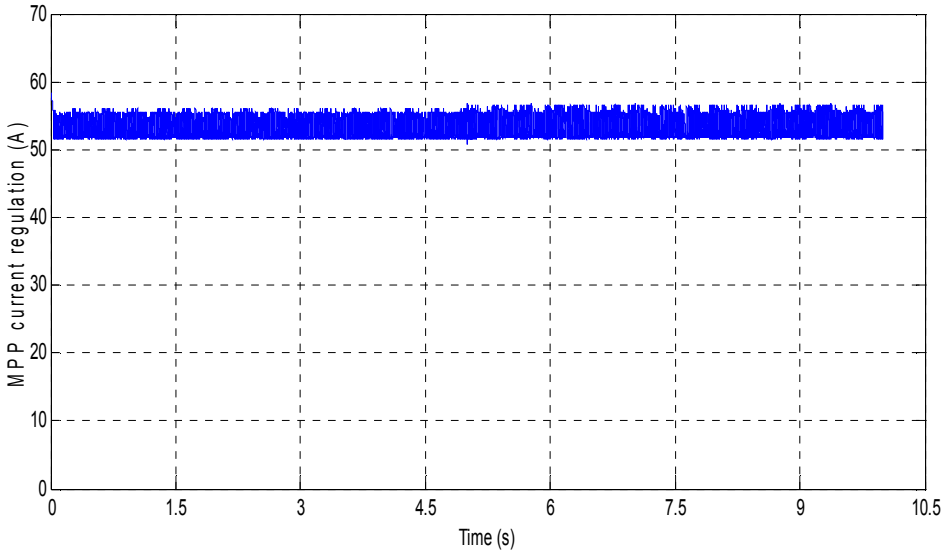

Figure (F.14): MPP current regulation for two different temperatures.

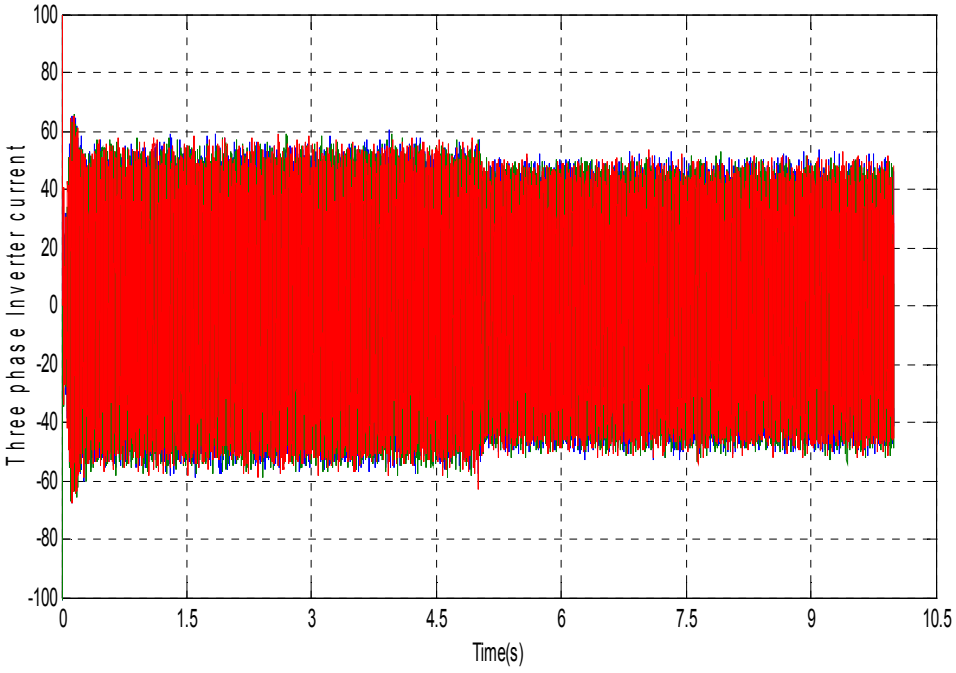

Figure (F.15): Three phase inverter current for two different temperatures.

www.manaraa.com

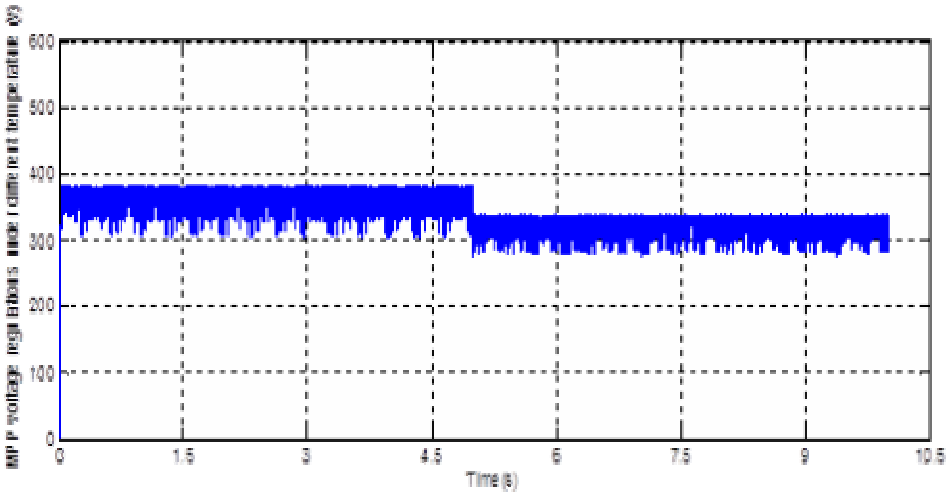

Figure (F.16): MPP voltage regulation for two different temperatures.

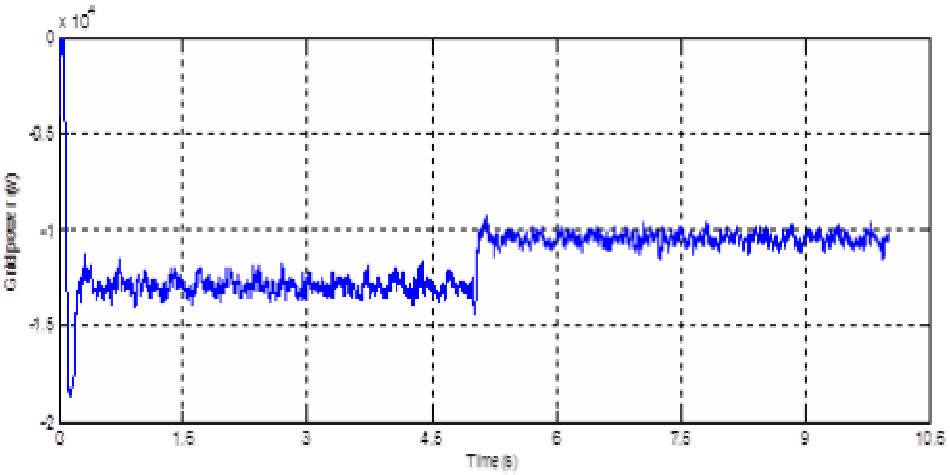

Figure (F.17): Grid power for two different temperatures.

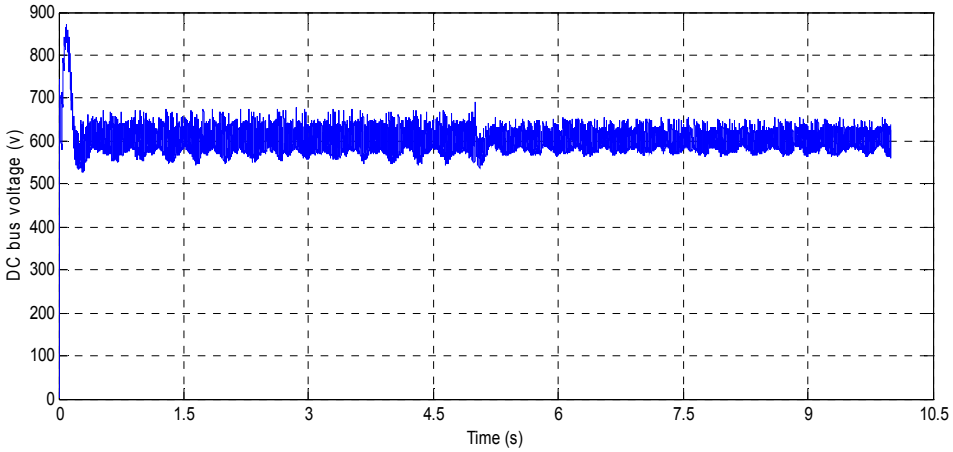

Figure (F.18): Dc bus voltage for two different temperatures.

www.manaraa.com

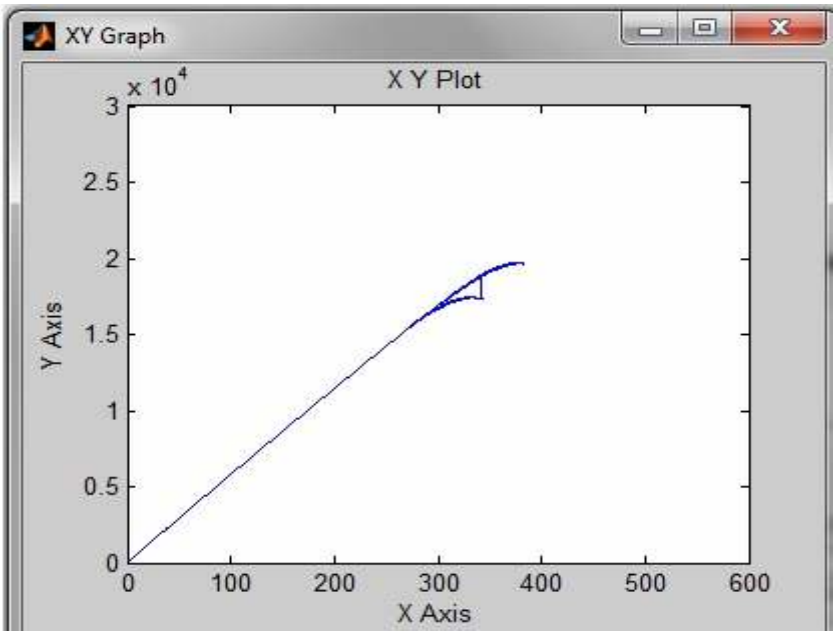

Figure (F.19): P-V Curve for two different temperature under MPP controller.

Simulation of the System for Different Loads

These conditions applied on the system, 25 ºC, 1000 W/m^2, 5kW load until 5s then 10kW.

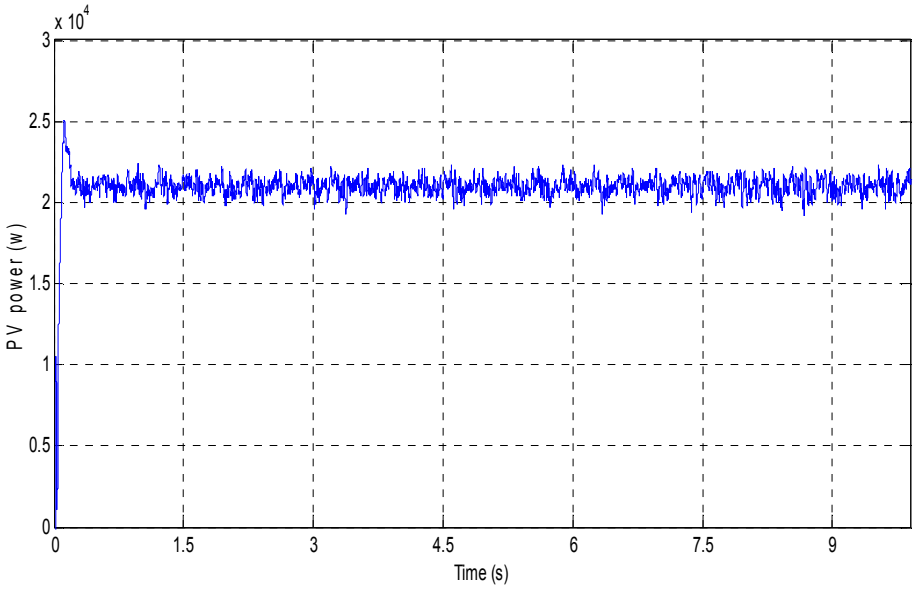

Figure (F.20): PV power for two different loads.

www.manaraa.com

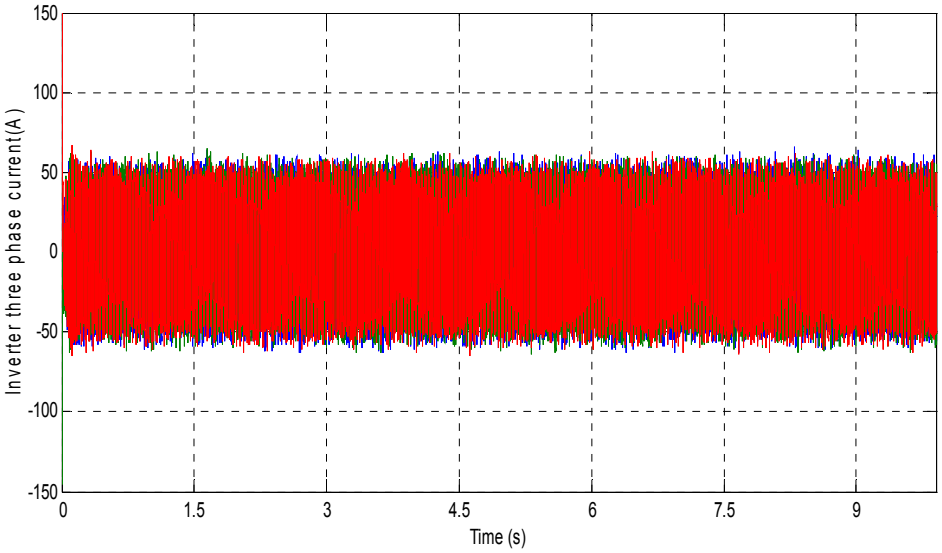

Figure (F.21): Three phase inverter current for two different loads.

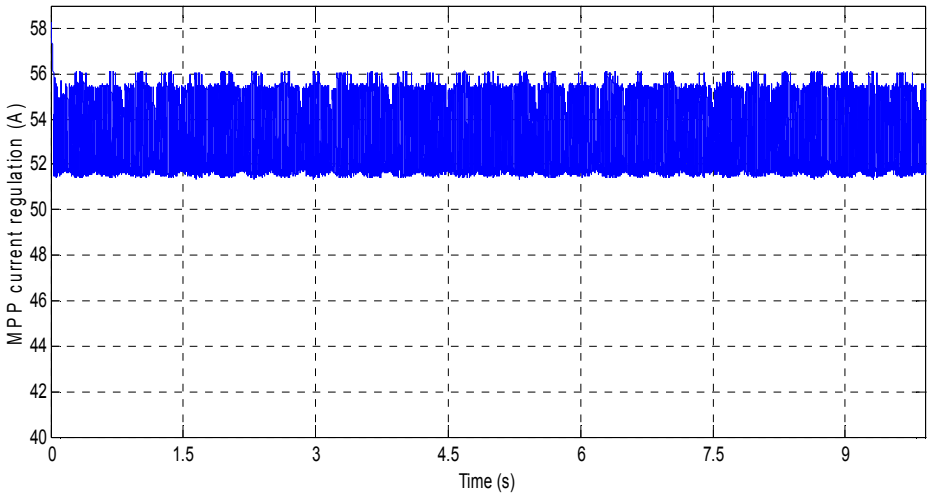

Figure (F.22): MPP current regulation for two different loads.

www.manaraa.com

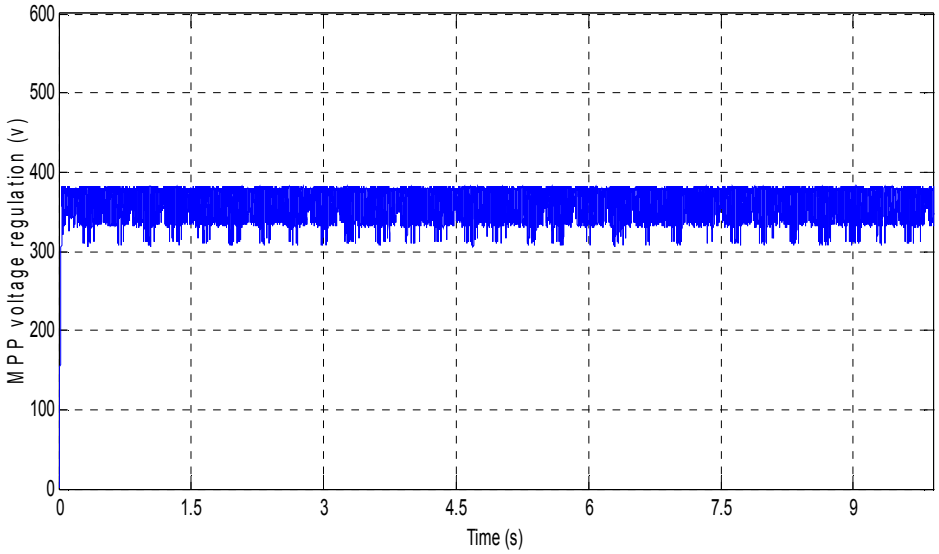

Figure (F.23): MPP voltage regulation for two different loads.

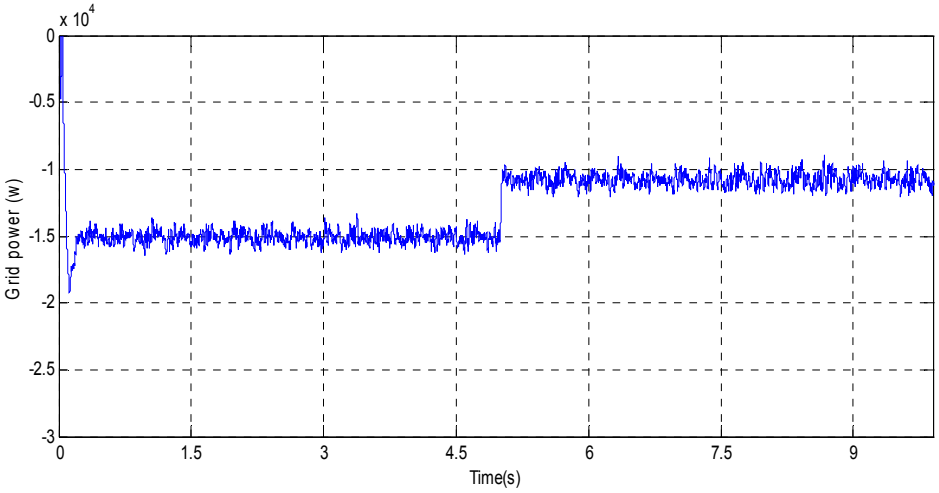

Figure (F.24): Grid power for two different loads.

www.manaraa.com

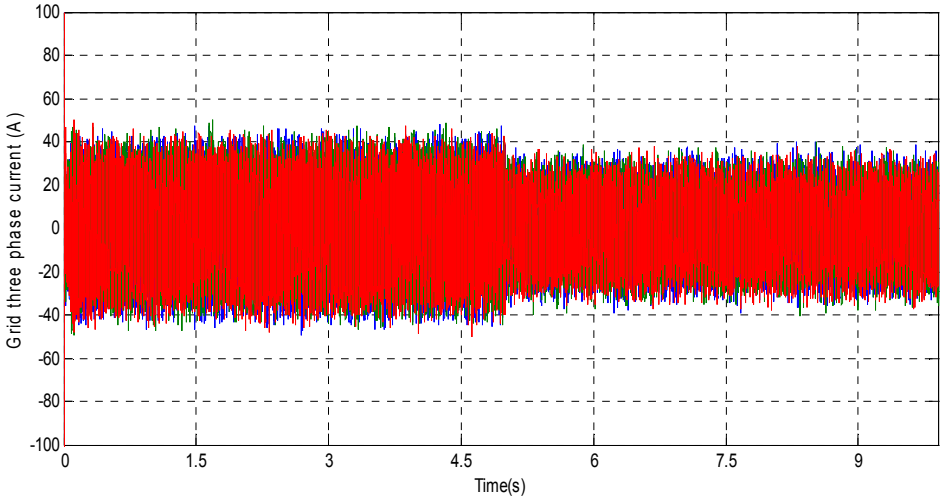

Figure (F.25): Three phase grid current for two different loads.

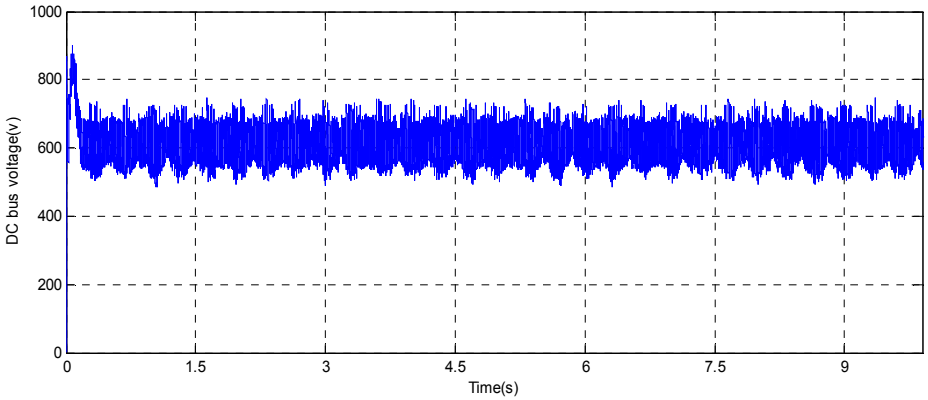

Figure (F.26): DC bus voltage for two different loads.

Simulation of the System for On and Off Grid Connection

At this condition when the grid at off mode the controller disconnects the grid, PV array and connect the standby diesel generator to the load.

www.manaraa.com

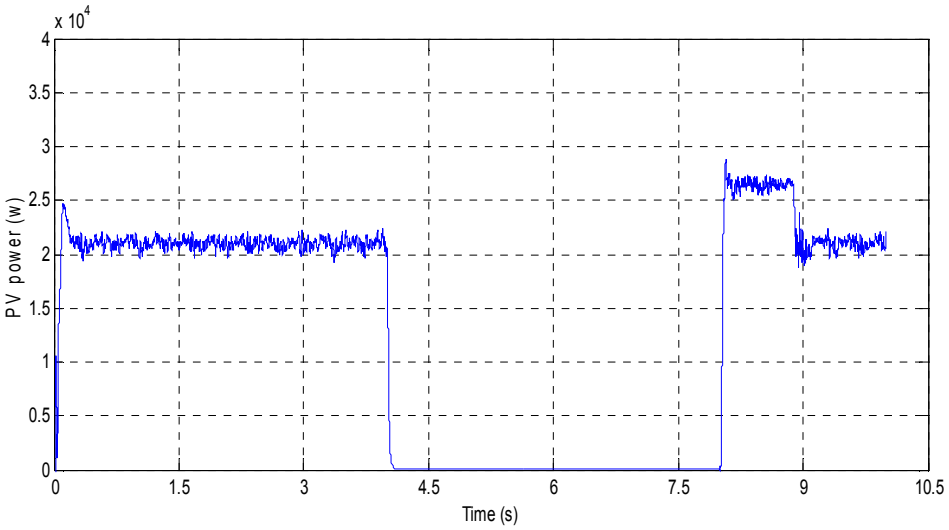

Figure (F.27): PV power for on and off grid.

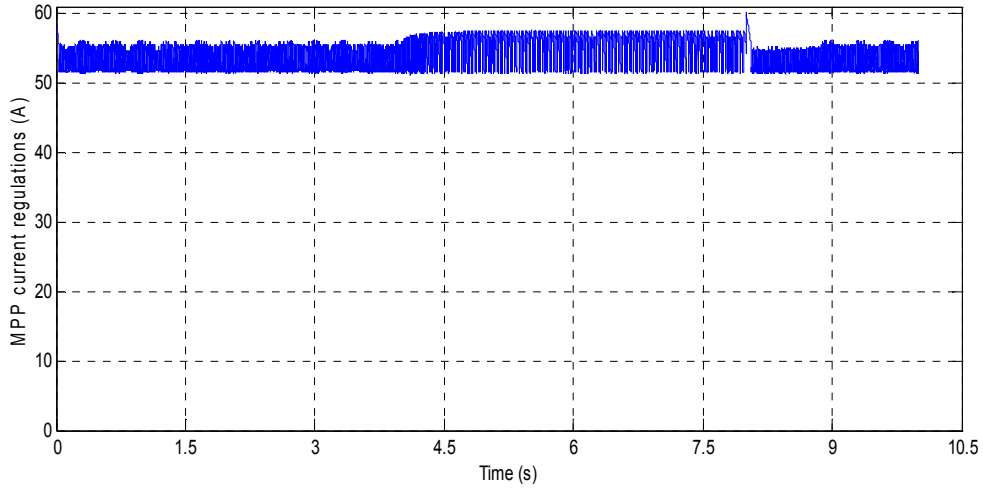

Figure (F.28): MPP current regulation for on and off grid.

www.manaraa.com

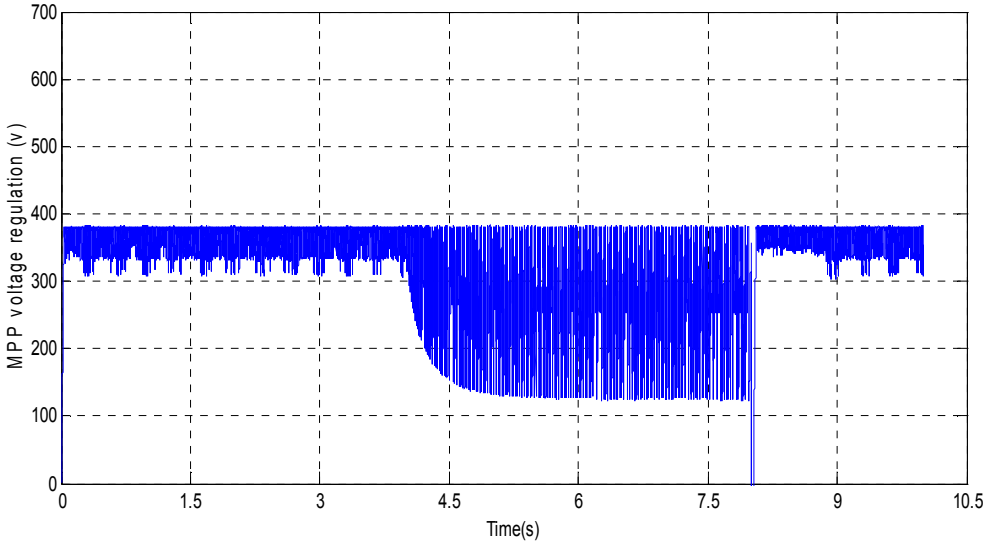

Figure (F.29): MPP voltage regulation for on and off grid.

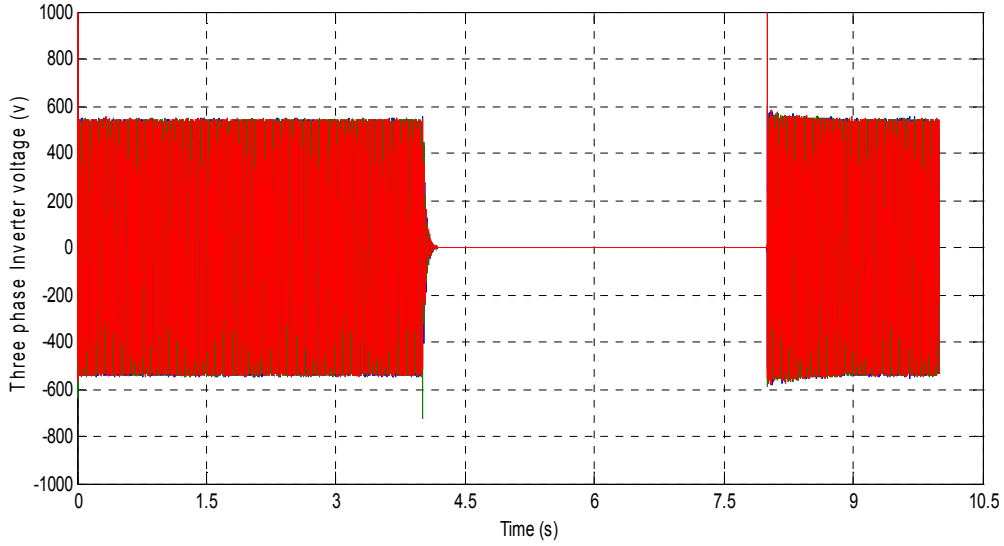

Figure (F.30): Three phase inverter voltage for on and off grid.

www.manaraa.com

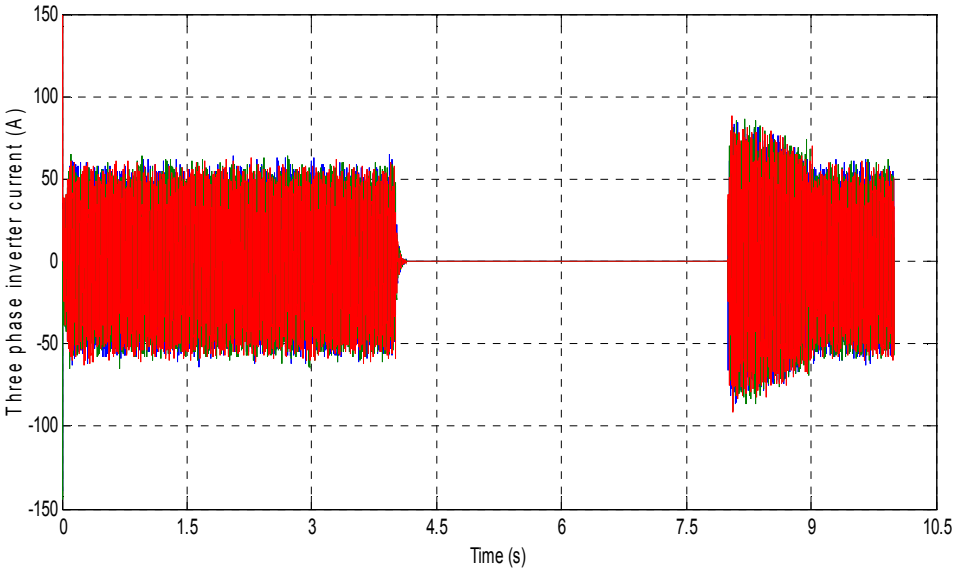

Figure (F.31): Three phase inverter current for on and off grid.

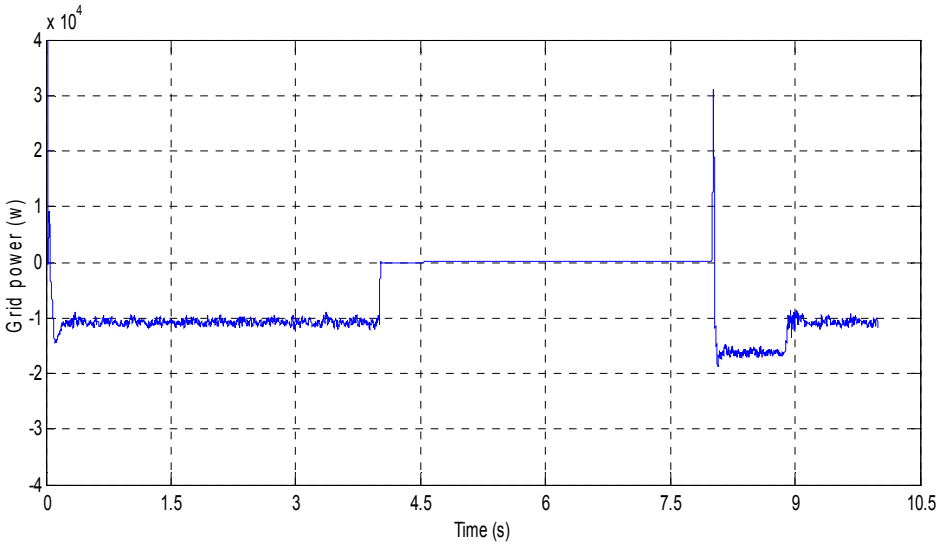

Figure (F.32): Grid power for on and off grid.

www.manaraa.com

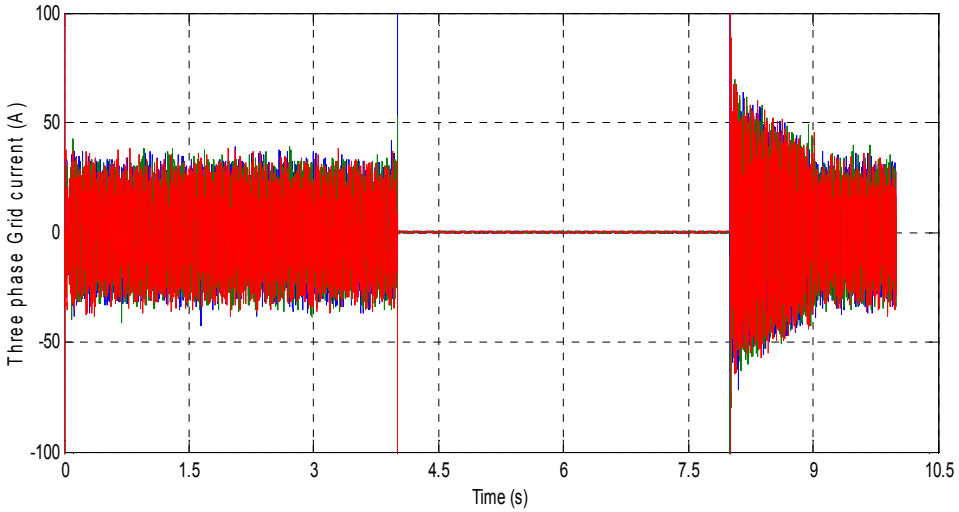

Figure (F.33): Three phase grid current for on and off grid.

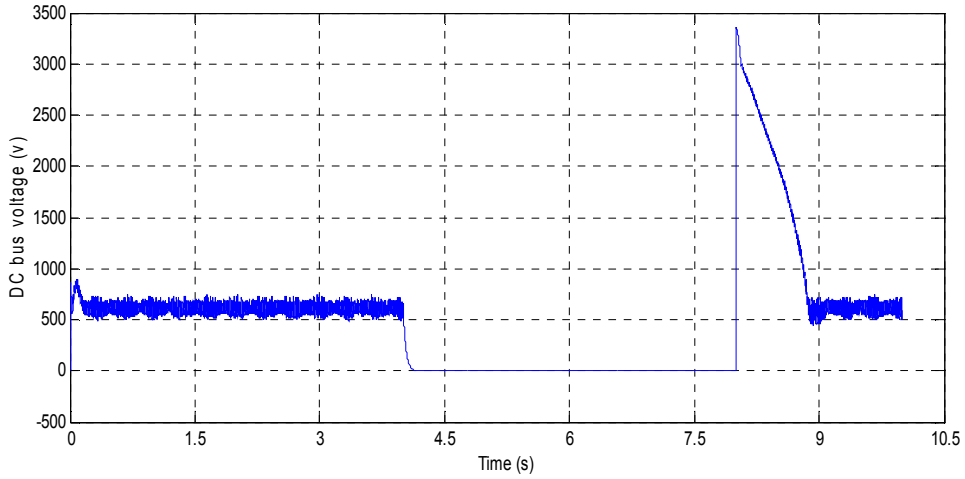

Figure (F.34): DC bus voltage for on and off grid.

www.manaraa.com

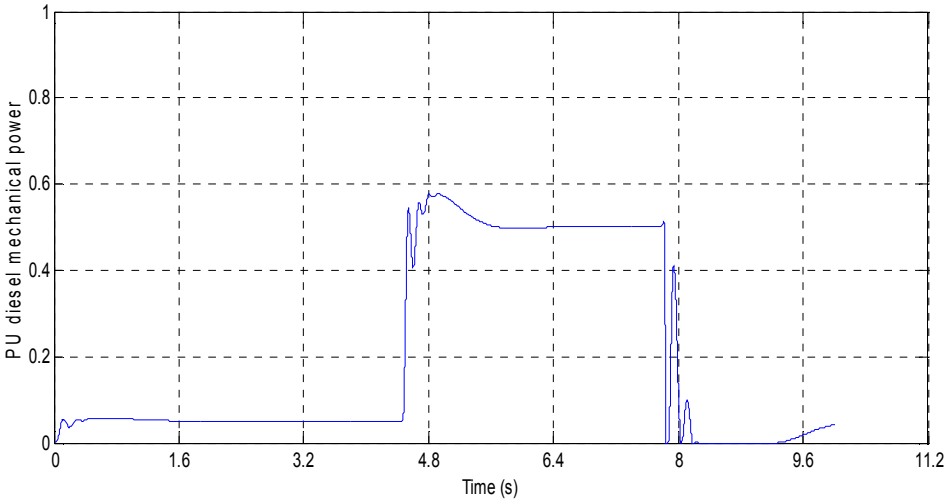

Figure (F.35): pu diesel generator mechanical power for on and off grid.

www.manaraa.com

جامعة النجاح الوطنية
كلية الدراسات العليا

التقييم والتحليل التقني والاقتصادي لربط شبكات الكهرباء مع الأنظمة الهجينة خلايا شمسية رياح في فلسطين/ قرية عطوف: دراسة حالة

إعداد
محمد حسين محمد دريدي

إشراف
د. عماد بريك

قدمت هذه الأطروحة استكمالا لمتطلبات الحصول على درجة الماجستير في هندسة الطاقة النظيفة وإستراتيجية الترشيد بكلية الدراسات العليا في جامعة النجاح الوطنية نابلس فلسطين.
2012

المنارة للاستشارات
www.manaraa.com

التقييم والتحليل التقني والاقتصادي لربط شبكات الكهرباء مع الأنظمة الهجينة خلايا شمسية رياح في فلسطين/ قرية عطوف : دراسة حالة

إعداد

محمد حسين محمد دريدي

إشراف

د. عماد بريك

الملخص

حيث أن الطاقة المتجددة أصبحت أكثر انتشارا, زادت الحاجة لمعرفة المزيد من المعلومات حول كيفية عمل الأنواع المختلفة من هذه التكنولوجيا. هذا البحث قائم على بناء نموذج رياضي محوسب لنظام كهربائي هجين مكون من ألواح شمسية وتوربين رياح موصولة مع شبكة الكهرباء, وذلك باستخدام برنامج الماتلاب سيميولينك من اجل دراسة وتحليل الأداء الفني والاقتصادي لبناء هذه الأنظمة بالاعتماد على تغير الظروف البيئية والبيانات المناخية المتوفرة مثل درجة الحرارة,كمية الإشعاع الشمسي,سرعة الرياح.

من خلال برنامج السيميولينك الذي تم إنشائه يتم معرفة تصميم القدرة اللازمة بالاعتماد على تغير درجة الحرارة,كمية الإشعاع الشمسي,سرعة الرياح و يمكن إجراء مقارنة جنبا إلى جنب بين الأحجام والتوصيلات المختلفة للنظام الهجين,حيث أن نماذج التنبؤ الحالية مفيدة جدا في حالة الأنظمة المتصلة بالشبكة الكهربائية والتي تعمل عند نقطة القدرة القصوى.وبالتالي تم عمل تعديلات على النماذج السابقة بحيث أن هذا النموذج المصمم يتم من خلاله عمل محاكاة لمعرفة نتائج تشغيل عناصر النظام لكل فترة زمنية محددة و يتنبأ أيضا بدقة عن كمية إنتاج الطاقة خلال هذه الفترات وبالاعتماد على البيانات المقاسه.

كذلك يتم من خلال البرنامج المحوسب الذي تم تصميمه معرفة كمية إنتاج الطاقة من الأنظمة الهجينة بتغيير ظروف التشغيل, زيادة درجة الحرارة أو كمية الإشعاع الشمسي ,وقد تم تحليل البيانات المقاسه من شبكة كهرباء عطوف كدراسة حالة.

المنارة للاستشارات

www.manaraa.com

هذا البحث مهم من الناحية العلمية لأنه يبين نواحي ضعف أداء النظـــام تحـــت تغيـــر الظروف المناخية للمواقع المحددة ,ويمكن من خلاله مقارنة أشكال مختلفـــة لمكونـــات النظـــام المقترح. كذلك يبين أن تصميم الأنظمة الهجينة من خلال الاعتماد علـــى نقطـــة واحـــدة مـــن الظروف المناخية (قيمة متوسطة) ليس بالضروري أن يعطي أفضل معايير تشغيل وأداء عنـــد وصلة مع الشبكة الكهربائية .وبالتحديد أن هذا البحث يبين كمية إنتاج الطاقة واقتصاديات النظام الناتج عن تشغيل أنظمة الخلايا الشمسية (وتوربينات الرياح),وذلك عند تحديد قـــدرة عناصـــر النظام ونسبة المشاركة في تغذية الأحمال الكهربائية.

المنارة للاستشارات
www.manaraa.com